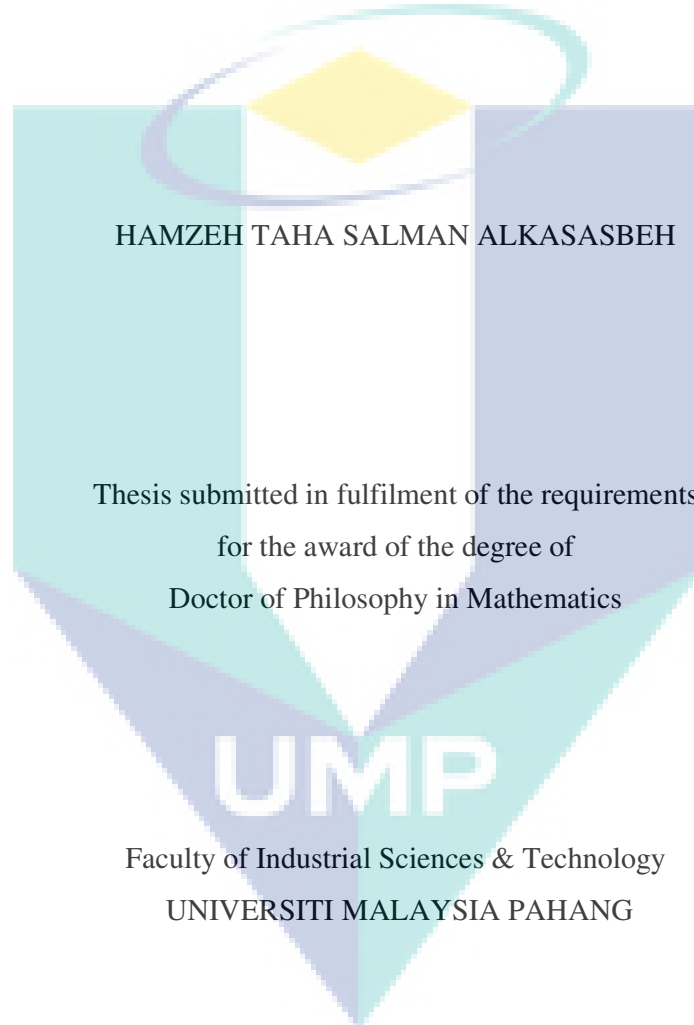


NUMERICAL SOLUTIONS FOR CONVECTIVE BOUNDARY LAYER FLOW
OVER A SOLID SPHERE OF NEWTONIAN AND NON-NEWTONIAN FLUIDS



OCTOBER 2015

UNIVERSITI MALAYSIA PAHANG

DECLARATION OF THESIS AND COPYRIGHT

Author's full name : HAMZEH TAHA SALMAN ALKASASBEH
Date of birth : 25 JANUARY 1982
Title : NUMERICAL SOLUTIONS FOR CONVECTIVE
BOUNDARY LAYER FLOW OVER A SOLID SPHERE
OF NEWTONIAN AND NON-NEWTONIAN FLUIDS
Academic Session : 2015/2016

I declare that this thesis is classified as:

- CONFIDENTIAL** (contains confidential information under the official secret Act 1972)*
 RESTRICTED (contains restricted information as specified by the organization where research was done)*
 OPEN ACCESS I agree that my thesis to be published as online open access (Full text)

I acknowledge the Universiti Malaysia Pahang reserve the right as follows:

1. The thesis is the property of University Malaysia Pahang.
2. The library of University Malaysia Pahang has the right to make copies for purpose of research only.
3. The library has the right to make copies of the thesis for academic exchange.

Certified By:

(Student's Signature)

M127535

New IC/ Passport Number

Date: /10/ 2015

(Signature of Supervisor)

ASSOC. PROF. DR. MOHD ZUKI SALLEH

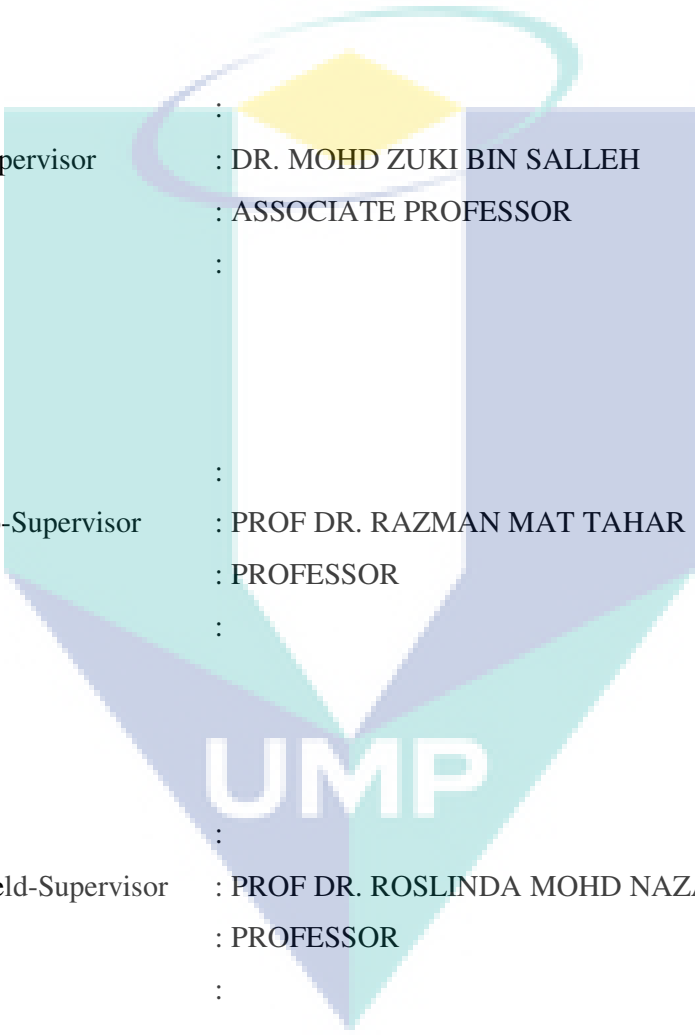
(Name of Supervisor)

Date: /10/ 2015

NOTES : * If the thesis is CONFIDENTIAL or RESTRICTED, please attach with the letter from the organization with period and reasons for confidentiality or restriction.

SUPERVISOR'S DECLARATION

I hereby declare that I have checked this thesis and in my opinion, this thesis is adequate in terms of scope and quality for the award of the degree of Doctor of Philosophy in Mathematics.

The background of the declaration form features a large, semi-transparent watermark of the UMP logo. The logo is a shield-shaped emblem with a yellow diamond at the top, a white vertical bar in the center, and teal and blue triangular sections at the bottom. The letters 'UMP' are prominently displayed in white at the base of the shield.

Signature :
Name of Supervisor : DR. MOHD ZUKI BIN SALLEH
Position : ASSOCIATE PROFESSOR
Date :

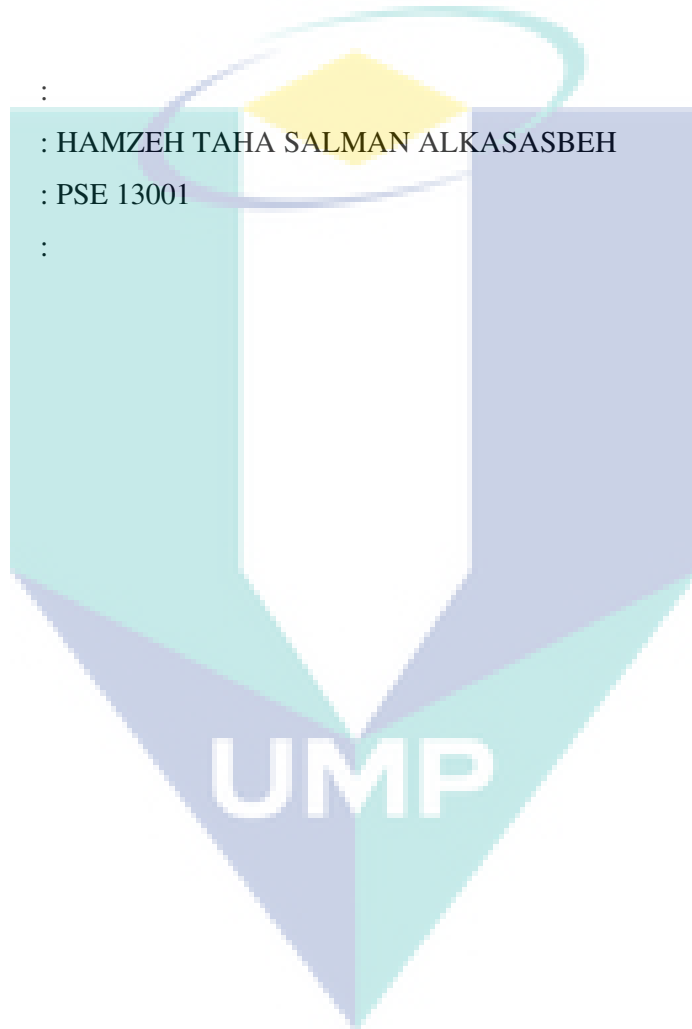
Signature :
Name of Co-Supervisor : PROF DR. RAZMAN MAT TAHAR
Position : PROFESSOR
Date :

Signature :
Name of Field-Supervisor : PROF DR. ROSLINDA MOHD NAZAR
Position : PROFESSOR
Date :

STUDENT'S DECLARATION

I hereby declare that the work in this thesis is my own except for quotations and summaries which have been duly acknowledged. This thesis has not been accepted for any degree and is not concurrently submitted for award of the other degree.

Signature :
Name : HAMZEH TAHA SALMAN ALKASASBEH
ID Number : PSE 13001
Date :



ACKNOWLEDGEMENTS

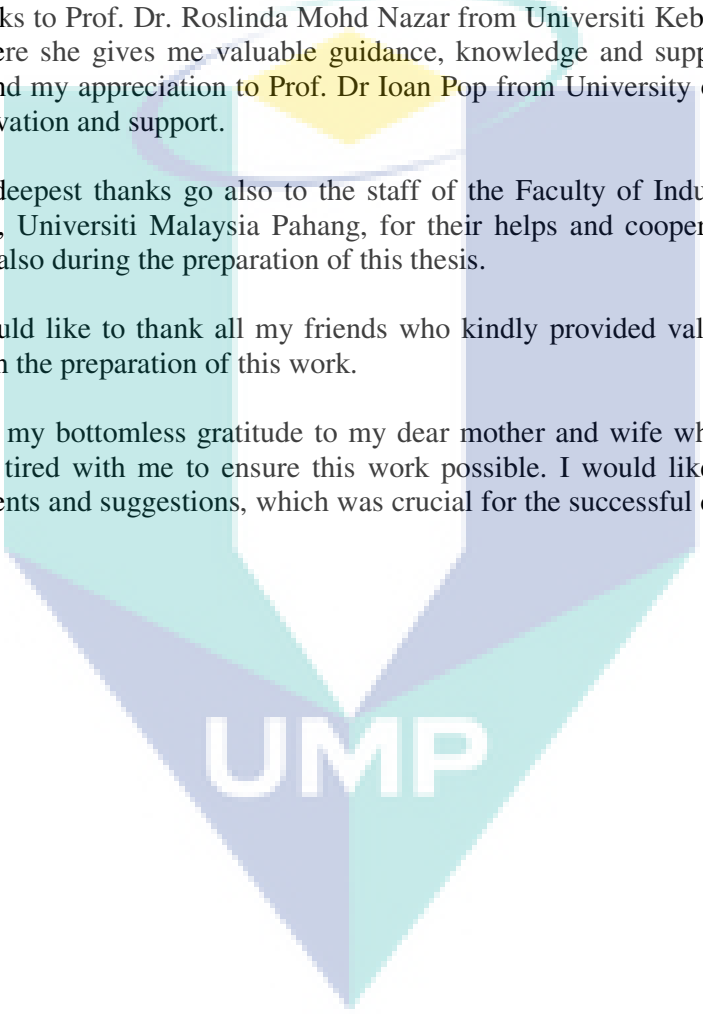
First of all, I am grateful to Allah for His bounty that helps me to complete this work. I would like to express my sincere gratitude and thanks to my supervisor, Associate Professor Dr. Mohd Zuki Salleh for his encouragement, generous support and valuable suggestion as without it, this thesis would not appear in this final form. I am deeply indebted to him and have enjoyed working with him.

My sincere thanks go to my co-supervisors; Prof Dr Razman Mat Tahar and special thanks to Prof. Dr. Roslinda Mohd Nazar from Universiti Kebangsaan Malaysia (UKM) where she gives me valuable guidance, knowledge and support. I would also like to extend my appreciation to Prof. Dr Ioan Pop from University of Cluj, Romania, for his motivation and support.

My deepest thanks go also to the staff of the Faculty of Industrial Sciences & Technology, Universiti Malaysia Pahang, for their helps and cooperations during my studies and also during the preparation of this thesis.

I would like to thank all my friends who kindly provided valuable and helpful comments in the preparation of this work.

Finally, my bottomless gratitude to my dear mother and wife who have sacrificed and getting tired with me to ensure this work possible. I would like to acknowledge their comments and suggestions, which was crucial for the successful completion of this thesis.



UMP

ABSTRACT

In this thesis, the mathematical modelling for the six main problems on convection boundary layer flows over a solid sphere has been considered. The first two problems on the effect of radiation on magnetohydrodynamic for steady free convection boundary layer flows in a viscous and micropolar fluid have been investigated. Further, the other four problems were mixed convection boundary layer flows in a viscous, micropolar, nanofluid and a porous medium filled with a nanofluid, respectively. All these problems focused on the solid sphere with convective boundary conditions in which the heat is supplied through a bounding surface of finite thickness and finite heat capacity. In order to solve these problems, the dimensional equations that governed the fluid flow and heat transfer were transformed into dimensionless equations by using appropriate dimensionless variables. Stream functions were introduced, yielding a function representing velocities. Similarity variables were used to deduce the dimensionless governing equations into a system of nonlinear partial differential equations. This system was solved numerically by using the numerical scheme, namely as Keller-box method. Numerical solutions were obtained for the local heat transfer coefficient, the local wall temperature, the local Nusselt number and the local skin friction coefficient, as well as the velocity, temperature and angular velocity profiles. The features of the fluid flow and heat transfer characteristics for different values of the Prandtl number Pr , magnetic parameter, radiation parameter, micropolar parameter, nanoparticle volume fraction, mixed convection parameter conjugate parameter and coordinate running along the surface of the sphere x , were analyzed and discussed. In conclusion, when the radiation parameter increased, the values of the temperature, velocity and skin friction coefficient decreased while the heat transfer coefficient increased. Next, as magnetic parameter increased the temperature increased but the velocity, skin friction coefficient and heat transfer coefficient decreased. Furthermore, the conjugate parameter increased the values of the local heat transfer coefficient and thus, the local skin friction coefficient increased. Additionally, the mixed convection parameter increased the values of the local heat transfer coefficient and hence the local skin friction coefficient also increased. On the other hand, the copper nanoparticles have the highest local heat transfer coefficient compared to aluminum oxide and titanium dioxide nanoparticles. Moreover, the copper nanoparticles also have the highest the local skin friction coefficient, followed by titanium dioxide and aluminum oxide nanoparticles.

ABSTRAK

Dalam tesis ini, pemodelan matematik bagi enam masalah pada aliran lapisan sempadan olakan terhadap sfera pejal telah dipertimbangkan. Dua masalah pertama adalah berkenaan kesan radiasi ke atas hydrodinamik magnet bagi aliran lapisan sempadan olakan bebas dalam bendalir likat dan mikrokutub telah dikaji. Di samping itu, empat masalah aliran lapisan sempadan olakan campuran yang terbenam masing-masing dalam bendalir likat, mikrokutub, bendalir nano dan medium berliang yang dipenuhi dengan bendalir nano turut diberi perhatian. Semua masalah ini memberi tumpuan kepada sfera pejal dengan syarat sempadan olakan di mana haba dibekalkan melalui permukaan dengan ketebalan dan muatan haba yang terbatas. Bagi menyelesaikan masalah ini, persamaan dimensi yang merupakan persamaan menakluk bagi aliran dan pemindahan haba dijelmakan menjadi persamaan tak berdimensi dengan menggunakan pemboleh ubah tak berdimensi yang sesuai. Fungsi aliran diperkenalkan bagi menghasilkan fungsi yang mewakili halaju. Pembolehubah keserupaan digunakan untuk menurunkan persamaan tertakluk tak berdimensi kepada sistem persamaan pembezaan separa tak linear. Sistem ini telah diselesaikan secara berangka dengan menggunakan kaedah berangka yang dikenali sebagai kaedah kotak Keller. Penyelesaian berangka diperoleh bagi pekali pemindahan haba setempat, suhu dinding setempat, nombor Nusselt setempat dan pekali geseran kulit setempat, serta profil halaju, suhu dan halaju sudut. Ciri-ciri aliran dan pemindahan haba untuk nilai yang berbeza bagi parameter-parameter seperti nombor Prandtl Pr, magnet, radiasi, mikrokutub, jumlah pecahan nanopartikel, olakan campuran konjugat dan koordinat di sepanjang permukaan sfera x , dianalisis dan dibincangkan. Kesimpulannya, apabila radiasi meningkat, nilai bagi suhu, halaju dan pekali geseran permukaan berkurangan manakala pekali pemindahan haba meningkat. Seterusnya, apabila parameter magnet meningkat, suhu meningkat tetapi halaju, pekali geseran permukaan dan pekali pemindahan haba menurun. Sebagai tambahan, parameter konjugat meningkatkan nilai pekali pemindahan haba setempat dan dengan itu, pekali geseran permukaan setempat meningkat. Selain itu, parameter olakan campuran meningkatkan nilai pekali pemindahan haba setempat dan dengan itu pekali geseran permukaan setempat juga meningkat. Manakala, nanopartikel tembaga mempunyai pekali pemindahan haba setempat yang paling tinggi berbanding aluminium oksida dan titanium dioksida. Selain itu juga, nanopartikel tembaga mempunyai pekali geseran permukaan setempat yang paling tinggi, diikuti dengan nanopartikel titanium dioksida dan oksida aluminium.

CHAPTER 2	GOVERNING EQUATIONS AND NUMERICAL METHOD	
2.1	Governing Equations	18
	2.1.1 The Dimensional Equations Boussinesq Approximation	18
	2.1.2 Non-similar Transformation	26
2.2	Numerical Method: The Keller-box Method	27
	2.2.1 Finite Difference Method	28
	2.2.2 Newton Method	33
	2.2.3 The Block Elimination Technique	37
	2.2.4 Starting Conditions	44
	2.2.5 Initial Profile	45
CHAPTER 3	THE EFFECT OF RADIATION ON MAGNETOHYDRODYNAMIC FREE CONVECTION BOUNDARY LAYER FLOW OVER A SOLID SPHERE IN A VISCOUS FLUID	
3.1	Introduction	49
3.2	Mathematical Formulation	50
3.3	Results and Discussion	53
3.4	Conclusions	69
CHAPTER 4	THE EFFECT OF RADIATION ON MAGNETOHYDRODYNAMIC FREE CONVECTION BOUNDARY LAYER FLOW OVER A SOLID SPHERE IN A MICROPOLAR FLUID	
4.1	Introduction	70
4.2	Mathematical Formulation	71
4.3	Results and Discussion	74
4.4	Conclusions	93

CHAPTER 5	MIXED CONVECTION BOUNDARY LAYER FLOW OVER A SOLID SPHERE IN A VISCOUS FLUID	
5.1	Introduction	95
5.2	Mathematical Formulation	96
5.3	Results and Discussion	99
5.4	Conclusions	109
CHAPTER 6	MIXED CONVECTION BOUNDARY LAYER FLOW OVER A SOLID SPHERE IN A MICROPOLAR FLUID	
6.1	Introduction	110
6.2	Mathematical Formulation	111
6.3	Results and Discussion	114
6.4	Conclusions	122
CHAPTER 7	MIXED CONVECTION BOUNDARY LAYER FLOW OVER A SOLID SPHERE IN A NANOFLUID	
7.1	Introduction	124
7.2	Basic Equations	125
7.3	Results and Discussion	126
7.4	Conclusions	142
CHAPTER 8	MIXED CONVECTION FLOW OVER A SOLID SPHERE EMBEDDED IN A POROUS MEDIUM FILLED A NANOFLUID	
8.1	Introduction	143
8.2	Mathematical Formulation	144
8.3	Results and Discussion	146
8.4	Conclusions	157

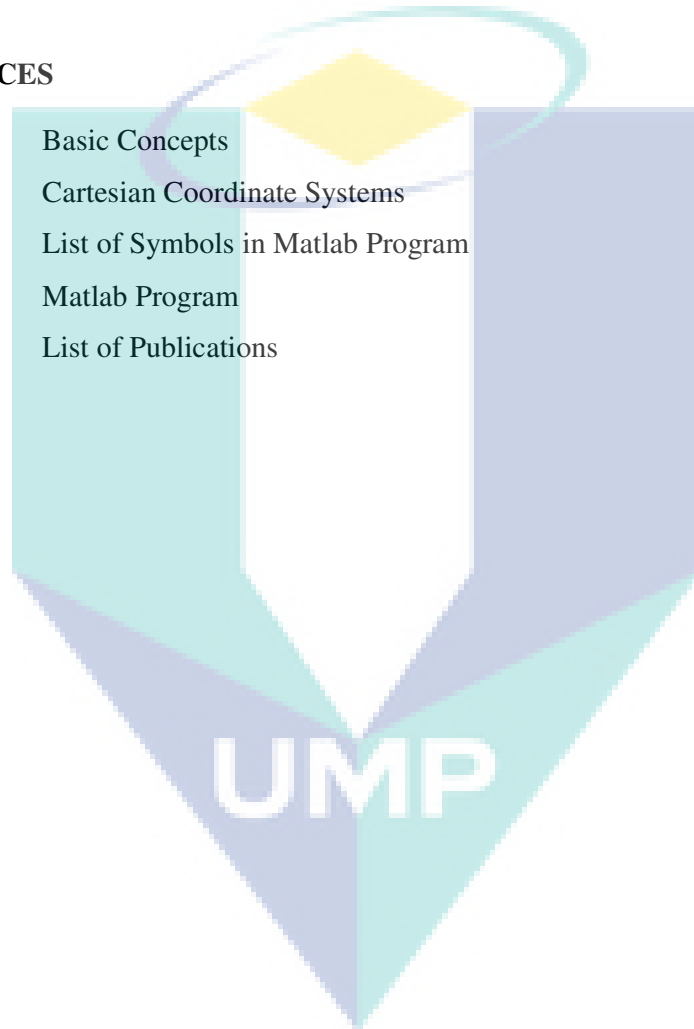
CHAPTER 9 CONCLUSIONS

9.1	Summary of the Research	158
9.2	Contribution of the Research	161
9.3	Future Studies	161

REFERENCES	162
-------------------	-----

APPENDICES

A	Basic Concepts	179
B	Cartesian Coordinate Systems	184
C	List of Symbols in Matlab Program	186
D	Matlab Program	187
E	List of Publications	194



LIST OF TABLES

Table No.	Title	Page
3.1	The heat transfer coefficient $-(\partial\theta/\partial y)(x,0)$ at the lower stagnation point of the sphere, $x \approx 0$, when $Pr = 0.7, 7$, without the effect of radiation and magnetohydrodynamic and $\gamma \rightarrow \infty$	57
3.2	The local heat transfer coefficient $Q_w(x)$ for various values of x when $Pr = 0.7, 7, 100, M = 0, N_R = 0$ and $\gamma = 0.1$	57
3.3	The local skin friction coefficient C_f for various values of x when $Pr = 0.7, 7, 100, M = 0, N_R = 0$ and $\gamma = 0.1$	58
3.4	The wall temperature $\theta(x,0)$, the heat transfer coefficient $-(\partial\theta/\partial y)$ and the skin friction coefficient $(\partial^2 f/\partial y^2)$ at the lower stagnation point of the sphere, $x \approx 0$, for various values of N_R when $Pr = 0.7, M = 0, 5$ and $\gamma = 0.1$	58
3.5	The local Nusselt number N_u for various values of x when $Pr = 1, 7, N_R = 3, M = 5$ and $\gamma = 0.1$	59
3.6	The local skin friction coefficient C_f for various values of x when $Pr = 1, 7, \gamma = 0.1, N_R = 3$ and $M = 5$	59
4.1	The heat transfer coefficient $-(\partial\theta/\partial y)$ at the lower stagnation point of the sphere, $x \approx 0$, for various values of K when $Pr = 0.7, 7$, without the effect of radiation and magnetohydrodynamic and $\gamma \rightarrow \infty$	78
4.2	The wall temperature $\theta(x,0)$ and the skin friction coefficient $(\partial^2 f/\partial y^2)$ at the lower stagnation point of the sphere, $x \approx 0$, for various values of K when $Pr = 0.7, M = 0, N_R = 0$ and $\gamma = 0.05, 0.1, 0.2$	78
4.3	The wall temperature $\theta(x,0)$ at the lower stagnation point of the sphere, $x \approx 0$, for various values of K when $Pr = 0.7, 1, 7, M = 0, N_R = 0$ and $\gamma = 0.1$	79
4.4	The heat transfer coefficient $-(\partial\theta/\partial y)$ at the lower stagnation point of the sphere, $x \approx 0$, for various values of K when $Pr = 0.7, 1, 7, M = 0, N_R = 0$ and $\gamma = 0.1$	79

4.5	The skin friction coefficient $(\partial^2 f / \partial y^2)$ at the lower stagnation point of the sphere, $x \approx 0$, for various values of K when $Pr = 0.7, 1, 7, M = 0, N_R = 0$ and $\gamma = 0.1$	79
4.6	The local heat transfer coefficient $Q_w(x)$ for various values of x when $Pr = 0.7, 1, \text{ and } 7, K = 0, M = 0, N_R = 0$ and $\gamma = 0.5$	80
4.7	The local skin friction coefficient C_f for various values of x when $Pr = 0.7, 1, 7, K = 0, M = 0, N_R = 0$ and $\gamma = 0.5$	80
4.8	The local heat transfer coefficient $Q_w(x)$ for various values of x when $Pr = 0.7, 1, 7, K = 2, M = 0, N_R = 0$ and $\gamma = 0.5$	81
4.9	The local skin friction coefficient C_f for various values of x when $Pr = 0.7, 1, 7, K = 2, M = 0, N_R = 0$ and $\gamma = 0.5$	81
4.10	The wall temperature $\theta(x, 0)$, the heat transfer coefficient $-(\partial\theta/\partial y)$ and the skin friction coefficient $(\partial^2 f / \partial y^2)$ at the lower stagnation point of the sphere, $x \approx 0$, for various values of N_R when $Pr = 7, K = 2, M = 0, 5$, and $\gamma = 0.1$	82
5.1	The heat transfer coefficient $-\theta'(0)$ and the skin friction coefficient $f''(0)$ at the lower stagnation point of the sphere, $x \approx 0$, for various values of λ when $Pr = 6.8$ and $\gamma \rightarrow \infty$	101
5.2	The wall temperature $\theta(x, 0)$, the heat transfer coefficient $-(\partial\theta/\partial y)$ and the skin friction coefficient $(\partial^2 f / \partial y^2)$ at the lower stagnation point of the sphere, $x \approx 0$, for various values of λ when $Pr = 0.7, 7$ and $\gamma = 0.5$	102
5.3	The local heat transfer coefficient $Q_w(x)$ at the different positions x for various values of λ when $Pr = 0.7$ and $\gamma = 1$	103
5.4	The local skin friction coefficient C_f at the different positions x for various values of λ when $Pr = 0.7$ and $\gamma = 1$	103
5.5	The local heat transfer coefficient $Q_w(x)$ for various values of x when $Pr = 0.7, 1, 7, \lambda = 10$ and $\gamma = 1$	104
5.6	Values of the local skin friction coefficient C_f for various values of x when $Pr = 0.7, 1, 7, \lambda = 10$ and $\gamma = 1$	104
6.1	The heat transfer coefficient $-\theta'(0)$ and the skin friction coefficient $f''(0)$ at the lower stagnation point of the sphere, $x \approx 0$, for various values of λ when $Pr = 7, K = 1$ and $\gamma \rightarrow \infty$	116

6.2	The local heat transfer coefficient $Q_w(x)$ at the different positions x for various values of λ when $Pr = 0.7$, $K = 1$ and $\gamma = 0.5$	116
6.3	The local skin friction coefficient, C_f at the different positions x for various values of λ when $Pr = 0.7$, $K = 1$ and $\gamma = 0.5$	117
6.4	The local heat transfer coefficient $Q_w(x)$ at the different positions x for various values of λ when $Pr = 0.7$, $K = 2$ and $\gamma = 0.5$	117
6.5	The local skin friction coefficient, C_f at the different positions x for various values of λ when $Pr = 0.7$, $K = 2$ and $\gamma = 0.5$	118
7.1	The thermophysical properties of fluid and nanoparticles	129
7.2	The heat transfer coefficient $-\theta'(0)$ and the skin friction coefficient $f''(0)$ at the lower stagnation point of the sphere, $x \approx 0$, for various values of λ when $\chi = 0$ (Newtonian fluid), $Pr = 6.8$ and $\gamma \rightarrow \infty$	129
7.3	The local heat transfer coefficient $Q_w(x)$ at the different positions x for $\chi = 0.1$ using Cu nanoparticles, $Pr = 6.2$, $\gamma = 0.5$ and various values of λ	130
7.4	The local skin friction coefficient, C_f at the different positions x for for $\chi = 0.1$ using Cu nanoparticles, $Pr = 6.2$, $\gamma = 0.5$ and various values of λ	130
7.5	The local heat transfer coefficient $Q_w(x)$ at the different positions x for $\chi = 0.2$ using Cu nanoparticles, $Pr = 6.2$, $\gamma = 0.5$ and various values of λ	131
7.6	The local skin friction coefficient, C_f at the different positions x for $\chi = 0.2$ using Cu nanoparticles, $Pr = 6.2$, $\gamma = 0.5$ and various values of λ	131
7.7	The local heat transfer coefficient $Q_w(x)$ at the different positions x for $\chi = 0.1$ using Al_2O_3 nanoparticles, $Pr = 6.2$, $\gamma = 0.5$ and various values of λ	132
7.8	The local skin friction coefficient, C_f at the different positions x for $\chi = 0.1$ using Al_2O_3 nanoparticles, $Pr = 6.2$, $\gamma = 0.5$ and various values of λ	132
7.9	The local heat transfer coefficient $Q_w(x)$ at the different positions x for $\chi = 0.2$ using Al_2O_3 nanoparticles, $Pr = 6.2$, $\gamma = 0.5$ and various values of λ	133

7.10	The local skin friction coefficient, C_f at the different positions x for for $\chi=0.2$ using Al_2O_3 nanoparticles, $Pr = 6.2$, $\gamma=0.5$ and various values of λ	133
7.11	The local heat transfer coefficient $Q_w(x)$ at the different positions x for $\chi=0.1$ using TiO_2 nanoparticles, $Pr = 6.2$, $\gamma=0.5$ and various values of λ	134
7.12	The local skin friction coefficient, C_f at the different positions x for $\chi=0.1$ using TiO_2 nanoparticles, $Pr = 6.2$, $\gamma=0.5$ and various values of λ	134
7.13	The local heat transfer coefficient $Q_w(x)$ at the different positions x for $\chi=0.2$ using TiO_2 nanoparticles, $Pr = 6.2$, $\gamma=0.5$ and various values of λ	135
7.14	The local skin friction coefficient, C_f at the different positions x for for $\chi=0.2$ using TiO_2 nanoparticles, $Pr = 6.2$, $\gamma=0.5$ and various values of λ	135
8.1	The local skin friction coefficient, $(Pr Pe^{1/2})C_f$ at the different positions x for for $\chi=0.1$ using Cu nanoparticles, $\gamma=0.5$ and various values of λ	149
8.2	The local skin friction coefficient, $(Pr Pe^{1/2})C_f$ at the different positions x for $\chi=0.2$ using Cu nanoparticles, $\gamma=0.5$ and various values of λ	150
8.3	The local skin friction coefficient, $(Pr Pe^{1/2})C_f$ at the different positions x for $\chi=0.1$ using TiO_2 nanoparticles, $\gamma=0.5$ and various values of λ	151
8.4	The local skin friction coefficient, $(Pr Pe^{1/2})C_f$ at the different positions x for for $\chi=0.2$ using TiO_2 nanoparticles, $\gamma=0.5$ and various values of λ	152
8.5	The local skin friction coefficient, $(Pr Pe^{1/2})C_f$ at the different positions x for $\chi=0.1$ using Al_2O_3 nanoparticles, $\gamma=0.5$ and various values of λ	153
8.6	The local skin friction coefficient, $(Pr Pe^{1/2})C_f$ at the different positions x for for $\chi=0.2$ using Al_2O_3 nanoparticles, $\gamma=0.5$ and various values of λ	154

LIST OF FIGURES

Figure No.	Title	Page
1.1	The velocity and thermal boundary layers	3
2.1	Physical model and coordinate system for the mixed convection	20
2.2	Net rectangle for difference approximations	29
2.3	Flow diagram for the Keller-box method	48
3.1	Physical model and coordinate system	50
3.2	Wall temperature $\theta(x,0)$ with conjugate parameter γ when $Pr = 0.7, 7, 100, M = 0$ and $N_R = 0$	60
3.3	Wall temperature $\theta(x,0)$ with Prandtl number Pr when $M = 0, N_R = 0$ and $\gamma = 0.05, 0.1, 0.2$	60
3.4	Temperature profiles $\theta(x, y)$ at $x = 0^\circ, 60^\circ, 90^\circ$ when $Pr = 0.7, 7, 100, M = 0, N_R = 0$ and $\gamma = 0.1$	61
3.5	Velocity profiles $(\partial f / \partial y)(x, y)$ at $x = 0^\circ, 60^\circ, 90^\circ$ when $Pr = 0.7, 7, 100, M = 0, N_R = 0$ and $\gamma = 0.1$	61
3.6	The local heat transfer coefficient with x when $Pr = 0.7, 7, 100, M = 0, N_R = 0$ and $\gamma = 0.1$	62
3.7	The skin friction coefficient with x when $Pr = 0.7, 7, 100, M = 0, N_R = 0$ and $\gamma = 0.1$	62
3.8	Wall temperature $\theta(x,0)$ with N_R when $Pr = 0.7, M = 5$ and $\gamma = 0.05, 0.1, 0.2$	63
3.9	Wall temperature $\theta(x,0)$ with M when $Pr = 0.7, N_R = 3$ and $\gamma = 0.05, 0.1, 0.2$	63
3.10	Temperature profiles $\theta(0, y)$ when $Pr = 7, M = 5, N_R = 0, 1, 3, 5$ and $\gamma = 0.1$	64
3.11	Velocity profiles $(\partial f / \partial y)(0, y)$ when $Pr = 7, M = 5, N_R = 0, 1, 3, 5$ and $\gamma = 0.1$	64
3.12	Temperature profiles $\theta(0, y)$ when $Pr = 7, N_R = 1, M = 5, 10, 15$ and $\gamma = 0.1$	65

3.13	Velocity profiles $(\partial f/\partial y)(0, y)$ when $Pr = 7$, $N_R = 1$, $M = 5, 10, 15$ and $\gamma = 0.1$	65
3.14	Temperature profiles $\theta(x, y)$ at $x = 0^\circ, 60^\circ, 90^\circ$ when $Pr = 0.7$, 7 , $N_R = 1$, $M = 5$ and $\gamma = 0.1$	66
3.15	Velocity profiles $(\partial f/\partial y)(x, y)$, at $x = 0^\circ, 60^\circ, 90^\circ$ when $Pr = 0.7, 7$, $N_R = 1$, $M = 5$ and $\gamma = 0.1$	66
3.16	The local Nusselt number N_u with x when $Pr = 0.7$, $N_R = 1$, $M = 5, 10, 15$ and $\gamma = 0.1$	67
3.17	The skin friction coefficient C_f with x when $Pr = 0.7$, $N_R = 1$, $M = 5, 10, 15$ and $\gamma = 0.1$	67
3.18	The local Nusselt number N_u with x when $Pr = 0.7$, $M = 5$, $N_R = 0, 1, 3, 5$ and $\gamma = 0.1$	68
3.19	The skin friction coefficient C_f with x when $Pr = 0.7$, $M = 5$, $N_R = 0, 1, 3, 5$ and $\gamma = 0.1$	68
4.1	Wall temperature $\theta(x, 0)$ with Prandtl number Pr when $K = 2$, $M = 0$, $N_R = 0$ and $\gamma = 0.05, 0.1, 0.2$	82
4.2	The skin friction coefficient $(\partial^2 f/\partial y^2)(x, 0)$ with Prandtl number Pr when $K = 2$, $M = 0$, $N_R = 0$ and $\gamma = 0.05, 0.1, 0.2$	83
4.3	Wall temperature $\theta(x, 0)$ with conjugate parameter γ when $Pr = 0.7, 1, 7$, $M = 0$, $N_R = 0$ and $K = 2$	83
4.4	Temperature profiles $\theta(0, y)$ for some values of $\gamma = 0.05, 0.1, 0.2$ when $Pr = 0.7$, $M = 0$, $N_R = 0$ and $K = 2$	84
4.5	Velocity profiles $(\partial f/\partial y)(0, y)$ for some values of $\gamma = 0.05, 0.1, 0.2$ when $Pr = 0.7$, $M = 0$, $N_R = 0$ and $K = 2$	84
4.6	Angular velocity profiles $h(0, y)$ for some values of $\gamma = 0.05, 0.1, 0.2$ when $Pr = 0.7$, $M = 0$, $N_R = 0$ and $K = 2$	85
4.7	Temperature profiles, $\theta(0, y)$ when $K = 0, 1, 2, 3$, $Pr = 1$, $M = 0$, $N_R = 0$ and $\gamma = 0.1$	85
4.8	Velocity profiles, $(\partial f/\partial y)(0, y)$ when $K = 0, 1, 2, 3$, $Pr = 1$, $M = 0$, $N_R = 0$ and $\gamma = 0.1$	86
4.9	Angular velocity profiles, $h(0, y)$ when $K = 0, 1, 2, 3$, $Pr = 1$, $M = 0$, $N_R = 0$ and $\gamma = 0.1$	86

4.10	Temperature profiles, $\theta(x, y)$ at $x = 0^\circ, 60^\circ, 90^\circ$ when $Pr = 0.7, 7, K = 2, M = 0, N_R = 0$ and $\gamma = 0.1$	87
4.11	Velocity profiles, $(\partial f / \partial y)(x, y)$ at $x = 0^\circ, 60^\circ, 90^\circ$ when $Pr = 0.7, 7, K = 2, M = 0, N_R = 0$ and $\gamma = 0.1$	87
4.12	Angular velocity profiles, $h(x, y)$ at $x = 0^\circ, 60^\circ, 90^\circ$ when $Pr = 0.7, 7, K = 2, M = 0, N_R = 0$ and $\gamma = 0.1$	88
4.13	Temperature profiles $\theta(0, y)$ when $Pr = 7, M = 5, K = 1, N_R = 0, 1, 3, 5$ and $\gamma = 0.1$	88
4.14	Velocity profiles $(\partial f / \partial y)(0, y)$ when $Pr = 7, K = 1, M = 5, N_R = 0, 1, 3, 5$ and $\gamma = 0.1$	89
4.15	Angular velocity profiles $h(0, y)$ when $Pr = 7, K = 1, M = 5, N_R = 0, 1, 3, 5$ and $\gamma = 0.1$	89
4.16	Temperature profiles $\theta(0, y)$ when $Pr = 7, K = 1, N_R = 1, M = 0, 5, 10$ and $\gamma = 0.1$	90
4.17	Velocity profiles $(\partial f / \partial y)(0, y)$ when $Pr = 7, K = 1, N_R = 1, M = 0, 5, 10$ and $\gamma = 0.1$	90
4.18	Angular velocity profiles $h(0, y)$ when $Pr = 7, K = 1, N_R = 1, M = 0, 5, 10$ and $\gamma = 0.1$	91
4.19	The local Nusselt number N_u with x when $Pr = 0.7, K = 1, N_R = 1, M = 0, 5, 10$ and $\gamma = 0.1$	91
4.20	The local skin friction coefficient C_f with x when $Pr = 0.7, K = 1, N_R = 1, M = 0, 5, 10$ and $\gamma = 0.1$	92
4.21	The local Nusselt number N_u with x when $Pr = 0.7, K = 1, M = 5, N_R = 0, 1, 3, 5$ and $\gamma = 0.1$	92
4.22	The local skin friction coefficient C_f with x when $Pr = 0.7, K = 1, M = 5, N_R = 0, 1, 3, 5$ and $\gamma = 0.1$	93
5.1	The local heat transfer coefficient $Q_w(x)$ with x when $Pr = 0.7, \gamma = 1$ and various values of λ .	105
5.2	The local skin friction coefficient C_f with x when $Pr = 0.7, \gamma = 1$ and various values of λ .	105
5.3	Temperature profiles $\theta(0, y)$, for various values of λ when $Pr = 0.7$ and $\gamma = 0.5$	106

5.4	Velocity profiles $(\partial f / \partial y)(0, y)$, for various values of λ when $\text{Pr} = 0.7$ and $\gamma = 0.5$	106
5.5	Temperature profiles $\theta(0, y)$, for various values of Pr when $\lambda = 10$ and $\gamma = 0.5$	107
5.6	Velocity profiles $(\partial f / \partial y)(0, y)$, for various values of Pr when $\lambda = 10$ and $\gamma = 0.5$	107
5.7	Temperature profiles $\theta(0, y)$, for various values of γ when $\lambda = 10$ and $\text{Pr} = 0.7$	108
5.8	Velocity profiles $(\partial f / \partial y)(0, y)$, for various values of γ when $\lambda = 10$ and $\text{Pr} = 0.7$	108
6.1	The local heat transfer coefficient $Q_w(x)$ with x when $\text{Pr} = 0.7$, $K = 1, 2$, $\lambda = 1$ and various values of γ	118
6.2	The local skin friction coefficient, C_f with x when $\text{Pr} = 0.7$, $K = 1, 2$, $\lambda = 1$ and various values of γ	119
6.3	Temperature profiles $\theta(0, y)$, for various values of λ when $\text{Pr} = 0.7$, $K = 1, 3$ and $\gamma = 0.1$	119
6.4	Velocity profiles $(\partial f / \partial y)(0, y)$, for various values of λ when $\text{Pr} = 0.7$, $K = 1, 3$ and $\gamma = 0.1$	120
6.5	Angular velocity profiles $h(0, y)$ for various values of λ when $\text{Pr} = 0.7$, $K = 1, 3$ and $\gamma = 0.1$	120
6.6	Temperature profiles $\theta(0, y)$, for various values of γ when $\lambda = 5$, $K = 1, 3$ and $\text{Pr} = 0.7$	121
6.7	Velocity profiles $(\partial f / \partial y)(0, y)$, for various values of γ when $\lambda = 5$, $K = 1, 3$ and $\text{Pr} = 0.7$	121
6.8	Angular velocity profiles $h(0, y)$ for various values of γ when $\lambda = 5$, $K = 1, 3$ and $\text{Pr} = 0.7$	122
7.1	The local heat transfer coefficient $Q_w(x)$ with x using various nanoparticles when $\text{Pr} = 6.2$, $\lambda = -1$, $\gamma = 0.5$ and $\chi = 0.1, 0.2$	136
7.2	The local skin friction coefficient C_f with x using various nanoparticles when $\text{Pr} = 6.2$, $\lambda = -1$, $\gamma = 0.5$ and $\chi = 0.1, 0.2$	136
7.3	The local heat transfer coefficient $Q_w(x)$ with x using various nanoparticles when $\text{Pr} = 6.2$, $\lambda = -1$, $\chi = 0.2$ and $\gamma = 0.3, 0.5$	137
7.4	The local skin friction coefficient C_f with x using various nanoparticles when $\text{Pr} = 6.2$, $\lambda = -1$, $\chi = 0.2$ and $\gamma = 0.3, 0.5$	137

7.5	The local heat transfer coefficient $Q_w(x)$ with x using various nanoparticles when $Pr = 6.2$, $\chi = 0.2$, $\gamma = 0.5$ and $\lambda = -1, 4$	138
7.6	The local skin friction coefficient C_f with x using various nanoparticles when $Pr = 6.2$, $\chi = 0.2$, $\gamma = 0.5$ and $\lambda = -1, 4$	138
7.7	Temperature profiles $\theta(0, y)$, using various nanoparticles when $Pr = 6.2$, $\lambda = 1$, $\gamma = 0.5$ and $\chi = 0.1, 0.2$	139
7.8	Velocity profiles $(\partial f / \partial y)(0, y)$, using various nanoparticles when $Pr = 6.2$, $\lambda = 1$, $\gamma = 0.5$ and $\chi = 0.1, 0.2$	139
7.9	Temperature profiles $\theta(0, y)$, using various nanoparticles when $Pr = 6.2$, $\lambda = 1$, $\chi = 0.2$ and $\gamma = 0.1, 0.3, 0.5$	140
7.10	Velocity profiles $(\partial f / \partial y)(0, y)$, using various nanoparticles when $Pr = 6.2$, $\lambda = 1$, $\chi = 0.2$ and $\gamma = 0.1, 0.3, 0.5$	140
7.11	Temperature profiles $\theta(0, y)$, using Cu nanoparticles when $Pr = 6.2$, $\chi = 0.1, 0.2$, $\lambda = 1$ and with various values of γ	141
7.12	Velocity profiles $(\partial f / \partial y)(0, y)$, using Cu nanoparticles when $Pr = 6.2$, $\chi = 0.1, 0.2$, $\lambda = 1$ and with various values of γ	141
8.1	The local skin friction coefficient $(Pr Pe^{1/2})C_f$ with x using various nanoparticles when $\lambda = -1$, $\gamma = 0.5$ and $\chi = 0.1, 0.2$	155
8.2	The local skin friction coefficient $(Pr Pe^{1/2})C_f$ with x using various nanoparticles when $\lambda = -1$, $\chi = 0.2$ and $\gamma = 0.5, 0.7, 1$	155
8.3	Temperature profiles $\theta(0, y)$, using various nanoparticles when $\lambda = -1$, $\gamma = 0.5$ and $\chi = 0.1, 0.2$	156
8.4	Temperature profiles $\theta(0, y)$, using various nanoparticles when $\lambda = -1$, $\chi = 0.2$ and $\gamma = 0.1, 0.3, 0.5$	156
8.5	Temperature profiles $\theta(0, y)$, using Cu nanoparticles when $\chi = 0.1, 0.2$, $\lambda = -1$ and with various values of γ	157

LIST OF SYMBOLS

a	Radius of sphere
C_f	Local skin friction coefficient
c_p	Specific heat.
f	Dimensionless stream function
g	Acceleration due to gravity
H	Microrotation component normal to the $x - y$ plane
Gr	Grashof number
h	Heat transfer coefficient
h_f	Heat transfer coefficient for convective boundary conditions
j	Microinertia density
k	Thermal conductivity
k^*	Mean absorption coefficient
K	Material or micropolar parameter
K_1	Permeability of the porous medium
k_f	Thermal conductivity of the fluid fraction
k_s	Thermal conductivity of the solid
k_{nf}	Effective thermal conductivity of the nanofluid
l	Coupling body
m	Power index
M	Magnetic parameter
n	Constant
N_R	Radiation parameter
N_u	Local Nusselt number
p, \bar{p}	Fluid pressure
Pe	Péclet number
Pr	Prandtl number
q_w	Surface heat flux
q_r	Radiative heat flux

Q_w	Local heat transfer
$\bar{r}(\bar{x})$	Radial distance from symmetrical axis to surface of the sphere
Ra	Rayleigh number
Re	Reynolds number
T	Fluid Temperature
T_f	Temperature of the hot fluid
T_∞	Ambient temperature
u, v	Non-dimensional velocity components along the x and y directions, respectively
$u_e(x)$	Non-dimensional velocity outside boundary layer
U_∞	Free stream velocity
\bar{V}	Velocity vector
x, y	Non Cartesian coordinates along the surface of the sphere and normal to it, respectively

Greek Symbol

α	Thermal diffusivity coefficient
α_{nf}	Thermal diffusivity of the nanofluid
β	Thermal expansion coefficient
β_f	Thermal expansion coefficient of the fluid fraction
β_s	Thermal expansion coefficient of the solid fraction
δ	Boundary layer thickness
δ_h	Velocity boundary layer thickness
δ_T	Thermal boundary layer thickness
γ	Conjugate parameter for convective boundary conditions
γ_c	Critical value of conjugate parameter for convective boundary conditions
λ	Mixed convection parameter
$\lambda_{\max}, \lambda_{\min}$	Maximum and Minimum of mixed convection parameter, respectively
μ	Dynamic viscosity
μ_{nf}	Viscosity of the nanofluid

κ	Vortex viscosity
ν	Kinematic viscosity
ν_f	Kinematic viscosity of the fluid
χ	Nanoparticle volume fraction or solid volume fraction of the nanofluid
ρ	Fluid density
ρ_f	Density of the fluid fraction
ρ_s	Density of the solid fraction
ρ_{nf}	Density of the nanofluid
ρ_∞	Fluid density at ambient temperature
$(\rho C_p)_{nf}$	Heat capacity of the nanofluid
σ	Electric conductivity
σ^*	Stefan-Boltzman constant
τ	Shear stress
τ_w	Surface shear stress
φ	Spin gradient viscosity
θ	Dimensionless temperature
ψ	Stream function
$\bar{\nabla}^2$	Laplacian operator

Subscript

w	Condition at the surface on the sphere
∞	Ambient/free stream condition

Superscript

'	Differentiation with respect to y
–	Dimensional variables

CHAPTER 1

PRELIMINARIES

1.1 INTRODUCTION

The convective mode of heat transfer is generally divided into two basic processes. If the motion of the fluid arises from an external agent then the process is termed forced convection. On the other hand, no such externally induced flow is provided and the flow arises from the effect of a density difference, resulting from a temperature or concentration difference, in a body force field such as the gravitational field, then the process is termed natural or free convection. The density difference gives rise to buoyancy forces which drive the flow and the main difference between free and forced convection lies in the nature of the fluid flow generation. In forced convection, the externally imposed flow is generally known, whereas in free convection it results from an interaction between the density difference and the gravitational field (or some other body force) and is therefore invariably linked with, and is dependent on, the temperature field. Thus, the motion that arises is not known at the onset and has to be determined from a consideration of the heat (or mass) transfer process coupled with a fluid flow mechanism. However, the effect of the buoyancy force in forced convection, or the effect of forced flow in free convection, becomes significant then the process is called mixed convection flows, or combined forced and free convection flows. The effect is especially pronounced in situations where the forced fluid flow velocity is low and/or the temperature difference is large (Ingham and Pop, 2001).

The mixed convection flows are characterized by the buoyancy or mixed convection parameter $\lambda = Gr/Re^n$ where Gr is the Grashof number, Re is the Reynolds number and n is a positive constant, which depends on the fluid flow configuration and the surface heating conditions. The mixed convection regime is generally defined in the range of $\lambda_{\min} \leq \lambda \leq \lambda_{\max}$, where λ_{\min} and λ_{\max} is the lower and the upper bounds of the regime of mixed convection flow respectively. The parameter λ provides a measure of the influence of free convection in comparison with that of

forced convection on the flow. Outside the mixed convection regime, $\lambda_{\min} \leq \lambda \leq \lambda_{\max}$, either the forced convection or the free convection analysis can be used to describe accurately the flow or the temperature field. Forced convection is the dominant mode of transport when $Gr/Re^n \rightarrow 0$, whereas free convection is the dominant mode when $Gr/Re^n \rightarrow \infty$ (Chen and Armaly, 1987). For detail explanations of Grashof, Prandtl and Reynolds number, see Appendix A.

1.2 BOUNDARY LAYER THEORY

The boundary layer theory was first introduced by Ludwig Prandtl, in his lecture on “Fluid motion with very small friction” at the Heidelberg Mathematical Congress in August 1904 (Schlichting, 1979). Using theoretical considerations together with some simple experiments, Prandtl showed that the flow past a body can be divided into two main parts. The larger part concerns on a free stream of fluid, far from any solid surface, which is considered to be inviscid. The smaller part is a thin layer adjacent to the solid surface in which the effects of viscosity are felt. This thin layer where friction effects cannot be ignored is called the boundary layer (Burmeister, 1993; Acheson, 1990).

The boundary layer can be divided into two types, which are velocity boundary layer and thermal boundary layer (Ozisik, 1985). To introduce the concept of boundary layer, fluid flow over a flat plate is considered. Interaction between the fluid and the surface of the flat plate will produce a region in the fluid where the y -component velocity u rises from zero at the surface (no slip condition) to an asymptotic value U_{∞} . This region is known as the velocity boundary layer where δ_h is the velocity boundary layer thickness as shown in Figure 1.1. This layer is characterized by the velocity gradient and the shear stress. On the other hand, the existence of temperature differences between the fluid and the surface area resulted in the formation of a region in the fluid where its temperature changes from the surface value T_s at $y = 0$ to T_{∞} at the outer flow. This region is called the thermal boundary layer where its thickness is represented by δ_t (Incropera et al., 2006). This thermal boundary layer is characterized by the temperature gradient and the heat transfer.

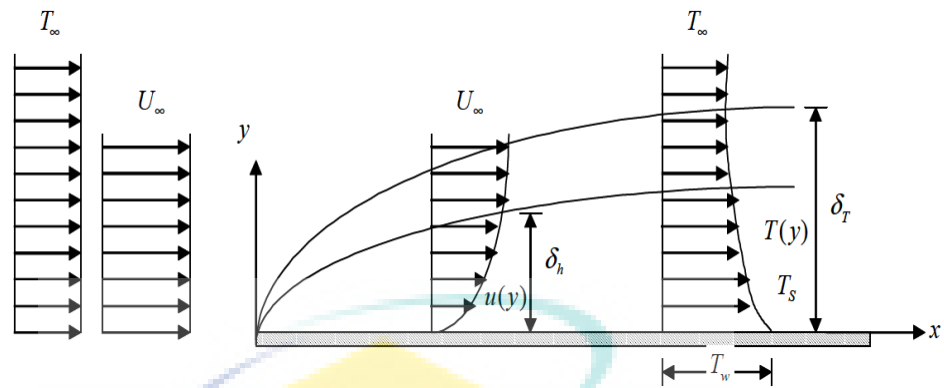


Figure 1.1: The velocity and thermal boundary layers

The boundary layer theory is used very frequently in solving fluid flow and heat transfer problems, see (Bejan, 1984; Cebeci and Bradshaw, 1988). This is because the boundary layer equations are parabolic and therefore, it can be solved much easier compared to the elliptic or sometimes, hyperbolic Navier-Stokes equations. However, the boundary layer equations are valid only up to the separation point (Ahmad, 2009).

1.3 VISCOUS FLUID

Fluids can be characterized as Newtonian or non-Newtonian fluids. Newtonian fluid is a fluid in which shear stress is linearly proportional to the velocity gradient in the direction of perpendicular to the plane of shear, i.e.

$$\tau = \mu \frac{du}{dy}, \quad (1.1)$$

where μ is a property of the fluid, and also known as the coefficient of dynamic viscosity (Acheson, 1990). Viscous fluid such as air and water are Newtonian fluid, while other fluids, which do not behave according to τ such as paints and polymers are called non-Newtonian fluids (Tanner, 1988). A key feature of a viscous fluid is that molecules of the fluid in contact with a solid surface remain bound to the surface. Hence, the appropriate condition at a boundary is the ‘no slip condition’, where the velocity of the fluid in contact with the solid boundary is the same as that of the

boundary (Acheson, 1990). This ‘no slip condition’ is an important boundary condition in viscous fluid mechanics (Ahmad, 2009).

1.4 MICROPOLAR FLUID

The essence of the micropolar fluid flow theory lies in the extension of the constitutive equations for Newtonian fluid, so that more complex fluids such as particle suspensions, animal blood, liquid crystal, turbulent shear flows and lubrication can be described by this theory. The theory of micropolar fluid was first proposed by Eringen (1965). This theory has generated much interest and many classical flows are being re-examined to determine the effects of the fluid microstructure. This theory is a special class in the theory of microfluids, in which the elements are allowed to undergo only rigid rotations without stretch. The theory of micropolar fluid requires that one must add a transport equation representing the principle of conservation of local angular momentum to the usual transport equations for the conservation of mass and momentum, and also additional local constitutive parameters are introduced.

Such applications include the extrusion of polymer liquids, solidification of liquid crystals, animal blood, etc., for which the classical Navier-Stokes theory is inadequate. The key points to note in the development of Eringen’s microcontinuum mechanics are the introduction of new kinematic variables, the gyration tensor and microinertia moment tensor. The addition of concept of body moments, stress moments, and micropolar fluids were discussed in a comprehensive review paper of the subject and application of micropolar fluid mechanics by Ariman et al. (1973). The recent books by Lukaszewicz (1999) and Eringen (2001) presented a useful account of the theory and extensive surveys of literature of micropolar fluid theory.

1.5 NANOFUID

Nanofluids are solid-liquid composite materials consisting of solid nanoparticles or nanofibers with sizes typically of 1-100 nm suspended in liquid. From the recent studies, a small amount (<1% volume fraction) of *Cu* nanoparticles with ethylene glycol or carbon nanotubes dispersed in oil is reported to increase the inherently poor thermal

conductivity of the liquid by 40% and 150%, respectively (Eastman et al., 2001; Choi et al., 2001). High concentrations (>10%) of particles are required to achieve such enhancement in case of conventional particle-liquid suspensions. High concentrations lead to amplified problems of stability. Some results in this rapidly evolving field include a surprisingly strong temperature dependence of the thermal conductivity (Patel et al., 2003) and a three-fold higher critical heat flux compared with the base fluids (Vassallo et al., 2004). Feasibility of nanofluids in nuclear applications by improving the performance of any water-cooled nuclear system, which is heat removal limited has been studied by You et al. (2003) at the Nuclear Science and Engineering Department of water reactor primary coolant, standby safety systems, accelerator targets, plasma diverters, etc. (Boungiorno et al., 2008). Nanofluids, where heat transfer can be reduced or enhanced at will, can be utilized where straight heat transfer enhancement is very important in many industrial applications, nuclear reactors, transportation as well as electronics and biomedicine. Studies indicate that nanofluids have the potential to conserve 1 trillion Btu of energy for U.S. industry by replacing the cooling and heating water with nanofluid. For U.S. electric power industry, using nanofluids in closed-loop cooling cycles could save about 10–30 trillion Btu per year (equivalent to the annual energy consumption of about 50,000–150,000 households). The related emissions reduction would be approximately 5.6 million metric tons of carbon dioxide; 8,600 metric tons of nitrogen oxides; and 21,000 metric tons of sulfur dioxide (Routbort et al., 2009). In geothermal power, energy extraction from the earth's crust involves high temperatures of around 5000°C to 10000°C and nanofluids can be employed to cool the pipes exposed to such high temperatures. When drilling, nanofluids can serve in cooling the machinery and equipment working in high temperature environment. Nanofluids could be used as a working fluid to extract energy from the earth core (Tran and Lyons, 2007). Fluids like Engine oils, automatic transmission fluids, coolants, lubricants etc. used in various automotive applications have inherently poor heat transfer properties. Using nanofluids by simply adding nanoparticles to these fluids could result in better thermal management (Chopkar et al., 2006). Nanofluids can be used for cooling of microchips in computers or elsewhere. They can be used in various biomedical applications like cancer therapeutics, nano-drug delivery, nanocryosurgery, cryopreservation and etc.

1.6 BOUNDARY CONDITIONS

In general, there are four common heating processes specifying the wall-to-ambient temperature distributions shown by Merkin (1994), namely

- (i) Prescribed wall temperature (PWT)
- (ii) Prescribed surface heat flux (PHF)
- (iii) Newtonian heating (NH)
- (iv) Convective boundary conditions (CBC)

For this study, only convective boundary conditions are considered.

The convective boundary conditions (sometimes called the Robin condition) are a weighted combination of Dirichlet boundary conditions and Neumann boundary conditions. This contrasts to mixed boundary conditions, which are boundary conditions of different types specified on different subsets of the boundary. Moreover, the convective boundary conditions are also called conjugate boundary conditions, from their application in electromagnetic problems or Robin boundary conditions, from their application in heat transfer problems (Hahn and Ozisk, 2012).

The convective boundary conditions, in which the heat is supplied through a bounding surface of finite thickness and finite heat capacity was recently used by Aziz (2009) who obtained the similarity solution for laminar thermal boundary layer over a flat plate with a convective surface boundary condition. Subsequently, Ishak (2010) and Ishak et al. (2011) obtained the similar solutions for flow and heat transfer over a permeable surface and the radiation effects on the thermal boundary layer flow over a moving plate with convective boundary conditions respectively. This Blasius flow with conjugate boundary conditions then, have been revisited by Rashidi and Erfani (2009) and Magyari (2010). Makinde and Aziz (2010) considered the hydromagnetic heat and mass transfer over a vertical plate. Ishak (2010) and Ishak et al. (2011) have studied the thermal boundary layer flow on a moving plate (Sakiadis flow) with radiation effects. Merkin and Pop (2011), Yao et al. (2011), Yacob et al. (2011) and Yacob and Ishak (2011) investigated the boundary layer flow past a shrinking /stretching sheet with convective boundary conditions in a viscous fluid, nanofluid and micropolar fluid respectively. The mixed convection boundary-layer flow past a horizontal circular cylinder embedded in a porous medium filled with a nanofluid with convective

boundary condition presented by Rashad et al. (2013). The numerical solutions of the steady magnetohydrodynamic two dimensional stagnation point flow of an incompressible nanofluid towards a stretching cylinder with convective boundary condition using fourth-order Runge-Kutta-Fehlberg method with a shooting technique has been investigated by Akbar et al. (2013). Mohamed et al. (2013), studied the numerical solutions of stagnation point flow over a stretching surface with convective boundary conditions using the Shooting method. Nadeem and Haq (2014) presented the comprehensive analysis of the effect of thermal radiation for magnetohydrodynamic boundary layer flow of a nanofluid past a stretching sheet with convective boundary conditions. Hayat et al. (2014) studied the analyses solving of the mixed convection flow by a porous sheet with convective boundary condition and variable thermal conductivity. Recently, the boundary layer flow of nanofluid over a nonlinear stretching sheet with convective boundary condition was presented by Mustafa et al. (2015).

1.7 OBJECTIVES AND SCOPE

The objectives of the present study are to construct mathematical models, to provide mathematical formulations and analyses and to develop numerical algorithms for the computations of the following six problems:

1. The effect of radiation on magnetohydrodynamic free convection boundary layer flow over a solid sphere with convective boundary conditions in a viscous fluid.
2. The effect of radiation on magnetohydrodynamic free convection boundary layer flow over a solid sphere with convective boundary conditions in a micropolar fluid.
3. Mixed convection boundary layer flow over a solid sphere with convective boundary conditions in a viscous fluid.
4. Mixed convection boundary layer flow over a solid sphere with convective boundary conditions in a micropolar fluid.
5. Mixed convection boundary layer flow over a solid sphere with convective boundary conditions in a nanofluid.
6. Mixed convection boundary layer flow over a solid sphere embedded in a porous medium filled with convective boundary conditions in a nanofluid.

The scope of the study is limited to problems involving steady, two-dimensional laminar free and mixed convection boundary layer flow over a solid sphere. The problems considered in this research involved the solid sphere that flow in three different fluids which are incompressible viscous fluid, micropolar fluid and nanofluid embedded in a porous medium saturated by a using the Buongiorno-Darcy model. The effects of various parameters of the physical conditions such as the magnetic, radiation, micropolar, mixed convection, conjugate parameters as well as Prandtl number and nanoparticle volume fraction have been studied accordingly in this thesis. This research also takes into account the boundary conditions with convective boundary conditions. The governing boundary layer equations for these problems are formulated using the non-similar transformation and solved numerically using an implicit finite difference scheme known as the Keller-box method.

1.8 SIGNIFICANCE OF THE RESEARCH

This thesis includes the analysis on the convective boundary layer problems of a viscous fluid, micropolar fluid and nanofluid over a solid sphere. The effect of magnetohydrodynamic free convection are basically concerned with the investigation on the macroscopic interaction of the electrically conducting fluid with the magnetic field. A fluid is said to have conducting characteristic if electric current can pass through it. In the magnetohydrodynamic discipline, the concentration results to the mechanics of electrically conducting fluids like magma, highly salted water and liquid metals. Moreover, the effects of radiation on free convection flow are important in the context of space technology and very little is known about the effects of radiation on the boundary layer flow of a radiating fluid past a body.

Mixed convection has attracted a great deal of attention from researchers because of its presence both in nature and engineering applications. In nature, convection cells formed from hot air rising due to sunlight which is a major feature in all weather systems. Convection is also seen in the rising plume of hot air from fire, oceanic currents, and sea-wind formation (where upward convection is also modified by Coriolis forces). In engineering applications, mixed convection is commonly visualized

in the formation of microstructures during the cooling of molten metal, fluid flows around shrouded heat-dissipation fins, and solar ponds.

On the other hand, convective flows in porous media have been extensively investigated during the last several decades and they have included several different physical effects. This interest is due to the many practical applications which can be modelled or approximated as transport phenomena in porous media. These flows appear in a wide variety of industrial applications, as well as in many natural circumstances such as geothermal extraction, storage of nuclear waste material, ground water flows, industrial and agricultural water distribution, oil recovery processes, thermal insulation engineering, pollutant dispersion in aquifers, cooling of electronic components, packed-bed reactors, food processing, casting and welding of manufacturing processes, liquid metal flow through endric structures in alloy casting and even for obtaining approximate solutions for flow through turbomachinery, to name just a few applications. This topic is of vital importance in all these applications, thereby generating the need for a full understanding of transport processes through porous media.

Therefore, the study on convective boundary layer flow over a solid sphere in a viscous fluid, micropolar fluid and nanofluid problems is important due to its imperative applications in real life, heat transfer plays a prominent role when dealing with fluid flow. Temperature of a fluid can influence the behavior of the fluid flow, especially when the flow involves buoyancy force. Among the types of heat transfer, convection is the most frequent case occurs in fluids. The result or output of this research enhances the understanding of the fluids flow phenomenon and improves the development of related industries, for example the manufacturing industries. Besides that, the generation of efficient algorithm helps in solving the problem of computational fluid dynamics for the future.

1.9 THESIS OUTLINE

This thesis is divided into nine chapters including this Introductory Chapter. Chapter 1 is preliminaries with general introduction to the boundary layer, types of fluids, boundary conditions, significance of the research, objective and scope of studies and the literature review.

Chapter 2 discusses about the governing equations and numerical method. The numerical method that has been used in this study, which is the Keller-box method, is discussed specifically for the fifth problem on the mixed convection boundary layer flow about a over a solid sphere with convective boundary conditions in a nanofluids. Step wise development of the method is presented. This method has been found to be suitable and flexible to deal with the problems of free and mixed convection. The Keller-box method used in this study is programmed through Matlab®5.3.1.

In Chapter 3, we discuss the first problem in a viscous fluid, which is the effect of radiation on magnetohydrodynamic free convection boundary layer flow over a solid sphere with convective boundary conditions. This chapter divided into four main sections, which are first, the introduction of the problem, second is the mathematical formulation, third is the results and discussion and lastly is the conclusion of these problems.

Discussion on relevant physical quantities of interest such as the local skin friction coefficient, Nusselt number and local wall heat transfer coefficient are presented in the results and discussion subsections. Some discussions on velocity and temperature profiles are also included. All related figures are presented and some results are also given in the form of tables in all chapters. Such tables are very important and they can serve as a reference against other exact or approximate solutions that can be compared in the future.

On the other hand, Chapter 4 discusses the second problem in a micropolar fluid, which is the effect of radiation on magnetohydrodynamic free convection boundary layer flow over a solid sphere with convective boundary conditions. The divisions of sections in this chapter are similar to those in Chapter 3.

The third, fourth and fifth problems are discussed in Chapter 5, 6 and 7 respectively. The mixed convection boundary layer flow over a solid sphere with convective boundary conditions in a viscous, micropolar fluid and nanofluids are analysed and discussed. The divisions of sections in these chapters are similar to those in Chapter 3. Some figures and tables related to temperature, velocity and angular velocity profiles, together with the local heat transfer coefficient and the local skin friction coefficient are also included.

Chapter 8 contains the last problem given in section 1.7 and also the divisions of sections in this chapter are similar to those in Chapter 3.

Lastly, Chapter 9 contains a summary, contributions of the research and some recommendations for future study based on present solutions. Additionally, all of the references are attached at the end of this chapter.

1.10 LITERATURE REVIEW

The discussion on the literature review will be presented in the next four subsections with regards to the six problems on viscous, micropolar fluids and nanofluid as mentioned in section 1.7. In addition, the Keller-box method, which presented in the last subsection.

1.10.1 The effect of Radiation on Magnetohydrodynamic Free Convection Boundary Layer Flow on a Sphere

The effect of radiation on boundary layer flow and heat transfer problems can be quite significant at high operating temperature such as gas turbines, nuclear power plant, and thermal energy store (Bataller, 2008a, 2008b). Since the process in engineering areas occurs at high temperature, the study on effect of radiation becomes very important for the design of the equipment. Molla et al. (2011) studied the natural convection laminar flow from an isothermal sphere immersed in a viscous incompressible optical dense fluid in the presence of radiation effects. Aktar et al. (2013) have investigated the effects of viscous dissipation on natural convection flow along a sphere with radiation and heat generation. The laminar boundary layer flow over

a moving plate in a moving fluid with convective surface boundary condition and in the presence of thermal radiation has been considered by Ishak et al. (2011). Salleh et al. (2012b) presented the mathematical modelling of free convection boundary layer flow over a permeable horizontal flat plate embedded in a porous medium under mixed thermal boundary conditions and radiation effects.

The application of the magnetohydrodynamic plays an important role in agriculture, engineering and petroleum industries. Bataller (2011) presented a numerical study of the flow and heat transfer of an incompressible upper-convected Maxwell (UCM) fluid in the presence of a uniform transverse magnetic field over a porous stretching sheet (Ganesan and Palani, 2004). Alam et al. (2007) and Molla et al. (2005) studied the viscous dissipation and magnetohydrodynamic effect on a natural convection flow over a sphere in the presence of heat generation, respectively. Molla et al. (2012) investigated the effect of temperature dependent viscosity on magnetohydrodynamic natural convection flow from an isothermal sphere.

The analysis performed to study the flow and heat transfer characteristics of laminar free, mixed and forced convection about a sphere has been presented by Chen and Mucoglu (1977). Salleh et al. (2010c; 2012a) considered the free convection boundary layer flow on a sphere with Newtonian heating (NH) in viscous fluid and micropolar fluid, respectively. El-kabeir and Gorla (2007) have investigated the magnetohydrodynamic effects on free convection in a micropolar fluid in a porous medium. The effects of radiation and chemical reaction on heat and mass transfer by free convection in a micropolar fluid saturated porous medium with streamwise temperature and species concentration variations were discussed by Rashad et al. (2014).

On the other hand, Nazar et al. (2002a, 2002b) studied the free convection boundary layer flows on a sphere in micropolar fluid with constant heat flux (CHF) and constant wall temperature (CWT), respectively. The natural convection heat and mass transfer from a sphere in micropolar fluid with constant wall temperature and concentration were presented by Cheng (2008).

Motivated by the above studies, we study the free convection boundary layer flow on a solid sphere with convective boundary conditions in a viscous and micropolar fluid in addition to the effect of radiation on magnetohydrodynamic free convection boundary layer flow on a sphere with same conditions and fluids. Therefore, four parameters are introduced in this study, which are, conjugate parameter, the micropolar parameter, magnetic parameter and the radiation parameter.

1.10.2 The Mixed Convection Boundary Layer Flow on a Sphere

The mixed convective heat transfer has received much attention due to a large number of applications, which are frequently encountered in many industrial and technical processes including solar central receivers exposed to winds, electronic devices cooled by fans, nuclear reactors cooled during emergency shutdown, and heat exchangers placed in a low-velocity environment from fixed or rotating bodies. This represents a problem that can be related to numerous engineering applications and industries (Kafoussias and Williams, 1995).

The problem of mixed, forced, and free convection on a sphere in a viscous incompressible fluid has received relatively little attention. To the best knowledge of the author, the only such studies, which have been reported are the experimental work by Yuge (1960) and Klyachko (1963) and the analytical work by Hieber and Gebhart, (1969). The mixed convection over a sphere with uniform surface temperature and uniform surface heat flux have been later studied by Chen and Mucoglu (1977, 1978), respectively. The solution depends on the non-dimensional mixed convection parameter $\lambda = Gr/Re^2$ for very large Reynolds number Re and Grashof number Gr using the boundary layer approximation. Nazar et al. (2002c) and Salleh et al. (2010a) studied the mixed convection boundary layer flow about a solid sphere in a viscous fluid with constant surface temperature and Newtonian heating, respectively. Yacob and Nazar (2006) considered the mixed convection boundary layer on a solid sphere with constant surface heat flux, and followed by Kotouc et al. (2008) who studied the loss of axisymmetry in the mixed convection (assisting flow) past a heated sphere. A detailed list of references on convective heat transfer problems can also be found in the recent book by Ingham and Pop (2001).

It appears that Lien and Chen (1987) were the first to study the steady mixed convection boundary layer flow problem on a sphere in a micropolar fluid and Wang and Kleinstreuer (1988) generalized the paper by Lien and Chen (1987) to two dimensional axisymmetric bodies with porous walls and heat flux or constant temperature. Lien and Chen (1987) used the Mangler transformation and potential outer flow velocity, while Wang and Kleinstreuer (1988) introduced a new coordinate transformation to reduce the streamwise dependence in the coupled boundary layer equations.

Motivated by the work of Nazar et al. (2002c,d ; 2003a) and Salleh et al. (2010a,b) for mixed convection boundary layer flow about a solid sphere in a viscous fluid and micropolar fluid with constant surface temperature, constant heat flux and Newtonian heating, respectively, the present study is going to tackle the problem of mixed convection boundary layer flows over a sphere in a viscous fluid and micropolar fluid with convective boundary conditions.

1.10.3 The Mixed Convection Boundary Layer Flow on a Sphere Embedded in a Porous Medium Filled in a Nanofluid

Nanofluids are engineered by suspending nanoparticles with average sizes below 100 nm in traditional heat transfer fluids such as water, oil, and ethylene glycol. A very small amount of guest nanoparticles that when dispersed uniformly and suspended stably in host fluids can provide dramatic improvements in the thermal properties of host fluids (Das et al., 2007).

The important theoretical and experimental research works on convective heat transfer appeared in the open literatures on the enhancement of heat transfer using suspensions of materials in nanometer-sized particles of solid, metallic or non-metallic heat transfer fluids in the base. Nanofluids are considered to offer important advantages over conventional heat transfer fluids. Over a decade ago, researchers focused on measuring and modelling the effective thermal conductivity and viscosity of nanofluids (Kakaç and Pramuanjaroenkij, 2009). The nanofluids contain the nanoparticles such as metals, carbon, oxides or carbides nanotubes, whereby these nanoparticles have unique physical and chemical characteristics (Abu-Nada and Oztop 2009). There are already

many studies that have been conducted to enhance the heat-transfer characteristics mechanism by nanofluids, including those by Khanafer et al. (2003), Putra et al. (2003), Maiga et al. (2005), Patel et al. (2006), Buongiorno (2006), Daungthongsuk and Wongwises (2007), Trisaksri and Wongwises (2007), Tiwari and Das (2007), Abu-Nada (2008), Oztop and Abu-Nada (2008), Wang and Mujumdar (2008), Muthtamilselvan et al. (2010), Talebi et al. (2010), Ghasemi and Aminossadati (2010), Yu and Xie (2012) and Jaluria et al. (2012). Recently, Tham et al. (2011) studied the mixed convection boundary layer flow about a solid sphere with constant surface temperature in a nanofluid.

On the other hand, the convection flow over a surface embedded in saturated porous media is encountered in many engineering problems such as the design of pebble-bed nuclear reactors, ceramic processing, crude oil drilling, geothermal energy conversion, use of fibrous material in the thermal insulation of buildings, catalytic reactors and compact heat exchangers, heat transfer from storage of agricultural products which generate heat as a result of metabolism, petroleum reservoirs, storage of nuclear wastes.

It is well known that conventional heat transfer fluids including oil, water and ethylene glycol mixtures have poor heat transfer performances, because the thermal conductivity of these fluids plays an important role in the heat transfer coefficients between the heat transfer medium and the heat-transfer surface. An innovative technique for improving heat transfer by using ultra fine solid particles in the fluids has been widely used during the last years. The term “nanofluid” refers to these kinds of fluids by suspending nanoscale particles in the base fluids and has been presented by Choi (1995).

Numerical and experimental studies on nanofluids have been performed, including the study on thermal conductivity (Kang et al., 2006), separated flow (Abu-Nada, 2008) and convective heat transfer (Jou and Tzeng, 2006). Duangthongsuk and Wongwises (2008) studied the influence of the thermo physical properties of nanofluids on the convective heat transfer and summarized various models used in the literature for predicting the thermophysical properties of nanofluids. Eastman et al. (2001) used pure copper nanoparticles of less than 10 nm in size and achieved a 40% increase in thermal

conductivity for only 0.3% volume fraction of the solid dispersed in ethylene glycol. Further references on nanofluids can be found in Das et al., (2007) and in the review paper by Buongiorno, (2006). The mixed convection boundary layer flow past a horizontal circular cylinder embedded in a bidisperse porous medium presented by Kumar et al. (2010). Nazar et al. (2011) and Rashad et al. (2013) have considered the mixed convection boundary layer flow from a horizontal circular cylinder embedded in a porous medium filled in a nanofluid under constant wall temperature and convective boundary condition, respectively. Furthermore, Rashad et al. (2011) considered the effect of chemical reaction on heat and mass transfer by mixed convection flow about a sphere in a saturated porous media. Recently, Tham and Nazar (2012) presented a steady laminar mixed convection boundary layer flow about an isothermal solid sphere embedded in a porous medium filled in a nanofluid for both cases of assisting and opposing flows with constant wall temperature.

Motivated by the studies conducted by Tham et al. (2011) and Tham and Nazar (2012) with constant surface temperature, the present study considers the mixed convection boundary layer flow over a solid sphere embedded in a porous medium filled with convective boundary conditions in nanofluid.

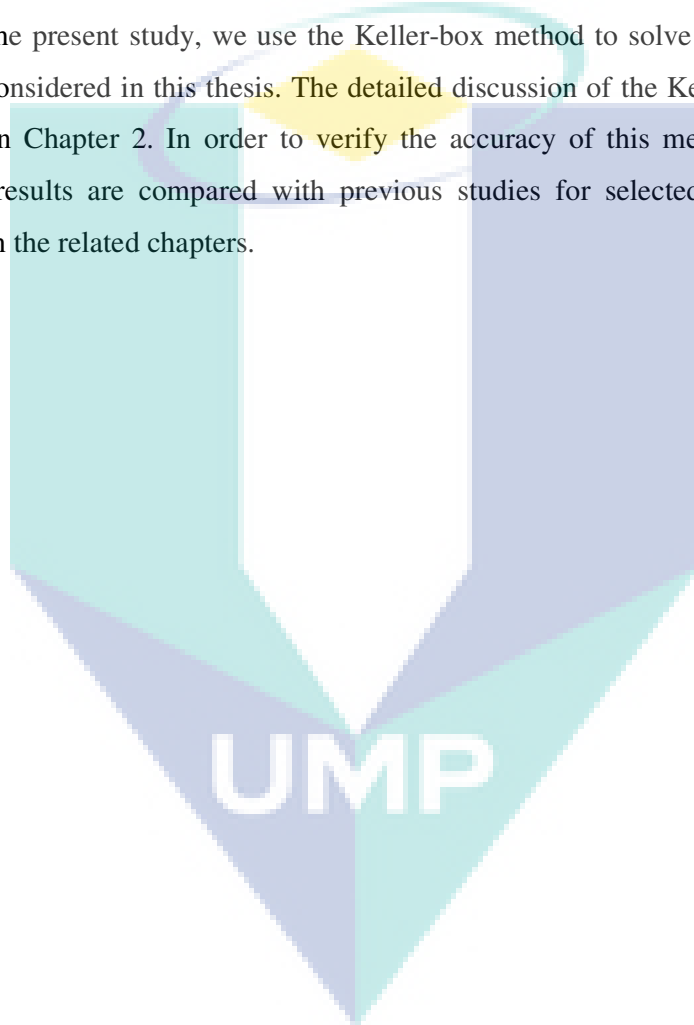
1.10.4 The Keller-box Method

The Keller-box method is an implicit finite difference scheme and it was introduced by Keller (1970.) This numerical method has shown to be particularly accurate for solving parabolic partial differential equations and also ordinary differential equations. It is also very suitable in dealing with non-linear problems. This method was later popularized by Cebeci and Bradshaw (1988).

This method seems to be the most flexible of the common methods. It is also being easily adapted to solve equations of any order. It had been tested on laminar boundary layer flows (Keller and Cebeci, 1971) and turbulent boundary layer flows (Keller and Cebeci, 1972, Cebeci and Smith, 1974). It had also been shown by Keller and Cebeci (1971) and Mucoglu and Chen (1978) to be more efficient and flexible to use, easier to program and has second-order accuracy.

Other researchers who used Keller-box in solving the boundary layer problems include Pop and Na (1999), Yih (1999), Nazar et al. (2002a, 2002b, 2002c, 2002d, 2002e, 2003a, 2003b, 2003c, 2004a, 2004b), Lok et al. (2003, 2005, 2006, 2007), Ishak et al. (2006a, 2006b, 2006c, 2007a, 2007b, 2008, 2010a, 2010b), Tham et al. (2011), Tham and Nazar (2012), Salleh et al. (2010a, 2010b, 2010c, 2010d, 2010e, 2010f, 2011, 2012a, 2012b), Mohamed et al (2012) and Kasim et al. (2012).

In the present study, we use the Keller-box method to solve all boundary layer problems considered in this thesis. The detailed discussion of the Keller-box method is presented in Chapter 2. In order to verify the accuracy of this method, the obtained numerical results are compared with previous studies for selected cases, which are discussed in the related chapters.



CHAPTER 2

GOVERNING EQUATIONS AND NUMERICAL METHOD

2.1 GOVERNING EQUATIONS

In this section, we derive the governing equations for the mixed convection boundary layer flow over a solid sphere with convective boundary conditions in a nanofluid, which is one of the considered problems as listed in section 1.7. The approximations and transformations employed in the analysis of this flow problem are outlined in the next subsections 2.2.1 to 2.2.3, namely the boundary layer and Boussinesq approximations, the non-dimensional transformation and the non-similarity transformation, respectively.

2.1.1 The Dimensional Equations Boussinesq Approximation

The complete dimensional form of continuity, momentum and thermal energy equations for a nanofluid of steady flow, is simplified only to the extent that we assume all the fluid properties, except the density, are constant and neglect the viscous dissipation effects. They are given in vectorial form as (see Ingham and Pop (2001)),

$$\text{Continuity equations} \quad \bar{\nabla} \cdot \bar{\nabla} = 0, \quad (2.1)$$

$$\text{Momentum equations} \quad (\bar{\nabla} \cdot \bar{\nabla}) \bar{\nabla} = -\frac{1}{\rho_{nf}} \bar{\nabla} \bar{p} + \frac{\mu_{nf}}{\rho_{nf}} \bar{\nabla}^2 \bar{\nabla} + \frac{(\rho_{nf} - \rho_{\infty})}{\rho_{\infty}} g, \quad (2.2)$$

$$\text{Thermal energy equations} \quad (\bar{\nabla} \cdot \bar{\nabla}) T = \alpha_{nf} \bar{\nabla}^2 T, \quad (2.3)$$

where $\bar{\nabla}$ is the velocity vector, g is the gravity acceleration, α_{nf} is the thermal diffusivity of the nanofluid, ρ_{nf} is the density of the nanofluid, μ_{nf} is the viscosity of the nanofluid, $\bar{\nabla}^2$ is the Laplacian operator, \bar{p} is the fluid pressure, T is the local temperature.

For many actual fluids and flow conditions, a simple and convenient way to express the density differences $(\rho_{nf} - \rho_\infty)$ in the buoyancy term of the momentum equations (2.2) is given by the Boussinesq approximation which there are flows in which the temperature varies little and therefore the density varies little, yet in which the buoyancy drives the motion. Thus the variation in density is neglected everywhere except in the buoyancy term. For small temperature difference between the top and bottom layer we can write. (Ingham and Pop, 2001),

$$\rho_{nf} = \rho_\infty [1 - \beta_{nf} (T - T_\infty)], \quad (2.4a)$$

where $\beta_{nf} = (\chi \rho_s \beta_s + (1 - \chi) \rho_f \beta_f)$ is the thermal expansion coefficient of the nanofluid β_f is the thermal expansion coefficient of the fluid fraction, β_s is the thermal expansion coefficient of the solid fraction, χ is the nanoparticle volume fraction or solid volume fraction of the nanofluid, ρ_∞ is the constant local density, ρ_f is the density of the fluid fraction, ρ_s is the density of the solid fraction and T_∞ is the temperature of the ambient medium. If the density ρ_{nf} varies linearly with T over the range of values of the physical quantities encountered in the transport process, β_{nf} in equation (2.4a) becomes

$$\beta_{nf} = -\frac{1}{\rho_\infty} \left(\frac{\partial \rho_{nf}}{\partial T} \right)_{\bar{p}}. \quad (2.4b)$$

Equation (2.4a) is a good approximation for the variation of the density, and it is known as the Boussinesq approximation (Ingham and Pop, 2001; Bejan, 1984), which stated that all variations in fluid properties can be completely ignored except for density in momentum equation and the density is considered to vary with temperature only, and its variations can be ignored everywhere except where they give rise to buoyancy force. The details of the Boussinesq approximation are discussed by Tritton (1988).

Now, consider the problem of two dimensional mixed convection boundary layer flow over solid sphere, placed in nanofluid of stream velocity, U_∞ and ambient temperature, T_∞ as shown in Figure 2.1.

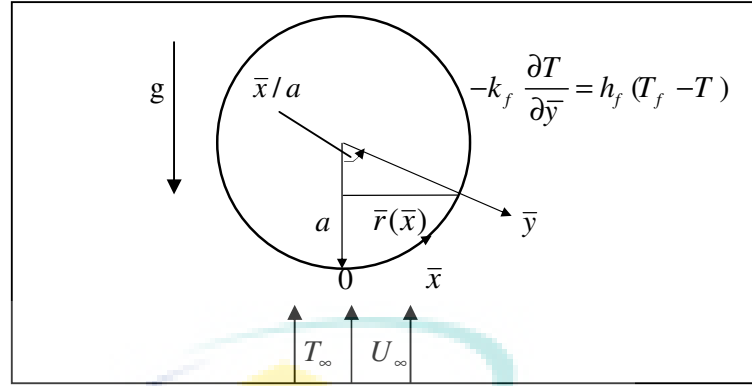


Figure 2.1: Physical model and coordinate system for the mixed convection

The governing dimensional equations (2.1)-(2.3) can be written in Cartesian coordinate system as follows (see appendix B)

Continuity equations
$$\frac{\partial}{\partial \bar{x}} (\bar{r} \bar{u}) + \frac{\partial}{\partial \bar{y}} (\bar{r} \bar{v}) = 0, \quad (2.5)$$

\bar{x} -momentum equation:

$$\begin{aligned} \bar{u} \frac{\partial \bar{u}}{\partial \bar{x}} + \bar{v} \frac{\partial \bar{u}}{\partial \bar{y}} = & -\frac{1}{\rho_{nf}} \frac{\partial \bar{p}}{\partial \bar{x}} + \frac{\mu_{nf}}{\rho_{nf}} \left(\frac{\partial^2 \bar{u}}{\partial \bar{x}^2} + \frac{\partial^2 \bar{u}}{\partial \bar{y}^2} \right) \\ & + \frac{\chi \rho_s \beta_s + (1-\chi) \rho_f \beta_f}{\rho_{nf}} g (T - T_\infty) \sin\left(\frac{\bar{x}}{a}\right), \end{aligned} \quad (2.6)$$

\bar{y} -momentum equation:

$$\begin{aligned} \bar{u} \frac{\partial \bar{v}}{\partial \bar{x}} + \bar{v} \frac{\partial \bar{v}}{\partial \bar{y}} = & -\frac{1}{\rho_{nf}} \frac{\partial \bar{p}}{\partial \bar{y}} + \frac{\mu_{nf}}{\rho_{nf}} \left(\frac{\partial^2 \bar{v}}{\partial \bar{x}^2} + \frac{\partial^2 \bar{v}}{\partial \bar{y}^2} \right) \\ & - \frac{\chi \rho_s \beta_s + (1-\chi) \rho_f \beta_f}{\rho_{nf}} g (T - T_\infty) \cos\left(\frac{\bar{x}}{a}\right), \end{aligned} \quad (2.7)$$

Energy equations
$$\bar{u} \frac{\partial T}{\partial \bar{x}} + \bar{v} \frac{\partial T}{\partial \bar{y}} = \alpha_{nf} \left(\frac{\partial^2 T}{\partial \bar{x}^2} + \frac{\partial^2 T}{\partial \bar{y}^2} \right), \quad (2.8)$$

where \bar{u} and \bar{v} are the velocity components along the \bar{x} and \bar{y} directions, respectively. Equation (2.5) is called the continuity equation. The order of magnitude for $\partial(\bar{r}\bar{u})/\partial\bar{x}$ and $\partial(\bar{r}\bar{v})/\partial\bar{y}$ in the continuity equation are defined as U_∞/L and

\bar{v}/δ , respectively, where L is a characteristic length of the wall and δ is boundary layer thickness. Note that $\partial(\bar{r}\bar{v})/\partial\bar{y}$ must be of the same order as $\partial(\bar{r}\bar{u})/\partial\bar{x}$ because $\partial(\bar{r}\bar{u})/\partial\bar{x} \neq 0$ in the boundary layer, therefore

$$\bar{v} = O\left(\frac{U_\infty \delta}{L}\right). \quad (2.9)$$

The \bar{x} component of momentum equation is given by (see equation (2.6))

$$\bar{u} \frac{\partial \bar{u}}{\partial \bar{x}} + \bar{v} \frac{\partial \bar{u}}{\partial \bar{y}} = -\frac{1}{\rho_{nf}} \frac{\partial \bar{p}}{\partial \bar{x}} + \frac{\mu_{nf}}{\rho_{nf}} \left(\frac{\partial^2 \bar{u}}{\partial \bar{x}^2} + \frac{\partial^2 \bar{u}}{\partial \bar{y}^2} \right),$$

and the order of magnitude of each term in the previous equation are

$$U_\infty \frac{U_\infty}{L}, \quad \frac{U_\infty \delta U_\infty}{L \delta}, \quad \frac{1}{\rho_{nf}} \frac{U_\infty^2}{L}, \quad \frac{\mu_{nf}}{\rho_{nf}} \frac{U_\infty}{L^2} \quad \text{and} \quad \frac{\mu_{nf}}{\rho_{nf}} \frac{U_\infty}{\delta^2},$$

respectively, where $\bar{p} = O(\rho_{nf} U_\infty^2)$ from Bernoulli's equation (which holds in the inviscid outer flow) since the pressure in the boundary layer is equivalent to the situation where it meets the inviscid outer flow. Multiplying all of the above terms with L/U_∞^2 ,

we get

$$O(1), \quad O(1), \quad O(1), \quad O\left(\frac{\mu_{nf}}{\rho_{nf}} \frac{U_\infty}{L}\right) \quad \text{and} \quad O\left(\frac{\mu_{nf}}{\rho_{nf}} \frac{U_\infty}{L} \left(\frac{L}{\delta}\right)^2\right).$$

Hence,

$$\frac{\partial^2 \bar{u}}{\partial \bar{y}^2} / \frac{\partial^2 \bar{u}}{\partial \bar{x}^2} = O\left(\frac{L}{\delta}\right)^2 \gg 1.$$

Therefore, we can neglect the term $\frac{\mu_{nf}}{\rho_{nf}} \frac{\partial^2 \bar{u}}{\partial \bar{x}^2}$ in the \bar{x} component of momentum

equation but we cannot neglect the term $\frac{\mu_{nf}}{\rho_{nf}} \frac{\partial^2 \bar{u}}{\partial \bar{y}^2}$ or we would get the inviscid solution.

All of the remaining terms are $O(1)$, thus

$$O\left(\frac{\mu_{nf}}{\rho_{nf}} \frac{U_{\infty}}{L} \left(\frac{L}{\delta}\right)^2\right) = O(1),$$

which gives

$$\delta \approx \left(\frac{\mu_{nf}}{\rho_{nf}} \frac{L}{U_{\infty}}\right)^{1/2}. \quad (2.10)$$

The \bar{y} component of momentum equation is given by (see equation (2.7))

$$\bar{u} \frac{\partial \bar{v}}{\partial \bar{x}} + \bar{v} \frac{\partial \bar{v}}{\partial \bar{y}} = -\frac{1}{\rho_{nf}} \frac{\partial \bar{p}}{\partial \bar{y}} + \frac{\mu_{nf}}{\rho_{nf}} \left(\frac{\partial^2 \bar{v}}{\partial \bar{x}^2} + \frac{\partial^2 \bar{v}}{\partial \bar{y}^2} \right),$$

and the order of magnitude of each term in the previous equation are

$$U_{\infty} \frac{U_{\infty} \delta}{L^2}, \quad \left(\frac{U_{\infty} \delta}{L}\right) \frac{1}{\delta}, \quad \frac{1}{\rho_{nf}} \frac{\rho_{nf} U_{\infty}^2}{\delta}, \quad \frac{\mu_{nf}}{\rho_{nf}} \frac{U_{\infty} \delta}{L} \frac{1}{L^2} \quad \text{and} \quad \frac{\mu_{nf}}{\rho_{nf}} \frac{U_{\infty} \delta}{L} \frac{1}{\delta^2}.$$

Multiplying all of the above terms with δ/U_{∞}^2 , we obtain

$$O(\delta^2/L^2), \quad O(\delta^2/L^2), \quad O(1), \quad O\left(\frac{\mu_{nf}}{\rho_{nf}} \frac{\delta^2}{U_{\infty} L^3}\right) \quad \text{and} \quad O\left(\frac{\mu_{nf}}{\rho_{nf}} \frac{1}{U_{\infty} L}\right).$$

Since $\delta \ll L$ therefore, all of the terms, except the pressure term, can be neglected because their values are very small compared to the pressure term (written as $O(1)$, in the previous equations).

On using the boundary layer approximation, equations (2.6) and (2.7) become

$$\bar{u} \frac{\partial \bar{u}}{\partial \bar{x}} + \bar{v} \frac{\partial \bar{u}}{\partial \bar{y}} = -\frac{1}{\rho_{nf}} \frac{\partial \bar{p}}{\partial \bar{x}} + \frac{\mu_{nf}}{\rho_{nf}} \frac{\partial^2 \bar{u}}{\partial \bar{y}^2} + \frac{\chi \rho_s \beta_s + (1-\chi) \rho_f \beta_f}{\rho_{nf}} g (T - T_{\infty}) \sin\left(\frac{\bar{x}}{a}\right), \quad (2.11)$$

$$0 = -\frac{1}{\rho_{nf}} \frac{\partial \bar{p}}{\partial \bar{y}}, \quad (2.12)$$

using the previous analysis, the energy equation (2.8) can be simplified as

$$\bar{u} \frac{\partial T}{\partial \bar{x}} + \bar{v} \frac{\partial T}{\partial \bar{y}} = \alpha_{nf} \frac{\partial^2 T}{\partial \bar{y}^2}. \quad (2.13)$$

Now, the dimensional equations for the mixed convection boundary layer flow over a solid sphere with convective boundary conditions in a nanofluid with convective boundary conditions are given in equations (2.5), (2.11) and (2.13),

subject to the boundary conditions

$$\begin{aligned} \bar{u} = \bar{v} = 0, \quad -k_f \frac{\partial T}{\partial \bar{y}} = h_f (T_f - T) \text{ at } \bar{y} = 0, \\ \bar{u} \rightarrow \bar{u}_e(\bar{x}), \quad p \rightarrow p_\infty, \quad T \rightarrow T_\infty \text{ as } \bar{y} \rightarrow \infty. \end{aligned} \quad (2.14)$$

Let $\bar{r}(\bar{x}) = a \sin(\bar{x}/a)$ be the radial distance from the symmetrical axis to the surface of the sphere and $\bar{u}_e(\bar{x}) = (3/2) U_\infty \sin(\bar{x}/a)$ is the local free stream velocity, T is the local temperature, g is the gravity acceleration, h_f is the heat transfer coefficient and k_f is the thermal conductivity of the fluid fraction, which are given by Oztop and Abu-Nada (2008)

$$\begin{aligned} \alpha_{nf} = \frac{k_{nf}}{(\rho C_p)_{nf}}, \quad \rho_{nf} = (1 - \chi)\rho_f + \chi\rho_s, \quad \mu_{nf} = \frac{\mu_f}{(1 - \chi)^{2.5}}, \\ (\rho C_p)_{nf} = (1 - \chi)(\rho C_p)_f + \chi(\rho C_p)_s, \\ \frac{k_{nf}}{k_f} = \frac{(k_s + 2k_f) - 2\chi(k_f - k_s)}{(k_s + 2k_f) + \chi(k_f - k_s)}, \end{aligned} \quad (2.15)$$

where k_{nf} is the effective thermal conductivity of the nanofluid, k_s is the thermal conductivity of the solid and $(\rho C_p)_{nf}$ is the heat capacity of the nanofluid.

We introduce now the following non-dimensional variables (Tham et al., 2011)

$$\begin{aligned} x = \frac{\bar{x}}{a}, \quad y = \text{Re}^{1/2} \left(\frac{\bar{y}}{a} \right), \quad r(x) = \frac{\bar{r}(\bar{x})}{a}, \\ u = \frac{\bar{u}}{U_\infty}, \quad v = \text{Re}^{1/2} \left(\frac{\bar{v}}{U_\infty} \right), \quad u_e(x) = \frac{\bar{u}_e(\bar{x})}{U_\infty}, \\ \theta = \frac{T - T_\infty}{T_f - T_\infty}, \quad p = \frac{\bar{p}}{\rho_{nf} U_\infty^2}, \end{aligned} \quad (2.16)$$

where $Re = U_\infty a / \nu_f$ is the Reynolds number and ν_f is the kinematic viscosity of the fluid. Substituting variables (2.16) into equation (2.5) then become

$$\begin{aligned} \frac{\partial(aU_\infty ru)}{\partial(ax)} + \frac{\partial(aRe^{-1/2}rv)}{\partial(aRe^{-1/2}y)} &= 0, \\ U_\infty \left(\frac{\partial}{\partial x}(ru) + \frac{\partial}{\partial y}(rv) \right) &= 0, \\ \frac{\partial}{\partial x}(ru) + \frac{\partial}{\partial y}(rv) &= 0. \end{aligned} \quad (2.17)$$

Substituting variables (2.16) into equation (2.11) then we have

$$\begin{aligned} \left(U_\infty u \frac{\partial(U_\infty u)}{\partial(ax)} + U_\infty Re^{-1/2}v \frac{\partial(U_\infty u)}{\partial(aRe^{-1/2}y)} \right) &= -\frac{1}{\rho_{nf}} \frac{\partial(p\rho_{nf}U_\infty^2)}{\partial(ax)} \\ &+ \frac{\mu_{nf}}{\rho_{nf}\nu_f} \frac{\partial^2(U_\infty u)}{\partial(aRe^{-1/2}y)^2} + g\beta(T - T_\infty)\sin\left(\frac{ax}{a}\right), \\ \frac{U_\infty^2}{a} \left(u \frac{\partial u}{\partial x} + v \frac{\partial u}{\partial y} \right) &= \frac{U_\infty^2}{a} \left(-\frac{\partial p}{\partial x} + \frac{\mu_{nf}}{\rho_{nf}\nu_f} \frac{\partial^2 u}{\partial y^2} + \frac{\chi\rho_s(\beta_s/\beta_f) + (1-\chi)\rho_f}{\rho_{nf}} \lambda\theta \sin x \right), \\ u \frac{\partial u}{\partial x} + v \frac{\partial u}{\partial y} &= -\frac{\partial p}{\partial x} + \frac{\mu_{nf}}{\rho_{nf}\nu_f} \frac{\partial^2 u}{\partial y^2} + \frac{\chi\rho_s(\beta_s/\beta_f) + (1-\chi)\rho_f}{\rho_{nf}} \lambda\theta \sin x. \end{aligned} \quad (2.18)$$

Finally, substituting variables (2.16) into equation (2.13) then we have

$$\begin{aligned} U_\infty u \frac{\partial(T_f - T_\infty)\theta}{\partial(ax)} + U_\infty Re^{-1/2}v \frac{\partial(T_f - T_\infty)\theta}{\partial(aRe^{-1/2}y)} &= \alpha_{nf} \frac{\partial^2(T_f - T_\infty)\theta}{\partial(aRe^{-1/2}y)^2}, \\ \frac{U_\infty}{a}(T_f - T_\infty) \left(u \frac{\partial\theta}{\partial x} + v \frac{\partial\theta}{\partial y} \right) &= \frac{U_\infty}{a}(T_f - T_\infty) \left(\alpha_{nf} Re \frac{\partial^2\theta}{\partial y^2} \right), \\ u \frac{\partial\theta}{\partial x} + v \frac{\partial\theta}{\partial y} &= \frac{1}{Pr} \frac{\alpha_{nf}}{\alpha_f} \frac{\partial^2\theta}{\partial y^2}. \end{aligned} \quad (2.19)$$

The boundary conditions (2.14) become

$$u = v = 0, \quad \frac{\partial\theta}{\partial y} = -\gamma(1-\theta) \text{ at } y = 0,$$

$$u_e(x) \rightarrow \frac{3}{2} \sin x, \quad \theta \rightarrow 0 \text{ as } y \rightarrow \infty, \quad (2.20)$$

where $\text{Pr} = \nu_f / \alpha_f$ is the Prandtl number, $\gamma = ah_f Gr^{-1/4} / k_f$ is the conjugate parameter for the convective boundary conditions and λ is the mixed convection parameter which is given by:

$$\lambda = \frac{Gr}{\text{Re}^2}, \quad (2.21)$$

with $Gr = g\beta(T_f - T_\infty)a^3 / \nu_f^2$ is the Grashof number for the convective boundary conditions. It is worth mentioning that $\lambda > 0$ corresponds to the aiding flow (heated sphere), $\lambda < 0$ corresponds to the opposing flow (cooled sphere) and $\lambda = 0$ corresponds to the forced convection flow, respectively.

From equation (2.18) we find $p = p(x)$, so we have

$$-\frac{\partial p}{\partial x} = u_e \frac{\partial u_e}{\partial x}. \quad (2.22)$$

Therefore, we have to solve the following boundary layer equations for the problem under consideration after substitute the values (2.15) and equation (2.22) in equations (2.17)-(2.19):

$$\frac{\partial}{\partial x}(ru) + \frac{\partial}{\partial y}(rv) = 0, \quad (2.23)$$

$$u \frac{\partial u}{\partial x} + v \frac{\partial u}{\partial y} = u_e \frac{\partial u_e}{\partial x} + \left[\frac{1}{(1-\chi)^{2.5}[(1-\chi) + (\chi\rho_s / \rho_f)]} \right] \frac{\partial^2 u}{\partial y^2} + \left[\frac{\chi\rho_s(\beta_s / \beta_f) + (1-\chi)\rho_f}{(1-\chi)\rho_f + \chi\rho_f} \right] \lambda\theta \sin x, \quad (2.24)$$

$$u \frac{\partial \theta}{\partial x} + v \frac{\partial \theta}{\partial y} = \frac{1}{\text{Pr}} \left[\frac{(k_s + 2k_f) - 2\chi(k_f - k_s)}{(k_s + 2k_f) + \chi(k_f - k_s)} \right] \frac{\partial^2 \theta}{\partial y^2}, \quad (2.25)$$

with the boundary conditions (2.20).

2.1.2 Non-similar Transformation

To solve equations (2.23)-(2.25), subjected to the boundary conditions (2.20), we assume the following variables:

$$\psi = xr(x)f(x, y), \quad \theta = \theta(x, y), \quad (2.26)$$

where ψ is the stream function defined as

$$u = \frac{1}{r} \frac{\partial \psi}{\partial y} \quad \text{and} \quad v = -\frac{1}{r} \frac{\partial \psi}{\partial x}, \quad (2.27)$$

so that $u = x \frac{\partial f}{\partial y}$ and $v = -\left((1+x \cot x)f + x \frac{\partial f}{\partial x} \right)$,

that satisfies the continuity equation (2.23). Thus, equations (2.24) and (2.25) become

$$\begin{aligned} & \left[\frac{1}{(1-\chi)^{2.5} [1-\chi+(\chi\rho_s/\rho_f)]} \right] \frac{\partial^3 f}{\partial y^3} + (1+x \cot x) f \frac{\partial^2 f}{\partial y^2} - \left(\frac{\partial f}{\partial y} \right)^2 \\ & + \left[\frac{\chi\rho_s(\beta_s/\beta_f) + (1-\chi)\rho_f}{(1-\chi)\rho_f + \chi\rho_f} \right] \lambda \frac{\sin x}{x} \theta + \frac{9 \sin x \cos x}{4 x} \\ & = x \left(\frac{\partial f}{\partial y} \frac{\partial^2 f}{\partial x \partial y} - \frac{\partial f}{\partial x} \frac{\partial^2 f}{\partial y^2} \right), \end{aligned} \quad (2.28)$$

$$\begin{aligned} & \frac{1}{\text{Pr}} \left[\frac{(k_s + 2k_f) - 2\chi(k_f - k_s)}{[(k_s + 2k_f) + \chi(k_f - k_s)][(1-\chi) + \chi(\rho C_p)_s / (\rho C_p)_f]} \right] \frac{\partial^2 \theta}{\partial y^2} \\ & + (1+x \cot x) f \frac{\partial \theta}{\partial y} = x \left(\frac{\partial f}{\partial y} \frac{\partial \theta}{\partial x} - \frac{\partial f}{\partial x} \frac{\partial \theta}{\partial y} \right), \end{aligned} \quad (2.29)$$

subject to the boundary conditions

$$f = \frac{\partial f}{\partial y} = 0, \quad \frac{\partial \theta}{\partial y} = -\gamma(1-\theta) \quad \text{at} \quad y = 0,$$

$$\frac{\partial f}{\partial y} \rightarrow \frac{3 \sin x}{2 x}, \quad \theta \rightarrow 0 \quad \text{as} \quad y \rightarrow \infty. \quad (2.30)$$

It can be seen that at the lower stagnation point of the sphere, $x \approx 0$, equations (2.28) and (2.29) reduce to the following ordinary differential equations:

$$\left[\frac{1}{(1-\chi)^{2.5}[1-\chi+(\chi\rho_s/\rho_f)]} \right] f''' + 2ff'' - f'^2 + \left[\frac{\chi\rho_s(\beta_s/\beta_f) + (1-\chi)\rho_f}{(1-\chi)\rho_f + \chi\rho_f} \right] \lambda\theta + \frac{9}{4} = 0, \quad (2.31)$$

$$\frac{1}{\text{Pr}} \left[\frac{(k_s + 2k_f) - 2\chi(k_f - k_s)}{[(k_s + 2k_f) + \chi(k_f - k_s)][(1-\chi) + \chi(\rho C_p)_s / (\rho C_p)_f]} \right] \theta'' + 2f\theta' = 0, \quad (2.32)$$

and the boundary conditions (2.24) become

$$\begin{aligned} f(0) = f'(0) = 0, \quad \theta'(0) = -\gamma(1-\theta(0)), \\ f' \rightarrow \frac{3}{2}, \quad \theta \rightarrow 0 \quad \text{as } y \rightarrow \infty, \end{aligned} \quad (2.33)$$

where primes denote differentiation with respect to y .

The physical quantities of interest in this problem are the local skin friction coefficient C_f and the local heat transfer coefficient $Q_w(x)$ which are defined by

$$C_f = \frac{1}{(1-\chi)^{2.5}} \frac{a}{U_\infty} \text{Re}^{-1/2} \mu_{nf} \left(\frac{\partial \bar{u}}{\partial \bar{y}} \right)_{\bar{y}=0}$$

and

$$Q_w(x) = \left[\frac{(k_s + 2k_f) - 2\chi(k_f - k_s)}{(k_s + 2k_f) + \chi(k_f - k_s)} \right] \frac{a}{(T_f - T_\infty)} \text{Re}^{-1/2} \left(\frac{\partial \bar{T}}{\partial \bar{y}} \right)_{\bar{y}=0}. \quad (2.34)$$

Using the non-dimensional variables (2.15) and (2.16), we have

$$C_f = \frac{1}{(1-\chi)^{2.5}} x \frac{\partial^2 f}{\partial y^2}(x, 0),$$

and

$$Q_w(x) = \gamma \left[\frac{(k_s + 2k_f) - 2\chi(k_f - k_s)}{(k_s + 2k_f) + \chi(k_f - k_s)} \right] (1 - \theta(x, 0)) \quad (2.35)$$

2.2 NUMERICAL METHOD: KELLER-BOX METHOD

In this study, all problems discussed are solved numerically using the Keller-box method and this method which was introduced by Keller (1970). It is a finite difference method usually used in solving parabolic partial differential equations. This method is

suitable and very efficient to solve the problems involve boundary layer theory. It can be modified in order to solve problem in any order. The Keller-box method used in this study is described clearly by Na (1979), Cebeci and Bradshaw (1988) and also Cebeci and Cousteix (2005). To simplify that, Keller-box method involve the following four steps:

1. Reduce the transformed equations to a first-order system
2. Write the difference equations using central differences
3. Linearize the resulting algebraic equations by Newton's method and write them in matrix-vector form
4. Solve the linear system by the block tridiagonal elimination technique

In this section, the detail about the Keller-box method will be discussed based on the fifth problem in chapter 7 which is the problem of mixed convection boundary layer flow over a solid sphere with convective boundary conditions in a nanofluid.

2.2.1 Finite Difference Method

As described in Cebeci and Bradshaw (1988) and Na (1979) equations (2.28) to (2.29) subject to the boundary conditions (2.30) are first written as a system of first-order equations. For this purpose, we introduce new dependent variables $u(x, y)$, $v(x, y)$, $t(x, y)$ and $s(x, y)$, where $s(x, y)$ replaces $\theta(x, y)$, as the variable for temperature and we obtain the following five first-order equations:

$$f' = u, \quad (2.36)$$

$$u' = v, \quad (2.37)$$

$$s' = t, \quad (2.38)$$

$$\left[\frac{1}{(1-\chi)^{2.5}[1-\chi+(\chi\rho_s/\rho_f)]} \right] v' + (1+x \cot x)fv - u^2 + \left[\frac{\chi\rho_s(\beta_s/\beta_f)+(1-\chi)\rho_f}{(1-\chi)\rho_f+\chi\rho_f} \right] \lambda \frac{\sin x}{x} s + \frac{9 \sin x \cos x}{4 x} = x \left(u \frac{\partial u}{\partial x} - v \frac{\partial f}{\partial x} \right), \quad (2.39)$$

$$\frac{1}{\text{Pr}} \left[\frac{(k_s + 2k_f) - 2\chi(k_f - k_s)}{[(k_s + 2k_f) + \chi(k_f - k_s)][(1 - \chi) + \chi(\rho C_p)_s / (\rho C_p)_f]} \right] t' + (1 + x \cot x) ft = x \left(u \frac{\partial s}{\partial x} - t \frac{\partial f}{\partial x} \right), \quad (2.40)$$

where primes denote differentiation with respect to y . In terms of the new dependent variables, the boundary conditions (2.30) becomes

$$f(x, 0) = u(x, 0) = 0, \quad t(x, 0) = -\gamma(1 - s(x, 0)),$$

$$u(x, \infty) = \frac{3 \sin x}{2x}, \quad s(x, \infty) = 0. \quad (2.41)$$

The net rectangle considered in the $x-y$ plane is shown in Figure 2.2 and the net points are denoted by:

$$\begin{aligned} x^0 &= 0, & x^n &= x^{n-1} + k_n, & n &= 1, 2, \dots, N, \\ y_0 &= 0, & y_j &= y_{j-1} + h_j, & j &= 1, 2, \dots, J, \end{aligned} \quad y_t \equiv y_\infty, \quad (2.42)$$

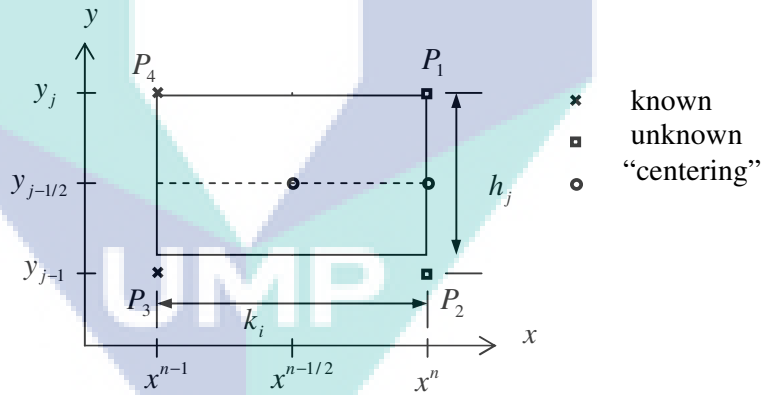


Figure 2.2: Net rectangle for difference approximations

where k_n is the Δx -spacing and h_j is the Δy -spacing. Here n and j are just sequence numbers that indicate the coordinate location (not tensor indices or exponents).

We approximate the quantities (f, u, v, s, t) at point (x^n, y_j) of the net by the net function given by $(f_j^n, u_j^n, v_j^n, s_j^n, t_j^n)$. We also use the notation $()_j^n$ for points and quantities midway between net points and for any net function:

$$x^{n-1/2} \equiv \frac{1}{2}(x^n + x^{n-1}), \quad (2.43)$$

$$y_{j-1/2} \equiv \frac{1}{2}(y_j + y_{j-1}), \quad (2.44)$$

$$(\)_j^{n-1/2} = \frac{1}{2}[(\)_j^n + (\)_j^{n-1}], \quad (2.45)$$

$$(\)_{j-1/2}^n = \frac{1}{2}[(\)_j^n + (\)_{j-1}^n]. \quad (2.46)$$

The derivatives in the $x-y$ direction are placed by finite difference. For any net function $(\)$, generally we have

$$\left(\frac{\partial u}{\partial x}\right)_{j-1/2}^{n-1/2} = \frac{u_{j-1/2}^n - u_{j-1/2}^{n-1}}{k_n}, \quad \left(\frac{\partial u}{\partial y}\right)_{j-1/2}^{n-1/2} = \frac{u_j^{n-1/2} - u_{j-1}^{n-1/2}}{h_j}. \quad (2.47)$$

We write the difference equations, that are to approximate equations (2.36) to (2.40) by considering one mesh rectangle as in Figure 2.2. We start by writing the finite difference approximations of the ordinary differential equations (2.36) to (2.38) for the midpoint $(x^n, y_{j-1/2})$ of the segment P_1P_2 using centered difference derivatives. This process is called “centering about $(x^n, y_{j-1/2})$ ”. Thus we get

$$\frac{f_j^n - f_{j-1}^n}{h_j} = \frac{1}{2}(u_j^n + u_{j-1}^n) = u_{j-1/2}^n, \quad (2.48)$$

$$\frac{u_j^n - u_{j-1}^n}{h_j} = \frac{1}{2}(v_j^n + v_{j-1}^n) = v_{j-1/2}^n, \quad (2.49)$$

$$\frac{s_j^n - s_{j-1}^n}{h_j} = \frac{1}{2}(t_j^n + t_{j-1}^n) = t_{j-1/2}^n. \quad (2.50)$$

The finite difference form of the nonlinear partial differential equations (2.39) and (2.40) is approximated by centering about the midpoint $(x^{n-1/2}, y_{j-1/2})$ of the rectangle $P_1P_2P_3P_4$. This can be done in two steps. In the first step, we center equations (2.39) and (2.40) about the point $(x^{n-1/2}, y)$ without specifying y . If we denote the left

hand side of equations (2.39) and (2.40) by L_1 and L_2 , respectively, then the difference approximations to equations (2.39) and (2.40) are

$$\frac{1}{2}(L_1^n + L_1^{n-1}) = x^{n-1/2} \left(u^{n-1/2} \frac{u^n - u^{n-1}}{k_n} - v^{n-1/2} \frac{f^n - f^{n-1}}{k_n} \right), \quad (2.51)$$

$$\frac{1}{2}(L_2^n + L_2^{n-1}) = x^{n-1/2} \left(u^{n-1/2} \frac{s^n - s^{n-1}}{k_n} - t^{n-1/2} \frac{f^n - f^{n-1}}{k_n} \right), \quad (2.52)$$

respectively. Rearranging these equations the difference approximation to equations (2.39) and (2.40) at $x^{n-1/2}$ become

$$\begin{aligned} K(v')^n + A(fv)^n - (u^2)^n + M Bs^n - \alpha(u^2)^n + \alpha(fv)^n + C \\ + \alpha v^{n-1} f^n - \alpha f^{n-1} v^n = [-L_1 + \alpha(fv) - \alpha(u^2)]^{n-1}, \\ K(v')^n + (A + \alpha)(fv)^n - (1 + \alpha)(u^2)^n + M Bs^n + C \\ + \alpha v^{n-1} f^n - \alpha f^{n-1} v^n = [-L_1 + \alpha(fv) - \alpha(u^2)]^{n-1}, \end{aligned} \quad (2.53)$$

$$\begin{aligned} \frac{1}{\text{Pr}} N(t')^n + A(ft)^n - \alpha(us)^n + \alpha(ft)^n + \alpha s^{n-1} u^n - \alpha u^{n-1} s^n \\ - \alpha f^{n-1} t^n + \alpha t^{n-1} f^n = [-L_2 + \alpha(ft) - \alpha(us)]^{n-1}, \\ \frac{1}{\text{Pr}} N(t')^n + (A + \alpha)(ft)^n - \alpha(us)^n + \alpha s^{n-1} u^n - \alpha u^{n-1} s^n \\ - \alpha f^{n-1} t^n + \alpha t^{n-1} f^n = [-L_2 + \alpha(ft) - \alpha(us)]^{n-1}, \end{aligned} \quad (2.54)$$

where

$$\alpha = \frac{x^{n-1/2}}{k_n}, \quad (2.55)$$

$$A = 1 + x^{n-1/2} \cot x^{n-1/2}, \quad (2.56)$$

$$B = \frac{\sin x^{n-1/2}}{x^{n-1/2}}, \quad (2.57)$$

$$C = \frac{9 \sin x^{n-1/2} \cos x^{n-1/2}}{4 x^{n-1/2}}, \quad (2.58)$$

$$K = \left[\frac{1}{(1-\chi)^{2.5}[1-\chi+(\chi\rho_s/\rho_f)]} \right], \quad (2.59)$$

$$M = \left[\frac{\chi\rho_s(\beta_s/\beta_f)+(1-\chi)\rho_f}{(1-\chi)\rho_f+\chi\rho_f} \right] \lambda, \quad (2.60)$$

$$N = \left[\frac{(k_s+2k_f)-2\chi(k_f-k_s)}{[(k_s+2k_f)+\chi(k_f-k_s)][(1-\chi)+\chi(\rho C_p)_s/(\rho C_p)_f]} \right], \quad (2.62)$$

$$(L_1)^{n-1} = [(1+K)v' + A(fv) - (u^2) + Bs - Mu + Kp]^{n-1}, \quad (2.63)$$

$$(L_2)^{n-1} = \left[\frac{1}{\text{Pr}} \left(1 + \frac{4}{3} N_R \right) t' + A(ft) \right]^{n-1}, \quad (2.64)$$

where the identity sign introduces a useful shorthand $[]^{n-1}$ means that quantities in square bracket are evaluated at $x = x^{n-1}$.

Next, we center equations (2.53) and (2.54) about the point $(x^{n-1/2}, y_{j-1/2})$ by using equation (2.47) and we get

$$\begin{aligned} & K \frac{(v_j^n - v_{j-1}^n)}{h_j} + (A + \alpha) f_{j-1/2}^n v_{j-1/2}^n - (1 + \alpha) (u_{j-1/2}^n)^2 \\ & + \alpha v_{j-1/2}^{n-1} f_{j-1/2}^n - \alpha f_{j-1/2}^{n-1} v_{j-1/2}^n + M B s_{j-1/2}^n + C \\ & = \left[-(L_1)_{j-1/2} + \alpha f_{j-1/2} v_{j-1/2} - \alpha (u_{j-1/2})^2 \right]^{n-1}, \end{aligned} \quad (2.65)$$

$$\begin{aligned} & \frac{1}{\text{Pr}} N \frac{(t_j^n - t_{j-1}^n)}{h_j} + (A + \alpha) f_{j-1/2}^n t_{j-1/2}^n - \alpha u_{j-1/2}^n s_{j-1/2}^n \\ & + \alpha s_{j-1/2}^{n-1} u_{j-1/2}^n - \alpha u_{j-1/2}^{n-1} s_{j-1/2}^n - \alpha f_{j-1/2}^{n-1} t_{j-1/2}^n + \alpha t_{j-1/2}^{n-1} f_{j-1/2}^n \\ & = \left[-(L_2)_{j-1/2} + \alpha f_{j-1/2} t_{j-1/2} - \alpha u_{j-1/2} s_{j-1/2} \right]^{n-1}, \end{aligned} \quad (2.66)$$

where

$$\begin{aligned} (L_1)_{j-1/2}^{n-1} &= \left[K \frac{(v_j - v_{j-1})}{h_j} + f_{j-1/2} y_{j-1/2} - (u_{j-1/2})^2 + M B s_{j-1/2} + C \right]^{n-1}, \\ (L_2)_{j-1/2}^{n-1} &= \left[\frac{1}{\text{Pr}} N \frac{(t_j - t_{j-1})}{h_j} + f_{j-1/2} t_{j-1/2} \right]^{n-1}. \end{aligned}$$

At $x = x^n$ the boundary conditions (2.41) become

$$\begin{aligned} f_0^n &= 0, u_0^n = 0, t_0^n = -\gamma(1 - s_0^n), \\ u_j^n &= \frac{3}{2}B, s_j^n = 0. \end{aligned} \quad (2.67)$$

2.2.2 Newton Method

Suppose $f_j^{n-1}, u_j^{n-1}, v_j^{n-1}, s_j^{n-1}, t_j^{n-1}$ are known for $0 \leq j \leq J$, then the solution for the unknown variable $(f_j^n, u_j^n, v_j^n, s_j^n, t_j^n)$, $j = 0, 1, \dots, J$ should be define. In order to simplify the writing, the unknown variable $(f_j^n, u_j^n, v_j^n, s_j^n, t_j^n)$ at $x = x^{n-1}$ can be written as $(f_j, u_j, v_j, s_j, t_j)$. By using the equation (2.47), the system of equations (2.48) to (2.50) and (2.65) and (2.66) can be written as

$$f_j - f_{j-1} - \frac{h_j}{2}(u_j + u_{j-1}) = 0, \quad (2.68)$$

$$u_j - u_{j-1} - \frac{h_j}{2}(v_j + v_{j-1}) = 0, \quad (2.69)$$

$$s_j - s_{j-1} - \frac{h_j}{2}(t_j + t_{j-1}) = 0, \quad (2.70)$$

$$\begin{aligned} &K(v_j - v_{j-1}) + \frac{(A + \alpha)}{4}h_j(f_j + f_{j-1})(v_j + v_{j-1}) \\ &- \frac{(1 + \alpha)}{4}h_j(u_j + u_{j-1})^2 + \frac{\alpha}{2}h_j v_{j-1/2}^{n-1}(f_j + f_{j-1}) \\ &- \frac{\alpha}{2}h_j f_{j-1/2}^{n-1}(v_j + v_{j-1}) + M B h_j (s_j + s_{j-1}) + C = (R_1)_{j-1/2}^{n-1}, \end{aligned} \quad (2.71)$$

$$\begin{aligned} &\frac{1}{Pr}N(t_j - t_{j-1}) + \frac{(A + \alpha)}{4}h_j(f_j + f_{j-1})(t_j + t_{j-1}) \\ &- \frac{\alpha}{4}h_j(u_j + u_{j-1})(s_j + s_{j-1}) + \frac{\alpha}{2}h_j s_{j-1/2}^{n-1}(u_j + u_{j-1}) \\ &- \frac{\alpha}{2}h_j u_{j-1/2}^{n-1}(s_j + s_{j-1}) - \frac{\alpha}{2}h_j f_{j-1/2}^{n-1}(t_j + t_{j-1}) \\ &+ \frac{\alpha}{2}h_j t_{j-1/2}^{n-1}(f_j + f_{j-1}) = (R_2)_{j-1/2}^{n-1}, \end{aligned} \quad (2.72)$$

where

$$(\mathbf{R}_1)_{j-1/2}^{n-1} = h_j \left[K \frac{(v_j - v_{j-1})}{h_j} + (A - \alpha) f_{j-1/2} v_{j-1/2} - (\alpha - 1) (u_{j-1/2})^2 + M B s_{j-1/2} + C \right]^{n-1}, \quad (2.73)$$

$$(\mathbf{R}_2)_{j-1/2}^{n-1} = h_j \left[\frac{1}{\text{Pr}} N \frac{(t_j - t_{j-1})}{h_j} + (A - \alpha) f_{j-1/2} t_{j-1/2} - \alpha u_{j-1/2} s_{j-1/2} \right]^{n-1} \quad (2.74)$$

In order to linearize the nonlinear equation system (2.68) to (2.74), by using the Newton's method, we introduce the following iterates.

$$\begin{aligned} f_j^{(i+1)} &= f_j^{(i)} + \delta f_j^{(i)}, & u_j^{(i+1)} &= u_j^{(i)} + \delta u_j^{(i)}, \\ v_j^{(i+1)} &= v_j^{(i)} + \delta v_j^{(i)}, & s_j^{(i+1)} &= s_j^{(i)} + \delta s_j^{(i)}, \\ t_j^{(i+1)} &= t_j^{(i)} + \delta t_j^{(i)}. \end{aligned} \quad (2.75)$$

Substitute the iterates (2.75) into the system of equations (2.68) to (2.74), we get

$$(f_j^{(i)} + \delta f_j^{(i)}) - (f_{j-1}^{(i)} + \delta f_{j-1}^{(i)}) - \frac{h_j}{2} (u_j^{(i)} + \delta u_j^{(i)} + u_{j-1}^{(i)} + \delta u_{j-1}^{(i)}) = 0, \quad (2.76)$$

$$(u_j^{(i)} + \delta u_j^{(i)}) - (u_{j-1}^{(i)} + \delta u_{j-1}^{(i)}) - \frac{h_j}{2} (v_j^{(i)} + \delta v_j^{(i)} + v_{j-1}^{(i)} + \delta v_{j-1}^{(i)}) = 0, \quad (2.77)$$

$$(s_j^{(i)} + \delta s_j^{(i)}) - (s_{j-1}^{(i)} + \delta s_{j-1}^{(i)}) - \frac{h_j}{2} (t_j^{(i)} + \delta t_j^{(i)} + t_{j-1}^{(i)} + \delta t_{j-1}^{(i)}) = 0, \quad (2.78)$$

$$\begin{aligned} & K \left[(v_j^{(i)} + \delta v_j^{(i)}) - (v_{j-1}^{(i)} + \delta v_{j-1}^{(i)}) \right] + \frac{(A + \alpha)}{4} h_j (f_j^{(i)} + \delta f_j^{(i)} + f_{j-1}^{(i)} + \delta f_{j-1}^{(i)}) \\ & (v_j^{(i)} + \delta v_j^{(i)} + v_{j-1}^{(i)} + \delta v_{j-1}^{(i)}) - \frac{(1 + \alpha)}{4} h_j (u_j^{(i)} + \delta u_j^{(i)} + u_{j-1}^{(i)} + \delta u_{j-1}^{(i)})^2 \\ & + \frac{\alpha}{2} h_j v_{j-1/2}^{n-1} (f_j^{(i)} + \delta f_j^{(i)} + f_{j-1}^{(i)} + \delta f_{j-1}^{(i)}) - \frac{\alpha}{2} h_j f_{j-1/2}^{n-1} (v_j^{(i)} + \delta v_j^{(i)} + v_{j-1}^{(i)} + \delta v_{j-1}^{(i)}) \\ & + M B h_j (s_j^{(i)} + \delta s_j^{(i)} + s_{j-1}^{(i)} + \delta s_{j-1}^{(i)}) + C = (\mathbf{R}_1)_{j-1/2}^{n-1}, \end{aligned} \quad (2.79)$$

$$\begin{aligned}
& \frac{1}{\text{Pr}} N \left[(t_j^{(i)} + \delta t_j^{(i)}) - (t_{j-1}^{(i)} + \delta t_{j-1}^{(i)}) \right] \\
& + \frac{(A+\alpha)}{4} h_j (f_j^{(i)} + \delta f_j^{(i)} + f_{j-1}^{(i)} + \delta f_{j-1}^{(i)}) (t_j^{(i)} + \delta t_j^{(i)} + t_{j-1}^{(i)} + \delta t_{j-1}^{(i)}) \\
& - \frac{\alpha}{4} h_j (u_j^{(i)} + \delta u_j^{(i)} + u_{j-1}^{(i)} + \delta u_{j-1}^{(i)}) (s_j^{(i)} + \delta s_j^{(i)} + s_{j-1}^{(i)} + \delta s_{j-1}^{(i)}) \\
& + \frac{\alpha}{2} h_j s_{j-1/2}^{n-1} (u_j^{(i)} + \delta u_j^{(i)} + u_{j-1}^{(i)} + \delta u_{j-1}^{(i)}) - \frac{\alpha}{2} h_j u_{j-1/2}^{n-1} (s_j^{(i)} + \delta s_j^{(i)} + s_{j-1}^{(i)} + \delta s_{j-1}^{(i)}) \\
& - \frac{\alpha}{2} h_j f_{j-1/2}^{n-1} (t_j^{(i)} + \delta t_j^{(i)} + t_{j-1}^{(i)} + \delta t_{j-1}^{(i)}) \\
& + \frac{\alpha}{2} h_j t_{j-1/2}^{n-1} (f_j^{(i)} + \delta f_j^{(i)} + f_{j-1}^{(i)} + \delta f_{j-1}^{(i)}) = (R_2)_{j-1/2}^{n-1}.
\end{aligned} \tag{2.80}$$

Next, we drop the quadratic and higher order terms in $(\delta f_j^{(i)}, \delta u_j^{(i)}, \delta v_j^{(i)}, \delta s_j^{(i)}, \delta t_j^{(i)})$. We have also dropped the superscript i for simplicity. After some algebraic manipulations, we obtain the following linear tridiagonal system of equations:

$$\delta f_j - \delta f_{j-1} - \frac{1}{2} h_j (\delta u_j + \delta u_{j-1}) = (r_1)_{j-1/2}, \tag{2.81}$$

$$\delta u_j - \delta u_{j-1} - \frac{1}{2} h_j (\delta v_j + \delta v_{j-1}) = (r_2)_{j-1/2}, \tag{2.82}$$

$$\delta s_j - \delta s_{j-1} - \frac{1}{2} h_j (\delta t_j + \delta t_{j-1}) = (r_3)_{j-1/2}, \tag{2.83}$$

$$\begin{aligned}
(a_1)_j \delta v_j + (a_2)_j \delta v_{j-1} + (a_3)_j \delta f_j + (a_4)_j \delta f_{j-1} + (a_5)_j \delta u_j + (a_6)_j \delta u_{j-1} \\
+ (a_7)_j \delta s_j + (a_8)_j \delta s_{j-1} = (r_4)_{j-1/2},
\end{aligned} \tag{2.84}$$

$$\begin{aligned}
(b_1)_j \delta t_j + (b_2)_j \delta t_{j-1} + (b_3)_j \delta f_j + (b_4)_j \delta f_{j-1} + (b_5)_j \delta u_j \\
+ (b_6)_j \delta u_{j-1} + (b_7)_j \delta s_j + (b_8)_j \delta s_{j-1} = (r_5)_{j-1/2},
\end{aligned} \tag{2.85}$$

where

$$\begin{aligned}
(a_1)_j &= K + h_j \left[\frac{(A + \alpha)}{2} f_{j-1/2} - \frac{\alpha}{2} f_{j-1/2}^{n-1} \right], \\
(a_2)_j &= -K + h_j \left[\frac{(A + \alpha)}{2} f_{j-1/2} - \frac{\alpha}{2} f_{j-1/2}^{n-1} \right] = (a_1)_j - 2K, \\
(a_3)_j &= h_j \left[\frac{(A + \alpha)}{2} v_{j-1/2} + \frac{\alpha}{2} v_{j-1/2}^{n-1} \right], \quad (a_4)_j = (a_3)_j, \\
(a_5)_j &= h_j \left[(1 + \alpha) u_{j-1/2} + \frac{M}{2} \right], \quad (a_6)_j = (a_5)_j, \\
(a_7)_j &= \frac{M B}{2} h_j, \quad (a_8)_j = (a_7)_j
\end{aligned} \tag{2.86}$$

$$\begin{aligned}
(b_1)_j &= \frac{1}{\text{Pr}} N + h_j \left[\frac{(A + \alpha)}{2} f_{j-1/2} - \frac{\alpha}{2} f_{j-1/2}^{n-1} \right], \\
(b_2)_j &= -\frac{1}{\text{Pr}} N + h_j \left[\frac{(A + \alpha)}{2} f_{j-1/2} - \frac{\alpha}{2} f_{j-1/2}^{n-1} \right] = (b_1)_j - \frac{2}{\text{Pr}} N, \\
(b_3)_j &= h_j \left[\frac{(A + \alpha)}{2} t_{j-1/2} + \frac{\alpha}{2} t_{j-1/2}^{n-1} \right], \quad (b_4)_j = (b_3)_j, \\
(b_5)_j &= h_j \left[-\frac{\alpha}{2} s_{j-1/2} + \frac{\alpha}{2} s_{j-1/2}^{n-1} \right], \quad (b_6)_j = (b_5)_j, \\
(b_7)_j &= h_j \left[-\frac{\alpha}{2} u_{j-1/2} + \frac{\alpha}{2} u_{j-1/2}^{n-1} \right], \quad (b_8)_j = (b_7)_j
\end{aligned} \tag{2.87}$$

$$(r_1)_{j-1/2} = f_{j-1} - f_j + h_j u_{j-1/2},$$

$$(r_2)_{j-1/2} = u_{j-1} - u_j + h_j v_{j-1/2},$$

$$(r_3)_{j-1/2} = s_{j-1} - s_j + h_j t_{j-1/2},$$

$$\begin{aligned}
(r_4)_{j-1/2} &= K (-v_j + v_{j-1}) + h_j \left[-(A + \alpha) f_{j-1/2} v_{j-1/2} \right] \\
&\quad + h_j \left[(1 + \alpha) u_{j-1/2}^2 - \alpha v_{j-1/2}^{n-1} f_{j-1/2} + \alpha f_{j-1/2}^{n-1} v_{j-1/2} \right] \\
&\quad + h_j \left[-M B s_{j-1/2} + C \right] + (R_1)_{j-1/2}^{n-1},
\end{aligned}$$

$$\begin{aligned}
(r_5)_{j-1/2} &= \frac{1}{\text{Pr}} N (-t_j + t_{j-1}) + h_j \left[-(A + \alpha) f_{j-1/2} t_{j-1/2} \right] \\
&\quad + h_j \left[\alpha u_{j-1/2} s_{j-1/2} - \alpha s_{j-1/2}^{n-1} u_{j-1/2} + \alpha u_{j-1/2}^{n-1} s_{j-1/2} \right] \\
&\quad + h_j \left[\alpha f_{j-1/2}^{n-1} t_{j-1/2} + \alpha t_{j-1/2}^{n-1} f_{j-1/2} \right] + (R_2)_{j-1/2}^{n-1}
\end{aligned} \tag{2.88}$$

System of equations (2.81) to (2.88) is subject to the boundary conditions (2.67), and according to Cebeci and Bradshaw (1988) they can be satisfied exactly with no iteration. In order to maintain the correct values in all the iterates, we take

$$\delta f_0 = 0, \delta u_0 = 0, \delta t_0 = 0, \delta u_J = 0, \delta s_J = 0 \quad (2.89)$$

2.2.3 The Block Elimination Technique

The linear system (2.81) to (2.85) can be solve by using the block elimination technique (Na, 1979). The linearized difference equations of the system (2.81) to (2.85) have a block -tridiagonal structure.

Commonly, the block tridiagonal structure consists of variables or constants, but here, for the Keller box method, it consists of block matrices. Before we can proceed further with the block elimination method, we will show how to get the elements of the block matrices from the linear system (2.81) to (2.85). We consider three cases namely when $j = 1$, $j = J - 1$, and $j = J$:

Case 1: $j = 1$

The linear systems (2.81) to (2.85) become

$$\delta f_1 - \delta f_0 - \frac{1}{2} h_1 (\delta u_1 + \delta u_0) = (r_1)_{1-1/2},$$

$$\delta u_1 - \delta u_0 - \frac{1}{2} h_1 (\delta v_1 + \delta v_0) = (r_2)_{1-1/2},$$

$$\delta s_1 - \delta s_0 - \frac{1}{2} h_1 (\delta t_1 + \delta t_0) = (r_3)_{1-1/2},$$

$$(a_1)_1 \delta v_1 + (a_2)_1 \delta v_0 + (a_3)_1 \delta f_1 + (a_4)_1 \delta f_0 + (a_5)_1 \delta u_1 + (a_6)_1 \delta u_0 \\ + (a_7)_1 \delta s_1 + (a_8)_1 \delta s_0 = (r_4)_{1-1/2},$$

$$(b_1)_1 \delta t_1 + (b_2)_1 \delta t_0 + (b_3)_1 \delta f_1 + (b_4)_1 \delta f_0 + (b_5)_1 \delta u_1 \\ + (b_6)_1 \delta u_0 + (b_7)_1 \delta s_1 + (b_8)_1 \delta s_0 = (r_5)_{1-1/2}$$

By letting $d_1 = -\frac{1}{2}h_1$ and using $\delta f_0 = 0$, $\delta u_0 = 0$, $\delta t_0 = 0$, from (2.89), the previous system of equations can be written in a matrix form as

$$\begin{bmatrix} 0 & 0 & 1 & 0 & 0 \\ d_1 & 0 & 0 & d_1 & 0 \\ 0 & -1 & 0 & 0 & d_1 \\ (a_2)_1 & (a_8)_1 & (a_3)_1 & (a_1)_1 & 0 \\ 0 & (b_8)_1 & (b_3)_1 & 0 & (b_1)_1 \end{bmatrix} \begin{bmatrix} \delta v_0 \\ \delta s_0 \\ \delta f_1 \\ \delta v_1 \\ \delta t_1 \end{bmatrix} + \begin{bmatrix} d_1 & 0 & 0 & 0 & 0 \\ 1 & 0 & 0 & 0 & 0 \\ 0 & 1 & 0 & 0 & 0 \\ (a_5)_1 & (a_7)_1 & 0 & 0 & 0 \\ (b_5)_1 & (b_7)_1 & 0 & 0 & 0 \end{bmatrix} \begin{bmatrix} \delta u_1 \\ \delta s_1 \\ \delta f_2 \\ \delta v_2 \\ \delta t_2 \end{bmatrix} = \begin{bmatrix} (r_1)_{1-(1/2)} \\ (r_2)_{1-(1/2)} \\ (r_3)_{1-(1/2)} \\ (r_4)_{1-(1/2)} \\ (r_5)_{1-(1/2)} \end{bmatrix}$$

For simplicity, case 1: $j = 1$, can be written as $[A_1][\delta_1] + [C_1][\delta_2] = [r_1]$.

Case 2: $j = J - 1$

The linear system (2.81) to (2.85) become

$$\delta f_{J-1} - \delta f_{J-2} - \frac{1}{2}h_{J-1}(\delta u_{J-1} + \delta u_{J-2}) = (r_1)_{(J-1)-1/2},$$

$$\delta u_{J-1} - \delta u_{J-2} - \frac{1}{2}h_{J-1}(\delta v_{J-1} + \delta v_{J-2}) = (r_2)_{(J-1)-1/2},$$

$$\delta s_{J-1} - \delta s_{J-2} - \frac{1}{2}h_{J-1}(\delta t_{J-1} + \delta t_{J-2}) = (r_3)_{(J-1)-1/2},$$

$$\begin{aligned} & (a_1)_{J-1} \delta v_{J-1} + (a_2)_{J-1} \delta v_{J-2} + (a_3)_{J-1} \delta f_{J-1} + (a_4)_{J-1} \delta f_{J-2} \\ & + (a_5)_{J-1} \delta u_{J-1} + (a_6)_{J-1} \delta u_{J-2} + (a_7)_{J-1} \delta s_{J-1} \\ & + (a_8)_{J-1} \delta s_{J-2} = (r_4)_{(J-1)-1/2}, \end{aligned}$$

$$\begin{aligned} & (b_1)_{J-1} \delta t_{J-1} + (b_2)_{J-1} \delta t_{J-2} + (b_3)_{J-1} \delta f_{J-1} + (b_4)_{J-1} \delta f_{J-2} + (b_5)_{J-1} \delta u_{J-1} \\ & + (b_6)_{J-1} \delta u_{J-2} + (b_7)_{J-1} \delta s_{J-1} + (b_8)_{J-1} \delta s_{J-2} = (r_5)_{(J-1)-1/2}. \end{aligned}$$

By letting $d_{j-1} = -\frac{1}{2}h_{j-1}$, the previous system of equations can be written in a matrix form as

$$\begin{aligned}
 & \begin{bmatrix} 0 & 0 & -1 & 0 & 0 \\ 0 & 0 & 0 & d_{j-1} & 0 \\ 0 & 0 & 0 & 0 & d_{j-1} \\ 0 & 0 & (a_4)_{j-1} & (a_2)_{j-1} & 0 \\ 0 & 0 & (b_4)_{j-1} & 0 & (b_2)_{j-1} \end{bmatrix} \begin{bmatrix} \delta u_{j-3} \\ \delta s_{j-3} \\ \delta f_{j-2} \\ \delta v_{j-2} \\ \delta t_{j-2} \end{bmatrix} \\
 + & \begin{bmatrix} d_{j-1} & 0 & 1 & 0 & 0 \\ -1 & 0 & 0 & d_{j-1} & 0 \\ 0 & -1 & 0 & 0 & d_{j-1} \\ (a_6)_{j-1} & (a_8)_{j-1} & (a_3)_{j-1} & (a_1)_{j-1} & 0 \\ (b_6)_{j-1} & (b_8)_{j-1} & (b_3)_{j-1} & 0 & (b_1)_{j-1} \end{bmatrix} \begin{bmatrix} \delta u_{j-2} \\ \delta s_{j-2} \\ \delta f_{j-1} \\ \delta v_{j-1} \\ \delta t_{j-1} \end{bmatrix} \\
 + & \begin{bmatrix} d_{j-1} & 0 & 0 & 0 & 0 \\ 1 & 0 & 0 & 0 & 0 \\ 0 & 1 & 0 & 0 & 0 \\ (a_5)_{j-1} & (a_7)_{j-1} & 0 & 0 & 0 \\ (b_5)_{j-1} & (b_7)_{j-1} & 0 & 0 & 0 \end{bmatrix} \begin{bmatrix} \delta u_{j-1} \\ \delta s_{j-1} \\ \delta f_j \\ \delta v_j \\ \delta t_j \end{bmatrix} = \begin{bmatrix} (r_1)_{(j-1)-(1/2)} \\ (r_2)_{(j-1)-(1/2)} \\ (r_3)_{(j-1)-(1/2)} \\ (r_4)_{(j-1)-(1/2)} \\ (r_5)_{(j-1)-(1/2)} \end{bmatrix}
 \end{aligned}$$

Hence, for all values of $j = 2, 3, \dots, J-1$, we have

$$[B_j][\delta_{j-1}] + [A_j][\delta_j] + [C_j][\delta_{j+1}] = [r_j].$$

Case 3: $j = J$,

The linear system (2.81) to (2.85) become

$$\delta f_J - \delta f_{J-1} - \frac{1}{2}h_J(\delta u_J + \delta u_{J-1}) = (r_1)_{J-1/2},$$

$$\delta u_J - \delta u_{J-1} - \frac{1}{2}h_J(\delta v_J + \delta v_{J-1}) = (r_2)_{J-1/2},$$

$$\delta g_J - \delta g_{J-1} - \frac{1}{2}h_J(\delta p_J + \delta p_{J-1}) = (r_3)_{J-1/2},$$

$$\delta s_J - \delta s_{J-1} - \frac{1}{2} h_J (\delta t_J + \delta t_{J-1}) = (r_3)_{J-1/2},$$

$$(a_1)_J \delta v_J + (a_2)_J \delta v_{J-1} + (a_3)_J \delta f_J + (a_4)_J \delta f_{J-1} + (a_5)_J \delta u_J + (a_6)_J \delta u_{J-1} + (a_7)_J \delta s_J + (a_8)_J \delta s_{J-1} = (r_4)_{J-1/2},$$

$$(b_1)_J \delta t_J + (b_2)_J \delta t_{J-1} + (b_3)_J \delta f_J + (b_4)_J \delta f_{J-1} + (b_5)_J \delta u_J + (b_6)_J \delta u_{J-1} + (b_7)_J \delta s_J + (b_8)_J \delta s_{J-1} = (r_5)_{J-1/2}$$

By letting $d_j = -\frac{1}{2}h_j$ and using $\delta u_j = 0$ and $\delta s_j = 0$. From (2.89), the previous system of equations can be written in a matrix form as

$$\begin{bmatrix} 0 & 0 & -1 & 0 & 0 \\ 0 & 0 & 0 & d_j & 0 \\ 0 & 0 & 0 & 0 & d_j \\ 0 & 0 & (a_4)_J & (a_2)_J & 0 \\ 0 & 0 & (b_4)_J & 0 & (b_2)_J \end{bmatrix} \begin{bmatrix} \delta u_{J-2} \\ \delta s_{J-2} \\ \delta f_{J-1} \\ \delta v_{J-1} \\ \delta t_{J-1} \end{bmatrix} + \begin{bmatrix} d_j & 0 & 0 & 0 & 0 \\ -1 & 0 & 0 & 0 & 0 \\ 0 & -1 & 0 & 0 & 0 \\ (a_6)_J & (a_8)_J & (a_3)_J & (a_1)_J & 0 \\ (b_6)_J & (b_8)_J & (b_3)_J & 0 & (b_1)_J \end{bmatrix} \begin{bmatrix} \delta u_{J-1} \\ \delta s_{J-1} \\ \delta f_J \\ \delta v_J \\ \delta t_J \end{bmatrix} = \begin{bmatrix} (r_1)_{J-(1/2)} \\ (r_2)_{J-(1/2)} \\ (r_3)_{J-(1/2)} \\ (r_4)_{J-(1/2)} \\ (r_5)_{J-(1/2)} \end{bmatrix}$$

Hence, for all value of $j = J$, we have $[B_j][\delta_{j-1}] + [A_j][\delta_j] = [r_j]$.

Therefore, in overall, for $j = 1, 2, 3, \dots, J-1, J$, we can simplify that

$$j=1 \quad : [A_1][\delta_1] + [C_1][\delta_2] = [r_1],$$

$$j=2 \quad : [B_2][\delta_1] + [A_2][\delta_2] + [C_2][\delta_3] = [r_2],$$

$$j=3 \quad : [B_3][\delta_2] + [A_3][\delta_3] + [C_3][\delta_4] = [r_3],$$

⋮

$$j=J-1 : [B_{j-1}][\delta_{j-2}] + [A_{j-1}][\delta_{j-1}] + [C_{j-1}][\delta_j] = [r_{j-1}],$$

$$j=J \quad : [B_j][\delta_{j-1}] + [A_j][\delta_j] = [r_j].$$

Generally, in matrix vector form, it can be written as

$$\mathbf{A}\boldsymbol{\delta} = \mathbf{r}, \quad (2.90)$$

where

$$\mathbf{A} = \begin{bmatrix} [A_1] & [C_1] \\ [B_2] & [A_2] & [C_2] \\ \vdots & \vdots & \vdots \\ [B_{j-1}] & [A_{j-1}] & [C_{j-1}] \\ [B_j] & [A_j] \end{bmatrix}, \quad \boldsymbol{\delta} = \begin{bmatrix} [\delta_1] \\ [\delta_2] \\ \vdots \\ [\delta_{j-1}] \\ [\delta_j] \end{bmatrix}, \quad \mathbf{r} = \begin{bmatrix} [r_1] \\ [r_2] \\ \vdots \\ [r_{j-1}] \\ [r_j] \end{bmatrix}$$

The elements of the matrices are as follows:

$$[A_1] = \begin{bmatrix} 0 & 0 & 1 & 0 & 0 \\ d_1 & 0 & 0 & d_1 & 0 \\ 0 & -1 & 0 & 0 & d_1 \\ (a_2)_1 & (a_8)_1 & (a_3)_1 & (a_1)_1 & 0 \\ 0 & (b_8)_1 & (b_3)_1 & 0 & (b_1)_1 \end{bmatrix}, \quad (2.91)$$

$$[A_j] = \begin{bmatrix} d_j & 0 & 0 & 0 & 0 \\ -1 & 0 & 0 & 0 & 0 \\ 0 & -1 & 0 & 0 & d_j \\ (a_6)_j & (a_8)_j & (a_3)_j & (a_1)_j & 0 \\ (b_6)_{j-1} & (b_8)_j & (b_3)_j & 0 & (b_1)_j \end{bmatrix}, \quad 2 \leq j \leq J \quad (2.92)$$

$$[B_j] = \begin{bmatrix} 0 & 0 & -1 & 0 & 0 \\ 0 & 0 & 0 & d_j & 0 \\ 0 & 0 & 0 & 0 & d_j \\ 0 & 0 & (a_4)_j & (a_2)_j & 0 \\ 0 & 0 & (b_4)_j & 0 & (b_2)_j \end{bmatrix}, \quad 2 \leq j \leq J \quad (2.93)$$

$$[C_j] = \begin{bmatrix} d_j & 0 & 0 & 0 & 0 \\ 1 & 0 & 0 & 0 & 0 \\ 0 & 1 & 0 & 0 & 0 \\ (a_5)_j & (a_7)_j & 0 & 0 & 0 \\ (b_5)_j & (b_7)_j & 0 & 0 & 0 \end{bmatrix}, \quad 1 \leq j \leq J-1 \quad (2.94)$$

$$[\delta_i] = \begin{bmatrix} \delta v_0 \\ \delta s_0 \\ \delta f_1 \\ \delta v_1 \\ \delta t_1 \end{bmatrix}, \quad [\delta_j] = \begin{bmatrix} \delta u_{j-1} \\ \delta s_{j-1} \\ \delta f_j \\ \delta v_j \\ \delta t_j \end{bmatrix}, \quad 2 \leq j \leq J \quad (2.95)$$

and

$$[r_j] = \begin{bmatrix} (r_1)_{j-(1/2)} \\ (r_2)_{j-(1/2)} \\ (r_3)_{j-(1/2)} \\ (r_4)_{j-(1/2)} \\ (r_5)_{j-(1/2)} \end{bmatrix}, \quad 2 \leq j \leq J \quad (2.96)$$

The coefficient matrix A in equation (2.90) is known as tridiagonal matrix with zero elements, except at its main diagonal. The equation (2.90) can be solve by using a block elimination technique (Na, 1979) with assume that A is nonsingular and it can be factored into

$$A=LU, \quad (2.97)$$

where

$$L = \begin{bmatrix} [\alpha_1] & & & & \\ [B_2] & [\alpha_2] & & & \\ & \ddots & \ddots & \ddots & \\ & & & [\alpha_{j-1}] & \\ & & & [B_j] & [\alpha_j] \end{bmatrix} \text{ and } U = \begin{bmatrix} [I] & [\Gamma_1] & & & \\ & [I] & [\Gamma_2] & & \\ & & \ddots & \ddots & \\ & & & & [I][\Gamma_{j-1}] \\ & & & & [I] \end{bmatrix},$$

$[I]$ is the identity matrix of order 5 and $[\alpha_i]$, and $[\Gamma_i]$ are 5×5 matrices which elements are determined by the following equations:

$$[\alpha_1] = [A_1], \quad (2.98)$$

$$[A_1] [\Gamma_1] = [C_1], \quad (2.99)$$

$$[\alpha_j] = [A_j] - [B_j] [\Gamma_{j-1}], \quad j = 2, 3, \dots, J, \quad (2.100)$$

$$[\alpha_j] [\Gamma_j] = [C_j], \quad j = 2, 3, \dots, J-1 \quad (2.101)$$

By substitute (2.97) is into equation (2.90), we get

$$LU \delta = r \quad (2.102)$$

If we define

$$U \delta = W, \quad (2.103)$$

then the equation (2.102) becomes

$$LW = r, \quad (2.104)$$

where

$$W = \begin{bmatrix} [W_1] \\ [W_2] \\ \vdots \\ [W_{J-1}] \\ [W_J] \end{bmatrix},$$

and $[W_j]$ are 5×1 column matrices. The elements W can be solved from equation (2.104) which is

$$[\alpha_1][W_1] = [r_1], \quad (2.105)$$

$$[\alpha_j][W_j] = [r_j] - [B_j][W_{j-1}], \quad 2 \leq j \leq J. \quad (2.106)$$

The step in which Γ_j , α_j and W_j are calculated is usually referred to as the forward sweep. Once the elements of W are found, Equation (2.103) then gives the solution δ in the so-called backward sweep, in which the elements are obtained by the following relations:

$$[\delta_j] = [W_j], \quad (2.107)$$

$$[\delta_j] = [W_j] - [\Gamma_j][\delta_{j+1}], \quad 1 \leq j \leq J-1. \quad (2.108)$$

Then, when the elements of δ are found, equations (2.81) to (2.85) then can be used to find $(i+1)^{\text{th}}$ iterates for equation (2.75).

These calculations are repeated until some convergence criterion is satisfied. In laminar boundary layer calculations, the wall shear stress parameter $v(x,0)$ is commonly used as convergence criterion (Cebeci and Bradshaw, 1988). This is probably because of boundary layer calculations, the greatest errors usually occurred in the wall shear stress parameter. Therefore, the wall shear stress parameter is used as convergence criterion in this study. Calculations are stopped when

$$|\delta v_0^{(i)}| < \varepsilon_1, \quad (2.109)$$

where ε_1 is a small fixed value. In this study, $\varepsilon_1 = 10^{-7}$ is used, which gives the precise values until six decimal places, as suggested by Cebeci and Bradshaw (1988).

2.2.4 Starting Conditions

In numerical calculation, the suitable step size Δy and boundary layer thickness y_∞ must be determined. These suitable values must be defined so that the numerical results for the quantities discussed is not affected by Δy and y_∞ . Usually, it is done by try and error approach. The computation can starts by determining the value of y_∞ with referring to velocity and temperature profile. The non suitable values of boundary layer thickness y_∞ , which is too large or too small may not fulfill the boundary conditions $y \rightarrow \infty$ ($y = y_\infty$). Next, after the value of y_∞ is determined, the suitable value of Δy must be define. Usually, we choose the step size $\Delta y = 0.01$ and we run the simulation until $y_\infty = 206$. Moreover, the step size for position x is chosen as $\Delta x = \pi/20$ and the time step $\Delta t = 0.05$ is sufficient to provide accurate numerical results. The appropriate value of step size Δy must not affect the converged results appreciably, for an example, the value of skin friction coefficient must free from the value of step size Δy chosen.

Too small values of Δy may cause an increase waiting time in calculation while large values of Δy cause a little time in calculation but may produce inaccurate results.

2.2.5 Initial Profile

In order to proceed with the numerical computation, it is necessary to make an initial guesses for the function f , u , v , s and t in the boundary layer flow. The initial guesses can start with velocity u and temperature distribution s at $y=0$ and $y=y_\infty$. It is because u and s have both boundary conditions at $y=0$ and $y \rightarrow \infty$ ($y=y_\infty$). When the initial guesses of u and s have been defined, other functions of f , v and t also can be defined with differentiation and integration. There are few possibilities in the selection of distribution curves, as long as they satisfy the boundary condition (2.41). In problem considered here, there is one possibility distribution curve for u and s suggested by Bejan (1984), Burmeister (1983) and Bejan and Kraus (2003).

$$u = \frac{df}{dy} = \frac{3 \sin x}{4 x} \left(\frac{y}{y_\infty} \right) \left(3 - \left(\frac{y}{y_\infty} \right)^2 \right), \quad (2.110)$$

$$s = \theta(y) = - \left(\frac{y}{y_\infty} \right)^2 + 1 \quad (2.111)$$

Integrate equation (2.110) with respect to y produce

$$f = \int_{y=0}^{y=y_\infty} u dy = \frac{3 \sin x}{8 x} \left(\frac{y^2}{y_\infty} \right) \left(3 - \frac{1}{2} \left(\frac{y}{y_\infty} \right)^2 \right), \quad (2.112)$$

$$v = \frac{du}{dy} = \frac{9 \sin x}{4 x} \left(\frac{1}{y_\infty} \right) \left(1 - \left(\frac{y}{y_\infty} \right)^2 \right), \quad (2.113)$$

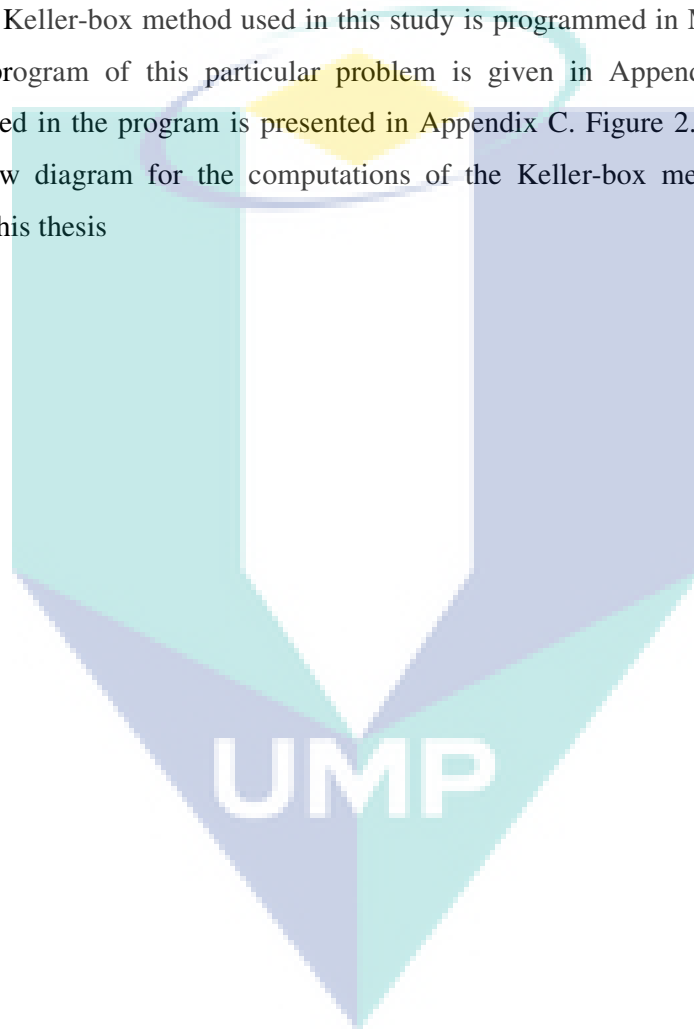
Similarly, differentiating equation (2.111) with respect to y , we get

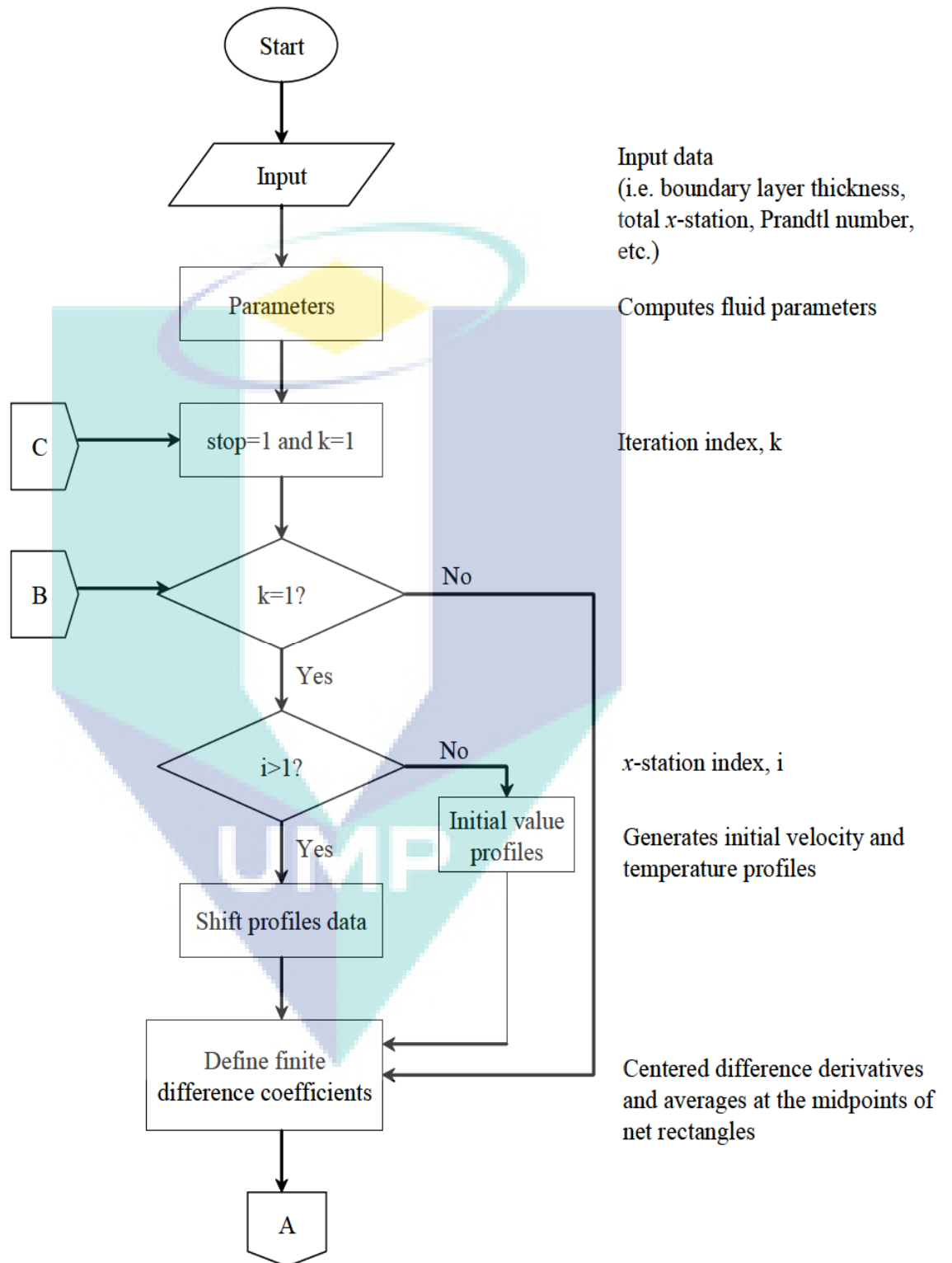
$$t = \frac{ds}{dy} = - \frac{2}{y_\infty} \left(\frac{y}{y_\infty} \right). \quad (2.114)$$

The complete numerical results of this particular problem as described in this chapter, namely the problem on the mixed convection boundary layer flow over a solid

sphere with convective boundary conditions in a nanofluid, are presented in Chapter 7. From our numerical results, the Keller-box method is found and proven to be suitable and accurate to solve this problem in nanofluid. Therefore, we are confident to proceed further using the Keller-box method to solve other effect of radiation on magnetohydrodynamic free and mixed convection boundary layer problems in a viscous fluid, micropolar fluid and nanofluid as presented in Chapter 3 to 8.

The Keller-box method used in this study is programmed in Matlab® 5.3.1. The complete program of this particular problem is given in Appendix D. The list of symbols used in the program is presented in Appendix C. Figure 2.3 below shows the general flow diagram for the computations of the Keller-box method for problems studied in this thesis





continued on the next page....

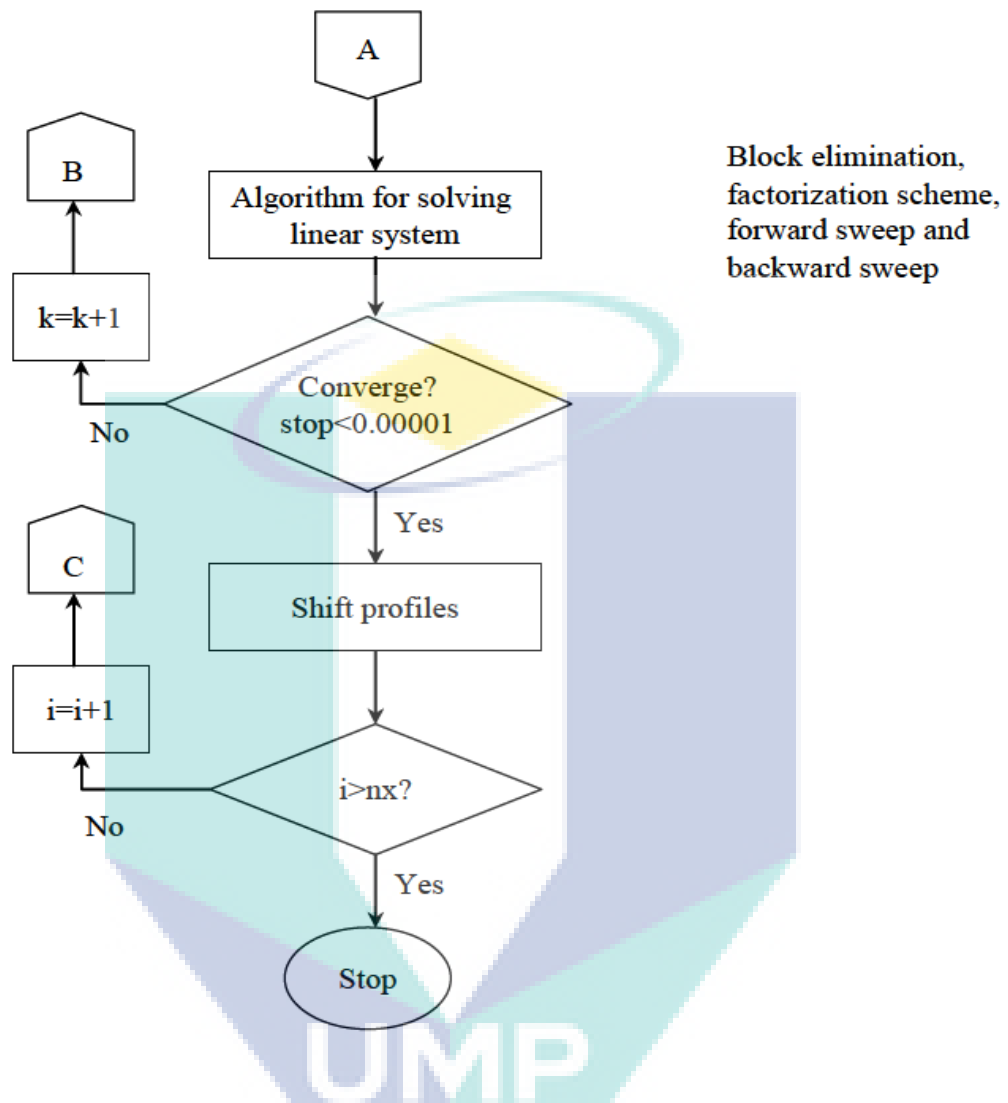


Figure 2.3: Flow diagram for the Keller-box method

CHAPTER 3

THE EFFECT OF RADIATION ON MAGNETOHYDRODYNAMIC FREE CONVECTION BOUNDARY LAYER FLOW OVER A SOLID SPHERE IN A VISCOUS FLUID

3.1 INTRODUCTION

The problem of the effect of radiation on magnetohydrodynamic free convection boundary layer flow over a solid sphere in a viscous fluid with convective boundary conditions is considered and discussed in this chapter. The effect of radiation on magnetohydrodynamic flow for heat and mass transfer problems have become industrially more important due to many engineering processes occur at high temperatures and the knowledge of radiation in heat transfer leads to significant role in the designing of equipment. Nuclear power plants, gas turbines and various propulsion devices for aircraft, missiles, satellites and space vehicles are examples of such engineering processes. At high operating temperature, the radiation effect can be quite significant (Sivaiah et al., 2010). This problem has been considered by several people, as listed in the literature review section in Chapter 1.

The obtained results are compared with those reported by Huang and Chen (1987) and Nazar et al. (2002a) without the effect of radiation and magnetohydrodynamic when $M = 0$, $N_R = 0$ and $\gamma \rightarrow \infty$.

In the current work, the basic equations of boundary layer are transformed into a non-dimensional form and reduced to nonlinear systems of partial differential equations. They are solved numerically using an implicit finite difference scheme known as the Keller-box method. Numerical solutions are obtained for the local wall temperature, the local heat transfer coefficient, local Nusselt number and the local skin friction coefficient, as well as the velocity and temperature profiles. The features of the flow and heat transfer characteristics for various values of the Prandtl number, the magnetic parameter, the radiation parameter, the conjugate parameter and the coordinate running along the surface of the sphere are analyzed and discussed.

3.2 MATHEMATICAL FORMULATION

Consider a heated sphere of radius a , which is immersed in a viscous fluid of ambient temperature T_∞ . The surface of the sphere is subjected to a convective boundary conditions as shown in Figure 3.1. Therefore, the equation of continuity as (2.5) but the momentum and energy equations can be written as

$$\bar{u} \frac{\partial \bar{u}}{\partial \bar{x}} + \bar{v} \frac{\partial \bar{u}}{\partial \bar{y}} = \nu \frac{\partial^2 \bar{u}}{\partial \bar{y}^2} + g \beta (T - T_\infty) \sin\left(\frac{\bar{x}}{a}\right) - \frac{\sigma \beta^2}{\rho} \bar{u}, \quad (3.1)$$

$$\bar{u} \frac{\partial T}{\partial \bar{x}} + \bar{v} \frac{\partial T}{\partial \bar{y}} = \alpha \frac{\partial^2 T}{\partial \bar{y}^2} - \frac{1}{\rho c_p} \frac{\partial q_r}{\partial \bar{y}}, \quad (3.2)$$

subject to the boundary conditions (Salleh et al., 2010c and Aziz, 2009)

$$\begin{aligned} \bar{u} = \bar{v} = 0, \quad -k_f \frac{\partial T}{\partial \bar{y}} = h_f (T_f - T) \text{ at } \bar{y} = 0, \\ \bar{u} \rightarrow 0, \quad T \rightarrow T_\infty \text{ as } \bar{y} \rightarrow \infty, \end{aligned} \quad (3.3)$$

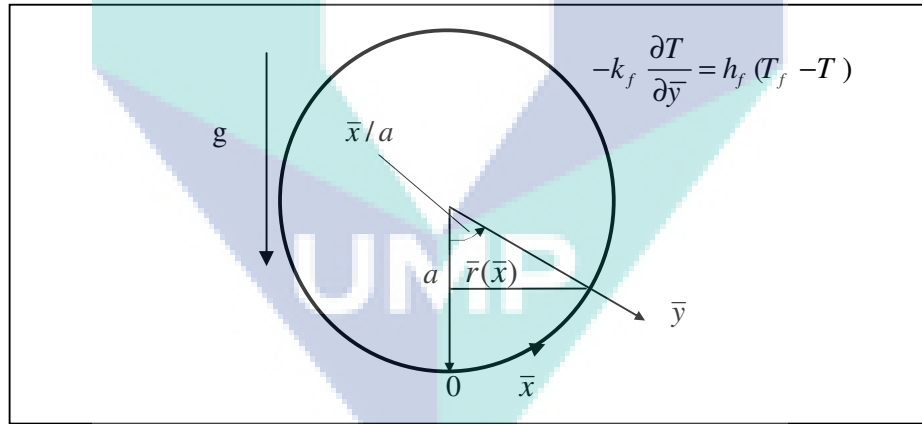


Figure 3.1: Physical model and coordinate system

where $\bar{r}(\bar{x}) = a \sin(\bar{x}/a)$, \bar{u} and \bar{v} are the velocity components along the \bar{x} and \bar{y} directions, respectively, T is the local temperature, g is the gravity acceleration, β is the thermal expansion coefficient, ν is the kinematic viscosity, ρ is the fluid density, σ is the electrical conductivity, c_p the specific heat, α is the thermal diffusivity, T_f is the temperature of the hot fluid, k_f is the thermal conductivity and h_f is the heat transfer coefficient fluid.

We introduce now the following non-dimensional variables (Salleh et al., 2010c; Aziz, 2009)

$$x = \frac{\bar{x}}{a}, \quad y = Gr^{1/4} \left(\frac{\bar{y}}{a} \right), \quad r = \frac{\bar{r}}{a},$$

$$u = \left(\frac{a}{\nu} \right) Gr^{-1/2} \bar{u}, \quad v = \left(\frac{a}{\nu} \right) Gr^{-1/4} \bar{v}, \quad \theta = \frac{T - T_{\infty}}{T_f - T_{\infty}}, \quad (3.4)$$

where $Gr = g\beta(T_f - T_{\infty}) \frac{a^3}{\nu^2}$ is the Grashof number for convective boundary conditions.

Using the Rosseland approximation for radiation (Bataller, 2008a,b) the radiative heat flux is simplified as

$$q_r = -\frac{4\sigma^*}{3k^*} \frac{\partial T^4}{\partial y}, \quad (3.5)$$

where σ^* and k^* are the Stefan-Boltzmann constant and the mean absorption coefficient, respectively. We assume that the temperature differences within the flow through the porous medium such as that the term T^4 may be expressed as a linear function of temperature. Hence, expanding T^4 in a Taylor series about T_{∞} and neglecting higher-order terms, we get

$$T^4 \cong 4T_{\infty}^3 T - 3T_{\infty}^4, \quad (3.6)$$

Substituting variables (3.4)–(3.6) into (3.1) and (3.2) then become

$$u \frac{\partial u}{\partial x} + v \frac{\partial u}{\partial y} = \frac{\partial^2 u}{\partial y^2} + \theta \sin x - Mu, \quad (3.7)$$

$$u \frac{\partial \theta}{\partial x} + v \frac{\partial \theta}{\partial y} = \frac{1}{Pr} \left(1 + \frac{4}{3} N_R \right) \frac{\partial^2 \theta}{\partial y^2}, \quad (3.8)$$

where $Pr = \frac{\nu}{\alpha}$ is the Prandtl number, $M = \frac{\sigma\beta^2 a^2}{\nu\rho Gr^{1/2}}$ is the magnetic parameter, and

$N_R = \frac{4\sigma^* T_{\infty}^3}{\alpha k^* \rho c_p}$ is the radiation parameter. The boundary conditions (3.3) become

$$u=v=0, \quad \frac{\partial \theta}{\partial y} = -\gamma(1-\theta) \quad \text{on } y=0,$$

$$u \rightarrow 0, \quad \theta \rightarrow 0 \quad \text{as } y \rightarrow \infty, \quad (3.9)$$

where $\gamma = ah_f Gr^{-1/4} / k_f$ is the conjugate parameter for the convective boundary conditions. It is noticed that if we write the boundary condition $\theta = 1 + \frac{\partial \theta / \partial y}{\gamma}$ at $y=0$ and when $\gamma \rightarrow \infty$ we have $\theta(0) = 1$ (CWT).

To solve (3.7) and (3.8), subjected to the boundary conditions (3.11), we assume the following variables:

$$\psi = xr(x)f(x, y), \quad \theta = \theta(x, y), \quad (3.10)$$

where ψ is the stream function defined as

$$u = \frac{1}{r} \frac{\partial \psi}{\partial y} \quad \text{and} \quad v = -\frac{1}{r} \frac{\partial \psi}{\partial x}, \quad (3.11)$$

which satisfies the continuity equation (2.17). Thus, equations (3.8) and (3.9) become

$$\frac{\partial^3 f}{\partial y^3} + (1+x \cot x) f \frac{\partial^2 f}{\partial y^2} - \left(\frac{\partial f}{\partial y} \right)^2 + \frac{\sin x}{x} \theta - M \frac{\partial f}{\partial y} = x \left(\frac{\partial f}{\partial y} \frac{\partial^2 f}{\partial x \partial y} - \frac{\partial f}{\partial x} \frac{\partial^2 f}{\partial y^2} \right), \quad (3.12)$$

$$\frac{1}{\text{Pr}} \left(1 + \frac{4}{3} N_R \right) \frac{\partial^2 \theta}{\partial y^2} + (1+x \cot x) f \frac{\partial \theta}{\partial y} = x \left(\frac{\partial f}{\partial y} \frac{\partial \theta}{\partial x} - \frac{\partial f}{\partial x} \frac{\partial \theta}{\partial y} \right), \quad (3.13)$$

subject to the boundary conditions

$$f = \frac{\partial f}{\partial y} = 0, \quad \frac{\partial \theta}{\partial y} = -\gamma(1-\theta) \quad \text{at } y=0,$$

$$\frac{\partial f}{\partial y} \rightarrow 0, \quad \theta \rightarrow 0 \quad \text{as } y \rightarrow \infty. \quad (3.14)$$

It can be seen that at the lower stagnation point of the sphere, $x \approx 0$, equations (3.12) and (3.13) are reduced to the following ordinary differential equations:

$$f''' + 2ff'' - f'^2 + \theta - Mf' = 0, \quad (3.15)$$

$$\frac{1}{\text{Pr}} \left(1 + \frac{4}{3} N_R \right) \theta'' + 2f\theta' = 0, \quad (3.16)$$

and the boundary conditions (3.14) become

$$\begin{aligned} f(0) = f'(0) = 0, \quad \theta'(0) = -\gamma(1 - \theta(0)), \\ f' \rightarrow 0, \quad \theta \rightarrow 0 \text{ as } y \rightarrow \infty, \end{aligned} \quad (3.17)$$

where primes denote differentiation with respect to y .

The physical quantities of interest in this problem are the local skin friction coefficient C_f , the local Nusselt number, N_u and the local heat transfer $Q_w(x)$ can be written as

$$C_f = \frac{Gr^{-3/4} a^2}{\mu v} \tau_w, \quad N_u = \frac{a Gr^{-1/4}}{k(T_f - T_\infty)} q_w, \quad (3.18)$$

where

$$\tau_w = \mu \left(\frac{\partial \bar{u}}{\partial y} \right)_{\bar{y}=0}, \quad q_w = -k \left(\frac{\partial T}{\partial y} \right)_{\bar{y}=0} + q_r. \quad (3.19)$$

Using the non-dimensional variables (3.4) and Rosseland approximation for radiation (3.5) with boundary condition (3.9) into equations (3.18) and (3.19), we get

$$C_f = x \frac{\partial^2 f}{\partial y^2}(x, 0), \quad N_u = \gamma \left(1 + \frac{4}{3} N_R \right) (1 - \theta(x, 0)) \text{ and } Q_w(x) = \gamma (1 - \theta(x, 0)) \quad (3.20)$$

3.3. RESULTS AND DISCUSSION

The nonlinear system of partial differential equations (3.12) and (3.13), subject to the boundary conditions (3.14) were solved numerically using an efficient, implicit finite-difference method known as the Keller-box scheme for convective boundary conditions with several parameters considered, namely the magnetic parameter M , the radiation parameter N_R , the Prandtl number Pr , the conjugate parameter γ and the coordinate running along the surface of the sphere, x . The numerical solutions start at the lower stagnation point of the sphere, $x \approx 0$, with initial profiles as given by the nonlinear ordinary differential equations (3.15) and (3.17), and proceed around the sphere up to 120° . The values of Pr considered are $Pr = 0.7, 1, 7$ and 100 . It is worth mentioning that small values of Pr ($\ll 1$) physically correspond to liquid metals, which have high thermal conductivity but low viscosity, while large values of Pr ($\gg 1$),

correspond to high-viscosity oils. It is also important to note that specifically, the Prandtl number considered in this study, namely $Pr = 0.7, 1, 7$ and 100 correspond to air, electrolyte solution such as salt water, water and engine oil respectively.

Table 3.1 shown the values of the heat transfer coefficient $-(\partial\theta/\partial y)(x,0)$ at the lower stagnation point of the sphere, $x \approx 0$, when $Pr = 0.7, 7$, without the effect of radiation and magnetohydrodynamic when $\gamma \rightarrow \infty$. In order to verify the accuracy of the present method, the present results are compared with those reported by Huang and Chen (1987) and Nazar et al. (2002a). It is found that the agreement between the previously published results with the present ones is excellent.

Tables 3.2, 3.3, 3.5 and 3.6 show the values of the local heat transfer coefficient, $Q_w(x)$, local Nusselt number N_u and the skin friction coefficient, C_f for various values of x when $Pr = 0.7, 1, 7, 100$, $M = 0, 5$, $N_R = 0, 3$ and $\gamma = 0.1$, respectively. It is found that as Pr increases, the values of $Q_w(x)$ and N_u increases and C_f decrease. On the other hand, for fixed Pr , as x increases, the values of $Q_w(x)$ and N_u decreased and C_f increased. From Tables 3.2 and 3.6, it showed that the values of $Q_w(x)$ and N_u is significantly higher at $x = 0^\circ$ than those at $x = 90^\circ$ and 120° because the sphere temperature is almost equal to fluid temperature at $x = 0^\circ$, and has a different value when $0^\circ < x \leq 90^\circ$ and $0^\circ < x \leq 120^\circ$. From Tables 3.3 and 3.7, it is found that the value of $C_f = 0$ at $x = 0^\circ$, because at this point, the value of the wall shear stress τ_w is very small. On the other hand, the maximum value of C_f appears when $x = 90^\circ$ and $x = 120^\circ$, because in this case, the value of τ_w is very high. From our numerical solutions, the reasons why we decided to stop the calculations at $x = 90^\circ$ for $M \neq 0$, $N_R \neq 0$ or $x = 120^\circ$ for $M = N_R = 0$ are because (1) starting from $x = 90^\circ$ or 120° , transition flow to turbulent flow or boundary separation will probably occur. (2) the values at $x = 90^\circ$ or $x = 120^\circ$ is the better values to computed values since it is $1/2$ or $2/3$ of 180° , respectively, compared to 125° , 130° , etc. (3) The values are physically unstable after $x = 90^\circ$ or 120° (see Nazar, 2003).

Table 3.4 shows the values of the wall temperature $\theta(x,0)$, the heat transfer coefficient $-(\partial\theta/\partial y)(x,0)$ and the skin friction coefficient $(\partial^2 f/\partial y^2)(x,0)$ at the lower stagnation point of the sphere, $x \approx 0$, for various values of N_R when $Pr = 0.7$, $\gamma = 0.1$ and $M = 0.5$. It is observed that, when the magnetic parameter M is fixed, an increase in the radiation parameter N_R causes the values of $\theta(x,0)$, $-(\partial\theta/\partial y)(x,0)$ and $(\partial^2 f/\partial y^2)$ to increase. Also when N_R is fixed and M increases, the value of $\theta(x,0)$, increases and the values of $(\partial^2 f/\partial y^2)(x,0)$ and $-(\partial\theta/\partial y)(x,0)$ decrease.

Figure 3.2 illustrates the variation of the wall temperature $\theta(x,0)$ with conjugate parameter γ when $Pr = 0.7, 7, 100$ and $M = 0$, and $N_R = 0$. From this graph, the critical value of γ and γ_c is 0.3766 when $Pr = 0.7$, 0.5971 when $Pr = 7$, and 0.6892 when $Pr = 100$. Besides, to get a physically acceptable solution, γ must be less than or equals to some critical value, say γ_c , i.e. $\gamma \leq \gamma_c$, depending on Pr .

The graphs of $\theta(x,0)$ for some values of the Prandtl number Pr when $\gamma = 0.05, 0.1, 0.2$ at $M = 0, N_R = 0$ are plotted in Figure 3.3. It is found that, as the Pr increases, the wall temperature $\theta(x,0)$ decreases, and $\theta(x,0)$ increases as γ increases. For small values of $Pr \ll 1$, the difference of value changing is higher than for large values of $Pr \gg 1$, and it is seen that the surface temperature is very sensitive to the Prandtl number variations.

Figures 3.4, 3.5, 3.14 and 3.15 display the temperature and velocity profiles, respectively, at $x = 0^\circ, 60^\circ, 90^\circ$ when $Pr = 0.7, 7, 100, M = 0, 5, N_R = 0, 1$ and $\gamma = 0.1$, respectively. It is found that as when x is fixed and Pr increases, the temperature and velocity decrease as well as the thermal boundary layer thickness. This is because for small values of the $Pr (\ll 1)$, the fluid is highly conductive. Physically, if Pr increases, the thermal diffusivity decreases and this phenomenon lead to the decreasing manner of the energy transfer ability that reduces the thermal boundary layer. On the other hand, in the same figure it has been found that when Pr is fixed and x increases, the temperature, velocity and the thermal boundary layer thickness increase.

Variation of the local heat transfer coefficient $Q_w(x)$ and the local skin friction coefficient C_f with various values of x when $Pr = 0.7, 7, 100, M = 0, N_R = 0$ and $\gamma = 0.1$ are plotted in Figures 3.6 and 3.7, respectively. It is found that as Pr increases, the local heat transfer coefficient also increases and the local skin friction coefficient decreases.

Figure 3.8 and 3.9 illustrates the variation of the wall temperature $\theta(x,0)$, with radiation parameter N_R and magnetic parameter M when $M = 5, N_R = 3, Pr = 0.7$, and $\gamma = 0.05, 0.1, 0.2$ respectively. It is found that the increasing value of M, N_R and the parameter γ caused the increasing value of wall temperature $\theta(x,0)$.

Figures 3.10 and 3.11 show the temperature $\theta(0,y)$ and velocity $(\partial f / \partial y)(0,y)$, profiles when $Pr = 7, M = 5, N_R = 0, 1, 3, 5$ and $\gamma = 0.1$, respectively. It is found that as N_R increases, the temperature and velocity increases, which means that higher radiation occurs for higher values of temperature that cause the increase of velocity as well.

The temperature $\theta(0,y)$ and velocity profiles $(\partial f / \partial y)(0,y)$, are presented in Figures 3.12 and 3.13, respectively, when $Pr = 0.7, N_R = 1, M = 5, 10, 15$ and $\gamma = 0.1$ show that when the value of M increases, it is found that the temperature also increase but the velocity decreases. This behavior is in accordance with the physical observation that the application of transverse magnetic field always results in a resistive type force also called Lorentz force.

Variation of the local Nusselt number N_u and the local friction coefficient C_f with various values of x when $Pr = 0.7, N_R = 1, M = 5, 10, 15$ and $\gamma = 0.1$ are plotted in Figures 3.16 and 3.17, respectively. It is found that as M increases, both values of local Nusselt number and the local skin friction coefficient decrease.

Figures 3.18 and 3.19 display the local Nusselt number N_u and the local friction coefficient C_f with various values of x when $Pr = 0.7, M = 5, N_R = 0, 1, 3, 5$ and $\gamma = 0.1$, respectively. It is found that as N_R increases, both values of local Nusselt

number and the local skin friction coefficient also increase so the effect of radiation parameter on local Nusselt number is more than on local skin friction coefficient.

Table 3.1: The heat transfer coefficient $-(\partial\theta/\partial y)(x, 0)$ at the lower stagnation point of the sphere, $x \approx 0$, when $Pr = 0.7$ and 7 , without the effect of radiation and magnetohydrodynamic and $\gamma \rightarrow \infty$

Pr	0.7			7		
	Huang and Chen (1987)	Nazar et al. (2002a)	Present	Huang and Chen (1987)	Nazar et al. (2002a)	Present
	0.4574	0.4576	0.457582	0.9581	0.9595	0.959498

Table 3.2: The local heat transfer coefficient $Q_w(x)$ for various values of x when $Pr = 0.7, 7, 100, M = 0, N_R = 0$ and $\gamma = 0.1$

Pr	0.7	7	100
x			
0°	0.083615	0.089018	0.092998
10°	0.083420	0.088868	0.092982
20°	0.083366	0.088832	0.092960
30°	0.083256	0.088769	0.092920
40°	0.083098	0.088673	0.092863
50°	0.082892	0.088551	0.092786
60°	0.082638	0.088400	0.092678
70°	0.082311	0.088213	0.092549
80°	0.081906	0.088005	0.092392
90°	0.081409	0.087735	0.092204
100°	0.080795	0.087446	0.091969
110°	0.080060	0.087112	0.091704
120°	0.079085	0.086677	0.091356

Table 3.3: The local skin friction coefficient C_f for various values of x
when $Pr = 0.7, 7, 100, M = 0, N_R = 0$ and $\gamma = 0.1$

Pr	0.7	7	100
x			
0°	0.000000	0.000000	0.000000
10°	0.024339	0.010401	0.003838
20°	0.047659	0.020366	0.007516
30°	0.071418	0.030349	0.011241
40°	0.094013	0.040072	0.014760
50°	0.115443	0.049131	0.018063
60°	0.135174	0.057400	0.021113
70°	0.153510	0.064763	0.023958
80°	0.169912	0.071107	0.026411
90°	0.184092	0.076146	0.028611
100°	0.195770	0.080327	0.030327
110°	0.204355	0.083037	0.031600
120°	0.209970	0.084369	0.032472

Table 3.4: The wall temperature $\theta(x,0)$, the heat transfer coefficient $-(\partial\theta/\partial y)(x,0)$
and the skin friction coefficient $(\partial^2 f/\partial y^2)(x,0)$ at the lower stagnation point of
the sphere, $x \approx 0$, for various values of N_R when $Pr = 0.7, M = 0, 5$ and $\gamma = 0.1$

N_R	$M = 0$			$M = 5$		
	$\theta(x,0)$	$-(\partial\theta/\partial y)$	$(\partial^2 f/\partial y^2)$	$\theta(x,0)$	$-(\partial\theta/\partial y)$	$(\partial^2 f/\partial y^2)$
0	0.238051	0.076195	0.260067	0.333977	0.066602	0.135855
1	0.285971	0.166607	0.333039	0.368856	0.147266	0.152026
2	0.311935	0.252290	0.371648	0.381992	0.226602	0.158119
3	0.328807	0.335597	0.396153	0.388949	0.305525	0.161346
4	0.340704	0.417554	0.413230	0.393268	0.384264	0.163349
5	0.349603	0.498638	0.425880	0.396232	0.462889	0.164722

Table 3.5: The local Nusselt number N_u for various values of x when $Pr = 1, 7$,

$$N_R = 3, M = 5 \text{ and } \gamma = 0.1$$

Pr	1	7
x		
0°	0.355676	0.396587
10°	0.355202	0.397462
20°	0.354661	0.396903
30°	0.353700	0.396008
40°	0.352421	0.394728
50°	0.350494	0.393054
60°	0.348294	0.390930
70°	0.345596	0.388080
80°	0.342404	0.384589
90°	0.338685	0.380433

Table 3.6: The local skin friction coefficient C_f for various values of x when $Pr = 1, 7$,

$$\gamma = 0.1, N_R = 3 \text{ and } M = 5$$

Pr	1	7
x		
0°	0.000000	0.000000
10°	0.020149	0.013344
20°	0.039303	0.026085
30°	0.058684	0.039092
40°	0.076283	0.050971
50°	0.091763	0.062019
60°	0.105630	0.071563
70°	0.117070	0.080116
80°	0.125645	0.087229
90°	0.131096	0.092433

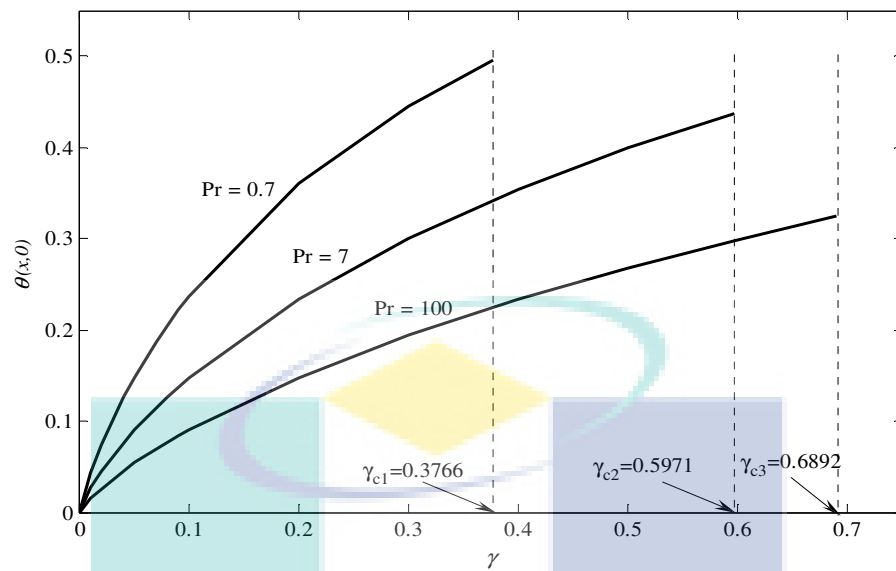


Figure 3.2: The wall temperature $\theta(x,0)$ with conjugate parameter γ when $Pr = 0.7, 7, 100, M = 0$ and $N_R = 0$

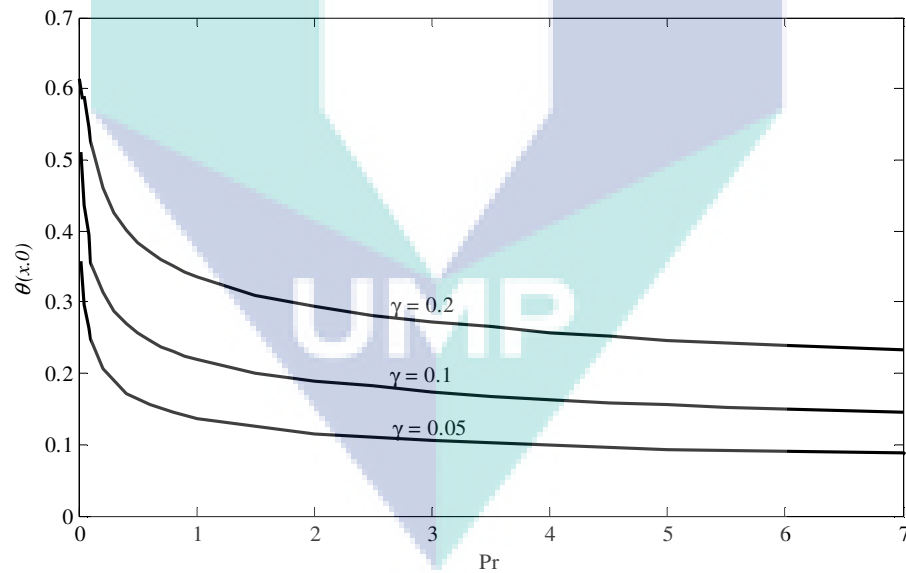


Figure 3.3: The wall temperature $\theta(x,0)$ with Prandtl number Pr when $M = 0, N_R = 0$ and $\gamma = 0.05, 0.1, 0.2$

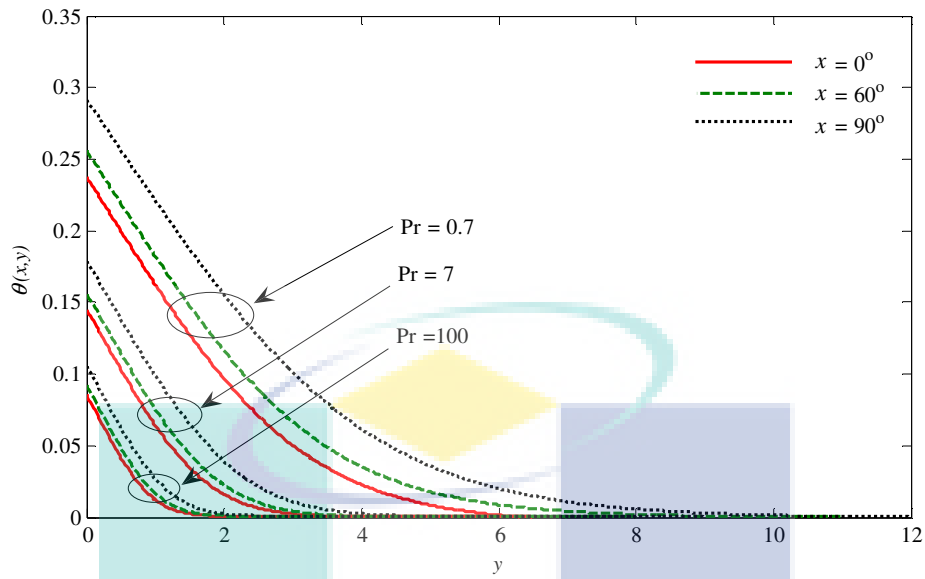


Figure 3.4: Temperature profiles $\theta(x, y)$ at $x = 0^\circ, 60^\circ, 90^\circ$ when $Pr = 0.7, 7, 100$,
 $M = 0, N_R = 0$ and $\gamma = 0.1$

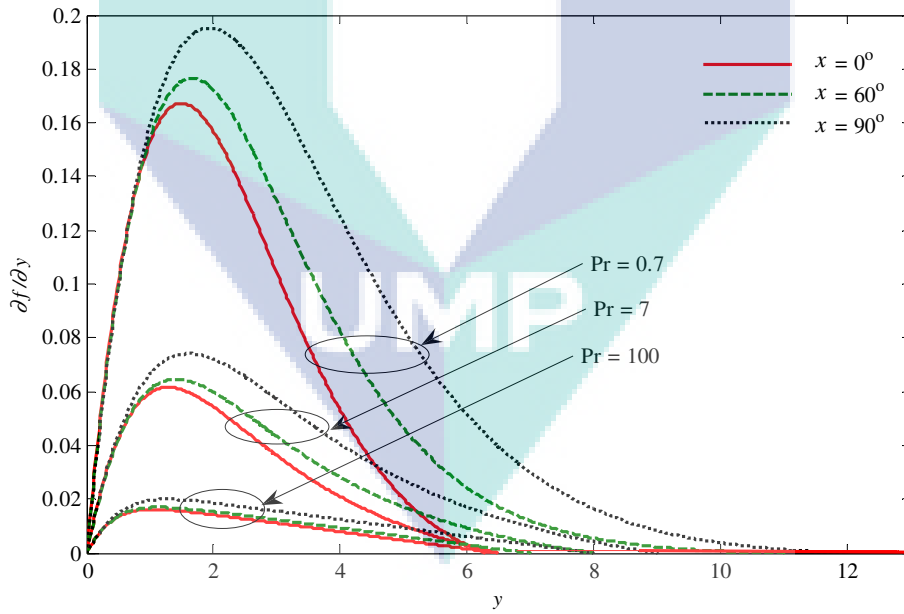


Figure 3.5: Velocity profiles $(\partial f / \partial y)(x, y)$ at $x = 0^\circ, 60^\circ, 90^\circ$ when $Pr = 0.7, 7, 100$,
 $M = 0, N_R = 0$ and $\gamma = 0.1$

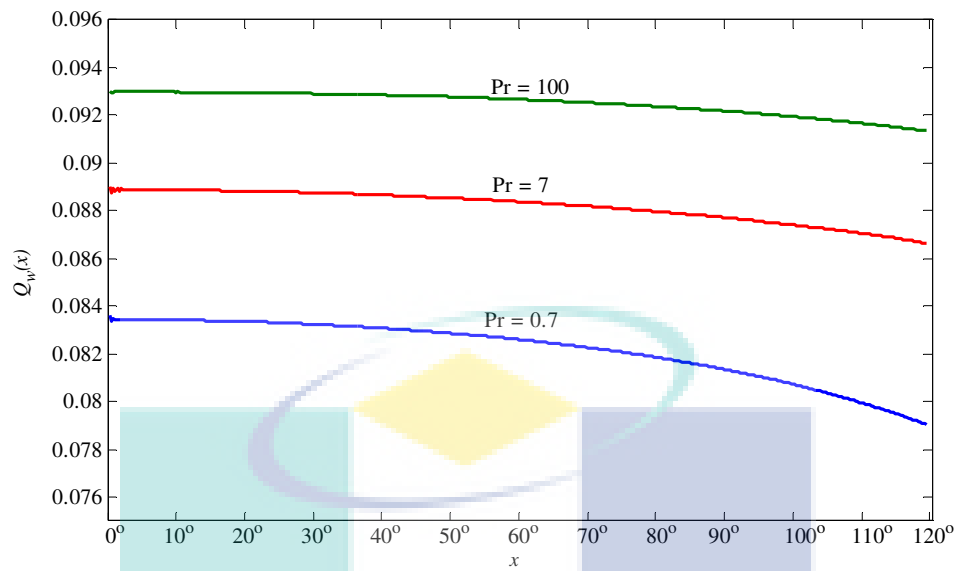


Figure 3.6: The local heat transfer coefficient with x when $Pr = 0.7, 7, 100$, $M = 0$, $N_R = 0$ and $\gamma = 0.1$

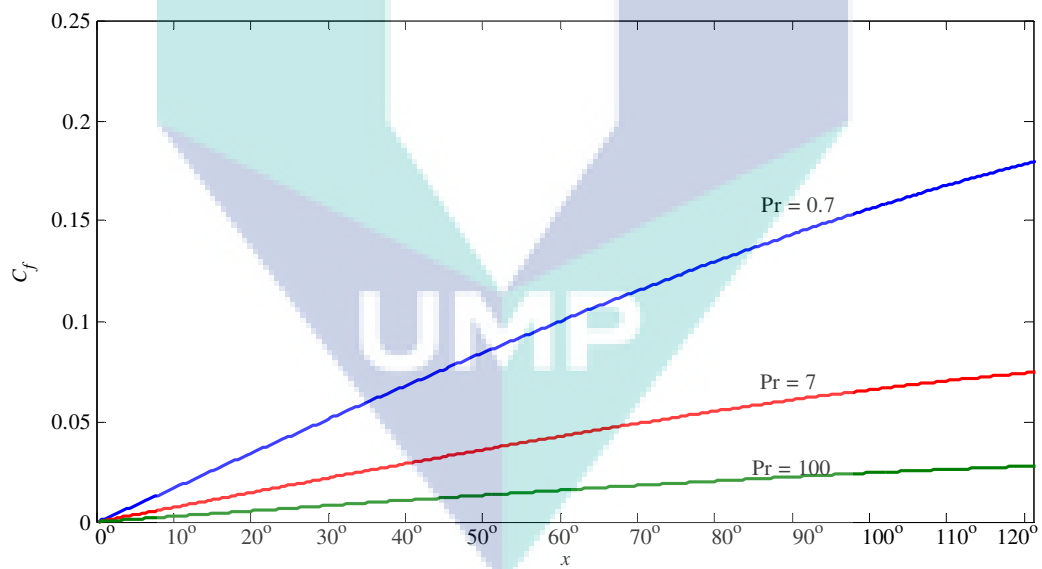


Figure 3.7: The skin friction coefficient C_f with x when $Pr = 0.7, 7, 100$ and $M = 0$, $N_R = 0$ and $\gamma = 0.1$

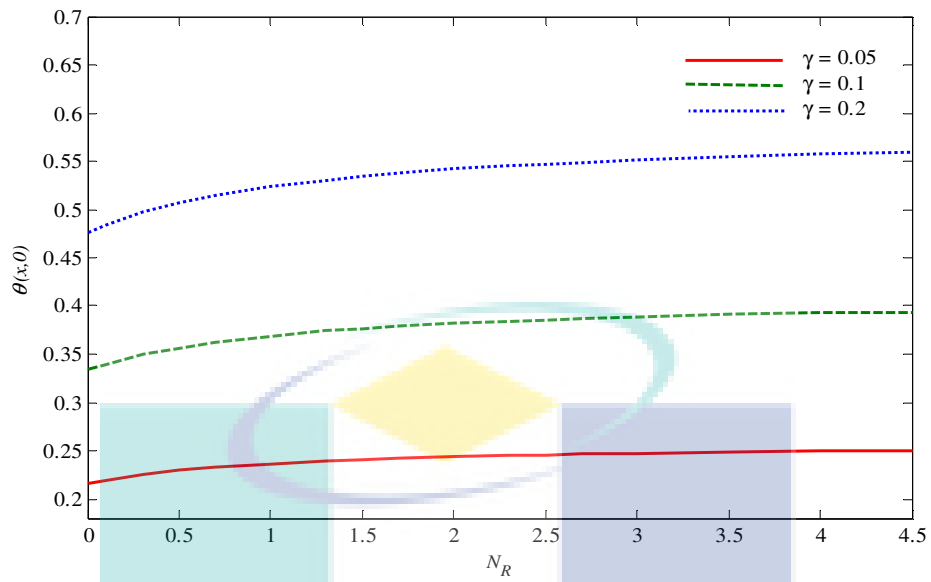


Figure 3.8: The wall temperature $\theta(x,0)$, with N_R when $Pr = 0.7$, $M = 5$ and $\gamma = 0.05, 0.1, 0.2$

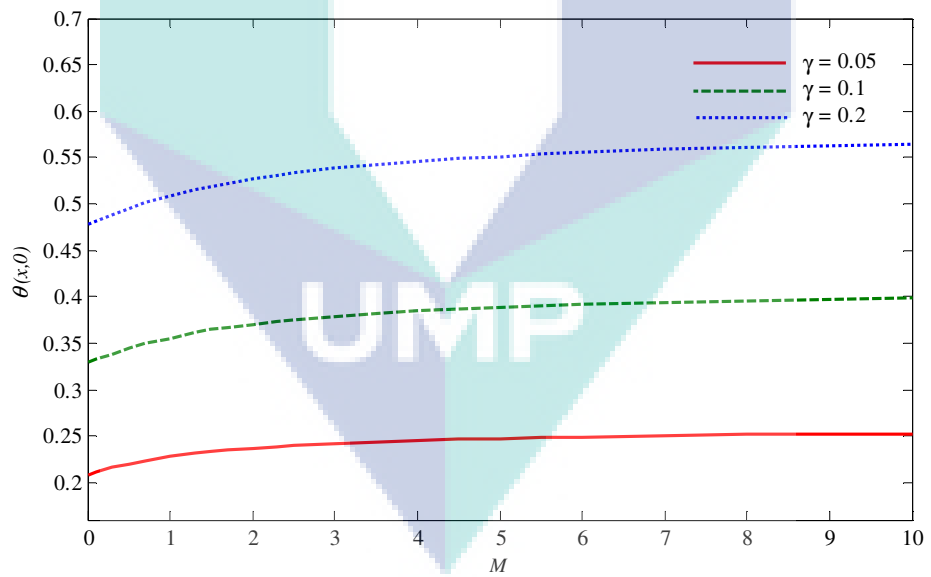


Figure 3.9: The wall temperature $\theta(x,0)$, with M when $Pr = 0.7$, $N_R = 3$ and $\gamma = 0.05, 0.1, 0.2$

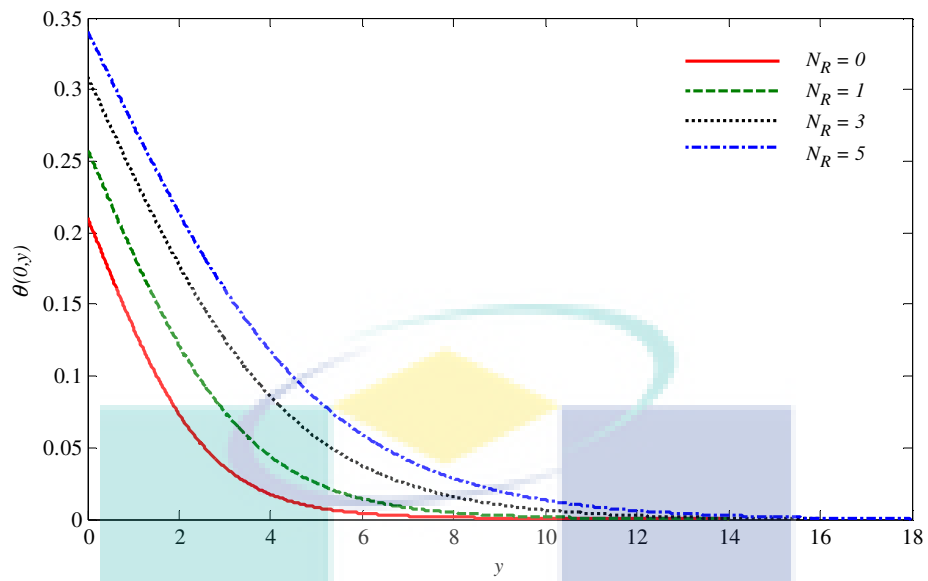


Figure 3.10: The temperature profiles $\theta(0, y)$ when $Pr = 7$, $M = 5$, $N_R = 0, 1, 3, 5$ and $\gamma = 0.1$

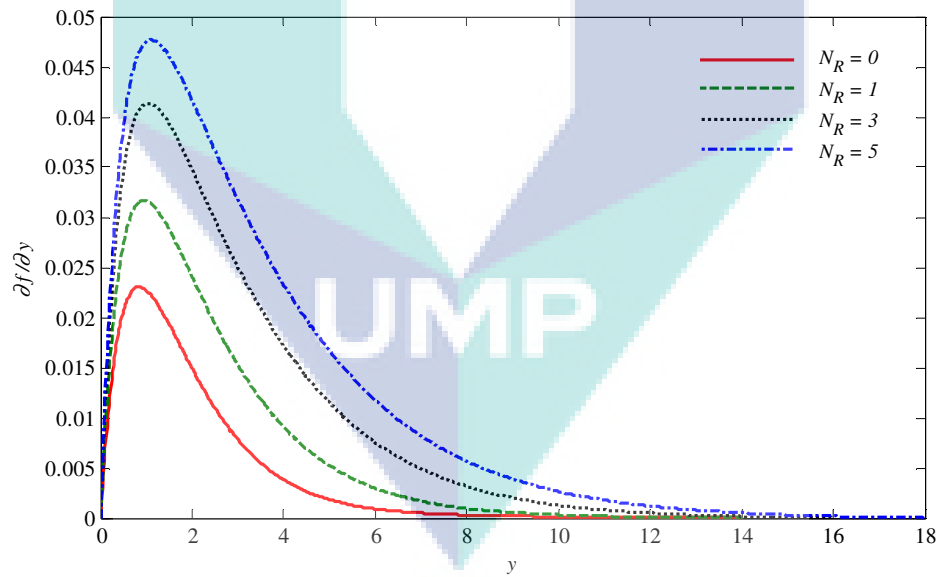


Figure 3.11: The velocity profiles $(\partial f / \partial y)(0, y)$ when $Pr = 7$, $M = 5$, $N_R = 0, 1, 3, 5$ and $\gamma = 0.1$

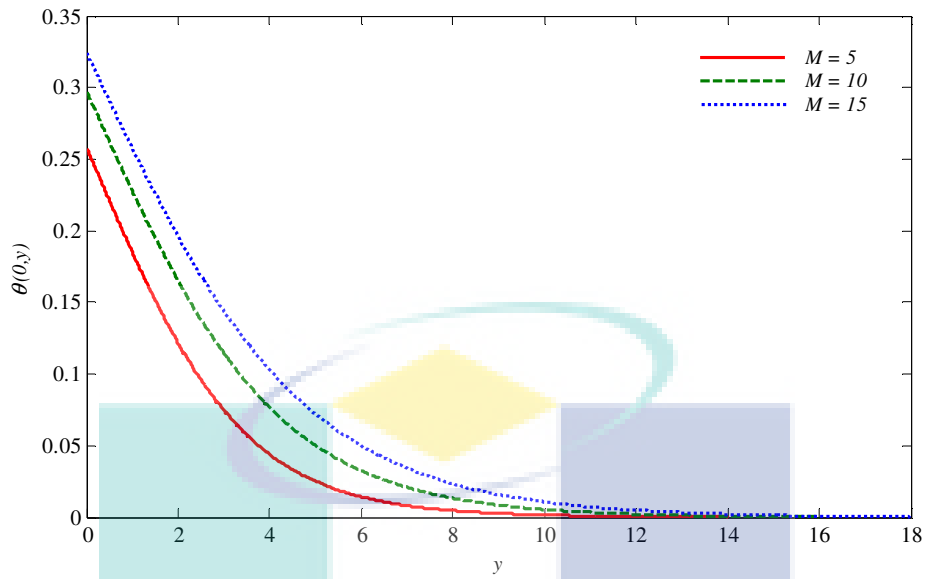


Figure 3.12: The temperature profiles $\theta(0, y)$ when $\text{Pr} = 7$, $N_R = 1$, $M = 5, 10, 15$ and $\gamma = 0.1$

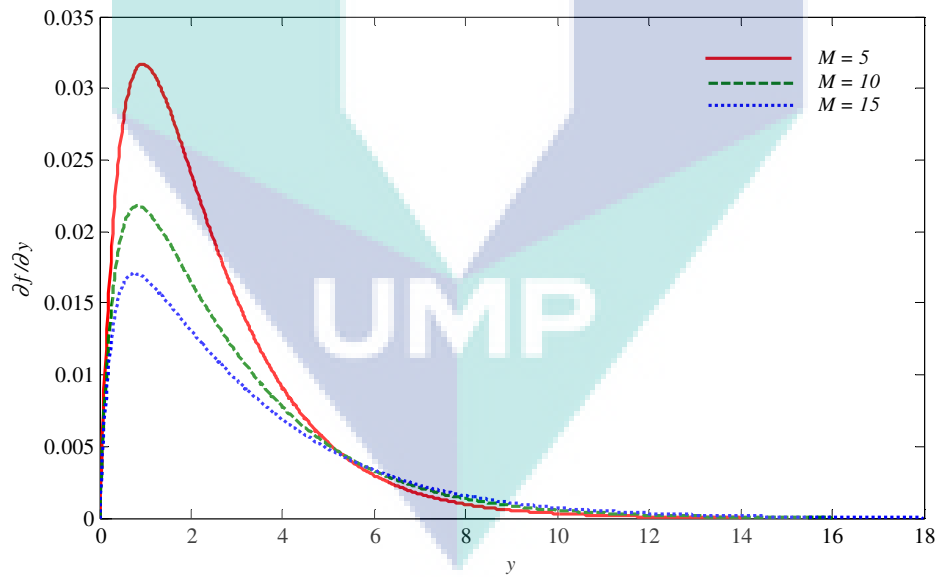


Figure 3.13: The velocity profiles $(\partial f / \partial y)(0, y)$ when $\text{Pr} = 7$, $N_R = 1$, $M = 5, 10, 15$ and $\gamma = 0.1$

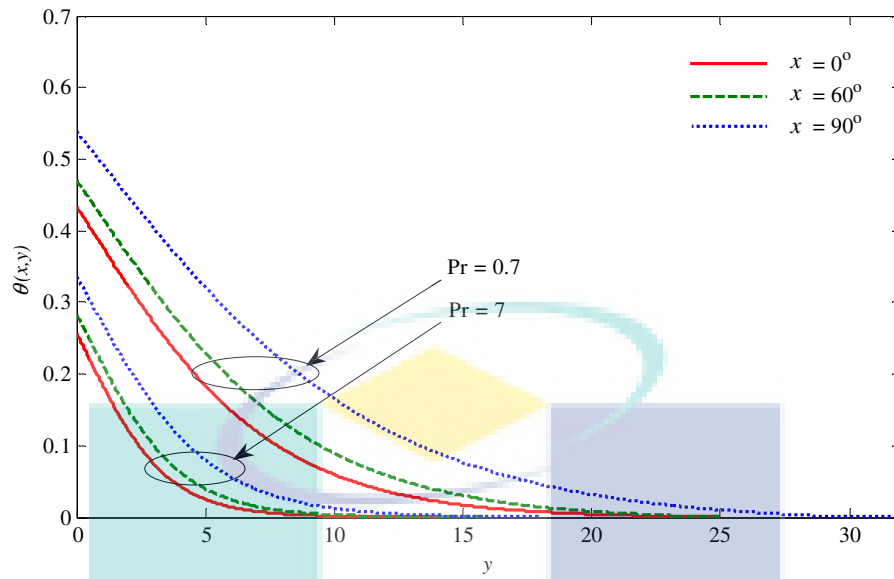


Figure 3.14: The temperature profiles $\theta(x, y)$ at $x = 0^\circ, 60^\circ, 90^\circ$ when $Pr = 0.7, 7$,
 $N_R = 1, M = 5$ and $\gamma = 0.1$

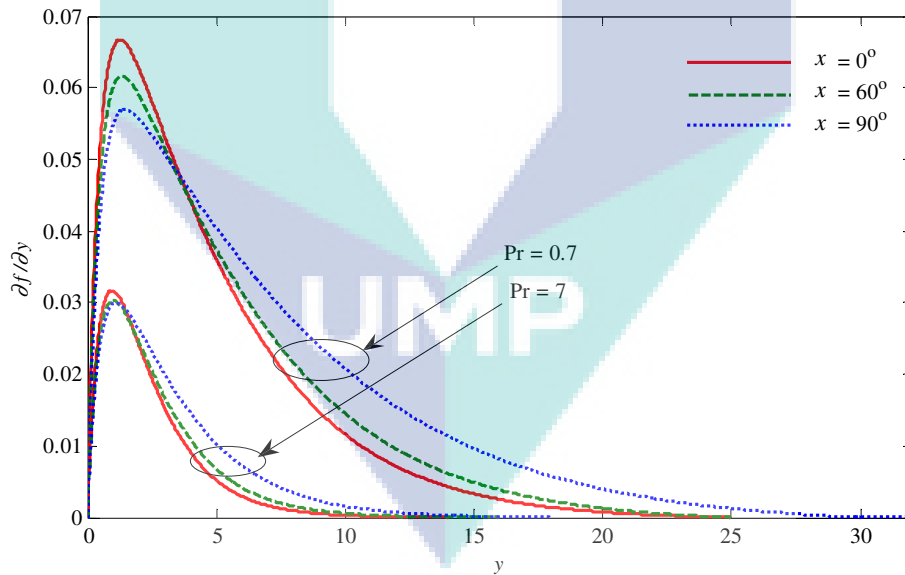


Figure 3.15: The velocity profiles $(\partial f / \partial y)(x, y)$, at $x = 0^\circ, 60^\circ, 90^\circ$ when $Pr = 0.7, 7$,
 $N_R = 1, M = 5$ and $\gamma = 0.1$

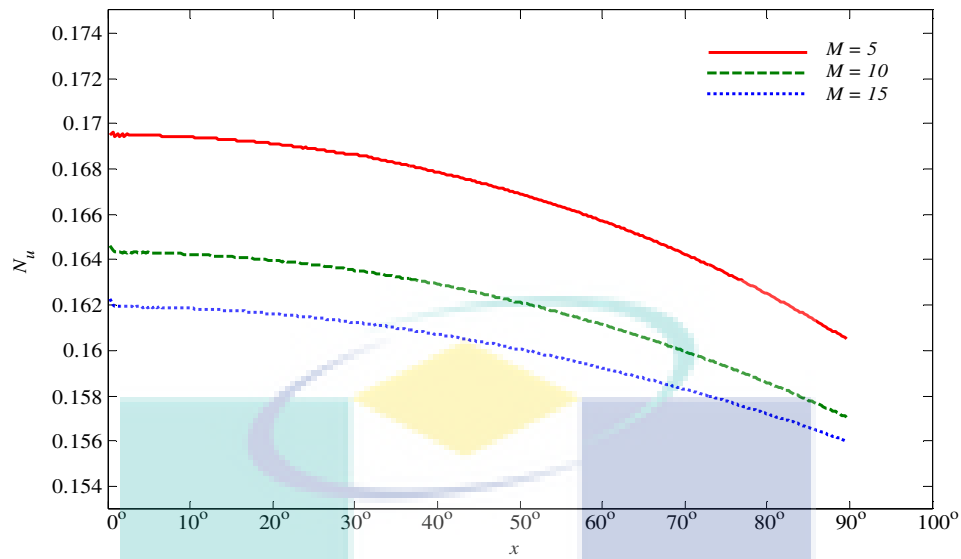


Figure 3.16: The local Nusselt number N_u with x when $Pr = 0.7$, $N_R = 1$, $M = 5, 10, 15$ and $\gamma = 0.1$

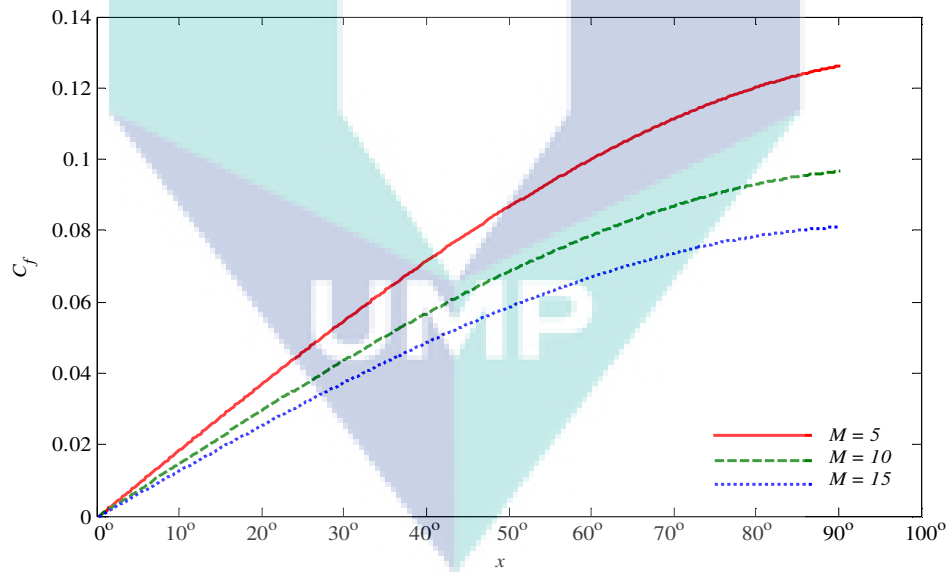


Figure 3.17: The skin friction coefficient C_f with x when $Pr = 0.7$, $N_R = 1$, $M = 5, 10, 15$ and $\gamma = 0.1$

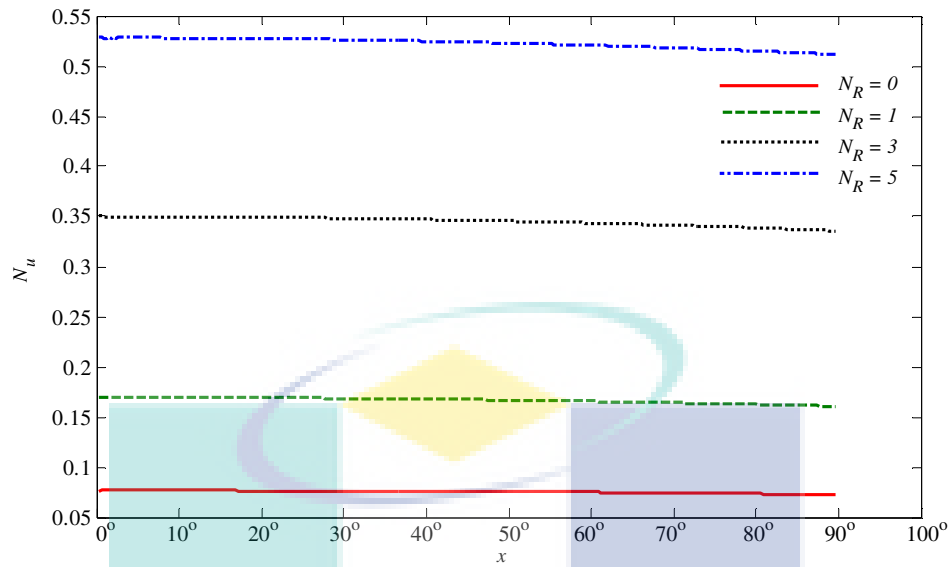


Figure 3.18: The local Nusselt number N_u with x when $Pr = 0.7$, $M = 5$, $N_R = 0, 1, 3, 5$ and $\gamma = 0.1$

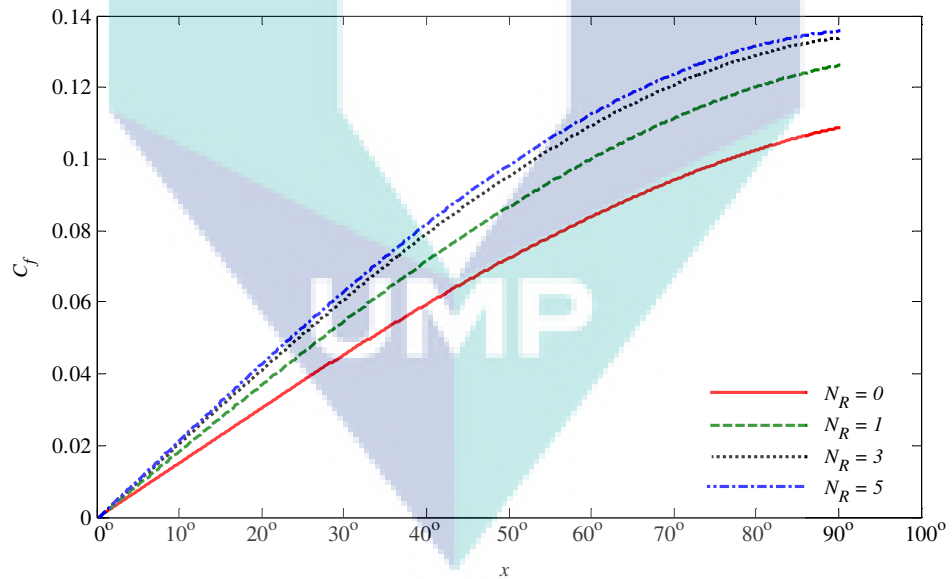


Figure 3.19: The skin friction coefficient C_f with x when $Pr = 0.7$, $M = 5$, $N_R = 0, 1, 3, 5$ and $\gamma = 0.1$

3.4 CONCLUSIONS

In this chapter, we have studied the problem of the effect of radiation on magnetohydrodynamic free convection boundary layer flow over a solid sphere in viscous fluids with convective boundary conditions. We are interested to see how the Prandtl number Pr , the magnetic parameter M and the radiation parameter N_R affect the flow and heat transfer characteristics. The transformed boundary layer equations in the form of partial differential equations are solved numerically using the Keller-box method. We can conclude that:

- When Pr , γ and M are fixed, as N_R increases, the temperature, velocity and skin friction coefficient decreases and the heat transfer coefficient increases. When Pr , γ and N_R are fixed, as M increases, the value of temperature increases and the velocity, skin friction coefficient and heat transfer coefficient decrease.
- When Pr , γ , N_R and M are fixed, as x increases, the local Nusselt number N_u and the local heat transfer coefficient $Q_w(x)$ decrease on the interval $0^\circ \leq x \leq 120^\circ$, but the local friction coefficient C_f increases on the same interval. If x , γ , N_R , and M are fixed as Pr increases, the values of the local Nusselt number N_u and the local heat transfer coefficient $Q_w(x)$ increase but the local friction coefficient C_f decrease.
- When Pr , γ , N_R and M are fixed, as x increases, the temperature and velocity increase, but when x , γ , N_R and M are fixed and Pr increases, the temperature and velocity decrease.
- When Pr , γ , and N_R are fixed, as M increases, both values of local Nusselt number and the local skin friction coefficient decreases and if Pr , γ and M are fixed, as N_R increases, the local Nusselt number increases but the local skin friction coefficient decrease.
- To get a physically acceptable solution, γ must be less than γ_c depending on Pr .

CHAPTER 4

THE EFFECT OF RADIATION ON MAGNETOHYDRODYNAMIC FREE CONVECTION BOUNDARY LAYER FLOW OVER A SOLID SPHERE IN A MICROPOLAR FLUID

4.1 INTRODUCTION

In this chapter, the problem of the effect of radiation on magnetohydrodynamic free convection boundary layer flow over a solid sphere in a micropolar fluid with convective boundary conditions is considered and discussed. The papers related to this problem but without the effect of radiation and magnetohydrodynamic have been investigated by Nazar et al. (2002a; 2002b) and Salleh et al. (2012a) where they studied the free convection boundary layer flows on a sphere in a micropolar fluid with constant heat flux, constant wall temperature and Newtonian heating, respectively. The natural convection heat and mass transfer from a sphere in micropolar fluid with constant wall temperature and concentration was presented by Cheng (2008).

The basic equations of boundary layer flow, which are transformed into a non-dimensional form and reduced to nonlinear systems of partial differential equations are solved numerically using an implicit finite difference scheme known as the Keller-box method.

The effect of the magnetic parameter M , the radiation parameter N_R , the micropolar parameter K , the Prandtl number Pr and the conjugate parameter γ on the local wall temperature, the local heat transfer coefficient, the local Nusselt number and the local skin friction coefficient, as well as the temperature, velocity and angular velocity profiles are illustrated through graphs and tables.

4.2 MATHEMATICAL FORMULATION

The flow of the fluid in this present problem is moving past a heated soled sphere of radius a , which is immersed in a incompressible micropolar fluid of ambient temperature, T_∞ . All assumptions considered are remained the same with previous problem in Chapter 3. By using continuity equation (2.5) and the energy equation (3.2) under the Boussinesq and boundary layer approximations, the momentum and angular momentum equations are

$$\bar{u} \frac{\partial \bar{u}}{\partial \bar{x}} + \bar{v} \frac{\partial \bar{u}}{\partial \bar{y}} = \frac{(\mu + \kappa)}{\rho} \frac{\partial^2 \bar{u}}{\partial \bar{y}^2} + g \beta (T - T_\infty) \sin\left(\frac{\bar{x}}{a}\right) + \frac{\kappa}{\rho} \frac{\partial \bar{H}}{\partial \bar{y}} - \frac{\sigma \beta^2}{\rho} \bar{u}, \quad (4.1)$$

$$\rho j \left(\bar{u} \frac{\partial \bar{H}}{\partial \bar{x}} + \bar{v} \frac{\partial \bar{H}}{\partial \bar{y}} \right) = -\kappa \left(2\bar{H} + \frac{\partial \bar{u}}{\partial \bar{y}} \right) + \varphi \frac{\partial^2 \bar{H}}{\partial \bar{y}^2}, \quad (4.2)$$

subject the boundary conditions of (Salleh et al., 2012a ; Aziz, 2009)

$$\begin{aligned} \bar{u} = \bar{v} = 0, \quad -k_f \frac{\partial T}{\partial \bar{y}} = h_f (T_f - T), \quad \bar{H} = -n \frac{\partial \bar{u}}{\partial \bar{y}} \quad \text{as } \bar{y} = 0, \\ \bar{u} \rightarrow 0, \quad T \rightarrow T_\infty, \quad H \rightarrow 0 \quad \text{as } \bar{y} \rightarrow \infty, \end{aligned} \quad (4.3)$$

where \bar{H} is the angular velocity of micropolar fluid, It is worth mentioning that in boundary conditions (4.5), n is a constant and $0 \leq n \leq 1$. The value $n = 0$, which indicates $\bar{H} = 0$ at the wall, represents concentrated particle flows in which the particle density is sufficiently great that microelements close to the wall are unable to rotate or called as “strong” concentration of microelements (Guram and Smith, 1980; Jena and Mathur, 1981). The case corresponding to $n = 1/2$ results in the vanishing of antisymmetric part of the stress tensor and represents “weak” concentration of microelements (Guram and Smith, 1980). In this case, the particle rotation is equal to fluid vorticity at the boundary for fine particle suspension. When $n = 1$, we have flows which are representative of turbulent boundary layer (Ahmadi, 1976). The case of $n = 1/2$ is considered in this study.

Let $\bar{r}(\bar{x})$ be the radial distance from the symmetrical axis to the surface of the sphere and φ is the spin gradient viscosity, which are given by

$$\bar{r}(\bar{x}) = a \sin(\bar{x}/a), \quad \varphi = (\mu + (\kappa/2))j. \quad (4.4)$$

We are now introduced the following non-dimensional variables see (Salleh, et al., 2012a and Aziz, 2009):

$$x = \frac{\bar{x}}{a}, \quad y = Gr^{1/4} \left(\frac{\bar{y}}{a} \right), \quad r = \frac{\bar{r}}{a},$$

$$u = \left(\frac{a}{\nu} \right) Gr^{-1/2} \bar{u}, \quad v = \left(\frac{a}{\nu} \right) Gr^{-1/4} \bar{v}, \quad H = \left(\frac{a^2}{\nu} \right) Gr^{-3/4} \bar{H},$$

$$\theta = \frac{T - T_\infty}{T_f - T_\infty}, \quad (4.5)$$

where $Gr = g\beta(T_f - T_\infty) \frac{a^3}{\nu^2}$ is the Grashof number for convective boundary conditions, respectively. Using the Rosseland approximation for radiation the radiative heat flux is simplified as in equations (3.5) and (3.6).

Substituting variables (3.5), (3.6), (4.4) and (4.5) into (3.2), (4.1) and (4.2) then become

$$u \frac{\partial u}{\partial x} + v \frac{\partial u}{\partial y} = (1 + K) \frac{\partial^2 u}{\partial y^2} + \theta \sin x - Mu + K \frac{\partial H}{\partial y}, \quad (4.6)$$

$$u \frac{\partial \theta}{\partial x} + v \frac{\partial \theta}{\partial y} = \frac{1}{Pr} \left(1 + \frac{4}{3} N_R \right) \frac{\partial^2 \theta}{\partial y^2}, \quad (4.7)$$

$$u \frac{\partial H}{\partial x} + v \frac{\partial H}{\partial y} = -K \left(2H + \frac{\partial u}{\partial y} \right) + \left(1 + \frac{K}{2} \right) \frac{\partial^2 H}{\partial y^2}, \quad (4.8)$$

where $K = \frac{\kappa}{\mu}$ is the material or micropolar parameter, $Pr = \frac{\nu}{\alpha}$ is the Prandtl number,

$M = \frac{\sigma\beta^2 a^2}{\nu\rho Gr^{1/2}}$ is the magnetic parameter and $N_R = \frac{4\sigma^* T_\infty^3}{\alpha k^* \rho c_p}$ is the radiation parameter.

The boundary conditions (4.3) become

$$u = v = 0, \quad \frac{\partial \theta}{\partial y} = -\gamma(1 - \theta), \quad H = -\frac{1}{2} \frac{\partial u}{\partial y} \quad \text{at } y = 0,$$

$$u \rightarrow 0, \quad \theta \rightarrow 0, \quad H \rightarrow 0 \quad \text{as } y \rightarrow \infty, \quad (4.9)$$

where $\gamma = ah_f Gr^{-1/4} / k_f$ is the conjugate parameter for convective boundary conditions.

To solve equations (4.6) to (4.8), subjected to the boundary conditions (4.9), we assume the following variables:

$$\psi = xr(x)f(x, y), \quad \theta = \theta(x, y), \quad H = xh(x, y), \quad (4.10)$$

where ψ is the stream function defined as

$$u = \frac{1}{r} \frac{\partial \psi}{\partial y} \quad \text{and} \quad v = -\frac{1}{r} \frac{\partial \psi}{\partial x}, \quad (4.11)$$

which satisfies the continuity equation (2.17). Thus, (4.6) to (4.8) become

$$(1+K) \frac{\partial^3 f}{\partial y^3} + (1+x \cot x) f \frac{\partial^2 f}{\partial y^2} - \left(\frac{\partial f}{\partial y} \right)^2 + \frac{\sin x}{x} \theta - M \frac{\partial f}{\partial y} + K \frac{\partial h}{\partial y} = x \left(\frac{\partial f}{\partial y} \frac{\partial^2 f}{\partial x \partial y} - \frac{\partial f}{\partial x} \frac{\partial^2 f}{\partial y^2} \right), \quad (4.12)$$

$$\frac{1}{\text{Pr}} \left(1 + \frac{4}{3} N_R \right) \frac{\partial^2 \theta}{\partial y^2} + (1+x \cot x) f \frac{\partial \theta}{\partial y} = x \left(\frac{\partial f}{\partial y} \frac{\partial \theta}{\partial x} - \frac{\partial f}{\partial x} \frac{\partial \theta}{\partial y} \right), \quad (4.13)$$

$$\left(1 + \frac{K}{2} \right) \frac{\partial^2 h}{\partial y^2} + (1+x \cot x) f \frac{\partial h}{\partial y} - \frac{\partial f}{\partial y} h - K \left(2h + \frac{\partial^2 f}{\partial y^2} \right) = x \left(\frac{\partial f}{\partial y} \frac{\partial h}{\partial x} - \frac{\partial f}{\partial x} \frac{\partial h}{\partial y} \right), \quad (4.14)$$

subject to the boundary conditions

$$f = \frac{\partial f}{\partial y} = 0, \quad \frac{\partial \theta}{\partial y} = -\gamma(1-\theta), \quad h = -\frac{1}{2} \frac{\partial^2 f}{\partial y^2} \quad \text{at } y = 0,$$

$$\frac{\partial f}{\partial y} \rightarrow 0, \quad \theta \rightarrow 0, \quad h \rightarrow 0 \quad \text{as } y \rightarrow \infty \quad (4.15)$$

It can be seen that at the lower stagnation point of the sphere, ($x \approx 0$), equations (4.12) to (4.14) reduce to the following ordinary differential equations

$$(1+K) f''' + 2ff'' - f'^2 + \theta - Mf' + Kh' = 0, \quad (4.16)$$

$$\frac{1}{\text{Pr}} \left(1 + \frac{4}{3} N_R \right) \theta'' + 2f\theta' = 0, \quad (4.17)$$

$$\left(1 + \frac{K}{2}\right) h'' + 2f h' - f' h - K(2h + f'') = 0. \quad (4.18)$$

The boundary conditions (4.15) become

$$f(0) = f'(0) = 0, \quad \theta'(0) = -\gamma(1 - \theta(0)), \quad h(0) = -\frac{1}{2} f''(0),$$

$$f' \rightarrow 0, \quad \theta \rightarrow 0, \quad h \rightarrow 0 \quad \text{as } y \rightarrow \infty \quad (4.19)$$

The physical quantities of interest in this problem are the local skin friction coefficient C_f , the local Nusselt number N_u and the local heat transfer coefficient $Q_w(x)$ which are given by

$$C_f = \left(1 + \frac{K}{2}\right) x \frac{\partial^2 f}{\partial y^2}(x, 0), \quad N_u = \gamma \left(1 + \frac{4}{3} N_R\right) (1 - \theta(x, 0)),$$

and

$$Q_w(x) = \gamma(1 - \theta(x, 0)) \quad (4.20)$$

4.3 RESULTS AND DISCUSSION

The parameters considered in this chapter, namely, the micropolar parameter K , the magnetic parameter M , the radiation parameter N_R , the Prandtl number Pr , the conjugate parameter γ and the coordinate running along the surface of the sphere, x .

The heat transfer coefficient $-(\partial\theta/\partial y)(x, 0)$ at the lower stagnation point of the sphere, $x \approx 0$, for various values of K when $Pr = 0.7$ and 7 , without the effect of radiation and magnetohydrodynamic when $\gamma \rightarrow \infty$ are shown in Table 4.1. In order to verify the accuracy of the present method, the present results are again compared with those reported by Huang and Chen (1987) and Nazar et al. (2002a). It is found that the agreement between the previously published results with the present ones is excellent. We can conclude that this method also works efficiently for the present problem and we are also confident that the results presented here are accurate.

Table 4.2 shows the values of the wall temperature, $\theta(x, 0)$ and the skin friction coefficient, $(\partial^2 f / \partial y^2)$ at the lower stagnation point of the sphere, $x \approx 0$, for various

values of K when $Pr = 0.7$, $M = 0$, $N_R = 0$ and $\gamma = 0.05, 0.1, 0.2$. It is found that for fixed γ , as K increases, the values of $\theta(x, 0)$ increase but the values of $(\partial^2 f / \partial y^2)(x, 0)$ decrease. Besides, it is found that for fixed K , as γ increases, both $\theta(x, 0)$ and $(\partial^2 f / \partial y^2)(x, 0)$ increase.

Tables 4.3 to 4.5 show the values of the wall temperature $\theta(x, 0)$, the heat transfer coefficient $-(\partial\theta/\partial y)(x, 0)$ and the skin friction coefficient $(\partial^2 f / \partial y^2)(x, 0)$ at the lower stagnation point of the sphere, $x \approx 0$, for various values of K when $Pr = 0.7, 1, 7$, $M = 0$, $N_R = 0$ and $\gamma = 0.1$. It is found that for fixed Pr , as K increases, the value of $\theta(x, 0)$ is also increase but the values of $-(\partial\theta/\partial y)(x, 0)$ and $(\partial^2 f / \partial y^2)(x, 0)$ decrease. Other than that, it is found that for fixed K , as Pr increases, both $\theta(x, 0)$ and $(\partial^2 f / \partial y^2)(x, 0)$ decreases but $-(\partial\theta/\partial y)(x, 0)$ increase. From these tables, the values of $\theta(x, 0)$ are higher for micropolar fluid ($K \neq 0$) than those for Newtonian fluid ($K = 0$) but the values of $-(\partial\theta/\partial y)(x, 0)$ and $(\partial^2 f / \partial y^2)(x, 0)$ are lower for micropolar fluid ($K \neq 0$) than those for Newtonian fluid ($K = 0$).

Tables 4.8 to 4.9 present the values of the local heat transfer coefficient $Q_w(x)$ and the local skin friction coefficient C_f for various values of x when $Pr = 0.7, 1, 7$, $M = 0$, $N_R = 0$, $K = 0, 2$ and $\gamma = 0.5$, respectively. It is found that, for fixed K , as Pr increases, the $Q_w(x)$ increase and C_f decrease. From these tables, for a fixed Pr , as x increases, i.e. from the lower stagnation point of the sphere, $x \approx 0$ and proceeds around the sphere up to the point $x = 120^\circ$, where the values of $Q_w(x)$ decrease and C_f increase. On the other hand, the values of C_f are higher for micropolar fluid ($K = 2$) than those for Newtonian fluid ($K = 0$).

Table 4.10 shows the values of the wall temperature $\theta(x, 0)$, the heat transfer coefficient $-(\partial\theta/\partial y)(x, 0)$ and the skin friction coefficient $(\partial^2 f / \partial y^2)(x, 0)$ at the lower stagnation point of the sphere, $x \approx 0$, for various values of N_R when $Pr = 0.7$, $K = 2$, $\gamma = 0.1$ and $M = 0, 5$. It is observed that, when the magnetic parameter M is

fixed, an increase in the radiation parameter N_R , causes the values of $\theta(x,0)$, $-(\partial\theta/\partial y)(x,0)$ and $(\partial^2 f/\partial y^2)(x,0)$ to increase. Similarly when N_R is fixed and M increases, the value of $\theta(x,0)$, increases but the values of $(\partial^2 f/\partial y^2)(x,0)$ and $-(\partial\theta/\partial y)(x,0)$ decrease.

The graphs of $\theta(x,0)$ and $(\partial^2 f/\partial y^2)(x,0)$ for some values of the Prandtl number Pr when $\gamma = 0.05, 0.1, 0.2$ and $M = 0, N_R = 0$ are plotted in Figures 4.1 and 4.2, respectively. It is found that, as Pr increases, both $\theta(x,0)$ and $(\partial^2 f/\partial y^2)(x,0)$ decrease. For small values of $Pr (\ll 1)$, the value of $\theta(x,0)$ and $(\partial^2 f/\partial y^2)(x,0)$ is higher than for large values of $Pr (\gg 1)$ and it seems that the surface temperature is very sensitive to Prandtl number variations.

Figure 4.3 illustrates the variation of the wall temperature $\theta(x,0)$ with conjugate parameter γ when $Pr = 0.7, 1, 7, M = 0, N_R = 0$ and $K = 2$. Furthermore, in order to get a physically acceptable solution, γ must be less than or equals to some critical value, say γ_c , i.e. $\gamma \leq \gamma_c$, depending on Pr . It can be seen from this figure that $\theta(x,0)$ becomes larger as γ approaches the critical value of $\gamma_{c1} = 0.5103$ when $Pr = 0.7$, $\gamma_{c2} = 0.5592$ when $Pr = 1$ and $\gamma_{c3} = 1.019$ when $Pr = 7$.

Figures 4.4 to 4.6 illustrate the temperature $\theta(0, y)$, velocity $(\partial f/\partial y^2)(0, y)$ and angular velocity $h(0, y)$ profiles of the sphere for some values of γ , namely $\gamma = 0.05, 0.1, 0.2$ when $Pr = 0.7, M = 0, N_R = 0$ and $K = 2$, respectively. It is found that when K is fixed, as γ increases, the temperature, velocity and angular velocity increase.

Figures 4.7 and 4.8 display the temperature $\theta(0, y)$ and velocity $(\partial f/\partial y^2)(0, y)$ profiles for some values of K , namely $K = 0, 1, 2, 3$ when $Pr = 1, M = 0, N_R = 0$ and $\gamma = 0.1$, respectively. It is found that when Pr is fixed, as K increases, both the temperature and velocity are also increase. The angular velocity profiles $h(0, y)$, when

$K = 0, 1, 2, 3$, $Pr = 1$ and $\gamma = 0.1$ are plotted in Figure 4.9. These figures show that the angular velocity is completely negative for $K = 0$ and positive for $K \neq 0$ when $y \geq 2$.

Figures 4.10 to 4.12 display the temperature, velocity and angular velocity at $x = 0^\circ, 60^\circ, 90^\circ$ when $Pr = 0.7, 7$, $K = 2$, $M = 0$, $N_R = 0$ and $\gamma = 0.1$. From Figure 4.10, it is found that as Pr and x increase, the temperature decrease and so does the thermal boundary layer thickness. This is because for small values of the Prandtl number $Pr \ll 1$, the fluid is highly conductive. Physically, if Pr increases, the thermal diffusivity decreases and this phenomenon leads to the decreasing manner of the energy transfer ability that reduces the thermal boundary layer. Furthermore, in these figures shown for fixed K , as Pr increases, the velocity decrease and the angular velocity are also decrease. In the same figures, it has been found that when Pr is fixed and x increases, the temperature, velocity and angular velocity increase.

Figures 4.13 to 4.15 show the temperature $\theta(0, y)$, velocity $(\partial f / \partial y)(0, y)$ and angular velocity $h(0, y)$ when $Pr = 7$, $K = 1$, $M = 5$, $N_R = 0, 1, 3, 5$ and $\gamma = 0.1$, respectively. It is found that as N_R increases, the temperature, velocity and angular velocity are doing the same.

The temperature $\theta(0, y)$, velocity $(\partial f / \partial y)(0, y)$ and angular velocity profiles $h(0, y)$ presented in Figure 4.16 to 4.18, respectively, when $Pr = 7$, $K = 1$, $N_R = 1$, $M = 0, 5, 10$ and $\gamma = 0.1$ show that when the value of M increases, it is found that the temperature also increase, but the velocity and angular velocity decrease.

Variation of the local Nusselt number N_u and the local friction coefficient C_f with various values of x when $Pr = 0.7$, $K = 1$, $N_R = 1$, $M = 0, 5, 10$ and $\gamma = 0.1$ are plotted in Figures 4.19 and 4.20, respectively. It is found that as M increases, both values of local Nusselt number and the local skin friction coefficient decrease.

Figures 4.21 and 4.22 display the local Nusselt number N_u and the local friction coefficient C_f with various values of x when $Pr = 0.7$, $K = 1$, $M = 5$, $N_R = 0, 1, 3, 5$ and $\gamma = 0.1$, respectively. It is found that as N_R increases, both values of local Nusselt

number and the local skin friction coefficient increase. We notice that from Figure 4.19 and 4.21, it showed that the value of N_u is above $x = 0^\circ$ than those at $0^\circ < x \leq 90^\circ$, because the sphere temperature is almost equal to fluid temperature at $x = 0^\circ$, and has a different value when $0^\circ < x \leq 90^\circ$. From figure 4.20 and 4.22, it is found that the value of $C_f = 0$ at $x = 0^\circ$, because at this point, the value of the wall shear stress τ_w is very small and careless, and the maximum value of C_f appear when $x = 90^\circ$, because in this case, the value of τ_w is very high.

Table 4.1: The heat transfer coefficient $-(\partial\theta/\partial y)(x,0)$ at the lower stagnation point of the sphere, $x \approx 0$, for various values of K when $Pr = 0.7, 7$, without the effect of radiation and magnetohydrodynamic and $\gamma \rightarrow \infty$

Pr	0.7			7		
	Huang and Chen (1987)	Nazar et al. (2002a)	Present	Huang and Chen (1987)	Nazar et al. (2002a)	Present
K						
0	0.4574	0.4576	0.457582	0.9581	0.9595	0.959498
0.5	-	0.4336	0.433616	-	0.8905	0.890523
1	-	0.4166	0.416577	-	0.8443	0.844347
1.5	-	0.4035	0.403509	-	0.8096	0.809569
2	-	0.3930	0.393023	-	0.7805	0.780481

Table 4.2: The wall temperature $\theta(x,0)$ and the skin friction coefficient $(\partial^2 f/\partial y^2)(x,0)$ at the lower stagnation point of the sphere, $x \approx 0$, for various values of K when $Pr = 0.7, M = 0, N_R = 0$ and $\gamma = 0.05, 0.1, 0.2$

K	0.05		0.1		0.2	
	$\theta(x,0)$	$(\partial^2 f/\partial y^2)$	$\theta(x,0)$	$(\partial^2 f/\partial y^2)$	$\theta(x,0)$	$(\partial^2 f/\partial y^2)$
0	0.149501	0.184661	0.238308	0.262053	0.360667	0.357656
1	0.157545	0.133231	0.251021	0.183022	0.378091	0.244051
2	0.162725	0.111617	0.259056	0.149459	0.388925	0.195632
3	0.166740	0.099368	0.265189	0.130425	0.397069	0.168159

Table 4.3: The wall temperature $\theta(x,0)$ at the lower stagnation point of the sphere, $x \approx 0$, for various values of K when $Pr = 0.7, 1, 7, M = 0, N_r = 0$ and $\gamma = 0.1$

Pr	0.7	1	7
K			
0	0.238308	0.219728	0.144616
1	0.251021	0.232412	0.153825
2	0.259056	0.240367	0.159325
3	0.265189	0.246400	0.163335

Table 4.4: The heat transfer coefficient $-(\partial\theta/\partial y)(x,0)$ at the lower stagnation point of the sphere, $x \approx 0$, for various values of K when $Pr = 0.7, 1, 7, M = 0, N_r = 0$ and

$\gamma = 0.1$

Pr	0.7	1	7
K			
0	0.076169	0.078027	0.085538
1	0.074898	0.076759	0.084617
2	0.074094	0.075963	0.084067
3	0.073481	0.075360	0.083666

Table 4.5: The skin friction coefficient $(\partial^2 f/\partial y^2)(x,0)$ at the lower stagnation point of the sphere, $x \approx 0$, for various values of K when $Pr = 0.7, 1, 7, M = 0, N_r = 0$ and

$\gamma = 0.1$

Pr	0.7	1	7
K			
0	0.262053	0.232622	0.118772
1	0.183022	0.163781	0.089184
2	0.149459	0.134749	0.077445
3	0.130425	0.118279	0.070782

Table 4.6: The local heat transfer coefficient $Q_w(x)$ for various values of x
when $Pr = 0.7, 1, \text{ and } 7, K = 0, M = 0, N_R = 0$ and $\gamma = 0.5$

Pr	0.7	1	7
x			
0°	0.330798	0.332928	0.360684
10°	0.323643	0.327921	0.358815
20°	0.323202	0.327438	0.358336
30°	0.322499	0.326561	0.357508
40°	0.321294	0.325299	0.356348
50°	0.319768	0.323628	0.354863
60°	0.317876	0.321551	0.352915
70°	0.315431	0.318872	0.350475
80°	0.312381	0.315538	0.347495
90°	0.308578	0.311404	0.343626
100°	0.303817	0.306267	0.338416
110°	0.297992	0.300045	0.332281
120°	0.290076	0.291707	0.324164

Table 4.7: The local skin friction coefficient C_f for various values of x
when $Pr = 0.7, 1, 7, K = 0, M = 0, N_R = 0$ and $\gamma = 0.5$

Pr	0.7	1	7
x			
0°	0.000000	0.000000	0.000000
10°	0.034291	0.032424	0.019232
20°	0.068051	0.064377	0.038208
30°	0.100840	0.095508	0.056746
40°	0.132223	0.125369	0.074045
50°	0.161811	0.153571	0.091395
60°	0.188384	0.179001	0.106634
70°	0.213152	0.202794	0.120807
80°	0.235005	0.223868	0.133682
90°	0.253596	0.241800	0.144351
100°	0.268672	0.256273	0.153816
110°	0.279600	0.266518	0.160617
120°	0.286714	0.272626	0.164811

Table 4.8: The local heat transfer coefficient $Q_w(x)$ for various values of x
when $Pr = 0.7, 1, 7, K = 2, M = 0, N_R = 0$ and $\gamma = 0.5$

Pr	0.7	1	7
x			
0°	0.318250	0.322975	0.386933
10°	0.317922	0.322470	0.381694
20°	0.317658	0.322153	0.381362
30°	0.317211	0.321659	0.380709
40°	0.316598	0.320812	0.379754
50°	0.315804	0.319797	0.378451
60°	0.314858	0.318588	0.376841
70°	0.313697	0.317094	0.374693
80°	0.312337	0.315328	0.372073
90°	0.310761	0.313264	0.368721
100°	0.308944	0.310862	0.364647
110°	0.306907	0.308146	0.359724
120°	0.302652	0.304752	0.353513

Table 4.9: The local skin friction coefficient C_f for various values of x
when $Pr = 0.7, 1, 7, K = 2, M = 0, N_R = 0$ and $\gamma = 0.5$

Pr	0.7	1	7
x			
0°	0.000000	0.000000	0.000000
10°	0.063458	0.062299	0.047452
20°	0.126326	0.124072	0.094862
30°	0.188080	0.184866	0.142196
40°	0.248124	0.244147	0.189483
50°	0.305980	0.301498	0.236618
60°	0.359604	0.354889	0.282270
70°	0.411721	0.407061	0.329185
80°	0.460355	0.456068	0.375692
90°	0.505152	0.501525	0.422065
100°	0.545910	0.543212	0.467708
110°	0.581465	0.579857	0.511386
120°	0.627322	0.614398	0.556060

Table 4.10: The wall temperature $\theta(x,0)$, the heat transfer coefficient $-(\partial\theta/\partial y)(x,0)$ and the skin friction coefficient $(\partial^2 f/\partial y^2)(x,0)$ at the lower stagnation point of the sphere, $x \approx 0$, for various values of N_R when $Pr = 7$, $K = 2$, $M = 0, 5$, and $\gamma = 0.1$

N_R	$M = 0$			$M = 5$		
	$\theta(x,0)$	$-(\partial\theta/\partial y)$	$(\partial^2 f/\partial y^2)$	$\theta(x,0)$	$-(\partial\theta/\partial y)$	$(\partial^2 f/\partial y^2)$
0	0.159324	0.084067	0.077444	0.215447	0.078455	0.055249
1	0.190971	0.188773	0.098184	0.264358	0.171650	0.067778
2	0.209968	0.289678	0.111751	0.293693	0.258979	0.075365
3	0.224033	0.387983	0.122225	0.314982	0.342509	0.080891
4	0.235386	0.484256	0.130896	0.331738	0.423232	0.085250
5	0.244992	0.578840	0.138354	0.345481	0.501798	0.088828

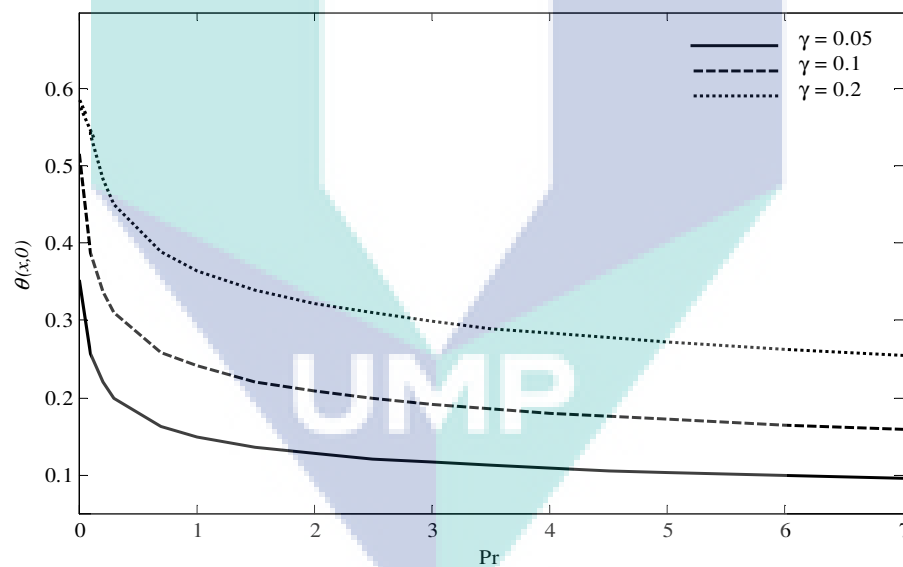


Figure 4.1: The wall temperature $\theta(x,0)$ with Prandtl number Pr when $K = 2$, $M = 0$, $N_R = 0$ and $\gamma = 0.05, 0.1, 0.2$

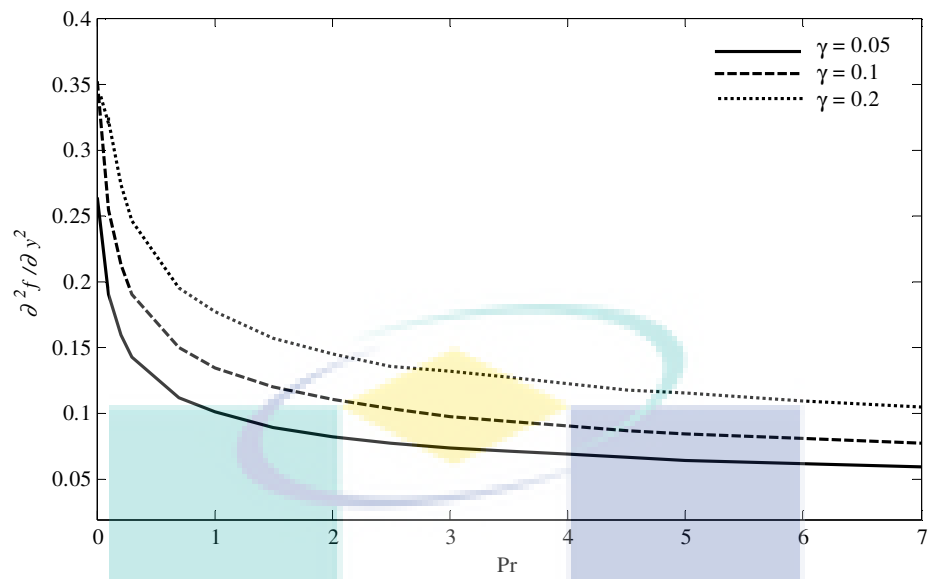


Figure 4.2: The skin friction coefficient $(\partial^2 f / \partial y^2)(x, 0)$ with Prandtl number Pr when $K = 2, M = 0, N_R = 0$ and $\gamma = 0.05, 0.1, 0.2$

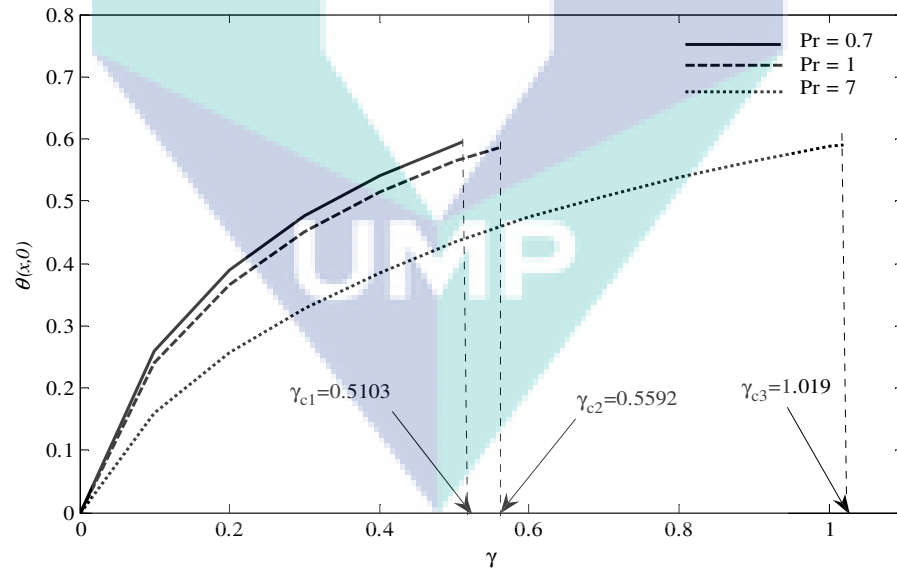


Figure 4.3: The wall temperature $\theta(x, 0)$ with conjugate parameter γ when $Pr = 0.7, 1, 7, M = 0, N_R = 0$ and $K = 2$

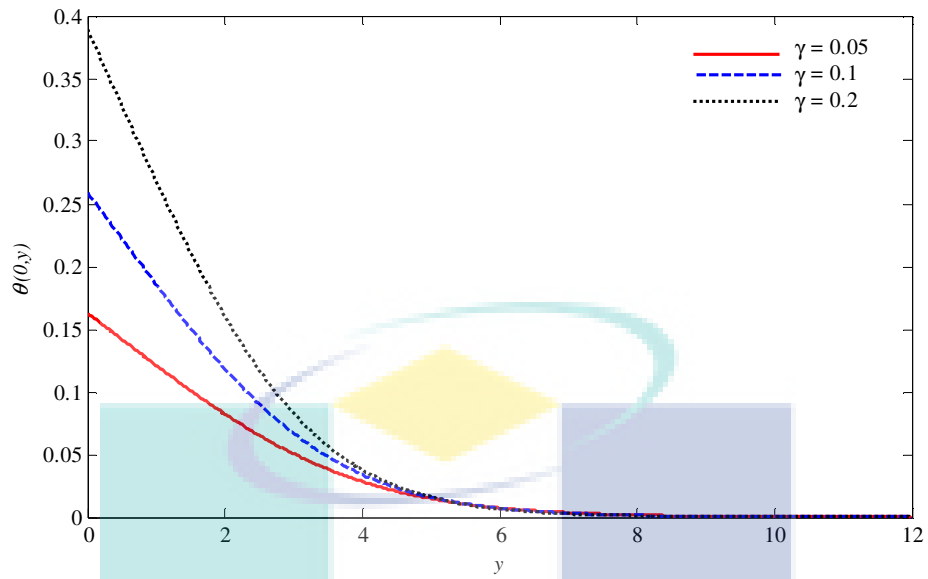


Figure 4.4: The temperature profiles $\theta(0, y)$ for some values of $\gamma=0.05, 0.1, 0.2$ when $Pr= 0.7, M = 0, N_R = 0$ and $K = 2$

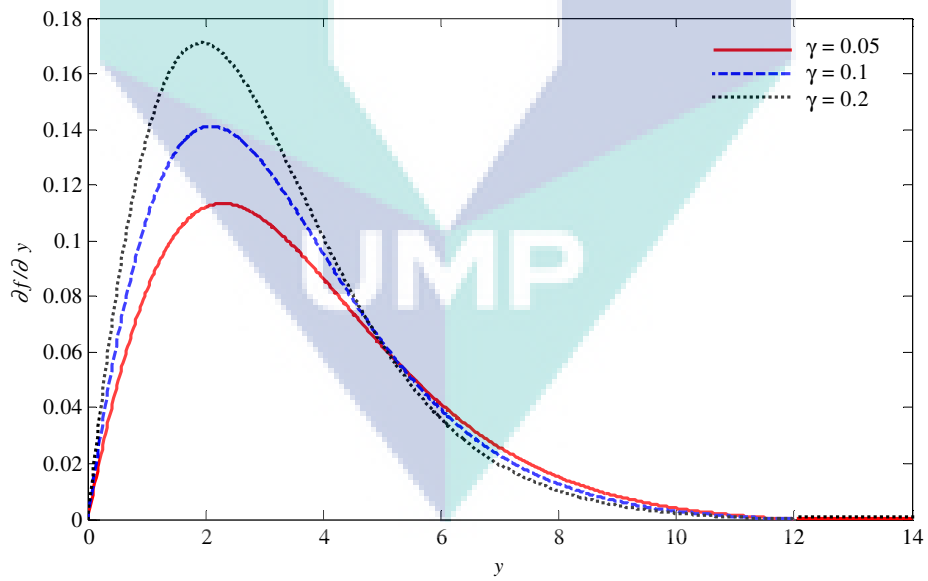


Figure 4.5: The velocity profiles $(\partial f / \partial y)(0, y)$ for some values of $\gamma=0.05, 0.1, 0.2$ when $Pr= 0.7, M = 0, N_R = 0$ and $K = 2$

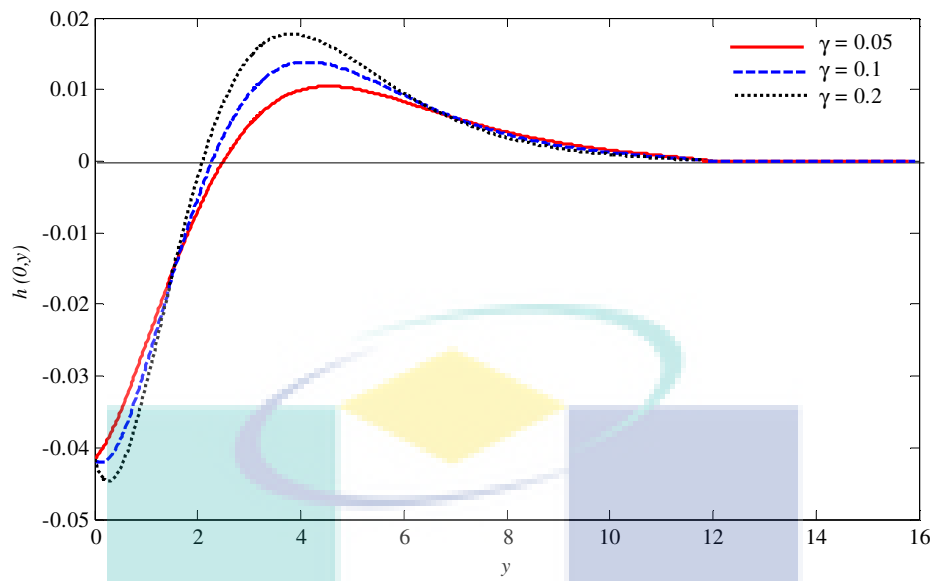


Figure 4.6: The angular velocity profiles $h(0, y)$ for some values of $\gamma=0.05, 0.1, 0.2$ when $Pr= 0.7, M = 0, N_R = 0$ and $K = 2$

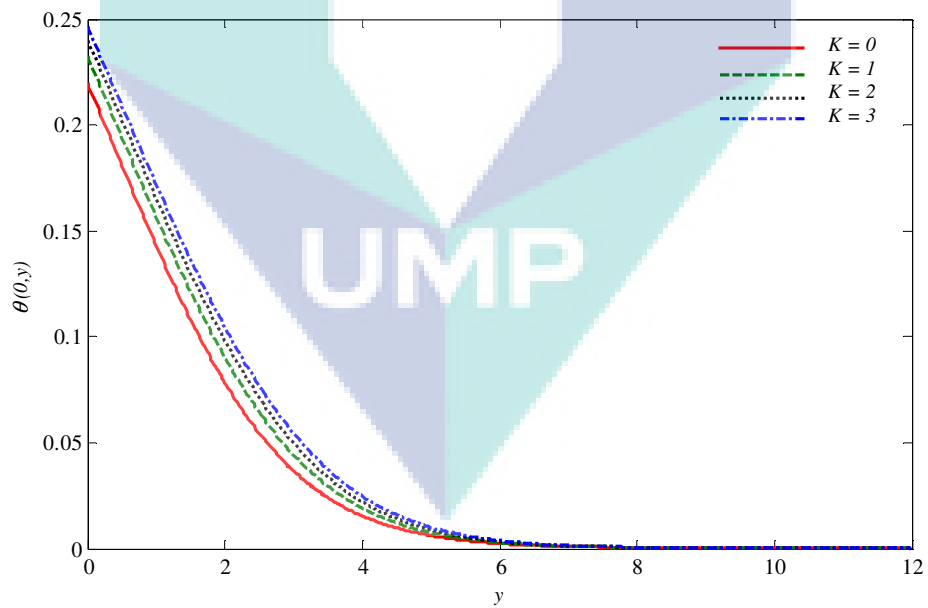


Figure 4.7: The temperature profiles $\theta(0, y)$ when $K = 0, 1, 2, 3, Pr = 1, M = 0, N_R = 0$ and $\gamma=0.1$

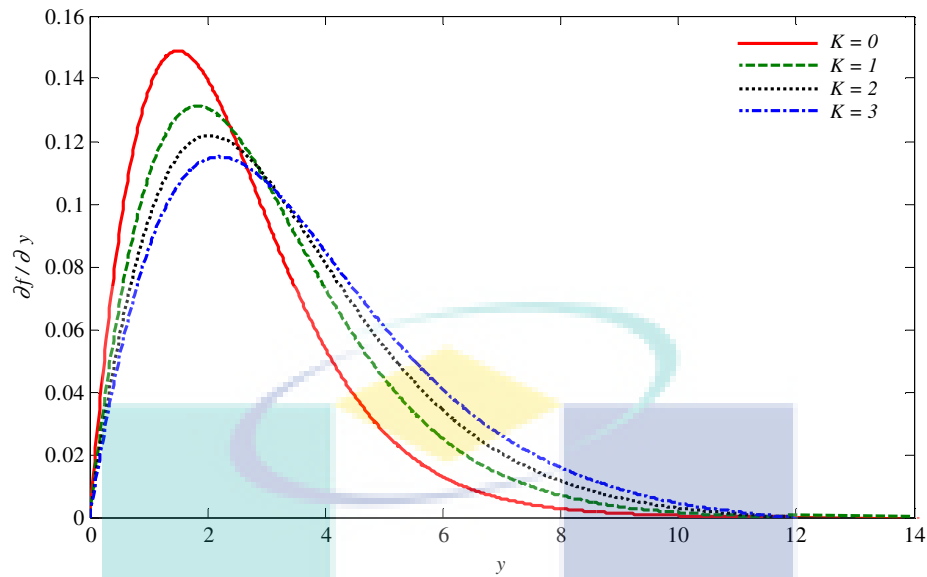


Figure 4.8: The velocity profiles $(\partial f / \partial y)(0, y)$ when $K = 0, 1, 2, 3$, $Pr = 1$, $M = 0$, $N_R = 0$ and $\gamma = 0.1$

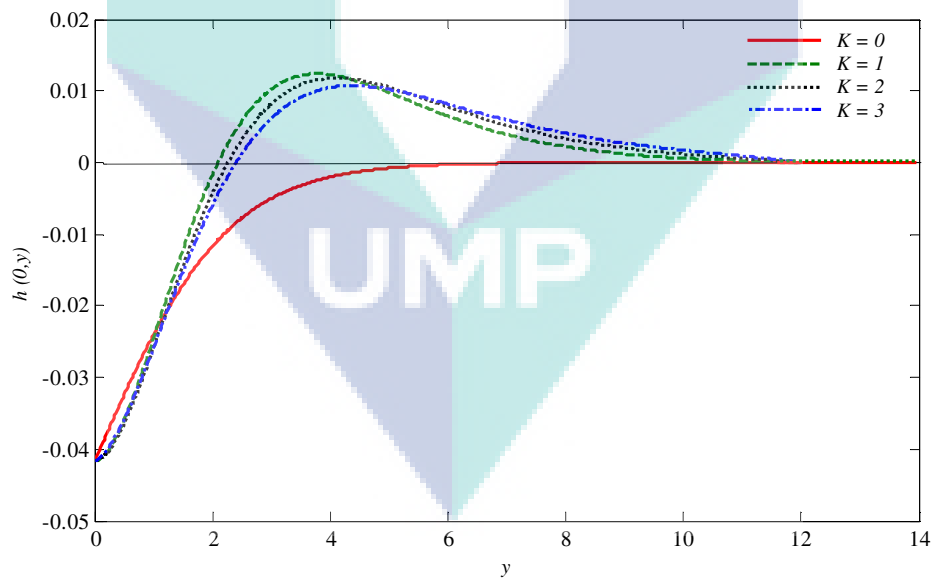


Figure 4.9: The angular velocity profiles $h(0, y)$ when $K = 0, 1, 2, 3$, $Pr = 1$, $M = 0$, $N_R = 0$ and $\gamma = 0.1$

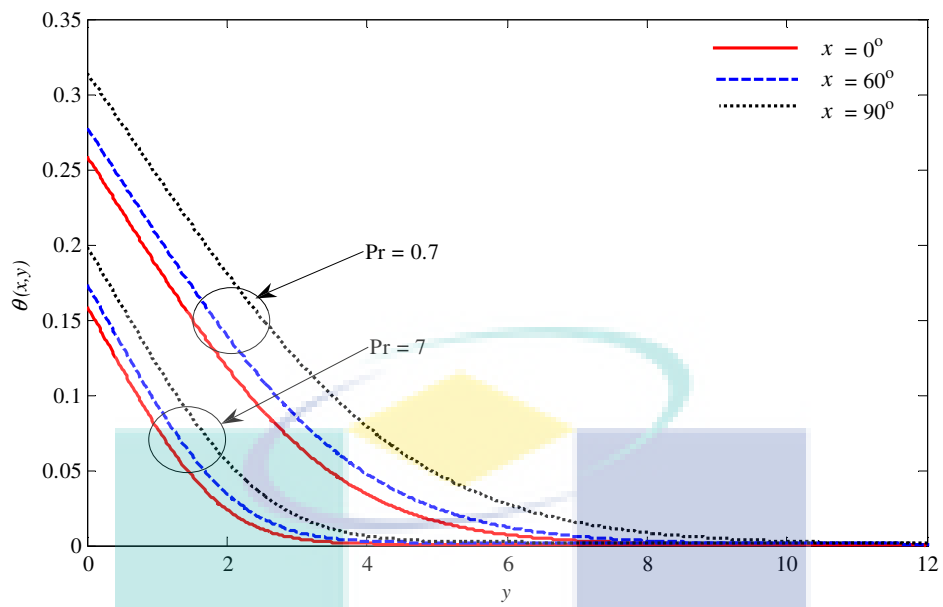


Figure 4.10: The temperature profiles $\theta(x, y)$ at $x = 0^\circ, 60^\circ, 90^\circ$ when $Pr = 0.7, 7$,
 $K = 2, M = 0, N_R = 0$ and $\gamma = 0.1$

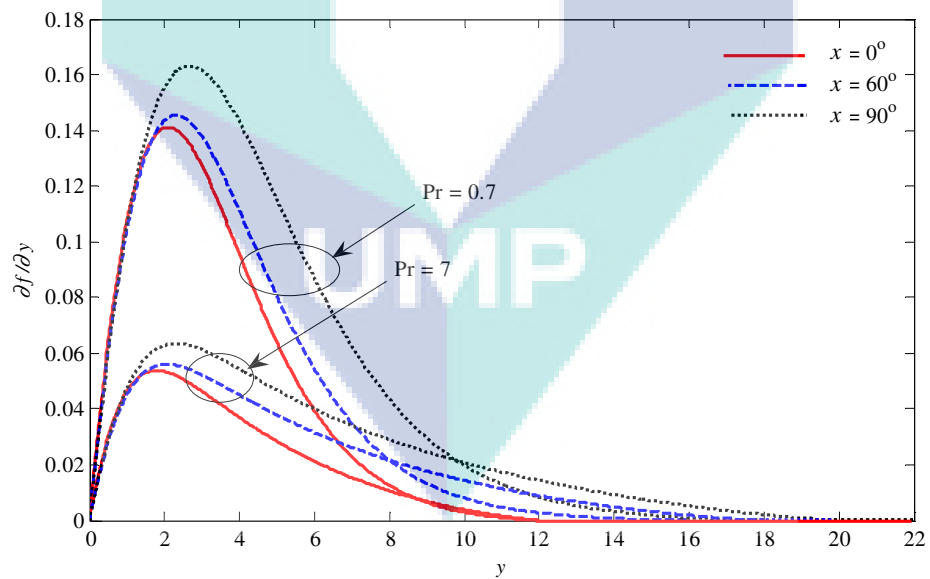


Figure 4.11: The velocity profiles, $(\partial f / \partial y)(x, y)$ at $x = 0^\circ, 60^\circ, 90^\circ$ when $Pr = 0.7, 7$,
 $K = 2, M = 0, N_R = 0$ and $\gamma = 0.1$

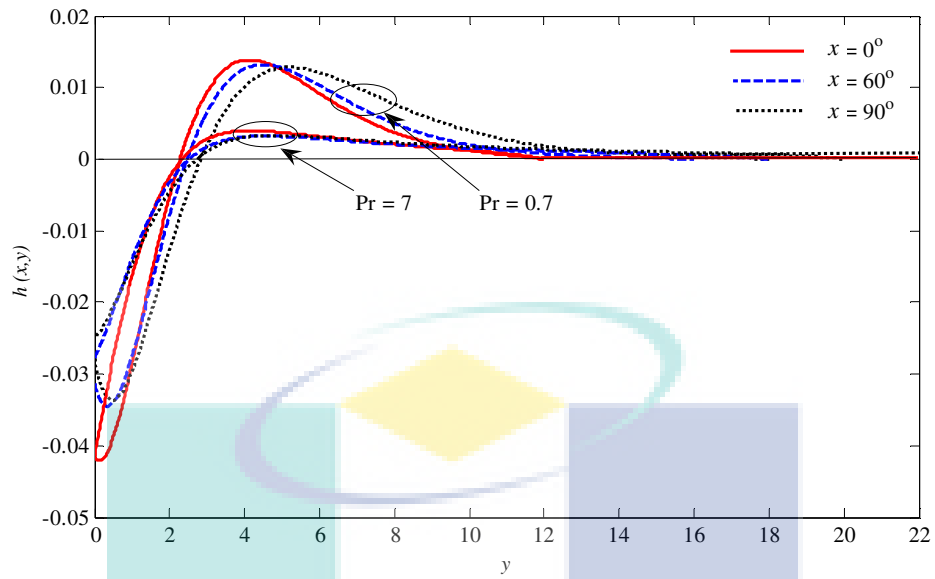


Figure 4.12: The angular velocity profiles, $h(x, y)$ at $x = 0^\circ, 60^\circ, 90^\circ$ when $Pr = 0.7, 7, K = 2, M = 0, N_R = 0$ and $\gamma = 0.1$

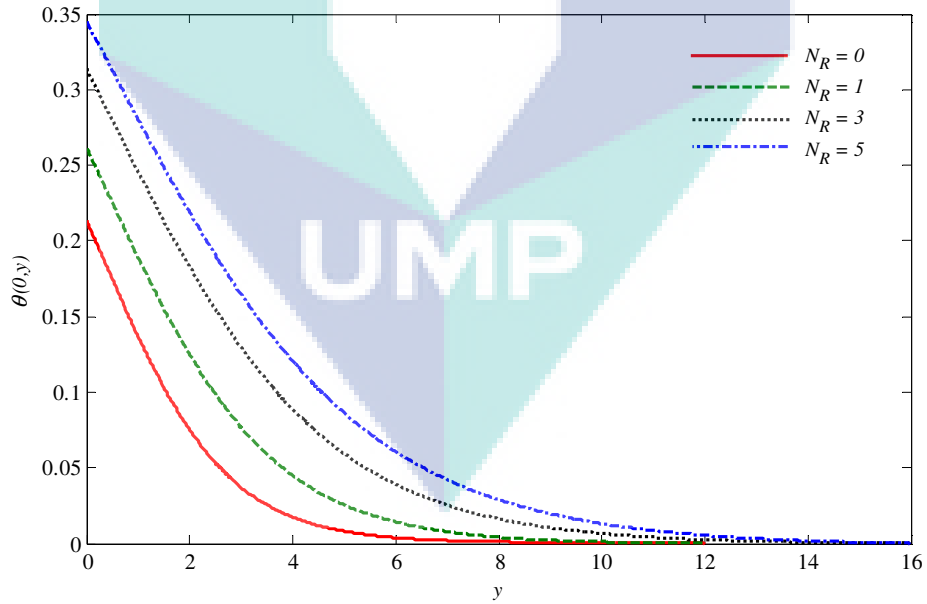


Figure 4.13: The temperature profiles $\theta(0, y)$ when $Pr = 7, M = 5, K = 1, N_R = 0, 1, 3, 5$ and $\gamma = 0.1$

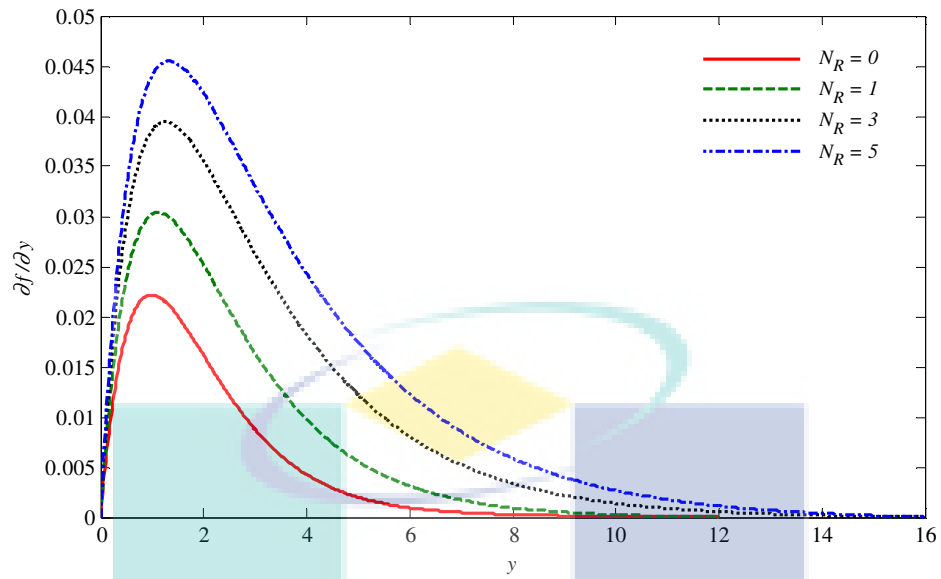


Figure 4.14: The velocity profiles $(\partial f / \partial y)(0, y)$ when $Pr = 7$, $K = 1$, $M = 5$, $N_R = 0, 1, 3, 5$ and $\gamma = 0.1$

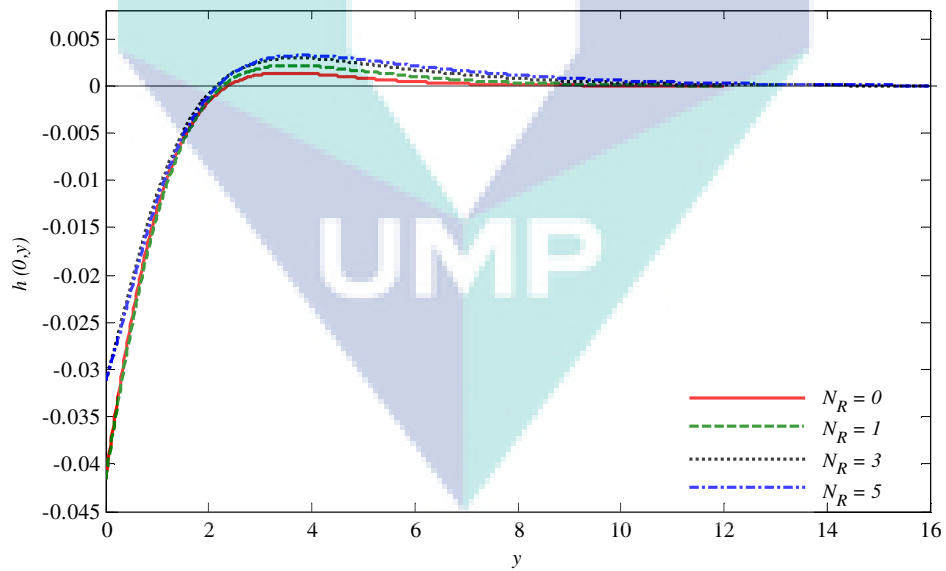


Figure 4.15: The angular velocity profiles $h(0, y)$ when $Pr = 7$, $K = 1$, $M = 5$, $N_R = 0, 1, 3, 5$ and $\gamma = 0.1$

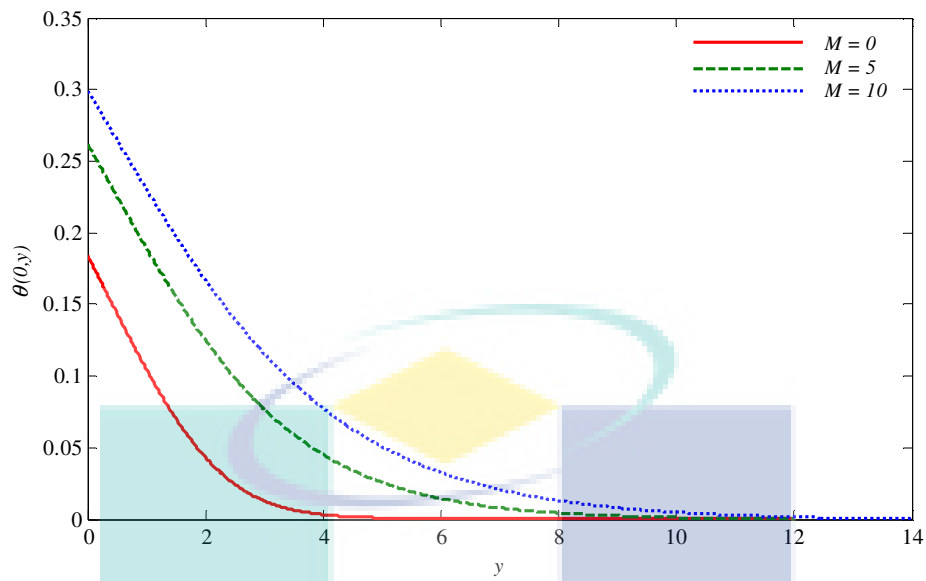


Figure 4.16: The temperature profiles $\theta(0, y)$ when $\text{Pr} = 7$, $K = 1$, $N_R = 1$, $M = 0, 5, 10$ and $\gamma = 0.1$

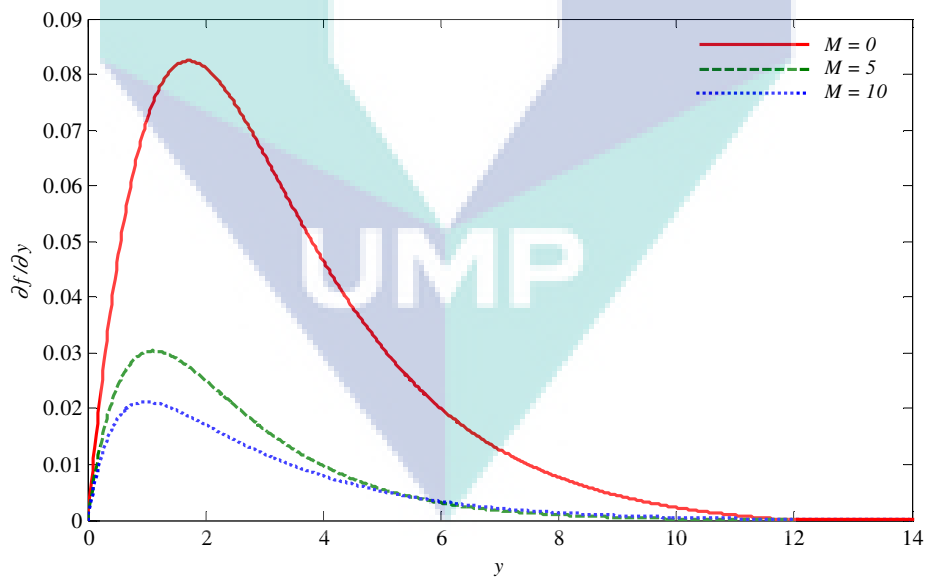


Figure 4.17: The velocity profiles $(\partial f / \partial y)(0, y)$ when $\text{Pr} = 7$, $K = 1$, $N_R = 1$, $M = 0, 5, 10$ and $\gamma = 0.1$

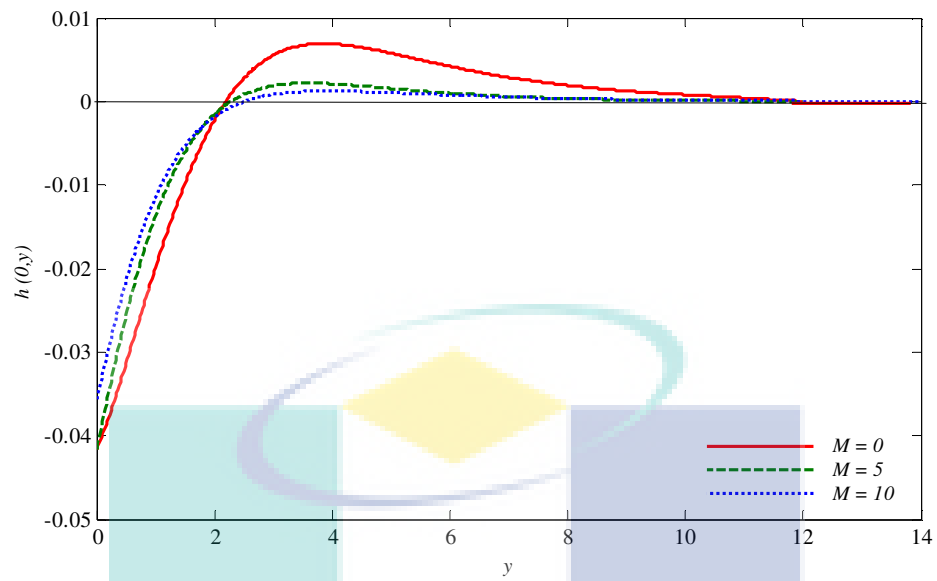


Figure 4.18: The angular velocity profiles $h(0, y)$ when $Pr = 7$, $K = 1$, $N_R = 1$, $M = 0, 5, 10$ and $\gamma = 0.1$

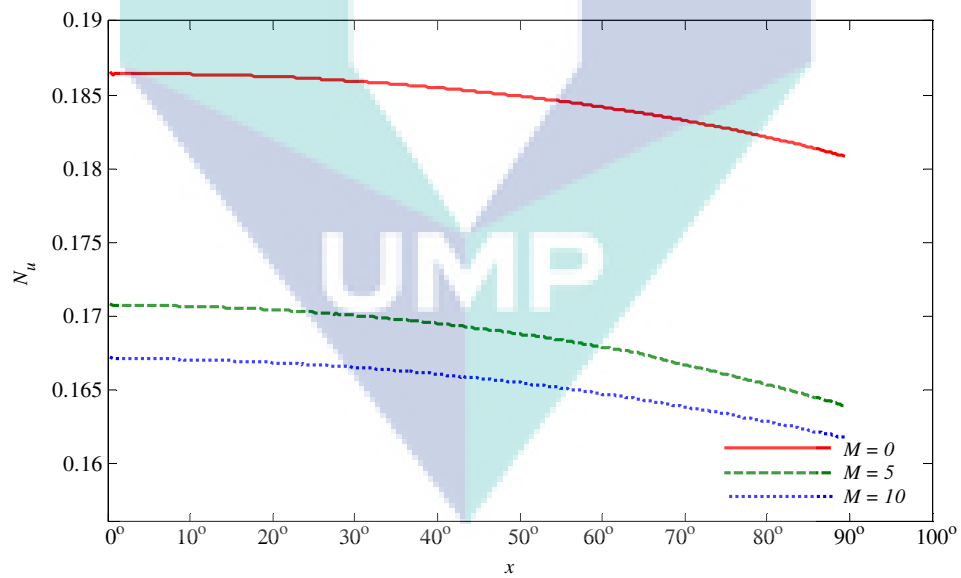


Figure 4.19: The local Nusselt number N_u with x when $Pr = 0.7$, $K = 1$, $N_R = 1$, $M = 0, 5, 10$ and $\gamma = 0.1$

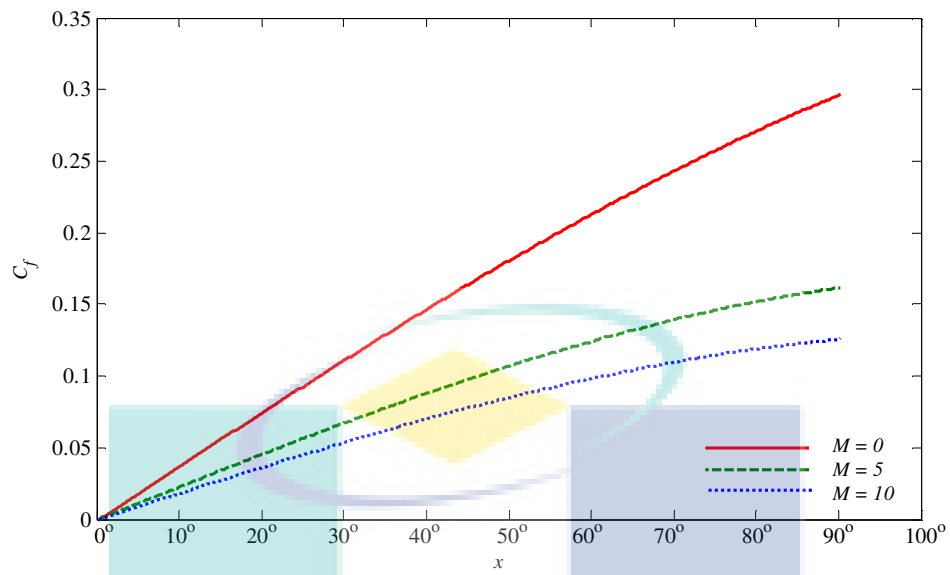


Figure 4.20: The local skin friction coefficient C_f with x when $Pr = 0.7$, $K = 1$, $N_R = 1$, $M = 0, 5, 10$ and $\gamma = 0.1$

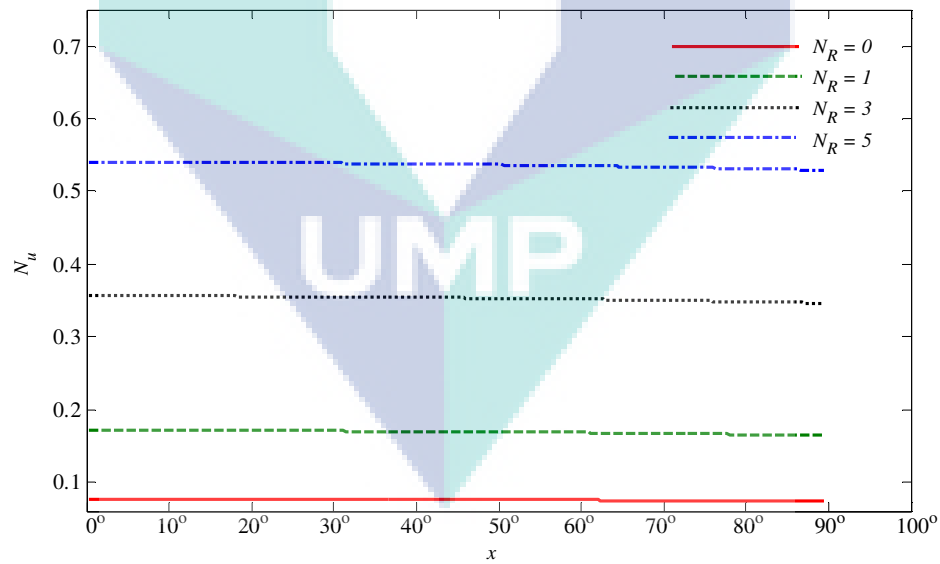


Figure 4.21: The local Nusselt number N_u with x when $Pr = 0.7$, $K = 1$, $M = 5$, $N_R = 0, 1, 3, 5$ and $\gamma = 0.1$

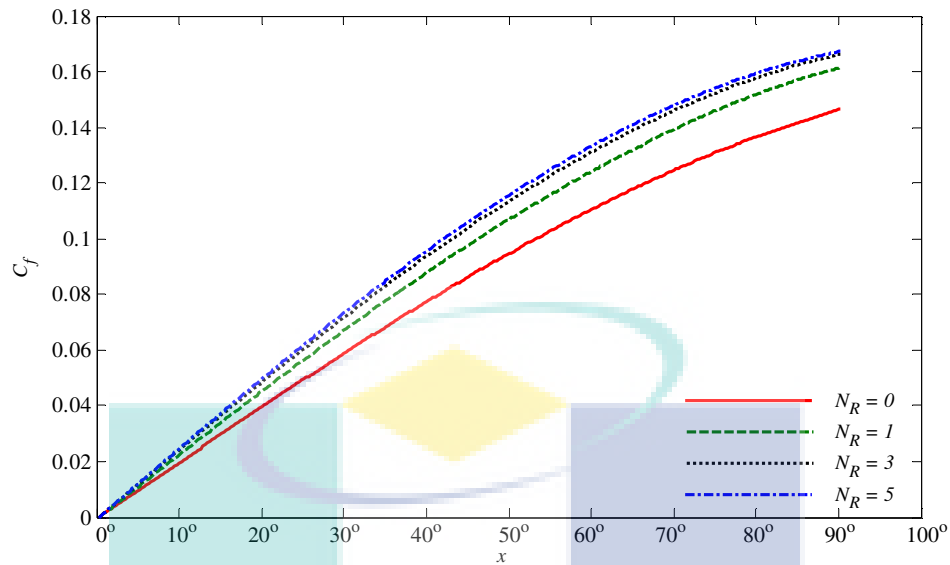


Figure 4.22: The local skin friction coefficient C_f with x when $Pr = 0.7$, $K = 1$, $M = 5$, $N_R = 0, 1, 3, 5$ and $\gamma = 0.1$

4.4 CONCLUSIONS

In this chapter, we have studied the problem of the effect of radiation on magnetohydrodynamic free convection boundary layer flow on a sphere in a micropolar fluid with convective boundary conditions. It is shown on how the Prandtl number Pr , micropolar parameter K , magnetic parameter M , thermal radiation parameter N_R , conjugate parameter γ and the coordinate running along the surface of the sphere x , affects the values of the temperature profiles $\theta(x,0)$, heat transfer coefficient $-(\partial\theta/\partial y)(0, y)$, velocity profiles $(\partial f/\partial y)(0, y)$, angular velocity profiles $h(x,0)$, the skin friction coefficient $(\partial^2 f/\partial y^2)(0, y)$, the Nusselt number N_u and the local friction coefficient C_f . The agreement between present results for $M = 0$, $N_R = 0$ and $\gamma \rightarrow \infty$ with those reported by Huang and Chen (1987) and Nazar et al. (2002a) are very good. From this study, we can come to the following conclusions:

- When Pr and γ are fixed, as K increases, the wall temperature increases but the skin friction coefficient decreases. On other hand, when K and γ are fixed, as Pr increases, the heat transfer coefficient, the skin friction coefficient, and the angular velocity decrease but the heat transfer coefficient increase.
- When K is fixed, an increase in γ leads to an increase of the wall temperature, skin friction coefficient, and temperature, velocity and angular velocity.
- When Pr and γ are fixed, the values of C_f are higher for micropolar fluids ($K \neq 0$) than those for a Newtonian fluid ($K = 0$).
- When Pr is fixed and x increases, the temperature, velocity and angular velocity increase.
- When K and γ are fixed, as Pr increases, the local heat transfer coefficient is doing the same but the local skin friction coefficient decrease.
- When Pr , γ and M are fixed, as N_R increases, the temperature, velocity, angular velocity, skin friction coefficient and the heat transfer coefficient increase, while when Pr , γ and N_R are fixed, as M increases, the temperature increases, and velocity, angular velocity, skin friction coefficient and heat transfer coefficient decrease.
- When Pr , γ and N_R are fixed, as M increases, both values of local Nusselt number and the local skin friction coefficient decreases, and if Pr , γ and M are fixed, as N_R increases, the local Nusselt number and the local skin friction coefficient increase.

CHAPTER 5

MIXED CONVECTION BOUNDARY LAYER FLOW OVER A SOLID SPHERE IN A VISCOUS FLUID

5.1 INTRODUCTION

This chapter discusses the mixed convection boundary layer flow over a solid sphere in a viscous fluid with convective boundary conditions. The mixed convection (free and forced) occur together and one would often like to know how much of the convection is due to external constraints, such as the fluid velocity in the pump, and how much is due to free convection occurring in the system. The relative magnitudes of the Grashof and Reynolds number squared determine which form of convection dominates.

Chen and Mucoglu (1977, 1978), considered the mixed convection over a sphere with uniform surface temperature and uniform surface heat flux, respectively. The mixed convection boundary layer flow about a solid sphere with constant heat flux and Newtonian heating (NH) in a viscous fluid was solved numerically using the Keller-box method presented by Nazar et al. (2002c) and Salleh et al. (2010a), respectively. Recently, the laminar mixed convection heat transfer from an isothermal sphere immersed in Bingham plastic fluids has been investigated by Nirmalkar et al. (2014).

Motivated by the above studies, we present the mixed convection boundary layer flow on a sphere with convective boundary conditions in a viscous fluid. We compare the present results with the previously published results reported by Nazar et al. (2002c). Thus, four parameters are discussed in this study, which are the Prandtl number, the coordinate running along the surface of the sphere, the conjugate parameter and the mixed convection parameter.

5.2 MATHEMATICAL FORMULATION

Consider a heated sphere of radius a , which is placed in a flow field with the undisturbed free stream velocity U_∞ and temperature T_∞ . The surface of the sphere is subjected to a convective boundary conditions, as shown in Figure 2.1. The convective forced flow is assumed to be moving upward, while the gravity vector g acts downward in the opposite direction, where the coordinates \bar{x} and \bar{y} are chosen such that \bar{x} measures the distance along the surface of the sphere from the lower stagnation point and \bar{y} measures the distance normal to the surface of the sphere. Therefore, by referring to equation (2.5) and following Salleh et al. (2010a) and Nazar et al. (2002c) the momentum and energy equations can be written as

$$\bar{u} \frac{\partial \bar{u}}{\partial \bar{x}} + \bar{v} \frac{\partial \bar{u}}{\partial \bar{y}} = \bar{u}_e \frac{d\bar{u}_e}{d\bar{x}} + \nu \frac{\partial^2 \bar{u}}{\partial \bar{y}^2} + g \beta (T - T_\infty) \sin\left(\frac{\bar{x}}{a}\right), \quad (5.1)$$

$$\bar{u} \frac{\partial T}{\partial \bar{x}} + \bar{v} \frac{\partial T}{\partial \bar{y}} = \alpha \frac{\partial^2 T}{\partial \bar{y}^2}, \quad (5.2)$$

subject to the boundary conditions (Salleh et al., 2010a ; Aziz, 2009)

$$\bar{u} = \bar{v} = 0, \quad -k_f \frac{\partial T}{\partial \bar{y}} = h_f (T_f - T) \text{ at } \bar{y} = 0,$$

$$\bar{u} \rightarrow \bar{u}_e(\bar{x}), \quad T \rightarrow T_\infty \text{ as } \bar{y} \rightarrow \infty \quad (5.3)$$

Let $\bar{r}(\bar{x})$ be the radial distance from the symmetrical axis to the surface of the sphere and \bar{u}_e is the local free stream velocity, which are given by:

$$\bar{r}(\bar{x}) = a \sin\left(\frac{\bar{x}}{a}\right), \quad \bar{u}_e(\bar{x}) = \frac{3}{2} U_\infty \sin\left(\frac{\bar{x}}{a}\right), \quad (5.4)$$

We introduce now the following non-dimensional variables (Salleh et al., 2010a ; Aziz, 2009)):

$$x = \frac{\bar{x}}{a}, \quad y = \text{Re}^{1/2} \left(\frac{\bar{y}}{a} \right), \quad r(x) = \frac{\bar{r}(\bar{x})}{a},$$

$$u = \frac{\bar{u}}{U_\infty}, \quad v = \text{Re}^{1/2} \left(\frac{\bar{v}}{U_\infty} \right), \quad u_e(x) = \frac{\bar{u}_e(\bar{x})}{U_\infty},$$

$$\theta = \frac{T - T_\infty}{T_f - T_\infty}, \quad (5.5)$$

where $Re = U_\infty \frac{a}{\nu}$, is the Reynolds number. Substituting variables (5.5) into (5.1) and (5.2) then become

$$u \frac{\partial u}{\partial x} + v \frac{\partial u}{\partial y} = u_e \frac{du_e}{dx} + \frac{\partial^2 u}{\partial y^2} + \lambda \theta \sin x, \quad (5.6)$$

$$u \frac{\partial \theta}{\partial x} + v \frac{\partial \theta}{\partial y} = \frac{1}{Pr} \frac{\partial^2 \theta}{\partial y^2}, \quad (5.7)$$

where $Pr = \frac{\nu}{\alpha}$ is the Prandtl number. The boundary conditions (5.3) become

$$\begin{aligned} u = v = 0, \quad \frac{\partial \theta}{\partial y} = -\gamma(1 - \theta) \quad \text{on } y = 0, \\ u_e(x) \rightarrow \frac{3}{2} \sin x, \quad \theta \rightarrow 0 \quad \text{as } y \rightarrow \infty, \end{aligned} \quad (5.8)$$

where $\gamma = ah_f Gr^{-1/4} / k_f$ is the conjugate parameter for convective boundary conditions and λ is the mixed convection parameter which is given by:

$$\lambda = \frac{Gr}{Re^2}, \quad (5.9)$$

with $Gr = g\beta(T_f - T_\infty) \frac{a^3}{\nu^2}$ is the Grashof number for the convective boundary conditions. It is worth mentioning that $\lambda > 0$ corresponds to the aiding flow (heated sphere), $\lambda < 0$ corresponds to the opposing flow (cooled sphere) and $\lambda = 0$ corresponds to the forced convection flow.

To solve equations (5.6) and (5.7), subjected to the boundary conditions (5.8), we using the variables (3.10) and stream function(3.11), which satisfies the continuity equation (2.17). Thus, the equations become

$$\begin{aligned} \frac{\partial^3 f}{\partial y^3} + (1 + x \cot x) f \frac{\partial^2 f}{\partial y^2} - \left(\frac{\partial f}{\partial y} \right)^2 + \lambda \frac{\sin x}{x} \theta + \frac{9 \sin x \cos x}{4 x} \\ = x \left(\frac{\partial f}{\partial y} \frac{\partial^2 f}{\partial x \partial y} - \frac{\partial f}{\partial x} \frac{\partial^2 f}{\partial y^2} \right), \end{aligned} \quad (5.10)$$

$$\frac{1}{\text{Pr}} \frac{\partial^2 \theta}{\partial y^2} + (1 + x \cot x) f \frac{\partial \theta}{\partial y} = x \left(\frac{\partial f}{\partial y} \frac{\partial \theta}{\partial x} - \frac{\partial f}{\partial x} \frac{\partial \theta}{\partial y} \right), \quad (5.11)$$

subject to the boundary conditions

$$\begin{aligned} f = \frac{\partial f}{\partial y} = 0, \quad \frac{\partial \theta}{\partial y} = -\gamma(1 - \theta) \text{ at } y = 0, \\ \frac{\partial f}{\partial y} \rightarrow \frac{3 \sin x}{2 x}, \quad \theta \rightarrow 0 \text{ as } y \rightarrow \infty. \end{aligned} \quad (5.12)$$

It can be seen that at the lower stagnation point of the sphere $x \approx 0$, equations (5.10) and (5.11) reduce to the following ordinary differential equations:

$$f''' + 2ff'' - f'^2 + \lambda\theta + \frac{9}{4} = 0, \quad (5.13)$$

$$\frac{1}{\text{Pr}} \theta'' + 2f\theta' = 0, \quad (5.14)$$

and the boundary conditions (5.12) become

$$\begin{aligned} f(0) = f'(0) = 0, \quad \theta'(0) = -\gamma(1 - \theta(0)), \\ f' \rightarrow \frac{3}{2}, \quad \theta \rightarrow 0 \text{ as } y \rightarrow \infty. \end{aligned} \quad (5.15)$$

The physical quantities of interest in this problem are the local skin friction coefficient, C_f and the local heat transfer coefficient, $Q_w(x)$ which are defined by

$$C_f = \frac{a}{U_\infty} \text{Re}^{-1/2} \mu \left(\frac{\partial \bar{u}}{\partial \bar{y}} \right)_{\bar{y}=0} \text{ and } Q_w(x) = \frac{a}{k(T_f - T_\infty)} \text{Re}^{-1/2} \left(\frac{\partial \bar{T}}{\partial \bar{y}} \right)_{\bar{y}=0}. \quad (5.16)$$

Using the non-dimensional variables (5.5), we have

$$C_f = x \frac{\partial^2 f}{\partial y^2}(x, 0) \text{ and } Q_w(x) = \gamma(1 - \theta(x, 0)) \quad (5.17)$$

5.3 RESULTS AND DISCUSSION

In this problem, we have solved the nonlinear partial differential equations (5.10) and (5.11) subject to the boundary conditions (5.11). The values of the skin friction coefficient C_f and the local heat transfer coefficient $Q_w(x)$ have been obtained at different positions x with various mixed convection parameter λ which $\lambda > 0$ is for the assisting flow (heated sphere) and $\lambda < 0$ is for the opposing flow (cooled sphere) and for the values of Prandtl number .

The values of the heat transfer coefficient $-\theta'(0)$ and the skin friction coefficient $f''(0)$ at the lower stagnation point of the sphere, $x \approx 0$, for various values of λ when $Pr = 6.8$ and $\gamma \rightarrow \infty$ are presented in Table 5.1. Some numerical results obtained by an implicit finite-difference scheme as reported by Nazar et al. (2002c) are also included in this table for comparison purposes. It is found that the agreement between the previously published results with the present ones is very good.

Table 5.2 shows the values of the wall temperature $\theta(x,0)$, the heat transfer coefficient $-(\partial\theta/\partial y)(x,0)$ and the skin friction coefficient $(\partial^2 f/\partial y^2)(x,0)$ at the lower stagnation point of the sphere, $x \approx 0$, for various values of λ when $Pr = 0.7, 7$ and $\gamma = 0.5$. It is found that, for fixed Pr , as λ increases, the value of $\theta(x,0)$ decrease but the values of $-(\partial\theta/\partial y)(x,0)$ and $(\partial^2 f/\partial y^2)(x,0)$ increases. Similarly, it is found that for fixed λ , as Pr increases, the values of $\theta(x,0)$ decreases and $-(\partial\theta/\partial y)(x,0)$ increases, but for the values of $(\partial^2 f/\partial y^2)(x,0)$, we must divide λ into three cases. Case 1: $\lambda > 0$ (heated sphere), when Pr increases the values of $(\partial^2 f/\partial y^2)(x,0)$ increases. Case 2: $\lambda < 0$ (cooled sphere), if Pr increases, it leads to the decrease of $(\partial^2 f/\partial y^2)(x,0)$. Case 3: $\lambda = 0$ corresponds to the forced convection flow, the values of $(\partial^2 f/\partial y^2)(x,0)$ are fixed when Pr increases.

Furthermore, Tables 5.3 and 5.4 show the values of local heat transfer coefficient $Q_w(x)$ and local skin friction coefficient C_f at different positions x and different values of λ for $Pr = 0.7$ and $\gamma = 1$, respectively. The variation of $Q_w(x)$ and

C_f is also illustrated in Figures 5.1 and 5.2. It is also seen from these tables and figures that $Q_w(x)$ and C_f increases as the mixed convection λ increase. Likewise, for a given value of λ , the local heat transfer coefficient $Q_w(x)$ is seems to decrease while the local skin friction coefficient C_f increases with the increment of the distance x from the stagnation point. Moreover, the numerical solutions indicate that the value of λ which first gives no separation, lies between 1.86 and 2.31 for fixed $Pr = 0.7$.

Tables 5.5 and 5.6 present the values of the local heat transfer coefficient $Q_w(x)$ and the local skin friction coefficient C_f for $\lambda = 10$ and $\gamma = 1$ and various values of Pr , respectively. It is found that, for fixed x , as Pr increases, $Q_w(x)$ increases but the values of C_f decreases. On the other hand, for fixed Pr , as x increases, that is, from the lower stagnation point of the sphere, $x \approx 0$, and proceeds round the sphere up to the point, $x = 120^\circ$, the values of $Q_w(x)$ decreases while C_f increase.

The temperature and velocity profiles are plotted in Figures 5.3 and 5.4 for some values of λ when $Pr = 0.7$ and $\gamma = 0.5$, respectively. We found that for fixed values of Pr , the velocity increase while the temperature decrease when the mixed convection parameter λ , increases.

Figures 5.5 and 5.6 display the temperature and velocity profiles when $\lambda = 10$ and $\gamma = 0.5$, respectively. It can be seen from these figures that, when Pr increases, the temperature and velocity decrease and so does the thermal boundary layer thickness. This is because for small values of the Prandtl number $Pr \ll 1$, the fluid is highly conductive. Physically, if Pr increases, the thermal diffusivity decreases and this phenomenon lead to the decreasing manner of the energy transfer ability that reduces the thermal boundary layer. From Figure 5.6, it is also noticed that there are overshoots of the velocity profiles when $Pr \leq 1$ where these overshoots take place higher for $Pr = 0.7$ than for $Pr > 1$.

The temperature and velocity profiles are presented in Figures 5.7 and 5.8 for some values of γ when $\lambda = 10$ and $Pr = 0.7$, respectively. It is found that for fixed

values of Pr and λ , the temperature and velocity are increases when the conjugate parameter γ , increases.

Table 5.1: The heat transfer coefficient $-\theta'(0)$ and the skin friction coefficient $f''(0)$ at the lower stagnation point of the sphere, $x \approx 0$, for various values of λ when $Pr = 6.8$ and $\gamma \rightarrow \infty$ (CWT)

λ	$-\theta'(0)$		$f''(0)$	
	Nazar et al. (2002c)	Present	Nazar et al. (2002c)	Present
-4	0.6534	0.653381	0.5028	0.502845
-3	0.7108	0.710804	1.0700	1.070014
-2	0.7529	0.752864	1.5581	1.558098
-1	0.7870	0.786997	2.0016	2.001582
-0.5	0.8021	0.802141	2.2115	2.211545
0	0.8162	0.816215	2.4151	2.415122
1	0.8463	0.846307	2.8064	2.806447
2	0.8648	0.864754	3.1804	3.180385
3	0.8857	0.885714	3.5401	3.540068
4	0.9050	0.905098	3.8880	3.887995
5	0.9230	0.922991	4.2257	4.225714
6	0.9397	0.939732	4.5546	4.554647
7	0.9555	0.955475	4.8756	4.875558
8	0.9704	0.970410	5.1896	5.189644
9	0.9846	0.984558	5.4974	5.497377
10	0.9981	0.998147	5.7995	5.799549
20	1.1077	1.107665	8.5876	8.587787

Table 5.2: The wall temperature $\theta(x,0)$, the heat transfer coefficient $-(\partial\theta/\partial y)(x,0)$ and the skin friction coefficient $(\partial^2 f/\partial y^2)(x,0)$ at the lower stagnation point of the sphere, $x \approx 0$, for various values of λ when $Pr = 0.7, 7$ and $\gamma = 0.5$

Pr	0.7			7		
	$\theta(x,0)$	$-(\partial\theta/\partial y)$	$\partial^2 f/\partial y^2$	$\theta(x,0)$	$-(\partial\theta/\partial y)$	$\partial^2 f/\partial y^2$
-3	0.389840	0.305080	1.925471	0.211142	0.394429	2.259568
-2	0.386181	0.306909	2.094082	0.210381	0.394810	2.310522
-1.5	0.384479	0.307760	2.175545	0.210009	0.394996	2.335714
-1	0.382851	0.308574	2.255307	0.209642	0.395179	2.360723
-0.5	0.381291	0.309354	2.333492	0.209281	0.395359	2.385553
0	0.379793	0.310103	2.410209	0.208926	0.395537	2.410209
0.5	0.378353	0.310824	2.485554	0.208575	0.395712	2.434695
1	0.376965	0.311517	2.559614	0.208230	0.395885	2.459016
2	0.374334	0.312833	2.704179	0.207554	0.396223	2.507174
3	0.371872	0.314064	2.844433	0.206896	0.396552	2.554713
4	0.369560	0.315220	2.980818	0.206255	0.396872	2.601661
5	0.367379	0.316311	3.113699	0.205631	0.397184	2.648042
6	0.365315	0.317343	3.243387	0.205023	0.397489	2.693880
7	0.363356	0.318322	3.370148	0.204429	0.397785	2.739197
8	0.361491	0.319254	3.494213	0.203850	0.398075	2.784014
9	0.359712	0.320144	3.615782	0.203284	0.398358	2.828348
10	0.358011	0.320994	3.735032	0.202731	0.398635	2.872218
20	0.344156	0.327922	4.827347	0.197731	0.401134	3.288498

Table 5.3: The local heat transfer coefficient $Q_w(x)$ at the different positions x for various values of λ when $Pr = 0.7$ and $\gamma = 1$

λ	-3	-2	-1	1	1.86	2.31	5
x							
0°	0.683935	0.684815	0.685683	0.687432	0.688103	0.688241	0.690616
10°	0.683495	0.684395	0.685060	0.686781	0.687654	0.687798	0.690184
20°	0.681063	0.681983	0.682166	0.683952	0.685434	0.685464	0.687889
30°		0.676049	0.677505	0.679389	0.681516	0.681637	0.684135
40°		0.670746	0.671288	0.673280	0.676329	0.676454	0.679037
50°		0.661292	0.663813	0.667043	0.669970	0.670098	0.672755
60°			0.655711	0.661106	0.662897	0.663027	0.665718
70°			0.646945	0.653784	0.654979	0.655105	0.657754
80°			0.638216	0.645811	0.646722	0.646840	0.649326
90°				0.636772	0.638416	0.638517	0.640682
100°				0.626214	0.630242	0.630317	0.631986
110°					0.621155	0.621673	0.623475
120°						0.611025	0.614075

Table 5.4: The local skin friction coefficient C_f at the different positions x for various values of λ when $Pr = 0.7$ and $\gamma = 1$

λ	-3	-2	-1	1	1.86	2.31	5
x							
0°	0.000000	0.000000	0.000000	0.000000	0.000000	0.000000	0.000000
10°	0.406697	0.418937	0.430987	0.454667	0.464625	0.466233	0.500114
20°	0.791331	0.815923	0.840044	0.887761	0.907680	0.910919	0.978930
30°		1.171430	1.207639	1.280024	1.309870	1.314756	1.417351
40°		1.470215	1.518447	1.616032	1.646752	1.662293	1.799711
50°		1.703085	1.763064	1.885548	1.935319	1.943514	2.115598
60°			1.935139	2.080385	2.140122	2.149860	2.354441
70°			2.050049	2.216719	2.285698	2.296890	2.532221
80°			2.114390	2.298812	2.375356	2.387767	2.649269
90°				2.343612	2.425039	2.438323	2.719015
100°				2.371532	2.453935	2.467650	2.758642
110°					2.481321	2.494489	2.784701
120°						2.536549	2.813363

Table 5.5: The local heat transfer coefficient $Q_w(x)$ for various values of x when

$Pr = 0.7, 1, 7, \lambda = 10$ and $\gamma = 1$

Pr	0.7	1	7
x			
0°	0.694311	0.725038	1.008014
10°	0.693886	0.723239	1.005625
20°	0.691622	0.7206167	1.003109
30°	0.687981	0.7164552	0.997069
40°	0.683015	0.7104188	0.988541
50°	0.676857	0.7030838	0.977925
60°	0.669892	0.6947445	0.965974
70°	0.661903	0.6851147	0.952394
80°	0.653291	0.6746465	0.937947
90°	0.644247	0.6635467	0.923018
100°	0.634895	0.6519518	0.907847
110°	0.625501	0.6402017	0.892856
120°	0.614950	0.6269539	0.876145

Table 5.6: The local skin friction coefficient C_f for various values of x when

$Pr = 0.7, 1, 7, \lambda = 10$ and $\gamma = 1$

Pr	0.7	1	7
x			
0°	0.000000	0.000000	0.000000
10°	0.553910	0.528024	0.281636
20°	1.086932	1.036460	0.549796
30°	1.580121	1.507612	0.797134
40°	2.017737	1.926877	1.016411
50°	2.388550	2.284000	1.204206
60°	2.679224	2.566542	1.357208
70°	2.906749	2.791441	1.489248
80°	3.066999	2.954954	1.604005
90°	3.170323	3.067061	1.712752
100°	3.231638	3.140626	1.827816
110°	3.261278	3.187926	1.956195
120°	3.277078	3.223147	2.117989

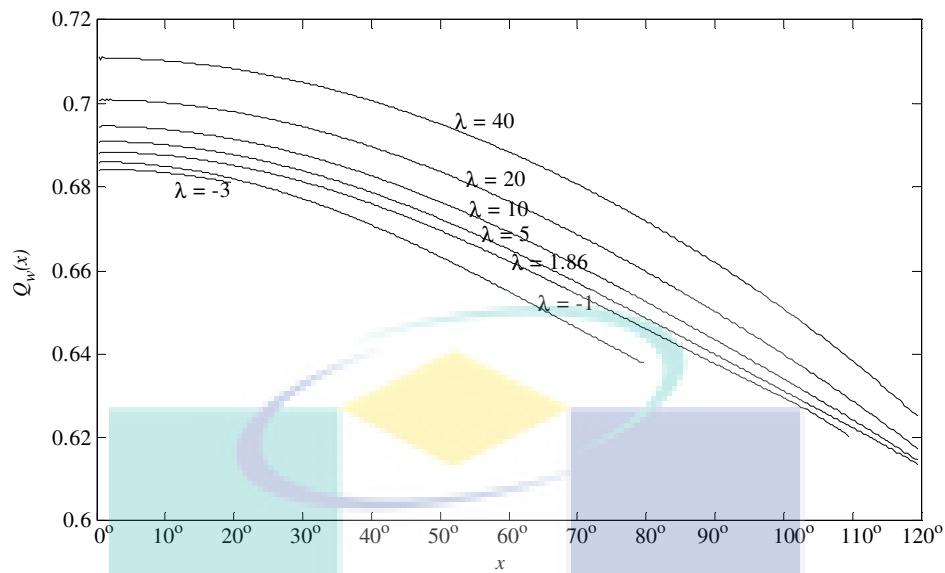


Figure 5.1: The local heat transfer coefficient $Q_w(x)$ with x when $Pr = 0.7$, $\gamma = 1$ and various values of λ

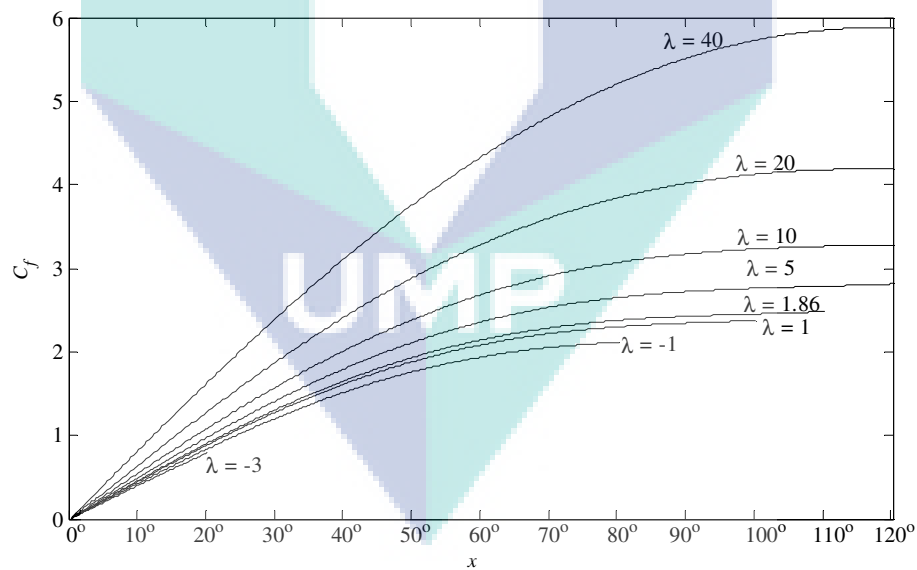


Figure 5.2: The local skin friction coefficient C_f with x when $Pr = 0.7$, $\gamma = 1$ and various values of λ

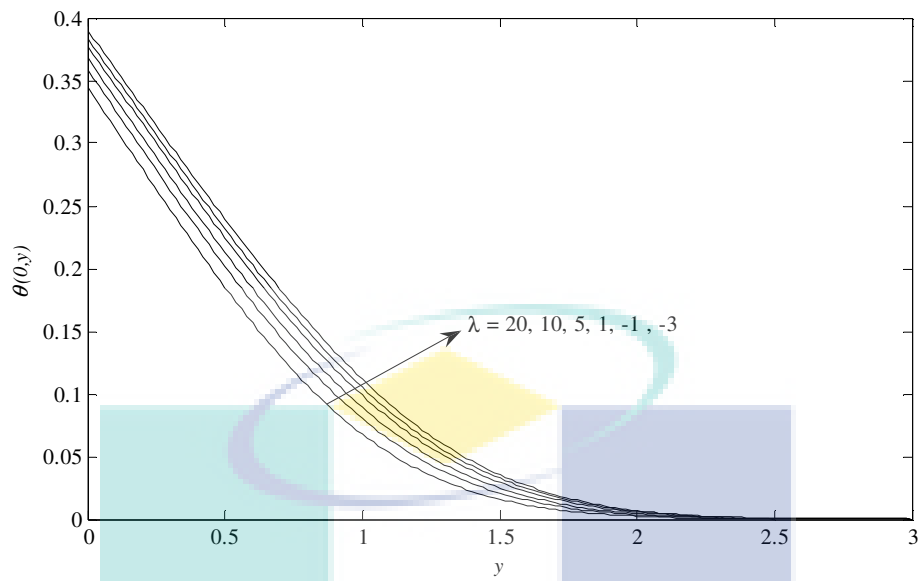


Figure 5.3: The temperature profiles $\theta(0, y)$, for various values of λ when $\text{Pr} = 0.7$ and $\gamma = 0.5$

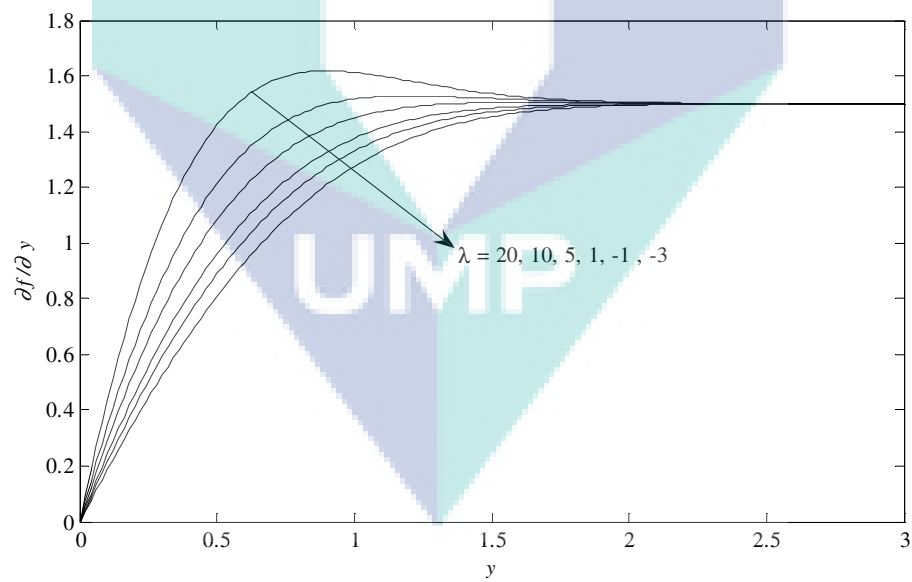


Figure 5.4: The velocity profiles $(\partial f / \partial y)(0, y)$, for various values of λ when $\text{Pr} = 0.7$ and $\gamma = 0.5$

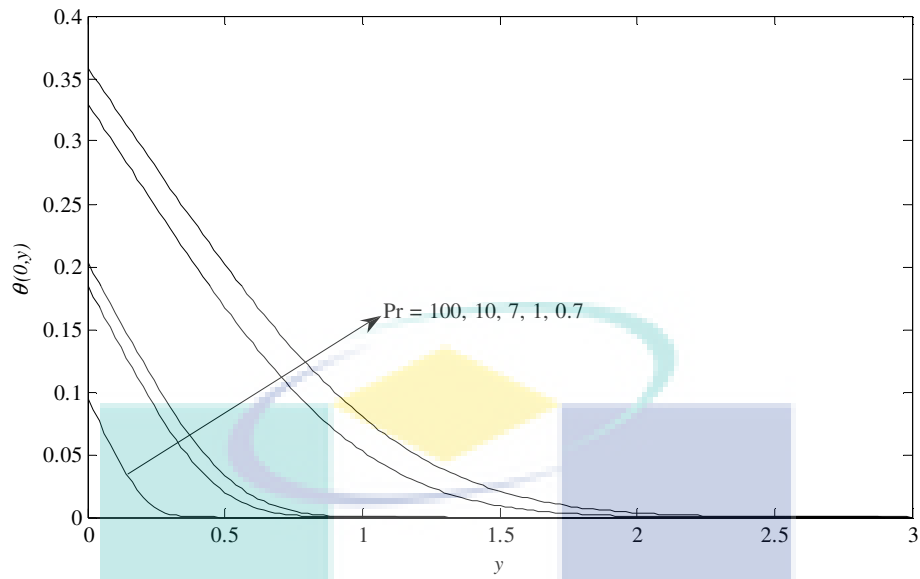


Figure 5.5: The temperature profiles $\theta(0, y)$, for various values of Pr when $\lambda = 10$ and $\gamma = 0.5$

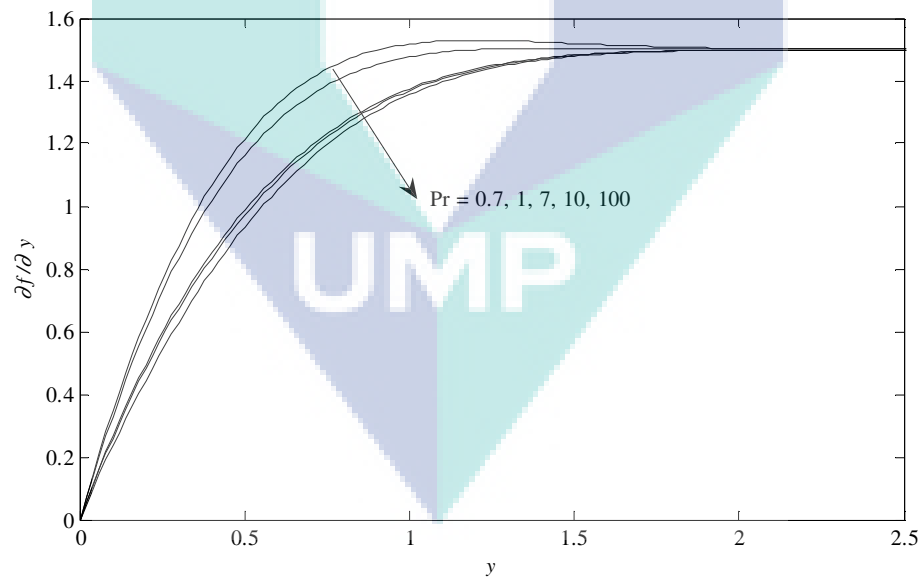


Figure 5.6: The velocity profiles $(\partial f / \partial y)(0, y)$, for various values of Pr when $\lambda = 10$ and $\gamma = 0.5$

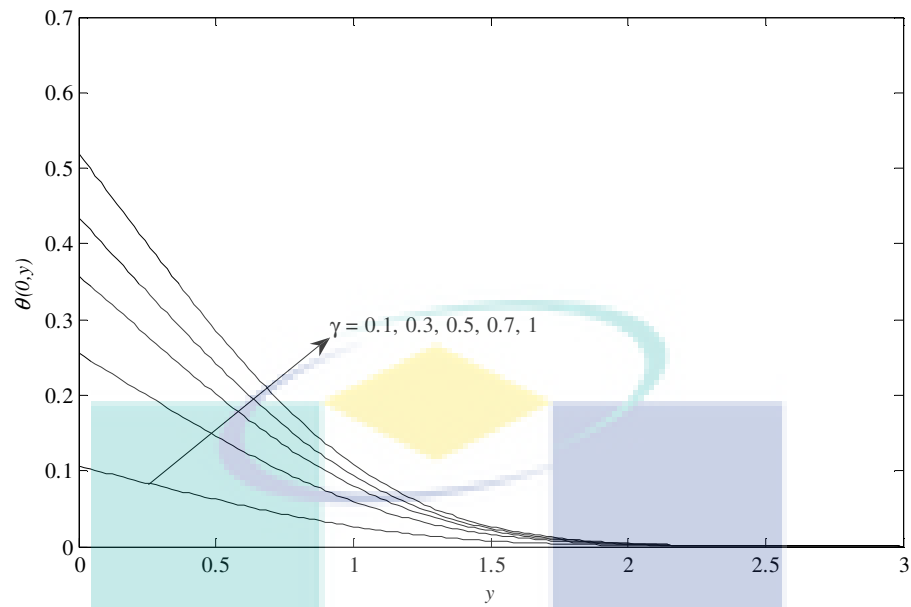


Figure 5.7: The temperature profiles $\theta(0, y)$, for various values of γ when $\lambda=10$ and $\text{Pr} = 0.7$

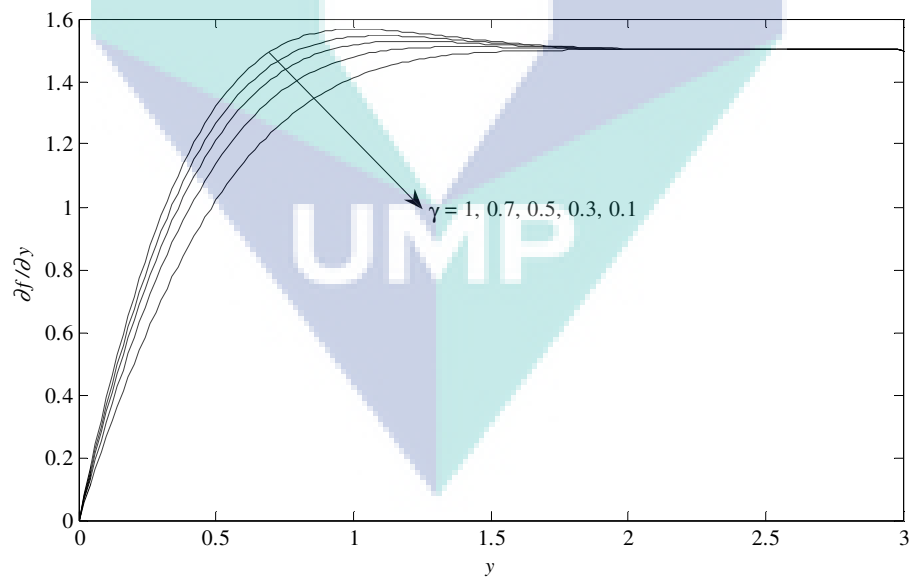


Figure 5.8: The velocity profiles $(\partial f / \partial y)(0, y)$, for various values of γ when $\lambda=10$ and $\text{Pr} = 0.7$

5.4 CONCLUSIONS

In this chapter, we have numerically studied the problem of mixed convection boundary layer flow over a solid sphere with convective boundary conditions using the Keller-box method. It shows how the mixed convection parameter λ , the Prandtl numbers Pr and the conjugate parameter γ , affects the values of heat transfer coefficient $-(\partial\theta/\partial y)(0, y)$, the skin friction coefficient $(\partial^2 f/\partial y^2)(0, y)$, the local skin friction coefficient C_f , the local heat transfer coefficient $Q_w(x)$, the temperature $\theta(0, y)$ and velocity profiles $(\partial f/\partial y)(0, y)$. We can conclude that:

- An increase in the value mixed parameter λ leads to the decrease of wall temperature value and an increase of values, the heat transfer coefficient and the skin friction coefficient. Besides, it is found that for fixed λ , as Pr increases, the values of the wall temperature decreases and the heat transfer coefficient increases. The values of the skin friction coefficient increases at $\lambda > 0$, decreases at $\lambda < 0$ and fixed when $\lambda = 0$.
- An increase in the value x leads to the decrease of the local heat transfer coefficient and an increase of the local skin friction coefficient for all λ . However, as the mixed parameter λ increases, the values of the local heat transfer coefficient and the local skin friction coefficient also increases. On the other hand, when Pr increases, the local heat transfer coefficient increases but the local skin friction coefficient decreases.
- The temperature increase and the velocity are decrease, when the mixed convection parameter λ decreases and also when Pr increases the temperature, velocity and the thermal boundary layer thickness decreases.
- When fixed values are for Pr and λ , if the conjugate parameter γ increases, the values of temperature and velocity increase.

CHAPTER 6

MIXED CONVECTION BOUNDARY LAYER FLOW OVER A SOLID SPHERE IN A MICROPOLAR FLUID

6.1 INTRODUCTION

This chapter discusses the problem of mixed convection boundary layer flow over a solid sphere in a micropolar fluid with convective boundary conditions. The analysis of heat transfer through a laminar mixed convection flow boundary layer over a body of arbitrary shape and arbitrarily, constitutes a very important problem in the field of heat transfer and has received extensive attention. The prediction of heat transfer under such conditions encompasses a wide range of technological applications, such as the cooling problems in turbine blades or electronic systems, the calculation of heat transfer from bodies moving through the atmosphere, manufacturing processes, process industries, and etc (Yaho, 1980).

The studies that are related to this present problem have been studied by Nazar et al. (2002d, 2003a) and Salleh et al. (2010b), in which they studied the mixed convection boundary layer flow about a solid sphere in micropolar fluid with different conditions, namely the constant surface temperature, constant heat flux and Newtonian heating, respectively. Recently, Dasman et al. (2013) have solved numerically the problem of mixed convection boundary layer flow of viscoelastic fluids past a sphere using the Keller-box method.

Motivated from the above contribution, the aim of this study is to investigate the mixed convection about sphere boundary layer flow on a solid sphere with convective boundary conditions in a micropolar fluid and we compared the present result with the previously published results reported by Nazar et al. (2003a). Therefore, five parameters are introduced in this study, which are the Prandtl number, the coordinate running along the surface of the sphere, the conjugate parameter, the material or micropolar parameter and the mixed convection parameter.

6.2 MATHEMATICAL FORMULATION

Similar as claimed in Section 5.2, and referring to equations (2.5) and (5.2). Under the Boussinesq and boundary layer approximations, the equations which govern the boundary layer flow are see (Salleh et al., 2010b; Nazar et al., 2002d, 2003a) the momentum and angular momentum equations can be written as

$$\bar{u} \frac{\partial \bar{u}}{\partial \bar{x}} + \bar{v} \frac{\partial \bar{u}}{\partial \bar{y}} = \bar{u}_e \frac{d\bar{u}_e}{d\bar{x}} + \left(\frac{\mu + \kappa}{\rho} \right) \frac{\partial^2 \bar{u}}{\partial \bar{y}^2} + g\beta(T - T_\infty) \sin\left(\frac{\bar{x}}{a}\right) + \frac{\kappa}{\rho} \frac{\partial \bar{H}}{\partial \bar{y}}, \quad (6.1)$$

$$\rho j \left(\bar{u} \frac{\partial \bar{H}}{\partial \bar{x}} + \bar{v} \frac{\partial \bar{H}}{\partial \bar{y}} \right) = -\kappa \left(2\bar{H} + \frac{\partial \bar{u}}{\partial \bar{y}} \right) + \varphi \frac{\partial^2 \bar{H}}{\partial \bar{y}^2}, \quad (6.2)$$

subject to the boundary conditions (Salleh et al., 2010b; Aziz, 2009)

$$\begin{aligned} \bar{u} = \bar{v} = 0, \quad -k_f \frac{\partial T}{\partial \bar{y}} = h_f (T_f - T), \quad \bar{H} = -n \frac{\partial \bar{u}}{\partial \bar{y}} \quad \text{as } \bar{y} = 0, \\ \bar{u} \rightarrow \bar{u}_e(\bar{x}), \quad T \rightarrow T_\infty, \quad H \rightarrow 0 \quad \text{as } \bar{y} \rightarrow \infty \end{aligned} \quad (6.3)$$

Let $\bar{r}(\bar{x})$ be the radial distance from the symmetrical axis to the surface of the sphere, φ is the spin gradient viscosity and \bar{u}_e is the local free stream velocity which are given by

$$\bar{r}(\bar{x}) = a \sin(\bar{x}/a), \quad \varphi = (\mu + (\kappa/2))j, \quad \bar{u}_e(\bar{x}) = \frac{3}{2} U_\infty \sin\left(\frac{\bar{x}}{a}\right), \quad (6.4)$$

we adopted now the following non-dimensional variables (Salleh et al., 2010b; Nazar et al., 2002d, 2003a and Aziz, 2009):

$$\begin{aligned} x = \frac{\bar{x}}{a}, \quad y = \text{Re}^{1/2} \left(\frac{\bar{y}}{a} \right), \quad r(x) = \frac{\bar{r}(\bar{x})}{a}, \\ u = \frac{\bar{u}}{U_\infty}, \quad v = \text{Re}^{1/2} \left(\frac{\bar{v}}{U_\infty} \right), \\ H = \left(\frac{a}{U_\infty} \right) \text{Re}^{1/2} \bar{H}, \quad \theta = \frac{T - T_\infty}{T_f - T_\infty}, \end{aligned} \quad (6.5)$$

where $Re = U_\infty \frac{a}{\nu}$, is the Reynolds number. Substituting variables (6.5) into equations (6.1) and (6.4) then become with equations (2.17) and (5.7)

$$u \frac{\partial u}{\partial x} + v \frac{\partial u}{\partial y} = u_e \frac{du_e}{dx} + (1+K) \frac{\partial^2 u}{\partial y^2} + \lambda \theta \sin x + K \frac{\partial H}{\partial y}, \quad (6.6)$$

$$u \frac{\partial H}{\partial x} + v \frac{\partial H}{\partial y} = -K \left(2H + \frac{\partial u}{\partial y} \right) + \left(1 + \frac{K}{2} \right) \frac{\partial^2 H}{\partial y^2}, \quad (6.7)$$

The boundary conditions (6.3) become

$$u = v = 0, \quad \frac{\partial \theta}{\partial y} = -\gamma(1-\theta), \quad H = -\frac{1}{2} \frac{\partial u}{\partial y} \quad \text{at } y = 0$$

$$u_e(x) \rightarrow \frac{3}{2} \sin x, \quad \theta \rightarrow 0, \quad H \rightarrow 0 \quad \text{as } y \rightarrow \infty, \quad (6.8)$$

where Pr is the Prandtl number, $\gamma = ah_f Gr^{-1/4} / k_f$ is the conjugate parameter for the convective boundary conditions, $K = \kappa/\mu$ is the material or micropolar parameter, λ is the mixed convection parameter and the Grashof number for convective boundary conditions which were given in previous chapter.

To solve the system of equations (2.17), (5.7), (6.6) and (6.11), subjected to the boundary conditions (6.12), we assume variables (4.10) and stream function (4.11). Thus, this equations become

$$(1+K) \frac{\partial^3 f}{\partial y^3} + (1+x \cot x) f \frac{\partial^2 f}{\partial y^2} - \left(\frac{\partial f}{\partial y} \right)^2 + \lambda \frac{\sin x}{x} \theta$$

$$+ \frac{9 \sin x \cos x}{4x} + K \frac{\partial h}{\partial y} = x \left(\frac{\partial f}{\partial y} \frac{\partial^2 f}{\partial x \partial y} - \frac{\partial f}{\partial x} \frac{\partial^2 f}{\partial y^2} \right), \quad (6.9)$$

$$\left(1 + \frac{K}{2} \right) \frac{\partial^2 h}{\partial y^2} + (1+x \cot x) f \frac{\partial h}{\partial y} - \frac{\partial f}{\partial y} h - K \left(2h + \frac{\partial^2 f}{\partial y^2} \right) = x \left(\frac{\partial f}{\partial y} \frac{\partial h}{\partial x} - \frac{\partial f}{\partial x} \frac{\partial h}{\partial y} \right), \quad (6.10)$$

$$\frac{1}{Pr} \frac{\partial^2 \theta}{\partial y^2} + (1+x \cot x) f \frac{\partial \theta}{\partial y} = x \left(\frac{\partial f}{\partial y} \frac{\partial \theta}{\partial x} - \frac{\partial f}{\partial x} \frac{\partial \theta}{\partial y} \right), \quad (6.11)$$

subject to the boundary conditions

$$f = \frac{\partial f}{\partial y} = 0, \quad \frac{\partial \theta}{\partial y} = -\gamma(1-\theta), \quad h = -\frac{1}{2} \frac{\partial^2 f}{\partial y^2} \text{ at } y = 0,$$

$$\frac{\partial f}{\partial y} \rightarrow \frac{3}{2} \frac{\sin x}{x}, \quad \theta \rightarrow 0, \quad h \rightarrow 0 \text{ as } y \rightarrow \infty. \quad (6.12)$$

It can be seen that at the lower stagnation point of the sphere $x \approx 0$, equations (6.9)-(6.11) reduce to the following ordinary differential equations:

$$(1+K)f''' + 2ff'' - f'^2 + Kh' + \lambda\theta + \frac{9}{4} = 0, \quad (6.13)$$

$$\left(1 + \frac{K}{2}\right)h'' + 2fh' - f'h - K(2h + f'') = 0, \quad (6.14)$$

$$\frac{1}{\text{Pr}}\theta'' + 2f\theta' = 0, \quad (6.15)$$

and the boundary conditions (6.12) become

$$f(0) = f'(0) = 0, \quad \theta'(0) = -\gamma(1-\theta(0)), \quad h(0) = -\frac{1}{2}f''(0),$$

$$f' \rightarrow \frac{3}{2}, \quad \theta \rightarrow 0, \quad h \rightarrow 0 \text{ as } y \rightarrow \infty. \quad (6.16)$$

The physical quantities of interest in this problem are the local skin friction coefficient, C_f and the local heat transfer coefficient, $Q_w(x)$ which are defined by

$$C_f = \frac{a}{U_\infty} \text{Re}^{-1/2} \left[(\mu + \kappa) \frac{\partial \bar{u}}{\partial \bar{y}} + \kappa H \right]_{\bar{y}=0} \quad \text{and} \quad Q_w(x) = \frac{a}{k(T_f - T_\infty)} \text{Re}^{-1/2} \left(\frac{\partial \bar{T}}{\partial \bar{y}} \right)_{\bar{y}=0}. \quad (6.17)$$

Using the non-dimensional variables (6.5), we have

$$C_f = \left(1 + \frac{K}{2}\right)x \frac{\partial^2 f}{\partial y^2}(x,0), \quad \text{and} \quad Q_w(x) = \gamma(1-\theta(x,0)) \quad (6.18)$$

6.3 RESULTS AND DISCUSSION

The nonlinear partial differential equations (6.9) to (6.12) subject to the boundary conditions (6.16) are solved numerically using Keller box-method. The values of the heat transfer coefficient $-\theta'(0)$ and the skin friction coefficient $f''(0)$ obtained by numerically solving equations (6.13) to (6.15) subject to boundary conditions (6.16) for the case at the lower stagnation point of the sphere, $x \approx 0$, for various values of λ when $Pr = 0.7$, $K=1$ and $\gamma \rightarrow \infty$ are presented in Table 6.1. Some numerical results are obtained by an implicit finite-difference scheme as reported by Nazar et al. (2003a) for the case of constant wall temperature. It is found that the agreement between the previously published results with the present ones is excellent. We can conclude that this numerical method works efficiently for the present problem and we are also confident that the results presented here are accurate.

Tables 6.2 to 6.5 show the values of the local heat transfer coefficient $Q_w(x)$ and the local skin friction coefficient C_f at different positions x for various values of λ when $Pr = 0.7$, $K = 1, 3$ and $\gamma=0.5$, respectively. It is found that the local heat transfer coefficient and the local skin friction coefficient increase as the mixed convection parameter λ also increases. Similarly, for a given value of λ , the local heat transfer coefficient $Q_w(x)$ is found to decrease with the increment of the distance x from the stagnation point. Furthermore, we can see from these tables that the increment of λ delays the separation and that separation can be completely suppressed in the range $0^\circ \leq x \leq 120^\circ$ for sufficiently large values of $\lambda > 0$. The actual value of $\lambda = \lambda_k$ which first gives no separation is difficult to be exactly determine as it has to be found by successive integrations of the equations. However, the numerical solutions indicate that the value of λ , which first gives no separation lies between 2.31 and 2.32 for $K = 1$ and between 2.54 and 2.55 for $K = 3$. For fixed x and λ , as the values of the micropolar parameter K increases from 1 to 2, this resulted in an increase of the value of the local skin friction coefficient, as well as a decrease in the values of the local heat transfer coefficient.

Figures 6.1 to 6.2 present the variation of the local heat transfer coefficient $Q_w(x)$ and local skin friction coefficient C_f with x when $Pr = 0.7$, $K = 1, 2$, $\lambda = 1$ and various values of the conjugate parameter γ , respectively. These figures show that the values of the local heat transfer coefficient and local skin friction coefficient increase with the increment of the conjugate parameter γ . From Figure 6.1, it is clear that the effect of the conjugate parameter is more pronounced than the effect of the micropolar parameter on the values of the local heat transfer coefficient but we found the contradict of it in Figure 6.2.

The temperature, velocity and angular velocity profiles at the lower stagnation point of the sphere, $x \approx 0$, are plotted in Figures 6.3 to 6.5 for some values of λ when $Pr = 0.7$, $K = 1, 3$ and $\gamma = 0.5$, respectively. It is found that for fixed values of K , the velocity and angular velocity increase, while the temperature decrease when the mixed convection parameter λ increases. Moreover, when λ is fixed, as the micropolar parameter K increases, the temperature also increase but the velocity and angular velocity decrease. In addition, we also notice that for $\lambda > 0$ (assisting flow), there is an overshoot of the velocity and angular velocity from the free stream velocity, which is smaller for higher values of the micropolar parameter K .

Figures 6.6 to 6.8 display the temperature, velocity and angular velocity profiles at the lower stagnation point of the sphere, $x \approx 0$, for some values of γ when $\lambda = 5$, $K = 1, 3$ and $Pr = 0.7$, respectively. It is found that for fixed values of K and λ , the temperature, velocity and angular velocity increase when the conjugate parameter γ increases. This is because, as the conjugate parameter increases, the convective heat transfers from the hot micropolar fluid side on the surface of the sphere to the cold micropolar fluid side increases leading to an increase in the temperature, velocity and the angular velocity.

Table 6.1: The heat transfer coefficient $-\theta'(0)$ and the skin friction coefficient $f''(0)$ at the lower stagnation point of the sphere, $x \approx 0$, for various values of λ when $Pr = 7$, $K = 1$ and $\gamma \rightarrow \infty$ (CWT)

λ	$-\theta'(0)$		$f''(0)$	
	Nazar et al. (2003a)	Present	Nazar et al. (2003a)	Present
-3	0.6770	0.677045	0.9383	0.938298
-2	0.7064	0.706388	1.2113	1.211342
-1	0.7312	0.731223	1.4617	1.461763
-0.5	0.7427	0.742699	1.5840	1.584003
1	0.7745	0.774456	1.9444	1.944369
2	0.7935	0.793543	2.1750	2.174998
3	0.8109	0.810897	2.3976	2.397570
4	0.8271	0.827102	2.6134	2.613378
5	0.8425	0.842549	2.8271	2.827117

Table 6.2: The local heat transfer coefficient $Q_w(x)$ at the different positions x for various values of λ when $Pr = 0.7$, $K = 1$ and $\gamma = 0.5$

λ	-5.4	-3	-1	1	2.31	2.32	3
x							
0°	0.458238	0.460309	0.469099	0.473775	0.477636	0.478117	0.480286
10°	0.453009	0.459147	0.465056	0.471706	0.475302	0.476477	0.479015
20°		0.457187	0.462258	0.468964	0.472645	0.473865	0.477146
30°		0.453200	0.456607	0.462923	0.466412	0.467575	0.472974
40°			0.448586	0.454249	0.457405	0.458462	0.466287
50°			0.438349	0.443087	0.445760	0.446662	0.456310
60°			0.426961	0.429974	0.432005	0.432697	0.443177
70°				0.414318	0.415470	0.415868	0.425321
80°				0.396785	0.396816	0.396823	0.404084
90°				0.375575	0.376045	0.376159	0.384742
100°					0.354905	0.355072	0.369892
110°					0.335943	0.336100	0.356285
120°						0.319876	0.349935

Table 6.3: The local skin friction coefficient, C_f at the different positions x for various values of λ when $Pr = 0.7$, $K = 1$ and $\gamma = 0.5$

λ	-5.4	-3	-1	1	2.31	2.32	3
x							
0°	0.000000	0.000000	0.000000	0.000000	0.000000	0.000000	0.000000
10°	0.434092	0.452117	0.471650	0.496164	0.510519	0.515420	0.526340
20°		0.879233	0.916987	0.963392	0.990862	1.000299	1.022354
30°		1.260321	1.312772	1.374291	1.411092	1.423795	1.458550
40°			1.639467	1.706404	1.747112	1.761265	1.808742
50°			1.883386	1.943530	1.981198	1.994455	2.050702
60°			2.034285	2.075047	2.101905	2.111604	2.169688
70°				2.109682	2.116533	2.119463	2.164476
80°				2.023588	2.031492	2.044413	2.053081
90°				1.830014	1.851889	1.872065	1.934970
100°					1.538420	1.555003	1.678325
110°					1.389932	1.416533	1.461896
120°						1.224859	1.271793

Table 6.4: The local heat transfer coefficient $Q_w(x)$ at the different positions x for various values of λ when $Pr = 0.7$, $K = 2$ and $\gamma = 0.5$

λ	-5.9	-3	-1	1	2.54	2.55	3
x							
0°	0.450823	0.455644	0.456113	0.460606	0.466133	0.466878	0.476956
10°	0.445287	0.450599	0.454811	0.459484	0.462772	0.463417	0.464603
20°		0.448208	0.452363	0.456998	0.460291	0.460947	0.462152
30°		0.443868	0.447490	0.451775	0.454830	0.455442	0.456740
40°		0.438636	0.440649	0.444392	0.447071	0.447609	0.448794
50°			0.432032	0.435053	0.437222	0.437659	0.438615
60°			0.422164	0.424313	0.425857	0.426168	0.426854
70°				0.411833	0.412604	0.412759	0.413126
80°				0.387110	0.398013	0.398188	0.398201
90°				0.372967	0.383083	0.381073	0.382724
100°					0.365929	0.366155	0.367487
110°					0.355189	0.352506	0.353630
120°						0.340081	0.340332

Table 6.5: The local skin friction coefficient, C_f at the different positions x for various values of λ when $Pr = 0.7$, $K = 2$ and $\gamma = 0.5$.

λ	-5.9	-3	-1	1	2.3	2.55	3
x							
0°	0.000000	0.000000	0.000000	0.000000	0.000000	0.000000	0.000000
10°	0.515240	0.533663	0.549936	0.569725	0.584709	0.587790	0.593512
20°		1.043496	1.073712	1.110818	1.139137	1.144990	1.155878
30°		1.508721	1.548308	1.596747	1.633995	1.641723	1.656520
40°		1.909917	1.954886	2.006314	2.046340	2.054689	2.070775
50°			2.280983	2.325340	2.360633	2.368063	2.382437
60°			2.516202	2.543347	2.566189	2.571101	2.580767
70°				2.677421	2.679633	2.680316	2.682070
80°				2.704267	2.710539	2.714652	2.735972
90°				2.700097	2.703001	2.707898	2.721561
100°					2.634895	2.617974	2.586765
110°					2.601425	2.580291	2.541319
120°						2.584262	2.541351

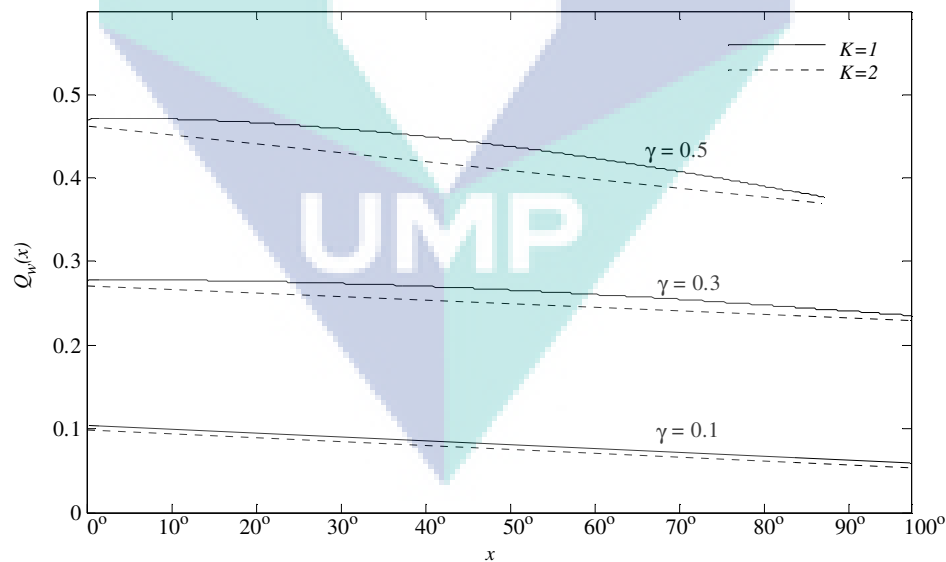


Figure 6.1: The local heat transfer coefficient $Q_w(x)$ with x when $Pr = 0.7$, $K = 1, 2$, $\lambda = 1$ and various values of γ

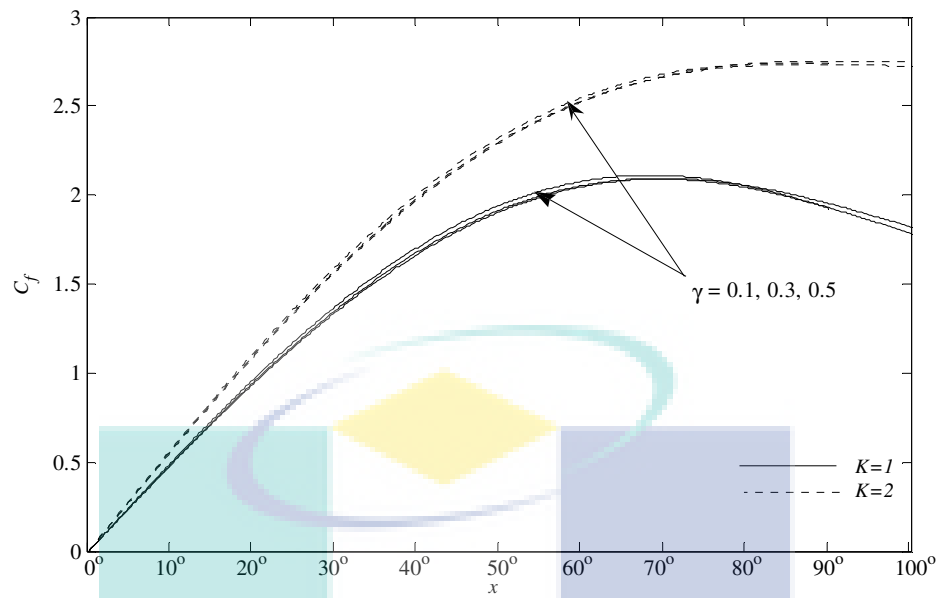


Figure 6.2: The local skin friction coefficient, C_f with x when $Pr = 0.7$, $K = 1, 2$, $\lambda = 1$ and various values of γ

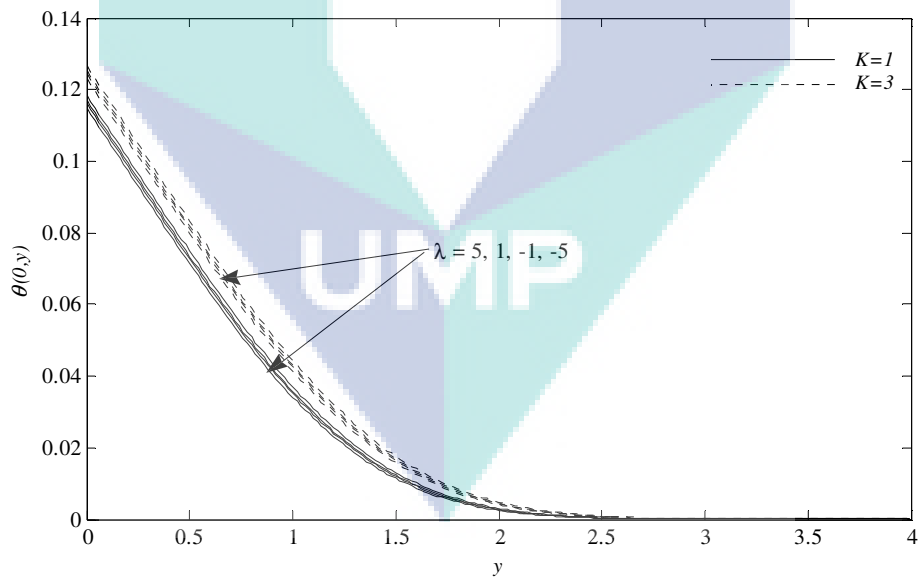


Figure 6.3: The temperature profiles $\theta(0, y)$, for various values of λ when $Pr = 0.7$, $K = 1, 3$ and $\gamma = 0.1$

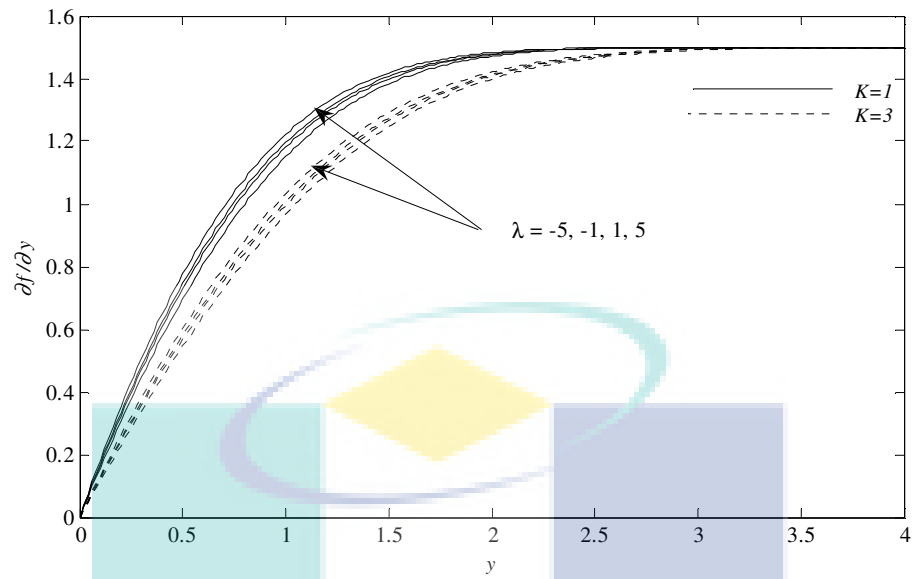


Figure 6.4: The velocity profiles $(\partial f / \partial y)(0, y)$, for various values of λ when $\text{Pr} = 0.7$, $K = 1, 3$ and $\gamma = 0.1$

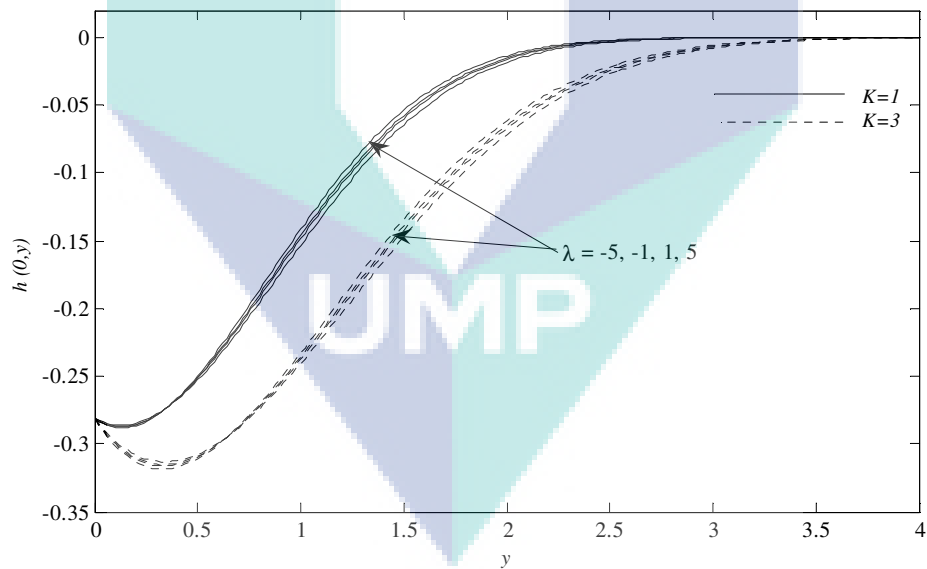


Figure 6.5: The angular velocity profiles $h(0, y)$ for various values of λ when $\text{Pr} = 0.7$, $K = 1, 3$, and $\gamma = 0.1$

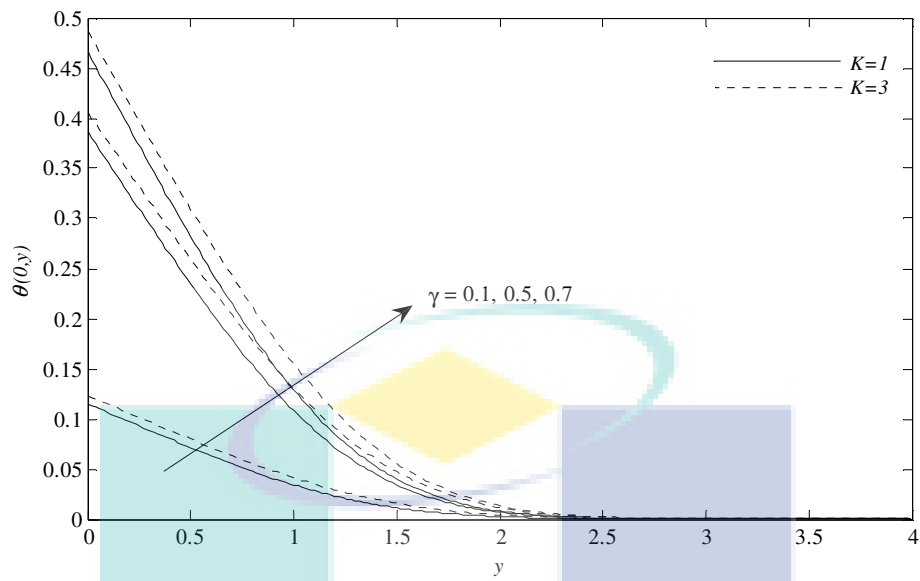


Figure 6.6: The temperature profiles $\theta(0, y)$, for various values of γ when $\lambda = 5$, $K = 1, 3$ and $Pr = 0.7$

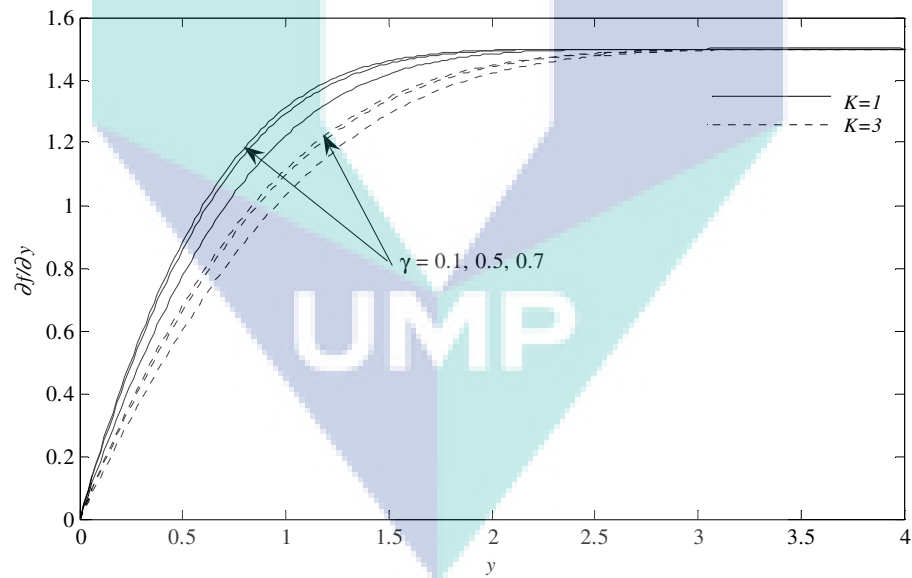


Figure 6.7: The velocity profiles $(\partial f / \partial y)(0, y)$, for various values of γ when $\lambda = 5$, $K = 1, 3$ and $Pr = 0.7$

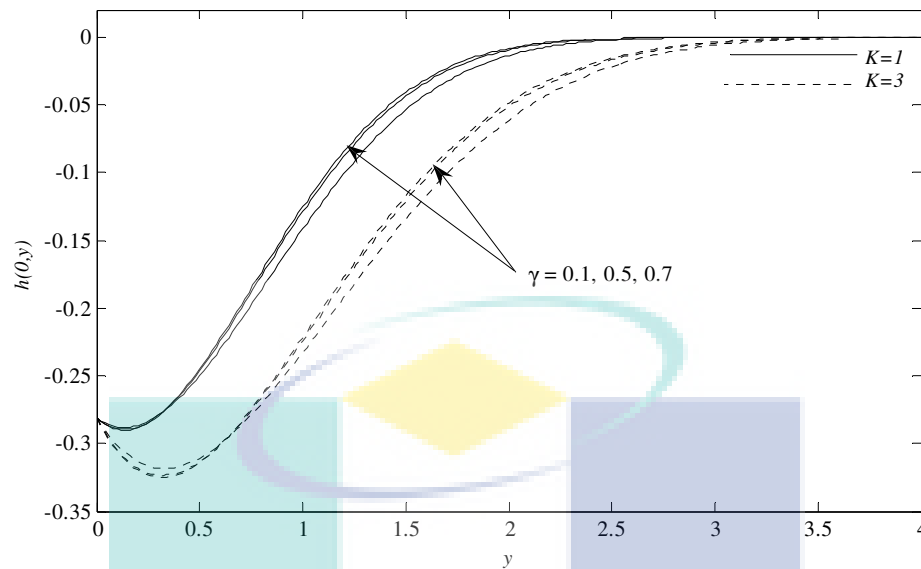


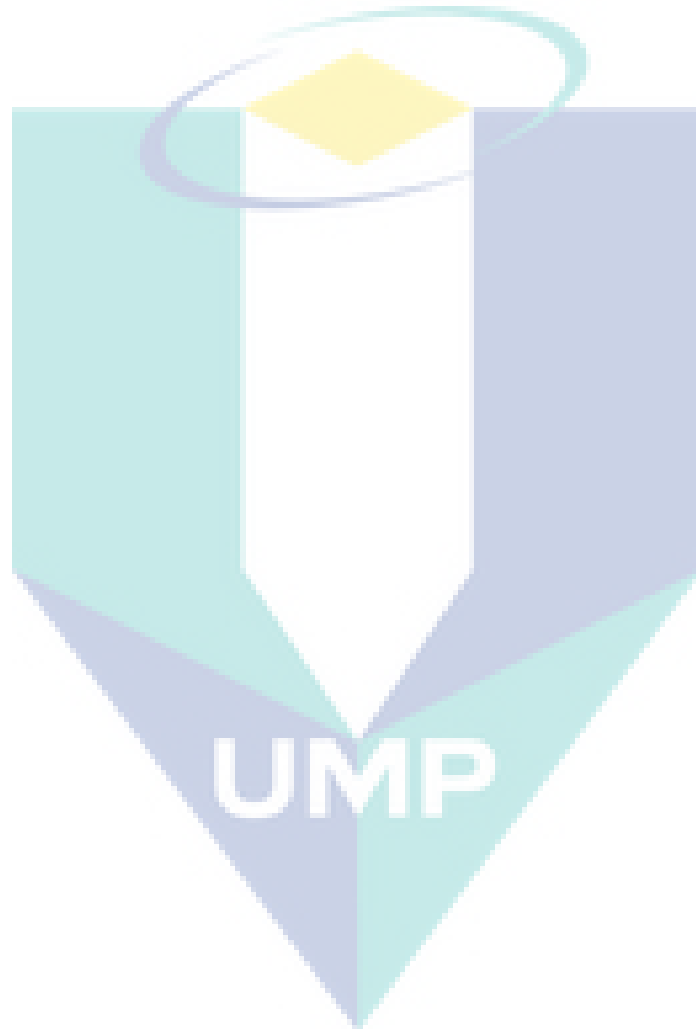
Figure 6.8: The angular velocity profiles $h(0, y)$ for various values of γ when $\lambda = 5$, $K = 1, 3$ and $Pr = 0.7$

6.4 CONCLUSIONS

In this chapter, we have numerically studied the problem of mixed convection boundary layer flow over a sphere with convective boundary conditions in micropolar fluid and solved it by using the Keller-box method. It shows how the mixed convection parameter λ , the micropolar parameter K and the conjugate parameter γ , affects the local skin friction coefficient C_f , the local heat transfer coefficient $Q_w(x)$, as well as the temperature $\theta(0, y)$, velocity $(\partial f / \partial y)(0, y)$ and angular velocity profiles $h(0, y)$. We can conclude that:

- When the conjugate parameter increases the values of the local heat transfer coefficient, so does the local skin friction coefficient. Also, as the mixed convection parameter λ increases the values of the local heat transfer coefficient, the same goes to the local skin friction coefficient.

- The temperature increases but the velocity and angular velocity decrease when the mixed convection parameter λ decreases, and also K increases the value of temperature while the velocity and angular velocity decrease.
- An increase in the values of the conjugate parameter γ leads to an increase of the temperature, velocity and angular velocity



CHAPTER 7

MIXED CONVECTION BOUNDARY LAYER FLOW OVER A SOLID SPHERE IN A NANOFLUID

7.1 INTRODUCTION

In this chapter, we study the mixed convection boundary layer flow over a solid sphere subjected to a convective boundary condition with nanofluid formed by the dilution of nanoparticles, such as copper Cu , aluminum oxide Al_2O_3 and titanium dioxide TiO_2 , in water. Nanofluids are primarily used as coolant in heat transfer equipment such as heat exchangers, electronic cooling system (such as flat plate) and radiators. Heat transfer over flat plate has been analyzed by many researchers. Graphene based nanofluid has been found to enhance Polymerase chain reaction efficiency. Nanofluids in solar collectors are another application where it is employed for their tunable optical properties (Wong and De Leon, 2010).

This problem has been considered by several people as listed in literature review section in Chapter 1. Recently, Tham et al. (2011) presented the mixed convection boundary layer flow about a solid sphere with constant surface temperature in nanofluid.

The aim of this study is to investigate the mixed convection boundary layer flow on a sphere with convective boundary conditions in a nanofluid. The accuracy of the current results is verified by comparing the numerical values with Nazar et al. (2002c) for limiting cases when nanoparticle volume fraction or solid volume fraction of the nanofluid $\chi = 0$ (Newtonian fluid), the Prandtl number $Pr = 6.8$ and the conjugate parameter $\gamma \rightarrow \infty$. It is found that the agreement between the previously published results with the present ones is very good. Therefore, we are confident that the numerical technique applied in this present problem is accurate. Numerical results

presented herein include velocity and temperature profiles as well as variation of skin friction and wall temperature.

7.2 BASIC EQUATIONS

The basic steady dimensional continuity, momentum and energy equations for a nanofluid are considered in Chapter 2. Therefore, we have to solve the following equations

$$\left[\frac{1}{(1-\chi)^{2.5} [1-\chi+(\chi\rho_s/\rho_f)]} \right] \frac{\partial^3 f}{\partial y^3} + (1+x \cot x) f \frac{\partial^2 f}{\partial y^2} - \left(\frac{\partial f}{\partial y} \right)^2 + \left[\frac{\chi\rho_s(\beta_s/\beta_f) + (1-\chi)\rho_f}{(1-\chi)\rho_f + \chi\rho_f} \right] \lambda \frac{\sin x}{x} \theta + \frac{9 \sin x \cos x}{4x} = x \left(\frac{\partial f}{\partial y} \frac{\partial^2 f}{\partial x \partial y} - \frac{\partial f}{\partial x} \frac{\partial^2 f}{\partial y^2} \right), \quad (7.1)$$

$$\frac{1}{\text{Pr}} \left[\frac{(k_s + 2k_f) - 2\chi(k_f - k_s)}{[(k_s + 2k_f) + \chi(k_f - k_s)][(1-\chi) + \chi(\rho C_p)_s / (\rho C_p)_f]} \right] \frac{\partial^2 \theta}{\partial y^2} + (1+x \cot x) f \frac{\partial \theta}{\partial y} = x \left(\frac{\partial f}{\partial y} \frac{\partial \theta}{\partial x} - \frac{\partial f}{\partial x} \frac{\partial \theta}{\partial y} \right), \quad (7.2)$$

with the boundary conditions

$$f = \frac{\partial f}{\partial y} = 0, \quad \frac{\partial \theta}{\partial y} = -\gamma(1-\theta) \text{ at } y = 0, \\ \frac{\partial f}{\partial y} \rightarrow \frac{3 \sin x}{2x}, \quad \theta \rightarrow 0 \text{ as } y \rightarrow \infty, \quad (7.3)$$

with the physical quantities of interest in this problem are the local skin friction coefficient C_f and the local heat transfer coefficient $Q_w(x)$ which are defined by

$$C_f = \frac{1}{(1-\chi)^{2.5}} x \frac{\partial^2 f}{\partial y^2}(x, 0) \text{ and } Q_w(x) = \gamma \left[\frac{(k_s + 2k_f) - 2\chi(k_f - k_s)}{(k_s + 2k_f) + \chi(k_f - k_s)} \right] (1-\theta(x, 0)) \quad (7.4)$$

7.3 RESULTS AND DISCUSSION

There are three different types of nanoparticles, namely Cu , Al_2O_3 and TiO_2 (with water as their base fluid), have been considered in this study. Results for the local skin friction coefficient C_f and the local heat transfer coefficient $Q_w(x)$ have been obtained at different positions x between the interval $0^\circ \leq x \leq 120^\circ$, with various values of the mixed convection parameter λ , the conjugate parameter γ , and the coordinate x measured along the surface of the sphere and the range of nanoparticle volume fraction $0 \leq \chi \leq 0.2$ when the Prandtl number $Pr = 0.7$ (for comparison purpose) and 6.2 (water-based nanofluid). We used the data related to the thermophysical properties of fluids and nanoparticles as listed in Table 7.1 and the one listed by Abu-Nada and Oztop (2009) to compute each case of nanofluid.

The numerical solutions are obtained for various values of λ when $\chi = 0$ (Newtonian fluid), $Pr = 6.8$ and $\gamma \rightarrow \infty$. The present results for some values of the heat transfer coefficient $-\theta'(0)$ and the skin friction coefficient $f''(0)$ at the lower stagnation point of the sphere, $x \approx 0$, are compared with those of Nazar et al. (2002c) in order to validate the numerical results obtained. The comparison shows that the numerical solutions (see Table 7.2) obtained by the present computation concurs very well with those of previous publication.

Tables 7.3 to 7.14 presented the values of the local heat transfer coefficient $Q_w(x)$ and the local skin friction coefficient C_f at the different positions x and various values of mixed parameter λ , $\chi = 0.1$ and $\chi = 0.2$ (nanofluid) with different nanoparticles (Cu , Al_2O_3 and TiO_2) when $Pr = 6.2$ and $\gamma = 0.5$, respectively. It is found that for fixed x and λ , as the value of nanoparticle volume fraction χ increases from 0.1 to 0.2, it resulted in an increase of the value of C_f and $Q_w(x)$ and these increases are applied in both heated sphere ($\lambda > 0$) and cooled sphere ($\lambda < 0$) cases. It is observed from these tables Cu (nanoparticles with high density) that it tends to have the highest local skin friction coefficient compared to TiO_2 and Al_2O_3 . In addition, Cu

also has the highest of local heat transfer coefficient $Q_w(x)$, followed by Al_2O_3 and TiO_2 (nanoparticles with low thermal conductivity). It can be seen from Tables 7.3 to 7.6 for the case Cu nanoparticles that the actual value of $\lambda = \lambda_s (> 0)$, which first gives no separation, is difficult to be exactly determine. However, the numerical solutions indicated that the value of λ_s , which first gives no separation, lies between 1.66 and 1.67 for $\chi = 0.1$ and between 2.08 and 2.09 for $\chi = 0.2$, when $Pr = 6.2$ and $\gamma = 0.5$. As well as in Tables 7.7 to 7.10 for the case of Al_2O_3 nanoparticles, the value of λ_s , lies between 0.80 and 0.81 for $\chi = 0.1$ and between 1.71 and 1.72 for $\chi = 0.2$ and for case of TiO_2 , nanoparticles in Tables 7.11 to 7.14, the value of λ_s , lies between 1.38 and 1.39 for $\chi = 0.1$ and between 1.94 and 1.95 for $\chi = 0.2$.

Figures 7.1 and 7.2 shows the local heat transfer coefficient $Q_w(x)$ and the local skin friction coefficient C_f with x using various nanoparticles (Cu , Al_2O_3 and TiO_2) when $Pr = 6.2$, $\lambda = -1$ (opposing flow), $\gamma = 0.5$ and the nanoparticle volume fraction $\chi = 0.1$ and 0.2 , respectively. It is found that for all the three nanoparticle cases, the local heat transfer coefficient $Q_w(x)$ and the local skin friction coefficient C_f increases with the increase of χ .

The variation of the local heat transfer coefficient $Q_w(x)$ and the local skin friction coefficient C_f with x using various nanoparticles (Cu , Al_2O_3 and TiO_2) when $Pr = 6.2$, $\lambda = -1$ (opposing flow), $\chi = 0.2$ and the conjugate parameter $\gamma = 0.3, 0.5$ are presented in Figures 7.3 and 7.4, respectively. It can be seen that for all nanoparticles cases, as the conjugate parameter increases, it causes an increase to the value of local heat transfer coefficient $Q_w(x)$ and the local skin friction coefficient C_f .

Figures 7.5 and 7.6 illustrate the local heat transfer coefficient $Q_w(x)$ and the local skin friction coefficient C_f with various x using different nanoparticles (Cu , Al_2O_3 and TiO_2) when $\lambda = 4$ (assisting flow) and $\lambda = -1$ (opposing flow), $Pr = 6.2$, $\chi = 0.2$, and $\gamma = 0.5$, respectively. It can be seen that Cu nanoparticles has the highest

local heat transfer coefficient compared to Al_2O_3 and TiO_2 . Moreover, Cu also has the highest local skin friction coefficient, followed by TiO_2 and Al_2O_3 nanoparticles due to the physical properties for all nanoparticles.

The temperature $\theta(0, y)$ and velocity $(\partial f / \partial y)(0, y)$ profiles using various nanoparticles when $Pr = 6.2$, $\lambda = 1$, $\gamma = 0.5$ and $\chi = 0.1, 0.2$ shown in Figures 7.7 and 7.8, respectively. It can be found that the temperature and velocity decreases from Cu to TiO_2 and to Al_2O_3 , when fixed nanoparticle volume fraction χ . In addition, as χ increases from 0.1 to 0.2, the temperature increases but the velocity decreases. However, Figures 7.9 and 7.10 presented the temperature $\theta(0, y)$ and velocity $(\partial f / \partial y)(0, y)$ of each nanoparticles when $Pr = 6.2$, $\lambda = 1$, $\chi = 0.2$ and various values of conjugate parameter γ . It is found that as γ increases, the temperature also increases but not for the velocity.

Finally, Figures 7.11 and 7.12 also presented the temperature $\theta(0, y)$ and velocity $(\partial f / \partial y)(0, y)$ profiles using Cu nanoparticles when $Pr = 6.2$, $\chi = 0.1, 0.2$, $\lambda = 1$ and with various values of γ . It is found that when the nanoparticle volume fraction χ is fixed and the values of conjugate parameter γ is increasing, it leads to an increment of temperature and the decrease of velocity. When γ is fixed, as χ increases the values of temperature also increases and the velocity decreases.

Table 7.1: The thermophysical properties of fluid and nanoparticles, (see Abu-Nada and Oztop, 2009)

Physical properties	Fluid phase (water)	<i>Cu</i>	<i>Al₂O₃</i>	<i>TiO₂</i>
C_p (J kg ⁻¹ K ⁻¹)	4179	385	765	686.2
ρ (kg m ⁻³)	997.1	8933	3970	4250
k (W m K ⁻¹)	0.613	400	40	8.9538
$\beta \times 10^{-5}$ (K ⁻¹)	21	1.67	0.85	0.9

Table 7.2: The heat transfer coefficient $-\theta'(0)$ and the skin friction coefficient $f''(0)$ at the lower stagnation point of the sphere, $x \approx 0$, for various values of λ when $\chi = 0$ (Newtonian fluid), Pr = 6.8 and $\gamma \rightarrow \infty$ (CWT)

λ	$-\theta'(0)$		$f''(0)$	
	Nazar et al. (2002c)	Present	Nazar et al. (2002c)	Present
-4	0.6534	0.653381	0.5028	0.502845
-3	0.7108	0.710804	1.0700	1.070014
-2	0.7529	0.752864	1.5581	1.558098
-1	0.7870	0.786997	2.0016	2.001582
-0.5	0.8021	0.802141	2.2115	2.211545
0	0.8162	0.816215	2.4151	2.415122
1	0.8463	0.846307	2.8064	2.806447
2	0.8648	0.864754	3.1804	3.180385
3	0.8857	0.885714	3.5401	3.540068
4	0.9050	0.905098	3.8880	3.887995
5	0.9230	0.922991	4.2257	4.225714
6	0.9397	0.939732	4.5546	4.554647
7	0.9555	0.955475	4.8756	4.875558
8	0.9704	0.970410	5.1896	5.189644
9	0.9846	0.984558	5.4974	5.497377
10	0.9981	0.998147	5.7995	5.799549
20	1.1077	1.107665	8.5876	8.587787

Table 7.3: The local heat transfer coefficient $Q_w(x)$ at the different positions x for $\chi = 0.1$ using Cu nanoparticles, $Pr = 6.2$, $\gamma = 0.5$ and various values of λ

λ	-8.4	-5	-3	-1	1.66	1.67	3
x							
0°	0.699239	0.700917	0.706494	0.709907	0.718013	0.718226	0.720395
10°	0.696899	0.700088	0.702805	0.707626	0.714704	0.714966	0.718091
20°		0.695225	0.700702	0.706001	0.713005	0.713352	0.716978
30°		0.692268	0.697835	0.703134	0.710450	0.711001	0.714869
40°		0.686903	0.692596	0.698282	0.705692	0.706290	0.710125
50°			0.685542	0.691174	0.698963	0.699646	0.703716
60°			0.676868	0.682608	0.690588	0.691038	0.695187
70°			0.666092	0.671890	0.680032	0.680478	0.684695
80°				0.659315	0.667462	0.667901	0.672113
90°				0.645037	0.653014	0.653440	0.657551
100°					0.637001	0.637400	0.641210
110°					0.620702	0.621059	0.624354
120°						0.603999	0.606565

Table 7.4: The local skin friction coefficient, C_f at the different positions x for $\chi = 0.1$ using Cu nanoparticles, $Pr = 6.2$, $\gamma = 0.5$ and various values of λ

λ	-8.4	-5	-3	-1	1.66	1.67	3
x							
0°	0.000000	0.000000	0.000000	0.000000	0.000000	0.000000	0.000000
10°	0.556168	0.582251	0.604018	0.629601	0.667094	0.668811	0.690223
20°		1.069944	1.138812	1.210485	1.306763	1.311066	1.363554
30°		1.577527	1.648544	1.730455	1.848871	1.854388	1.927223
40°		1.883223	2.002961	2.129722	2.303309	2.311200	2.407382
50°			2.304512	2.406458	2.599001	2.607241	2.727628
60°			2.445311	2.571299	2.760426	2.769380	2.880012
70°			2.425858	2.581351	2.803073	2.813355	2.940043
80°				2.505055	2.682437	2.691129	2.799639
90°				2.319423	2.504588	2.513444	2.623615
100°					2.236224	2.241833	2.313338
110°					2.006726	2.010015	2.052704
120°						1.833664	1.845827

Table 7.5: The local heat transfer coefficient $Q_w(x)$ at the different positions x for $\chi = 0.2$ using Cu nanoparticles, $Pr = 6.2$, $\gamma = 0.5$ and various values of λ

λ	-9.5	-5	-3	-1	2.08	2.09	3
x							
0°	0.878913	0.882791	0.885966	0.889000	0.893004	0.893049	0.896065
10°	0.874948	0.880829	0.884452	0.887174	0.891003	0.891312	0.895534
20°		0.880636	0.883471	0.886035	0.890800	0.890994	0.892463
30°		0.876238	0.879100	0.881642	0.886604	0.886798	0.888361
40°			0.871989	0.874707	0.879768	0.879947	0.881539
50°			0.862411	0.865243	0.870331	0.870501	0.872101
60°				0.853576	0.858677	0.858841	0.860445
70°				0.838975	0.844040	0.844199	0.845797
80°				0.821770	0.826658	0.826809	0.828362
90°				0.801765	0.806684	0.806825	0.808282
100°					0.784611	0.784733	0.786001
110°					0.762338	0.762435	0.763433
120°						0.739689	0.740383

Table 7.6: The local skin friction coefficient, C_f at the different positions x for $\chi = 0.2$ using Cu nanoparticles, $Pr = 6.2$, $\gamma = 0.5$ and various values of λ

λ	-9.5	-5	-3	-1	2.08	2.09	3
x							
0°	0.000000	0.000000	0.000000	0.000000	0.000000	0.000000	0.000000
10°	0.833418	0.859067	0.872208	0.886449	0.909786	0.910436	0.917934
20°		1.630962	1.670516	1.711068	1.773959	1.775700	1.795370
30°		2.350533	2.392733	2.438043	2.511469	2.513547	2.537247
40°			2.935165	3.005224	3.115399	3.118445	3.153217
50°			3.342572	3.405835	3.510152	3.513111	3.547111
60°				3.603195	3.711209	3.714297	3.749880
70°				3.609259	3.735984	3.739542	3.780475
80°				3.464352	3.548328	3.550827	3.579956
90°				3.193123	3.260213	3.262641	3.290856
100°					2.866059	2.866655	2.874157
110°					2.502076	2.503632	2.511022
120°						2.206889	2.243231

Table 7.7: The local heat transfer coefficient $Q_w(x)$ at the different positions x for $\chi = 0.1$ using Al_2O_3 nanoparticles, $Pr = 6.2$, $\gamma = 0.5$ and various values of λ

λ	-5.32	-4	-3	-1	0.80	0.81	3
x							
0°	0.625750	0.628957	0.630038	0.633788	0.636186	0.636570	0.639350
10°	0.624737	0.626547	0.629260	0.632871	0.635032	0.635530	0.638171
20°		0.625448	0.627119	0.630501	0.633311	0.633582	0.637660
30°		0.623499	0.625027	0.628231	0.630961	0.631252	0.635354
40°		0.619819	0.621383	0.624573	0.627358	0.627651	0.631714
50°			0.616975	0.620597	0.622578	0.622862	0.626753
60°			0.611645	0.614352	0.616941	0.617212	0.620896
70°				0.607767	0.610218	0.610474	0.613880
80°				0.600482	0.602680	0.602911	0.605912
90°				0.591514	0.594546	0.594752	0.597312
100°					0.585978	0.586151	0.588185
110°					0.577407	0.577550	0.579091
120°						0.568191	0.569272

Table 7.8: The local skin friction coefficient, C_f at the different positions x for $\chi = 0.1$ using Al_2O_3 nanoparticles, $Pr = 6.2$, $\gamma = 0.5$ and various values of λ

λ	-5.32	-4	-3	-1	0.80	0.81	3
x							
0°	0.000000	0.000000	0.000000	0.000000	0.000000	0.000000	0.000000
10°	0.583641	0.573564	0.570233	0.571822	0.579381	0.580352	0.597511
20°		1.086222	1.039575	1.096308	1.141010	1.145349	1.206084
30°		1.578830	1.579595	1.599992	1.631319	1.634951	1.694004
40°		1.861243	1.908717	1.995916	2.066241	2.073163	2.171891
50°			2.330184	2.352008	2.390496	2.395104	2.471446
60°			2.581973	2.595052	2.628437	2.632650	2.704761
70°				2.737622	2.803745	2.810277	2.904286
80°				2.873231	2.878243	2.879804	2.915951
90°				2.933893	2.938217	2.941651	2.990225
100°					2.902026	2.900310	2.935620
110°					2.901501	2.906319	2.921218
120°						2.881120	2.898231

Table 7.9: The local heat transfer coefficient $Q_w(x)$ at the different positions x for $\chi = 0.2$ using Al_2O_3 nanoparticles, $Pr = 6.2$, $\gamma = 0.5$ and various values of λ

λ	-6.91	-4	-3	-1	1.71	1.72	3
x							
0°	0.835122	0.839807	0.841264	0.847369	0.851093	0.851838	0.857113
10°	0.832209	0.837538	0.839428	0.845214	0.851292	0.850590	0.855273
20°		0.836734	0.838875	0.843103	0.849055	0.849166	0.852204
30°		0.833067	0.835182	0.839236	0.845317	0.845430	0.848539
40°		0.826927	0.829015	0.833137	0.839313	0.839429	0.842531
50°			0.821091	0.825110	0.831201	0.831316	0.835662
60°			0.811626	0.815517	0.821484	0.821598	0.824520
70°			0.800244	0.803951	0.809712	0.809822	0.812608
80°				0.790946	0.796301	0.796405	0.798964
90°				0.776790	0.781659	0.781753	0.784037
100°					0.766170	0.766252	0.768167
110°					0.752633	0.750893	0.752436
120°						0.734594	0.735777

Table 7.10: The local skin friction coefficient, C_f at the different positions x for $\chi = 0.2$ using Al_2O_3 nanoparticles, $Pr = 6.2$, $\gamma = 0.5$ and various values of λ

λ	-6.91	-4	-3	-1	1.71	1.72	3
x							
0°	0.000000	0.000000	0.000000	0.000000	0.000000	0.000000	0.000000
10°	0.687926	0.694847	0.699508	0.711775	0.733366	0.733821	0.746132
20°		1.292834	1.319182	1.372090	1.444486	1.445873	1.481953
30°		1.915177	1.933688	1.978003	2.050465	2.051958	2.091946
40°		2.330184	2.372849	2.459558	2.580801	2.583156	2.644712
50°			2.788927	2.847762	2.946515	2.948578	2.990459
60°			3.035232	3.091680	3.189847	3.191930	3.247781
70°			3.117393	3.208009	3.337402	3.339959	3.407303
80°				3.261509	3.327254	3.328764	3.369857
90°				3.210189	3.295589	3.297301	3.342789
100°					3.174807	3.175079	3.183666
110°					3.005104	3.006208	3.060306
120°						3.000845	3.004621

Table 7.11: The local heat transfer coefficient $Q_w(x)$ at the different positions x for $\chi = 0.1$ using TiO_2 nanoparticles, $Pr = 6.2$, $\gamma = 0.5$ and various values of λ

λ	-8.86	-5	-3	-1	1.38	1.39	3
x							
0°	0.602300	0.609838	0.610016	0.613117	0.618572	0.618845	0.621754
10°	0.600313	0.605575	0.608282	0.611826	0.615145	0.615557	0.619039
20°		0.604394	0.607588	0.610702	0.614670	0.614792	0.617603
30°		0.602632	0.605549	0.608557	0.612449	0.612566	0.615421
40°		0.599031	0.602038	0.605042	0.608955	0.609064	0.611923
50°			0.597708	0.600503	0.604284	0.604385	0.607149
60°			0.592501	0.595131	0.598773	0.598868	0.601496
70°				0.588724	0.592186	0.592276	0.594711
80°				0.581619	0.584762	0.584844	0.586998
90°				0.573923	0.576740	0.576814	0.578654
100°					0.568265	0.568328	0.569793
110°					0.559794	0.559846	0.560959
120°						0.550637	0.551418

Table 7.12: The local skin friction coefficient, C_f at the different positions x for $\chi = 0.1$ using TiO_2 nanoparticles, $Pr = 6.2$, $\gamma = 0.5$ and various values of λ

λ	-8.86	-5	-3	-1	1.32	1.39	3
x							
0°	0.000000	0.000000	0.000000	0.000000	0.000000	0.000000	0.000000
10°	0.404805	0.577709	0.571819	0.575864	0.589027	0.589547	0.607189
20°		0.988313	1.050105	1.105418	1.167890	1.169796	1.214477
30°		1.176151	1.584848	1.610515	1.660531	1.662328	1.708181
40°		1.827998	1.923166	2.009496	2.109759	2.112845	2.186660
50°			2.333056	2.363232	2.427327	2.429653	2.490305
60°			2.580773	2.603908	2.662999	2.665223	2.724009
70°				2.744668	2.843060	2.846129	2.919604
80°				2.872038	2.895582	2.896787	2.931900
90°				2.929718	2.924742	2.925081	2.939602
100°					2.900924	2.901347	2.923890
110°					2.890790	2.894304	2.905076
120°						2.886900	2.897426

Table 7.13: The local heat transfer coefficient $Q_w(x)$ at the different positions x for $\chi = 0.2$ using TiO_2 nanoparticles, $Pr = 6.2$, $\gamma = 0.5$ and various values of λ

λ	-10.09	-5	-3	-1	1.94	1.95	3
x							
0°	0.779534	0.789780	0.795440	0.797143	0.802584	0.802778	0.806630
10°	0.778251	0.787927	0.792676	0.795177	0.801655	0.801731	0.804610
20°		0.786262	0.790040	0.794328	0.800579	0.800682	0.802887
30°		0.782911	0.786768	0.790809	0.797223	0.797354	0.799653
40°			0.781066	0.785149	0.791673	0.791812	0.794126
50°			0.773636	0.777636	0.784109	0.784246	0.786525
60°				0.768615	0.775001	0.775134	0.777366
70°				0.757693	0.763915	0.764043	0.766198
80°				0.745359	0.751224	0.751345	0.753354
90°				0.725541	0.737302	0.737413	0.739234
100°					0.722516	0.722614	0.724169
110°					0.707836	0.707921	0.709206
120°						0.692343	0.693353

Table 7.14: The local skin friction coefficient, C_f at the different positions x for $\chi = 0.2$ using TiO_2 nanoparticles, $Pr = 6.2$, $\gamma = 0.5$ and various values of λ

λ	-10.09	-5	-3	-1	1.94	1.95	3
x							
0°	0.000000	0.000000	0.000000	0.000000	0.000000	0.000000	0.000000
10°	0.689459	0.695929	0.707265	0.721356	0.747716	0.748212	0.759132
20°		1.282360	1.336468	1.391166	1.472897	1.474343	1.504991
30°		1.911445	1.953034	2.002788	2.089478	2.091130	2.126381
40°			2.397552	2.488969	2.628308	2.630833	2.683985
50°			2.807817	2.875828	2.996704	2.999033	3.048669
60°				3.115557	3.238653	3.241053	3.292267
70°				3.224943	3.380699	3.383569	3.444406
80°				3.264843	3.357930	3.359852	3.400948
90°				3.281776	3.311910	3.313999	3.358450
100°					3.171936	3.172658	3.188068
110°					3.063912	3.064344	3.077551
120°						3.004045	3.011284

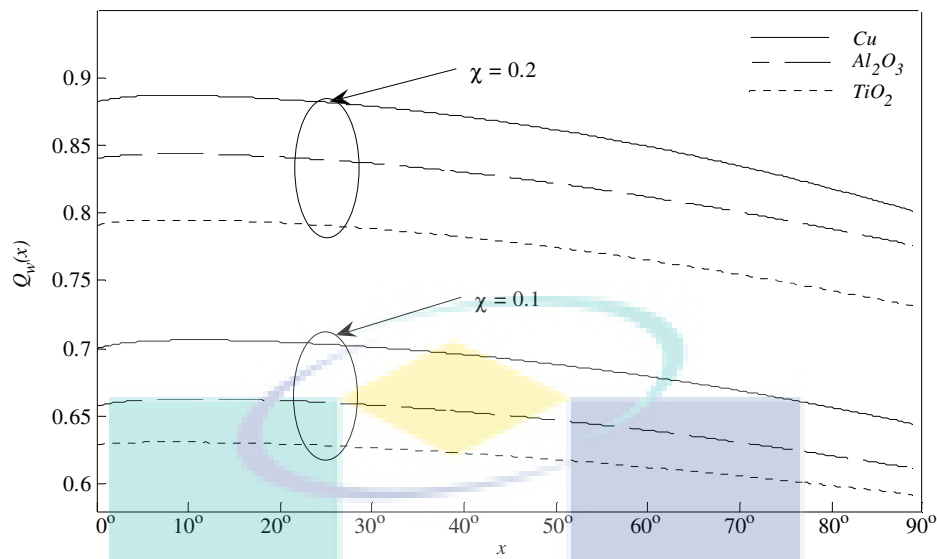


Figure 7.1: The local heat transfer coefficient $Q_w(x)$ with x using various nanoparticles when $Pr = 6.2$, $\lambda = -1$, $\gamma = 0.5$ and $\chi = 0.1, 0.2$

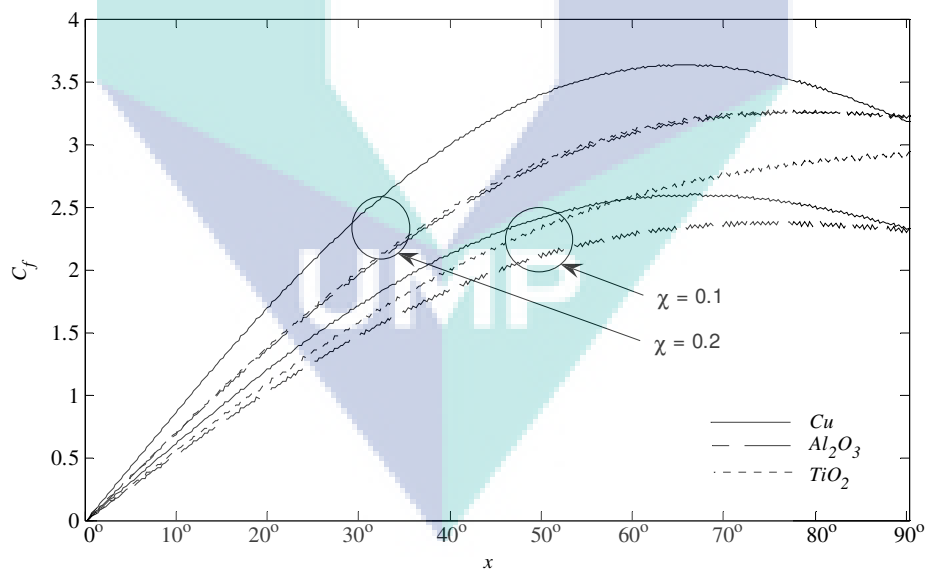


Figure 7.2: The local skin friction coefficient C_f with x using various nanoparticles when $Pr = 6.2$, $\lambda = -1$, $\gamma = 0.5$ and $\chi = 0.1, 0.2$

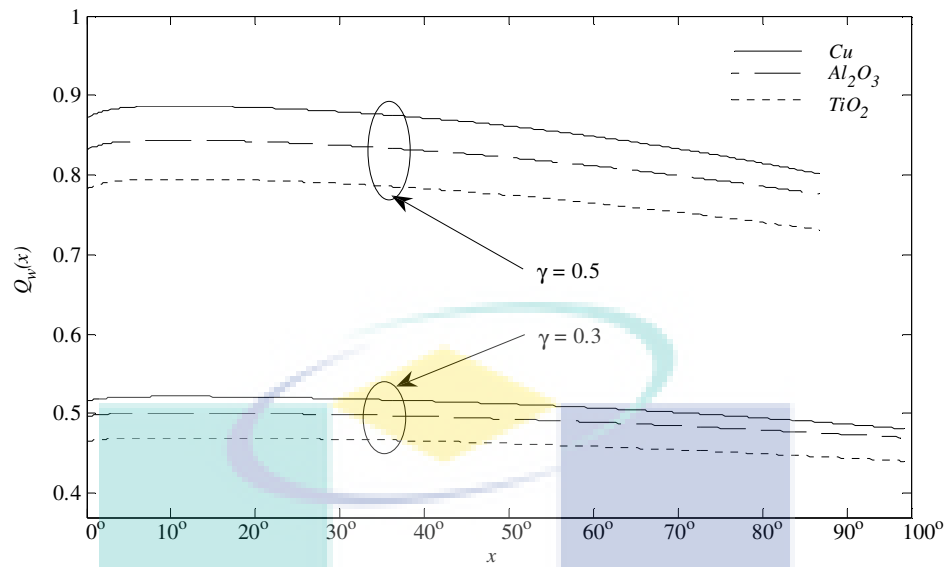


Figure 7.3: The local heat transfer coefficient $Q_w(x)$ with x using various nanoparticles when $Pr = 6.2$, $\lambda = -1$, $\chi = 0.2$ and $\gamma = 0.3, 0.5$

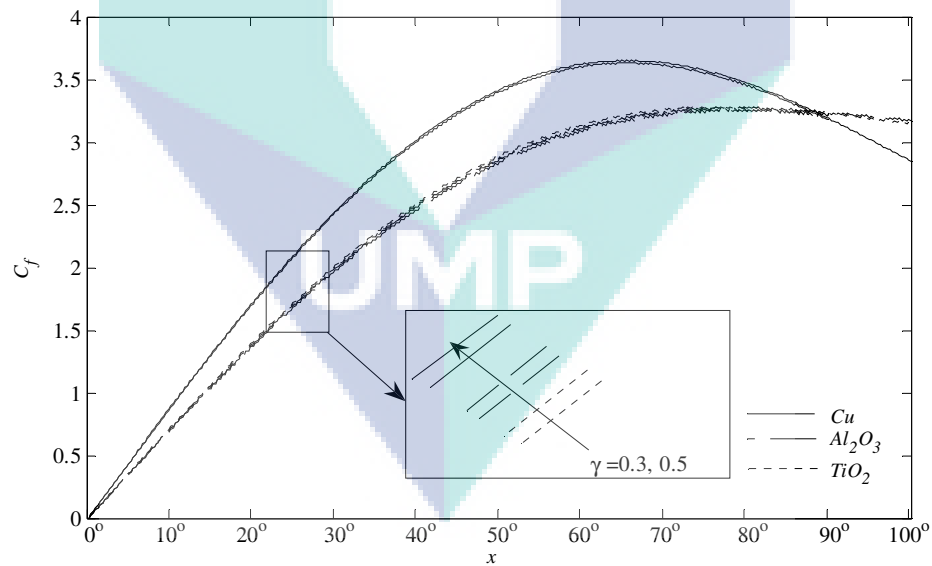


Figure 7.4: The local skin friction coefficient C_f with x using various nanoparticles when $Pr = 6.2$, $\lambda = -1$, $\chi = 0.2$ and $\gamma = 0.3, 0.5$

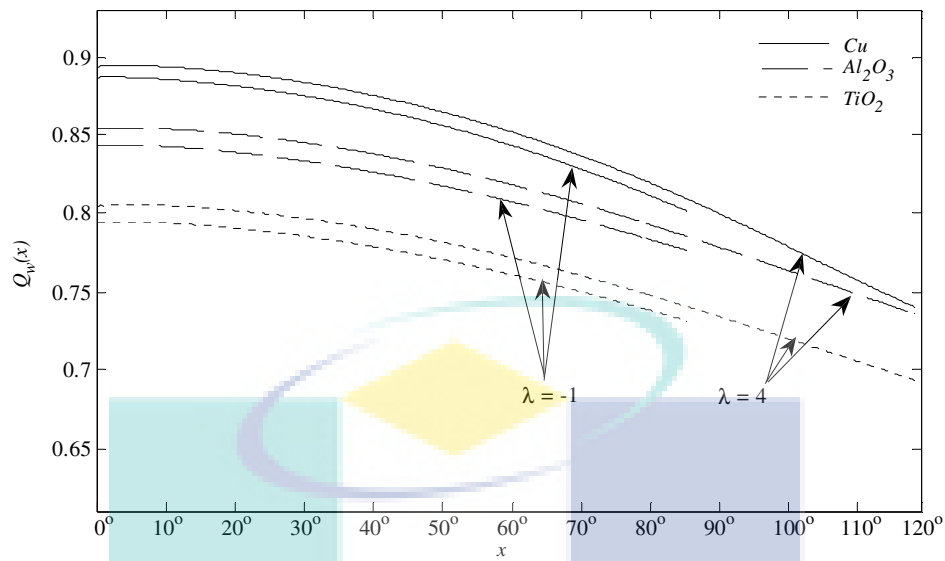


Figure 7.5: The local heat transfer coefficient $Q_w(x)$ with x using various nanoparticles when $Pr = 6.2$, $\chi = 0.2$, $\gamma = 0.5$ and $\lambda = -1, 4$

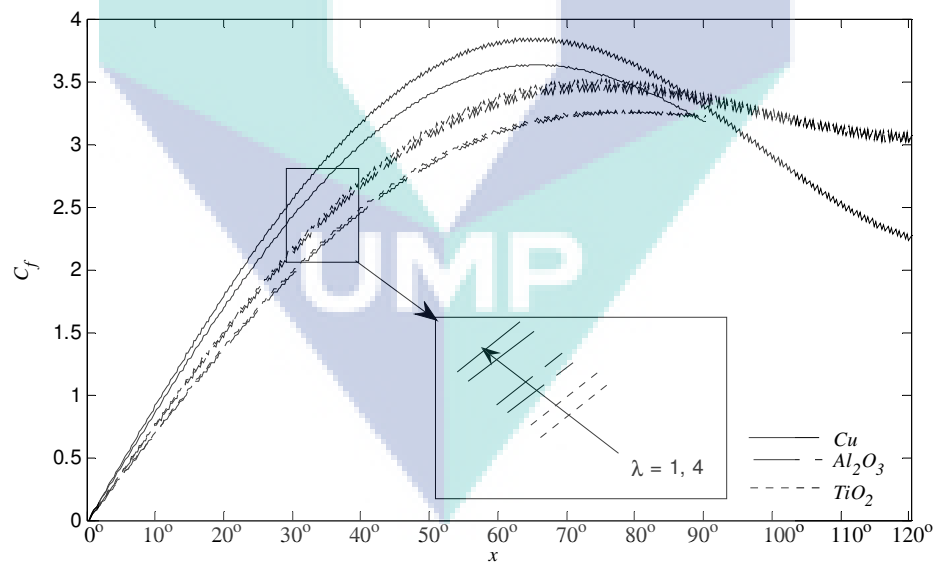


Figure 7.6: The local skin friction coefficient C_f with x using various nanoparticles when $Pr = 6.2$, $\chi = 0.2$, $\gamma = 0.5$ and $\lambda = -1, 4$

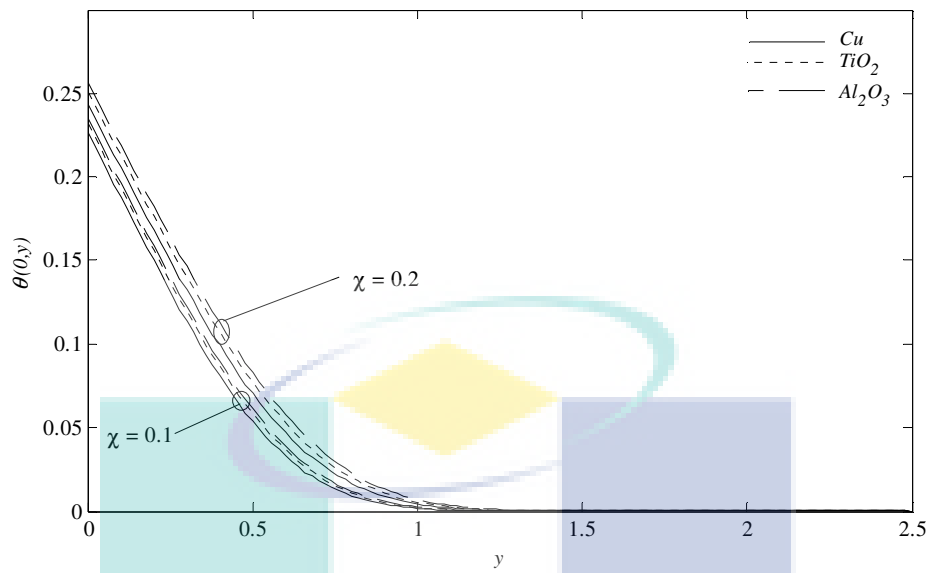


Figure 7.7: The temperature profiles $\theta(0, y)$, using various nanoparticles when $Pr = 6.2$, $\lambda = 1$, $\gamma = 0.5$ and $\chi = 0.1, 0.2$

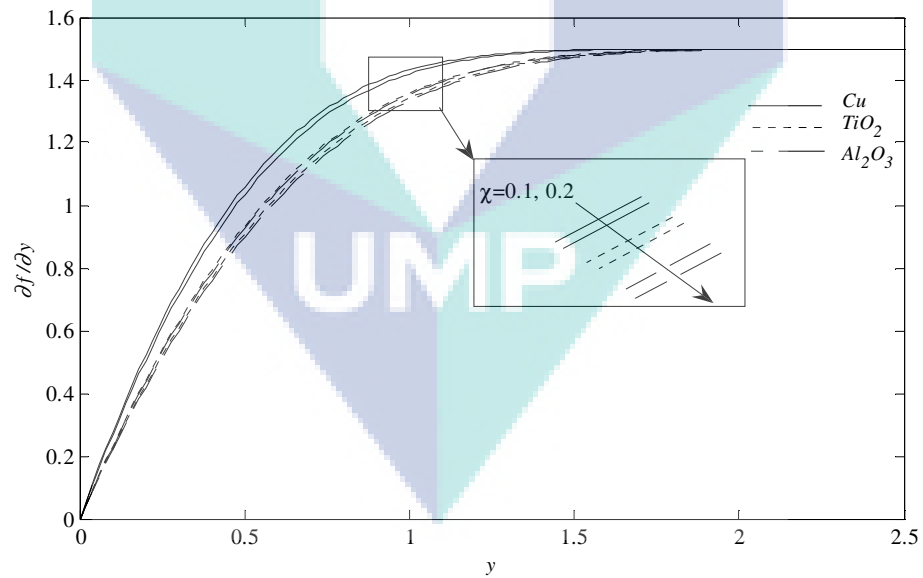


Figure 7.8: The velocity profiles $(\partial f / \partial y)(0, y)$, using various nanoparticles when $Pr = 6.2$, $\lambda = 1$, $\gamma = 0.5$ and $\chi = 0.1, 0.2$

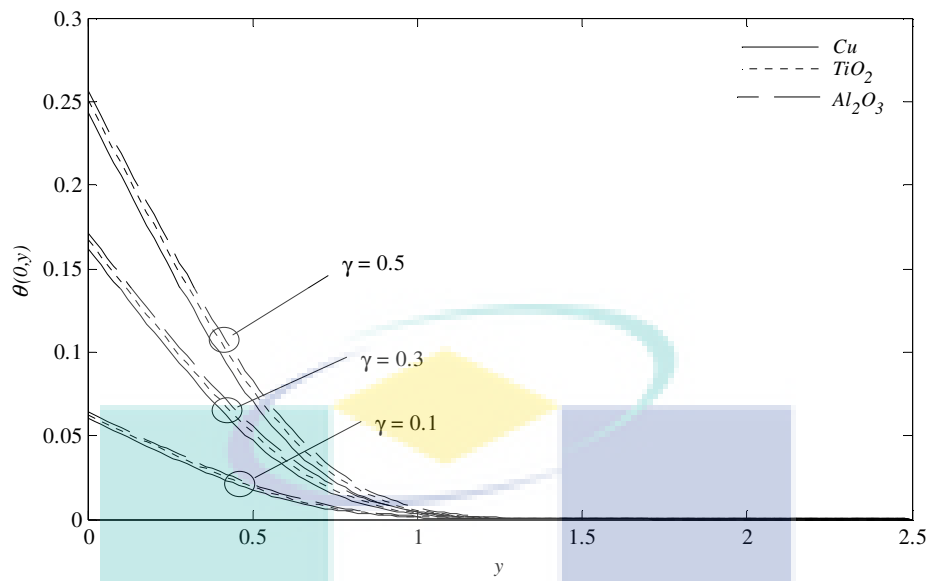


Figure 7.9: The temperature profiles $\theta(0, y)$, using various nanoparticles when $Pr = 6.2$, $\lambda = 1$, $\chi = 0.2$ and $\gamma = 0.1, 0.3, 0.5$

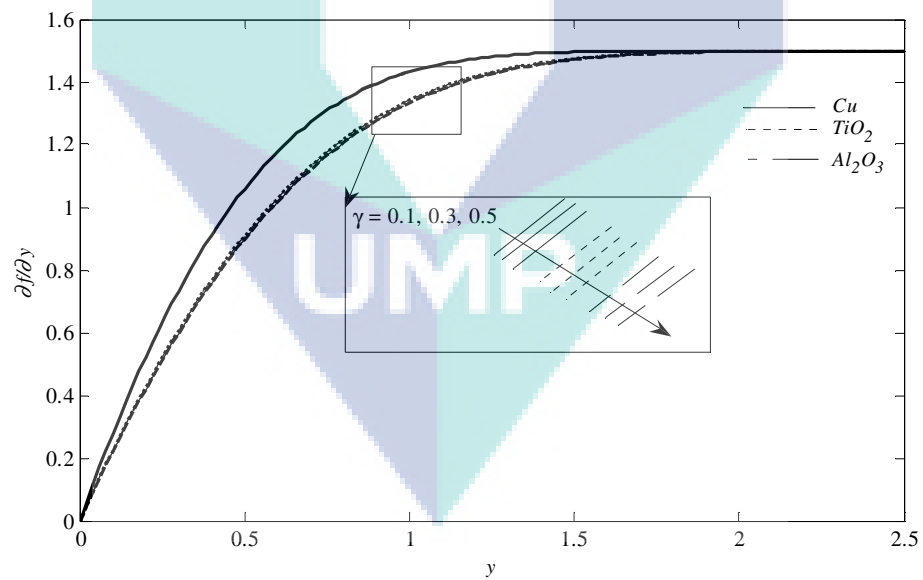


Figure 7.10: The velocity profiles $(\partial f / \partial y)(0, y)$, using various nanoparticles when $Pr = 6.2$, $\lambda = 1$, $\chi = 0.2$ and $\gamma = 0.1, 0.3, 0.5$

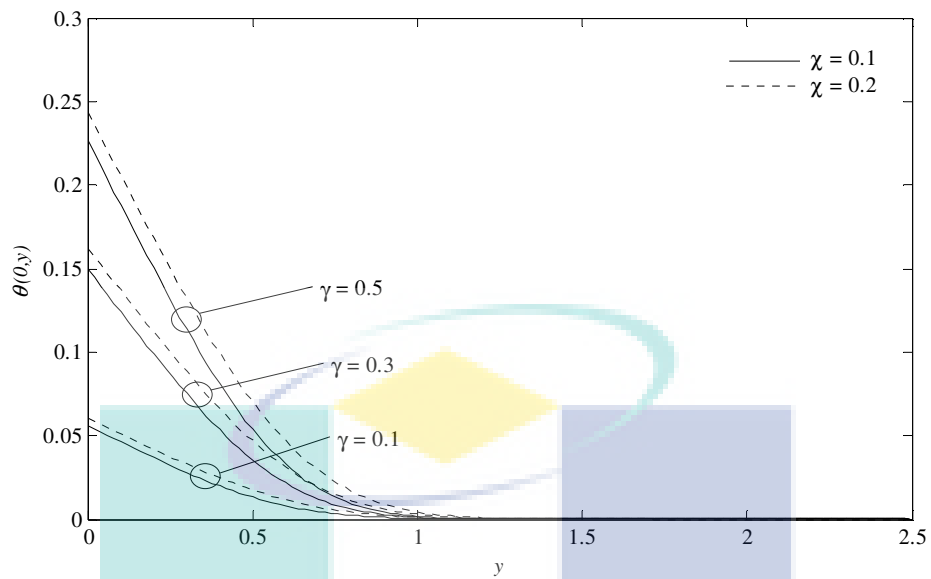


Figure 7.11: The temperature profiles $\theta(0, y)$, using *Cu* nanoparticles when $Pr = 6.2$, $\chi = 0.1, 0.2$, $\lambda = 1$ and with various values of γ

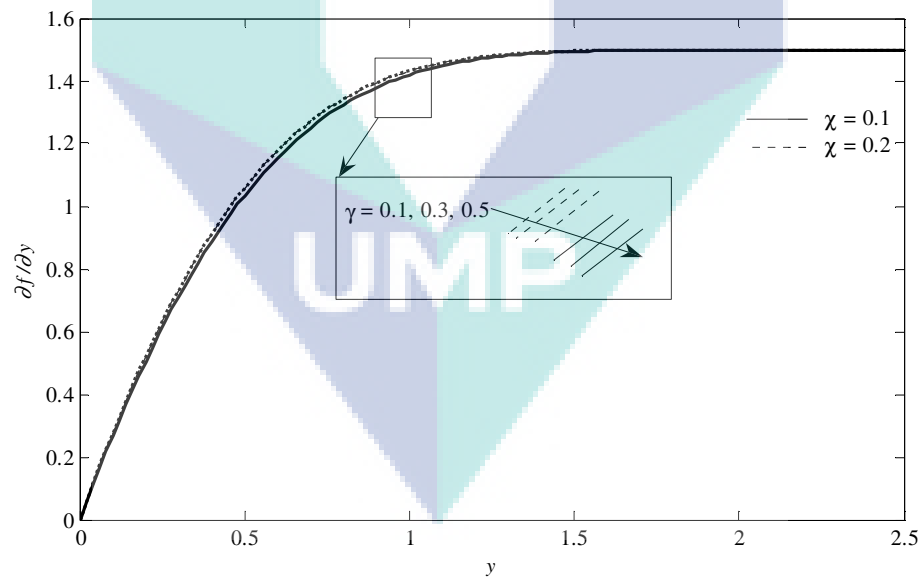


Figure 7.12: The velocity profiles $(\partial f / \partial y)(0, y)$, using *Cu* nanoparticles when $Pr = 6.2$, $\chi = 0.1, 0.2$, $\lambda = 1$ and with various values of γ

7.4 CONCLUSIONS

In this chapter, we have numerically studied the problem of mixed convection boundary layer flow about a sphere with convective boundary conditions in a nanofluid and solved by using the Keller-box method. It is shown how the mixed convection parameter λ , the type of nanoparticles (Cu , Al_2O_3 , TiO_2), the nanoparticle volume fraction χ and the conjugate parameter γ , affects the local skin friction coefficient C_f , the local heat transfer coefficient $Q_w(x)$, the temperature $\theta(0, y)$, and velocity $(\partial f / \partial y)(0, y)$. We can conclude that,

- An increase in both values of nanoparticle volume fraction χ and the conjugate parameter γ led to an increase of both local heat transfer coefficient $Q_w(x)$ and the local skin friction coefficient C_f .
- An increase in both values of nanoparticle volume fraction χ and the conjugate parameter γ led to an increase in the temperature but decreases the velocity.
- The Cu nanoparticles have the highest local heat transfer coefficient compared to Al_2O_3 and TiO_2 . Moreover, Cu also has the highest local skin friction coefficient, followed by TiO_2 and Al_2O_3 nanoparticles.

CHAPTER 8

MIXED CONVECTION FLOW OVER A SOLID SPHERE EMBEDDED IN A POROUS MEDIUM FILLED IN A NANOFLUID

8.1 INTRODUCTION

In this chapter, the nanofluid model that proposed by Tiwari and Das (2007) was used to study the present problem of mixed convection boundary layer flow over a solid sphere embedded in a porous medium filled with convective boundary conditions in a nanofluid and extending the paper by Tham and Nazar (2012) who studied the same problem but with different condition.

The study on convective flow in porous medium together with the influence of magnetic field have attracted many researchers due to its advance applications in engineering and industrial activities such as in the field of agricultural engineering and chemical engineering. In petroleum refineries, movement of oil, water and gas through porous medium for purification and filtration are areas that this research can be applied to.

In this problem, convective boundary conditions are considered with nanofluid. The results for the component, the local skin friction as well as temperature profiles are illustrated in the form of figures and tables with nanofluid formed by the dilution of nanoparticles, such as copper Cu , aluminum oxide Al_2O_3 and titanium dioxide TiO_2 , in water for a wide range of parameters such as mixed convection parameter, the conjugate parameter γ , the coordinate x measured along the surface of the sphere and the nanoparticle volume fraction.

8.2 MATHEMATICAL FORMULATION

The Boussinesq approximation is employed and homogeneity and local thermal equilibrium in the porous medium is assumed. All assumptions considered are remained the same as discussed in Section 5.2. It is assumed that the nanoparticles are suspended in the nanofluid using either surfactant or surface charge technology. In keeping with the Darcy law, and adopting the nanofluid model proposed by Tiwari and Das (2007), the basic steady dimensional continuity (2.5), energy equations (2.13) and momentum for a nanofluid in Cartesian coordinates \bar{x} and \bar{y} are

$$\frac{\mu_{nf}}{K_1} \bar{u} = -\frac{\partial \bar{p}}{\partial \bar{x}} + (\chi \rho_s \beta_s + (1-\chi) \rho_f \beta_f) g (T - T_\infty) \sin\left(\frac{\bar{x}}{a}\right), \quad (8.1)$$

subject to the boundary conditions

$$\begin{aligned} \bar{v}(\bar{x}, \bar{y}) = 0, \quad -k_f \frac{\partial T}{\partial \bar{y}}(\bar{x}, \bar{y}) = h_f (T_f - T(\bar{x}, \bar{y})) \text{ at } \bar{y} = 0, \quad 0 \leq \bar{x} \leq \pi, \\ \bar{u}(\bar{x}, \bar{y}) \rightarrow \bar{u}_e(\bar{x}), \quad T(\bar{x}, \bar{y}) \rightarrow T_\infty \text{ as } \bar{y} \rightarrow \infty, \quad 0 \leq \bar{x} \leq \pi. \end{aligned} \quad (8.2)$$

We introduce now the following non-dimensional variables

$$\begin{aligned} x = \frac{\bar{x}}{a}, \quad y = P e^{1/2} \left(\frac{\bar{y}}{a} \right), \quad r(x) = \frac{\bar{r}(\bar{x})}{a}, \\ u = \frac{\bar{u}}{U_\infty}, \quad v = P e^{1/2} \left(\frac{\bar{v}}{U_\infty} \right), \quad u_e(x) = \frac{\bar{u}_e(\bar{x})}{U_\infty}, \\ \theta = \frac{T - T_\infty}{T_f - T_\infty}, \quad P = \frac{\bar{P}}{\rho_{nf} U_\infty^2}, \end{aligned} \quad (8.3)$$

where $Pe = U_\infty a / \alpha_f$ is the Péclet number and K_1 is permeability of the porous medium. Eliminating \bar{P} from equation (8.1) by cross differentiation, substituting variables (8.3) into (8.1) then become

$$\frac{1}{(1-\chi)^{2.5}} \frac{\partial u}{\partial y} = \chi (\rho_s / \rho_f) (\beta_s / \beta_f) + (1-\chi) \frac{\partial \theta}{\partial y} \lambda \sin x. \quad (8.4)$$

The boundary conditions (8.2) become

$$v(x, y) = 0, \quad \frac{\partial \theta}{\partial y}(x, y) = -\gamma(1 - \theta(x, y)) \quad \text{at } y=0, \quad 0 \leq x \leq \pi,$$

$$u(x, y) \rightarrow u_e(x) = \frac{3}{2} \sin x, \quad \theta(x, y) \rightarrow 0 \quad \text{as } y \rightarrow \infty, \quad 0 \leq x \leq \pi, \quad (8.5)$$

where $\gamma = ah_f Ra^{-1/4} / k_f$ is the conjugate parameter for the convective boundary conditions and λ is the mixed convection parameter which is given by:

$$\lambda = \frac{Ra}{Pe}, \quad (8.6)$$

with $Ra = gK_1 \beta (T_f - T_\infty) a / \nu_f \alpha_f$ is the being the Rayleigh number for the porous medium. Integrating equation (8.4) and using the boundary conditions (8.5), we obtain

$$\frac{1}{(1-\chi)^{2.5}} u = \frac{3}{2} \frac{\sin x}{(1-\chi)^{2.5}} \left[\chi(\rho_s / \rho_s)(\beta_s / \beta_f) + (1-\chi) \right] \theta \lambda \sin x. \quad (8.7)$$

To solve equations (2.17), (2.19) and (8.7) subject to the boundary conditions (8.5), we use the variables stream function which defined in Chapter 3 :

which satisfies the continuity equation (2.17). Thus, equations (8.7) and (2.19) become

$$\frac{1}{(1-\chi)^{2.5}} \frac{\partial f}{\partial y} = \left[\frac{3}{2} \frac{1}{(1-\chi)^{2.5}} + \chi(\rho_s / \rho_s)(\beta_s / \beta_f) + (1-\chi) \lambda \theta \right] \frac{\sin x}{x}, \quad (8.8)$$

$$\left[\frac{(k_s + 2k_f) - 2\chi(k_f - k_s)}{[(k_s + 2k_f) + \chi(k_f - k_s)][(1-\chi) + \chi(\rho C_p)_s / (\rho C_p)_f]} \right] \frac{\partial^2 \theta}{\partial y^2} + (1 + x \cot x) f \frac{\partial \theta}{\partial y} = x \left(\frac{\partial f}{\partial y} \frac{\partial \theta}{\partial x} - \frac{\partial f}{\partial x} \frac{\partial \theta}{\partial y} \right), \quad (8.9)$$

subject to the boundary conditions

$$f(x, y) = 0, \quad \frac{\partial \theta}{\partial y}(x, y) = -\gamma(1 - \theta(x, y)) \quad \text{at } y=0, \quad 0 \leq x \leq \pi,$$

$$\frac{\partial f}{\partial y}(x, y) \rightarrow \frac{3 \sin x}{2x}, \quad \theta(x, y) \rightarrow 0 \quad \text{as } y \rightarrow \infty, \quad 0 \leq x \leq \pi. \quad (8.10)$$

It can be seen that at the lower stagnation point of the sphere, $x \approx 0$, equations (8.8) and (8.9) reduced to the following ordinary differential equations:

$$\frac{1}{(1-\chi)^{2.5}} f' = \frac{3}{2} \frac{1}{(1-\chi)^{2.5}} + [\chi(\rho_s / \rho_s)(\beta_s / \beta_f) + (1-\chi)] \lambda \theta, \quad (8.11)$$

$$\left[\frac{(k_s + 2k_f) - 2\chi(k_f - k_s)}{[(k_s + 2k_f) + \chi(k_f - k_s)][(1-\chi) + \chi(\rho C_p)_s / (\rho C_p)_f]} \right] \theta'' + 2f \theta' = 0, \quad (8.12)$$

and the boundary conditions (8.10) become

$$\begin{aligned} f(0) &= 0, \quad \theta'(0) = -\gamma(1-\theta(0)), \\ f' &\rightarrow \frac{3}{2}, \quad \theta \rightarrow 0 \quad \text{as } y \rightarrow \infty. \end{aligned} \quad (8.13)$$

Quantities of practical interest is the local skin friction coefficient, C_f which is defined as

$$C_f = \frac{1}{\rho_f U_\infty^2} \mu_{nf} \left(\frac{\partial \bar{u}}{\partial \bar{y}} \right)_{\bar{y}=0}, \quad (8.14)$$

substituting the variables (8.3) into (8.14), we obtain

$$(\text{Pr } Pe^{1/2}) C_f = \frac{1}{(1-\chi)^{2.5}} x \frac{\partial^2 f}{\partial y^2}(x, 0) \quad (8.21)$$

8.3 RESULTS AND DISCUSSION

The data related to the thermophysical properties of fluids and nanoparticles was used from the Table 7.1 (Abu-Nada and Oztop, 2009) to compute each case of nanofluid.

Tables 8.1 to 8.6 show the values of $(\text{Pr } Pe^{1/2}) C_f$ at different positions x and various values of the parameter λ for $\chi=0.1$ and $\chi=0.2$ (nanofluid) for different nanoparticles (Cu , Al_2O_3 and TiO_2) when the conjugate parameter $\gamma=0.5$, respectively. It is observed from these tables that the skin friction coefficients $(\text{Pr } Pe^{1/2}) C_f$ are negative when $\lambda > 0$ and positive when $\lambda < 0$ and zero when $\lambda = 0$ due to the definition of $(\text{Pr } Pe^{1/2}) C_f$ given in (8.22). It is found that for fixed x and λ ,

as the value of nanoparticle volume fraction χ increases from 0.1 to 0.2, it resulted in an increase of the value of $(Pr Pe^{1/2})C_f$ and these increases are applied in both heated sphere ($\lambda > 0$) and cooled sphere ($\lambda < 0$) cases. It is observed from Tables 8.1 and 8.2 for the case *Cu* nanoparticles that the actual value of $\lambda = \lambda_s (> 0)$, which first gives no separation, is difficult to be exactly determine. However, the numerical solutions indicated that the value of λ_s which first gives no separation, lies between -3.34 and -3.35 for $\chi = 0.1$ and between -3.89 and -3.9 for $\chi = 0.2$ as well as in Tables 8.3 and 8.4 for the case of *TiO₂* nanoparticles, the value of λ_s lies between -2.87 and -2.88 for $\chi = 0.1$ and between -3.05 and -3.06 for $\chi = 0.2$. The same trend can be observed for the cases of *Al₂O₃* nanoparticles in Tables 8.5 and 8.7 where the value of λ_s lies between -2.24 and -2.25 for $\chi = 0.1$ and between -2.61 and -2.62 for $\chi = 0.2$. It is found that the boundary layer started to separate the fastest (with highest values of λ_s) for the *Cu* nanoparticles, followed by *TiO₂* and *Al₂O₃*. This indicates that the *TiO₂* nanoparticles delay the start of the boundary layer separation from the sphere.

Figure 8.1 show the skin friction coefficient $(Pr Pe^{1/2})C_f$ for $\lambda = -1$ (opposing flow), when $\gamma = 0.5$ with various values of $\chi = 0.1$ and $\chi = 0.2$ for the three nanoparticles considered, namely *Cu*, *TiO₂* and *Al₂O₃*. It is seen from these figure that due to the definition of $(Pr Pe^{1/2})C_f$, the skin friction coefficients are positive when $\lambda < 0$ (opposing flow). The opposite trends are observed when $\lambda = -1$ (opposing flow) as shown in this Figure with the parabolic curve having a maximum value was shown in the tables 8.1 to 8.6. These phenomena are observed for the skin friction coefficient curves involving a sphere. It is possibly due to the shapes of sphere, which consequently leads to flow separation. It is also observed from these figures that the magnitude of the skin friction coefficient decreases as χ increases from 0.1 to 0.2. Among the three nanoparticles, the magnitude of the skin friction coefficient is the highest for *Al₂O₃* (nanoparticles with high density and thermal diffusivity), followed by *TiO₂* and the lowest is *Cu* (nanoparticles with low thermal diffusivity). It should be pointed out that nanofluids have lower skin friction coefficient compared with the base fluid, which is

good to be used as lubricant due to the suspended nanoparticles that can stay longer in the base fluid and the surface area per unit volume of nanoparticles is large. These two properties can enhance the flow characteristic of nanofluids.

The variation of the local skin friction coefficient $(Pr Pe^{1/2})C_f$ with x using various nanoparticles (Cu , Al_2O_3 and TiO_2) when $\lambda = -1$ (opposing flow), $\chi = 0.2$ and the conjugate parameter $\gamma = 0.5, 0.7, 1$ is presented in Figure 8.2. It can be seen that for all nanoparticles cases, as the conjugate parameter increases causing it to increase the value the local skin friction coefficient C_f . This is due by the definition of the conjugate parameter given as $\gamma = ah_f Ra^{-1/4} / k_f$.

The temperature profiles $\theta(0, y)$ using various nanoparticles when $\lambda = -1$, $\gamma = 0.5$ and $\chi = 0.1, 0.2$ are shown in Figure 8.3. It can be found that the temperature decreases from Cu to TiO_2 and to Al_2O_3 , when fixed nanoparticle volume fraction is χ . In addition, as χ increases from 0.1 to 0.2, the temperature increases. However, Figure 8.4 presented the temperature profiles $\theta(0, y)$ of each nanoparticles when $\lambda = -1$, $\chi = 0.2$ and various values of conjugate parameter is γ . It is found that as γ increases, the temperature also increase.

Finally, Figure 8.5 presented the temperature profiles $\theta(0, y)$ using Cu nanoparticles when $\chi = 0.1, 0.2$, $\lambda = -1$ and with various values of γ . It is found that when the nanoparticle volume fraction χ is fixed, an increment in the values of conjugate parameter γ lead to an increase of temperature, as well as when γ is fixed, χ increases the values of temperature.

Table 8.1: The local skin friction coefficient, $(Pr Pe^{1/2})C_f$ at the different positions x for for $\chi = 0.1$ using Cu nanoparticles, $\gamma = 0.5$ and

λ	various values of λ									
	-5.6	-5	-4	-3.35	-3.34	-2	-1	-0.5	1	3
x										
0°	0.000000	0.000000	0.000000	0.000000	0.000000	0.000000	0.000000	0.000000	0.000000	0.000000
10°	0.579030	0.482082	0.384253	0.320999	0.315264	0.244154	0.124044	0.033381	-0.330724	-0.526221
20°	0.652861	0.555914	0.458075	0.394821	0.389083	0.317976	0.197866	0.107202	-1.276386	-1.471883
30°		0.620563	0.522728	0.459474	0.453731	0.382629	0.262519	0.171855	-2.278712	-2.474209
40°		0.672130	0.574295	0.511041	0.50530	0.434196	0.314086	0.223422	-3.079677	-3.275174
50°		0.708079	0.610239	0.546985	0.541249	0.47014	0.35003	0.259366	-3.635956	-3.831453
60°			0.628642	0.565388	0.559653	0.488543	0.368433	0.277769	-3.922312	-4.117809
70°			0.629406	0.566152	0.560416	0.489307	0.369197	0.278533	-3.933269	-4.128766
80°			0.613462	0.550208	0.544477	0.473363	0.353253	0.262589	-3.684542	-3.880039
90°				0.519719	0.513988	0.442874	0.322764	0.23210	-3.211547	-3.407044
100°				0.478341	0.47266	0.401496	0.281386	0.190722	-2.568117	-2.763614
110°				0.430363	0.424624	0.353518	0.233408	0.142744	-1.821677	-2.017174
120°					0.374712	0.303607	0.183497	0.092833	-1.048335	-1.243832

Table 8.2: The local skin friction coefficient, $(Pr Pe^{1/2})C_f$ at the different positions x for $\chi = 0.2$ using Cu nanoparticles, $\gamma = 0.5$ and

	various values of λ									
λ	-6.5	-6	-5	-3.9	-3.89	-2	-1	-0.5	1	3
x										
0°	0.000000	0.000000	0.000000	0.000000	0.000000	0.000000	0.000000	0.000000	0.000000	0.000000
10°	0.631042	0.572081	0.506470	0.471922	0.454252	0.331373	0.307492	0.048741	-0.207410	-0.211821
20°	0.704860	0.645913	0.580291	0.545754	0.528074	0.405192	0.381315	0.122567	-1.153231	-1.157411
30°		0.710567	0.644944	0.610404	0.592727	0.469847	0.445963	0.187216	-2.155311	-2.159823
40°		0.762133	0.696517	0.661971	0.644294	0.521410	0.497536	0.238783	-2.956345	-2.960760
50°		0.798070	0.732459	0.697912	0.680238	0.557356	0.533477	0.274721	-3.512664	-3.517010
60°			0.750865	0.716311	0.698641	0.575762	0.551880	0.293134	-3.798978	-3.803478
70°			0.751621	0.717081	0.699405	0.576522	0.552641	0.293890	-3.809902	-3.814354
80°			0.735683	0.701133	0.683461	0.560585	0.536709	0.277951	-3.561223	-3.565634
90°				0.670648	0.652972	0.530090	0.506218	0.247463	-3.088211	-3.092623
100°				0.629270	0.611594	0.488711	0.464831	0.206087	-2.444795	-2.449233
110°				0.581281	0.563616	0.440733	0.416855	0.158100	-1.698334	-1.702745
120°					0.513705	0.390825	0.366944	0.108191	-0.925001	-0.929434

Table 8.3: The local skin friction coefficient, $(Pr Pe^{1/2})C_f$ at the different positions x for $\chi = 0.1$ using TiO_2 nanoparticles, $\gamma = 0.5$ and

	various values of λ									
λ	-5.77	-5	-4	-2.88	-2.87	-2	-1	-0.5	1	3
x										
0°	0.000000	0.000000	0.000000	0.000000	0.000000	0.000000	0.000000	0.000000	0.000000	0.000000
10°	0.601719	0.527588	0.433140	0.354262	0.355262	0.277461	0.205371	0.052061	-0.265323	-0.466231
20°	0.675541	0.60141	0.506972	0.428087	0.429083	0.351283	0.279199	0.125886	-1.210933	-1.411931
30°		0.666063	0.571626	0.492738	0.493733	0.415934	0.343842	0.190535	-2.213387	-2.414243
40°			0.623198	0.54438	0.54535	0.467576	0.395416	0.24213	-3.014209	-3.215265
50°			0.659134	0.580242	0.581247	0.503443	0.431358	0.278042	-3.570583	-3.771578
60°			0.677538	0.598646	0.599659	0.521847	0.449763	0.296454	-3.856921	-4.057832
70°			0.678301	0.599410	0.600411	0.522615	0.450527	0.297216	-3.867832	-4.068889
80°			0.662357	0.583461	0.584474	0.506660	0.434589	0.281278	-3.619155	-3.820043
90°				0.552982	0.553986	0.476184	0.404091	0.250789	-3.146163	-3.347212
100°				0.511610	0.512601	0.434811	0.362710	0.209400	-2.502787	-2.703654
110°				0.463622	0.46453	0.386825	0.314732	0.161421	-1.756232	-1.957287
120°					0.414711	0.336918	0.264829	0.111512	-0.982921	-1.183855

Table 8.4: The local skin friction coefficient, $(Pr Pe^{1/2})C_f$ at the different positions x for for $\chi = 0.2$ using TiO_2 nanoparticles, $\gamma = 0.5$ and

	various values of λ									
λ	-7.2	-6	-5	-3.06	-3.05	-2	-1	-0.5	1	3
x										
0°	0.000000	0.000000	0.000000	0.000000	0.000000	0.000000	0.000000	0.000000	0.000000	0.000000
10°	0.677481	0.613042	0.563035	0.447591	0.434143	0.385366	0.334261	0.053171	-0.101633	-0.114212
20°	0.751303	0.686863	0.636866	0.521413	0.507972	0.459188	0.408082	0.126995	-1.047345	-1.059866
30°		0.751512	0.701515	0.586066	0.572623	0.523841	0.472733	0.191643	-2.049609	-2.062176
40°			0.753087	0.637635	0.624194	0.575408	0.52435	0.243213	-2.850597	-2.863156
50°			0.789028	0.673570	0.660136	0.611352	0.560246	0.279165	-3.406845	-3.419489
60°			0.807429	0.691989	0.678537	0.629755	0.578647	0.297567	-3.693234	-3.705703
70°			0.808192	0.692741	0.679360	0.630519	0.579418	0.298328	-3.704123	-3.716723
80°			0.792246	0.67682	0.663352	0.614575	0.563469	0.282389	-3.455422	-3.468010
90°				0.646314	0.632865	0.584086	0.532988	0.251890	-2.982434	-2.995038
100°				0.604936	0.591497	0.542708	0.49166	0.210513	-2.33966	-2.351523
110°				0.556957	0.543519	0.49473	0.443625	0.162534	-1.592543	-1.605123
120°					0.493601	0.444819	0.393717	0.112622	-0.819256	-0.831820

Table 8.5: The local skin friction coefficient, $(Pr Pe^{1/2})C_f$ at the different positions x for $\chi = 0.1$ using Al_2O_3 nanoparticles, $\gamma = 0.5$ and

	various values of λ									
λ	-5.92	-5	-4	-2.24	-2.23	-2	-1	-0.5	1	3
x										
0°	0.000000	0.000000	0.000000	0.000000	0.000000	0.000000	0.000000	0.000000	0.000000	0.000000
10°	0.644262	0.577710	0.465261	0.389482	0.379361	0.282031	0.261933	0.055491	-0.220699	-0.433043
20°	0.718083	0.651544	0.539082	0.463331	0.453193	0.355868	0.335755	0.129312	-1.166361	-1.378722
30°		0.716193	0.603736	0.527951	0.517847	0.420513	0.400408	0.193975	-2.168687	-2.38132
40°		0.767767	0.655304	0.579522	0.569418	0.472081	0.451975	0.245536	-2.969652	-3.182110
50°			0.691245	0.615463	0.605356	0.508023	0.487919	0.281489	-3.525931	-3.738313
60°			0.709654	0.633871	0.623754	0.526426	0.506322	0.299886	-3.812287	-4.024609
70°			0.710414	0.634632	0.624529	0.527198	0.507086	0.300644	-3.823244	-4.035634
80°			0.694472	0.618693	0.608570	0.511245	0.491142	0.284701	-3.574517	-3.786923
90°				0.588244	0.578087	0.480756	0.460653	0.254211	-3.101522	-3.313945
100°				0.546822	0.536715	0.439383	0.419275	0.212833	-2.458092	-2.670409
110°				0.498841	0.488732	0.391401	0.371297	0.164865	-1.711652	-1.924543
120°					0.438820	0.341491	0.321386	0.114942	-0.938319	-1.150634

Table 8.6: The local skin friction coefficient, $(Pr Pe^{1/2})C_f$ at the different positions x for for $\chi = 0.2$ using Al_2O_3 nanoparticles, $\gamma = 0.5$ and

λ	various values of λ									
	-7.9	-6	-5	-2.62	-2.61	-2	-1	-0.5	1	3
x										
0°	0.000000	0.000000	0.000000	0.000000	0.000000	0.000000	0.000000	0.000000	0.000000	0.000000
10°	0.729831	0.675263	0.587581	0.414259	0.402251	0.397518	0.374161	0.073272	-0.011636	-0.020423
20°	0.803653	0.749082	0.661414	0.488087	0.476075	0.471347	0.447984	0.147094	-0.957300	-1.243121
30°		0.813736	0.726065	0.552734	0.540725	0.535996	0.512635	0.211743	-1.959611	-2.245433
40°		0.865309	0.777635	0.604330	0.592294	0.587565	0.564277	0.263312	-2.760522	-3.046356
50°			0.813576	0.640242	0.628237	0.623540	0.600146	0.299263	-3.316813	-3.602654
60°			0.831978	0.658646	0.646638	0.641932	0.618545	0.317666	-3.603244	-3.88933
70°			0.832747	0.659417	0.64744	0.642673	0.619314	0.318427	-3.614137	-3.899978
80°			0.816794	0.643468	0.631453	0.626725	0.603363	0.302485	-3.365439	-3.651212
90°				0.612978	0.600978	0.596236	0.572882	0.271994	-2.892423	-3.178289
100°				0.571660	0.559599	0.554867	0.531564	0.230610	-2.24945	-2.534854
110°				0.523622	0.511613	0.506883	0.483525	0.182639	-1.502511	-1.788365
120°					0.461720	0.456971	0.433615	0.132725	-0.729209	-1.015205

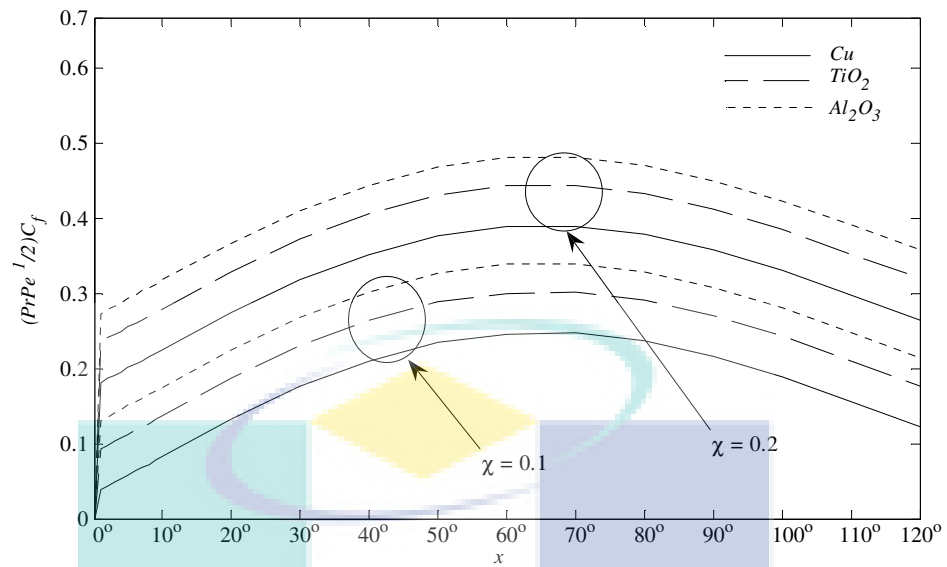


Figure 8.1: The local skin friction coefficient $(Pr Pe^{1/2})C_f$ with x using various nanoparticles when $\lambda = -1$, $\gamma = 0.5$ and $\chi = 0.1, 0.2$

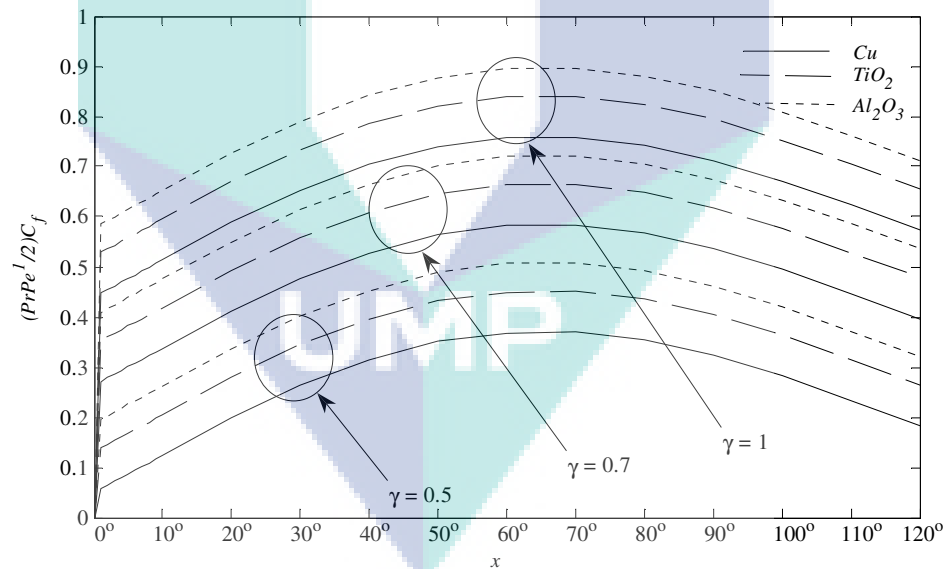


Figure 8.2: The local skin friction coefficient $(Pr Pe^{1/2})C_f$ with x using various nanoparticles when $\lambda = -1$, $\chi = 0.2$ and $\gamma = 0.5, 0.7, 1$

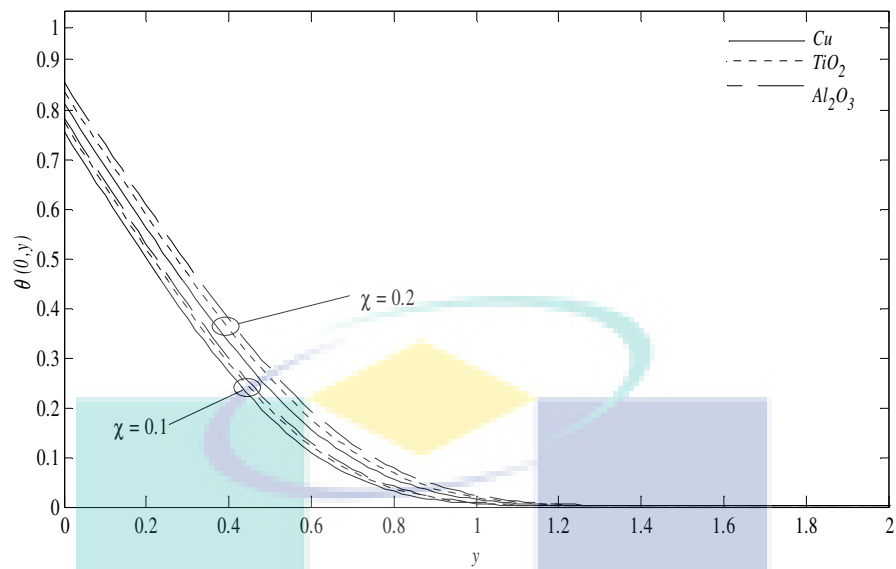


Figure 8.3: The temperature profiles $\theta(0, y)$, using various nanoparticles when $\lambda = -1$, $\gamma = 0.5$ and $\chi = 0.1, 0.2$

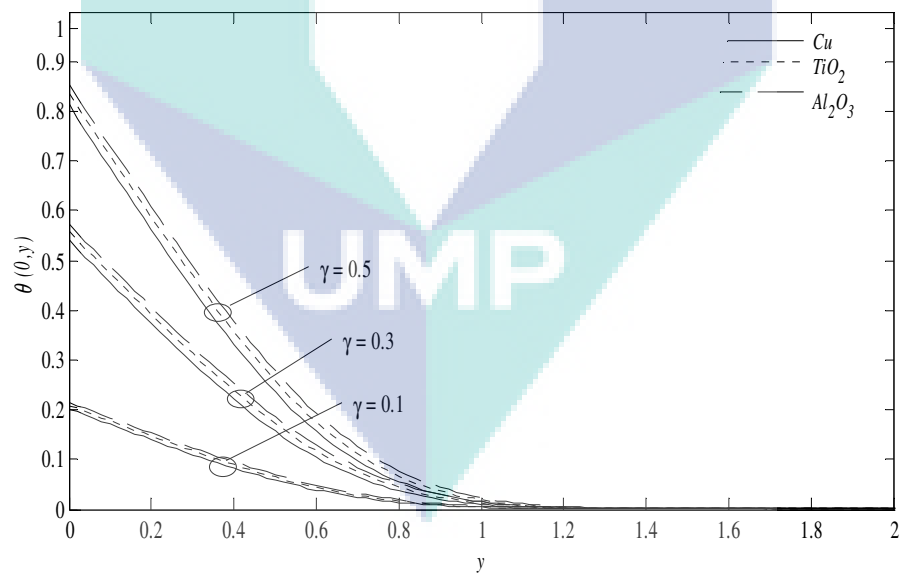


Figure 8.4: The temperature profiles $\theta(0, y)$, using various nanoparticles when $\lambda = -1$, $\chi = 0.2$ and $\gamma = 0.1, 0.3, 0.5$

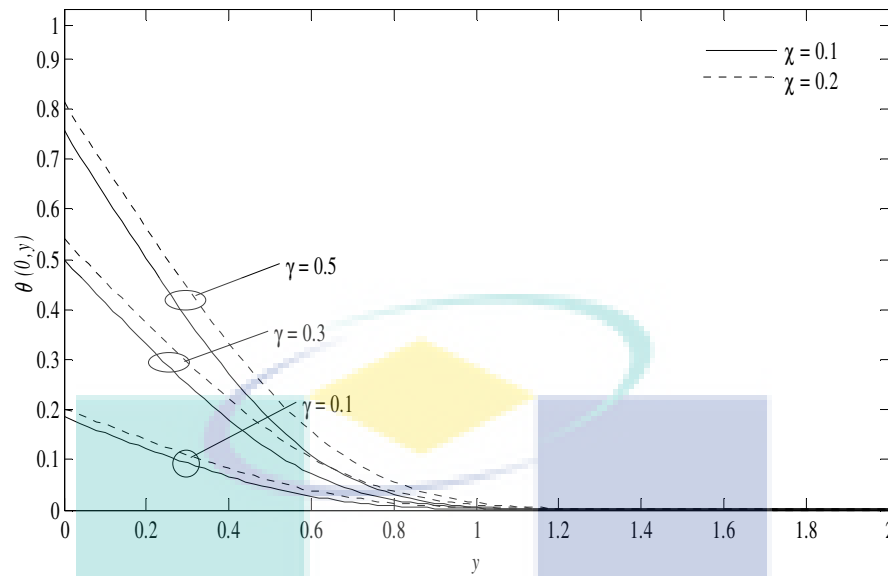


Figure 8.5: The temperature profiles $\theta(0, y)$, using *Cu* nanoparticles when $\chi = 0.1, 0.2$ $\lambda = -1$ and $\gamma = 0.1, 0.3, 0.5$

8.4 CONCLUSIONS

In this chapter, we have numerically studied the problem of mixed convection boundary layer flow about a sphere embedded in a porous medium filled with convective boundary conditions in a nanofluid and solved by using the Keller-box method. It is shown how the mixed convection parameter λ , the type of nanoparticles (*Cu*, Al_2O_3 , TiO_2), the nanoparticle volume fraction χ and the conjugate parameter γ , affects on the local skin friction coefficient $(Pr Pe^{1/2})C_f$ and the temperature $\theta(0, y)$. We can conclude that:

- An increase in the both values of nanoparticle volume fraction χ and the conjugate parameter γ led to an increase of the local skin friction coefficient.
- An increase in the both values of nanoparticle volume fraction χ and the conjugate parameter γ led to an increase temperature.
- The Al_2O_3 also has the highest local skin friction coefficient, followed by TiO_2 and the lowest is *Cu*.

CHAPTER 9

CONCLUSIONS

9.1 SUMMARY OF THE RESEARCH

This thesis presented six problems involving the free and mixed convection boundary layer flow over a solid sphere in a viscous, micropolar fluid and nanofluid with radiation and magnetohydrodynamic effects. All the problems in this study are examined with convective boundary conditions. These problems are solved numerically using an implicit finite difference scheme known as the Keller-box method.

Chapter 1 contains an introduction, the boundary layer theory, type of fluids, boundary conditions, significance of research, scope and objectives, thesis outline and literature review.

The governing equation for the problem considered and the details about the Keller-box method are discussed in Chapter 2. In this chapter, the focus is only given on the governing equation for the specific problem of the mixed convection boundary layer flow over a solid sphere with convective boundary conditions in a nanofluid. In summary, we had derived the governing equations into basic equations and transformed it to nonlinear partial differential equations before being solved numerically using the Keller-box method. The Keller-box method involves four steps, which are, reduce a system to a first order system, write the equations using central differences, linearize the resulting algebraic equations by Newton's method, and write them in the matrix-vector form and lastly solve the linear system by the block triadiagonal elimination technique; this method was programmed into Matlab® as given in Appendix D.

Chapter 3, we discussed a problem of steady effect of radiation on magnetohydro-dynamic free convection boundary layer flow over a solid sphere in a viscous fluid. The discussion on relevant physical quantities, such as the local wall

temperature, the local heat transfer coefficient, local Nusselt number and the local skin friction coefficient have been considered and presented in the results and discussion. The velocity and temperature have also been discussed. In conclusion, as radiation parameter increases, the temperature, velocity, and skin friction coefficient decreases but the local Nusselt number and the heat transfer coefficient increases. Also as the magnetic parameter increases, the value of temperature increases but the velocity, values of local Nusselt number, the local skin friction coefficient and heat transfer coefficient decreases. On the other hand, we have compared the present results with previous results without the effect of radiation and magnetohydrodynamic when $M = 0$, $N_R = 0$ and the conjugate parameter $\gamma \rightarrow \infty$ as we found that the agreement was very good. Results are presented in the form of figures and tables.

The problem of the effect of radiation on magnetohydrodynamic free convection boundary layer flow over a solid sphere in a micropolar fluids were studied and discussed in Chapter 4. The division of sections and subsections are similar to those in Chapter 3. The convective boundary conditions have been considered to all problems. The results obtained are the wall temperature, the local heat transfer coefficient, local Nusselt number and the local skin friction coefficient as well as the temperature, velocity and angular velocity. In conclusion, as micropolar parameter K increases. Also, the value of the wall temperature also increases but the skin friction coefficient decreases the values of local skin friction coefficient are higher for micropolar fluids ($K \neq 0$) than those for a Newtonian fluid ($K = 0$). Moreover as N_R increases the angular velocity increases, while when M increases the angular velocity decrease. We have also comparing the present results with previous results, without the effect of radiation and magnetohydrodynamic when $M = 0$, $N_R = 0$ and $\gamma \rightarrow \infty$ for various values of micropolar parameter. It is found that the agreement are very good.

Furthermore, the mixed convection boundary layer flow over a solid sphere with convective boundary conditions in a viscous and micropolar fluid has also been studied in both cases of heated and cooled sphere. The full discussions of both problems can be found in Chapter 5 and 6, respectively. For these problems, we started our discussion by comparing our present results for $\gamma \rightarrow \infty$ with the previously published results that were found to be very good. The numerical results of the local heat transfer coefficient

and the skin friction coefficient were obtained for various values in micropolar parameter, Prandtl number and the conjugate parameter for both assisting and opposing flows cases. In conclusion, when the conjugate parameter increases the values of the local heat transfer coefficient and the local skin friction coefficient increases. Also, as the mixed convection parameter increases the values of the local heat transfer coefficient, the same goes to the local skin friction coefficient.

Chapter 7 discussed the problem of mixed convection boundary layer flow over a solid sphere with convective boundary conditions in a nanofluid. As a conclusion, an increase in both values of nanoparticle volume fraction and the conjugate parameter led to an increase of both the local heat transfer coefficient and the local skin friction coefficient. On the other hand, the copper Cu nanoparticles have the highest local heat transfer coefficient compared to aluminum oxide Al_2O_3 and titanium dioxide TiO_2 . Moreover, copper Cu also has the highest local skin friction coefficient, followed by titanium dioxide TiO_2 and aluminum oxide Al_2O_3 by nanoparticles.

In Chapter 8, the study was on laminar of mixed convection boundary layer flow about a sphere embedded in a porous medium filled with convective boundary conditions in a nanofluid. The formulation, results and discussion are detailed. From this chapter, the conclusions that we have obtained are an increase in both values of nanoparticle volume fraction and the conjugate parameter led to an increase of the local skin friction coefficient. Moreover, an increase in both values of nanoparticle volume fraction and the conjugate parameter γ led to an increase of temperature. On other hand, the Al_2O_3 also has the highest local skin friction coefficient, followed by TiO_2 and the lowest is Cu .

For all problems considered in Chapters 3 to 8, the governing boundary layer equations were first transformed into non-dimensional form. Then, the non-similar transformations were used to solve the non-dimensional governing equations. The resulting nonlinear system of partial differential equations is then solved numerically using an implicit finite difference scheme known as the Keller-box method.

Finally, it is worth mentioning that all the results presented in this study are illustrated in the form of figures and tables. The tables are very important because they can serve as a reference against other exact or approximate solutions that can be compared in the future. It is also worth pointing out that some of the problems studied in this thesis have been published and the list of publications is presented in Appendix E.

9.2 CONTRIBUTION OF THE RESEARCH

The main contribution in this thesis is investigated on a viscous fluid, micropolar fluid and nanofluid in three different mathematical modelling such as solid sphere. Besides that, a few parameters like magnetic parameter, radiation parameter, the micropolar parameter, the nanoparticle volume fraction, the mixed convection parameter, the conjugate parameter and the coordinate running along the surface of the sphere, x as well as Prandtl number has been studied thoroughly. In each problem, the numerical algorithm has been developed. The results obtained in this thesis will be used for validation purposes in future.

9.3 FUTURE STUDIES

In this thesis, only incompressible viscous, micropolar fluid and nanofluid with convective boundary conditions are considered. Therefore, there are a lot of aspects that can be considered for future studies. For examples:

1. Other geometries such as vertical plate, stretching sheet and also elliptic circular cylinder.
2. Investigating this type of fluid flow like Eyring Powell, Casson, viscoelastic, Jeffrey and Maxwell fluids.
3. Include the other effects like chemical reaction, heat absorption and temperature dependent viscosity.
4. Study the effects of the boundary condition representing Hall current effect of slip and mixed thermal boundary conditions.

REFERENCES

- Abu-Nada, E. 2008. Application of nanofluids for heat transfer enhancement of separated flows encountered in a backward facing step. *International Journal of Heat and Fluid Flow*. **29**(1): 242-249.
- Abu-Nada, E. and Oztop, H. F. 2009. Effects of inclination angle on natural convection in enclosures filled with Cu–water nanofluid. *International Journal of Heat and Fluid Flow*. **30**(4): 669-678.
- Acheson, D. J. 1990. *Elementary fluid dynamics*. Oxford University.
- Ahmad, S. B. 2009. *Convection boundary layer flows over needles and cylinders in viscous fluids*. Ph.D Thesis, Universiti Putra Malaysia, Malaysia.
- Ahmadi, G. 1976. Self-similar solution of incompressible micropolar boundary layer flow over a semi-infinite flat plate. *International Journal of Engineering Science*. **14**(7): 639-646.
- Akbar, N. S. Nadeem, S., Haq, R. U. and Khan. Z. 2013. Radiation effects on MHD stagnation point flow of nano fluid towards a stretching surface with convective boundary condition. *Chinese Journal of Aeronautics*. **26**(6): 1389-1397.
- Aktar, S., Ruma, M. B. M. and Alim, M. A. 2013. Effects of viscous dissipation on natural convection flow along a sphere with radiation and heat generation. *Journal of Naval Architecture and Marine Engineering*. **10**(1): 13-24.
- Alam, M. M., Alim, M. and Chowdhury, M. M. 2007. Viscous dissipation effects on mhd natural convection flow over a sphere in the presence of heat generation. *Nonlinear Analysis: Modelling and Control*. **12**(4): 447-459.
- Ariman, T., Turk, M. and Sylvester, N. 1973. Microcontinuum fluid mechanics. *International Journal of Engineering Science*. **11**(8): 905-930.

- Aziz, A. 2009. A similarity solution for laminar thermal boundary layer over a flat plate with a convective surface boundary conditions. *Communications in Nonlinear Science and Numerical Simulation*. **14**(4): 1064-1068.
- Baehr, H. D. and Stephan, K. 2006. *Heat and mass transfer*. Berlin Heidelberg: Springer Verlag.
- Bataller, R. C. 2008a. Radiation effects for the blasius and sakiadis flows with a convective surface boundary conditions. *Applied Mathematics and Computation*. **206**(2): 832-840.
- Bataller, R. C. 2008b. Radiation effects in the Blasius flow. *Applied Mathematics and Computation*. **198**(1): 333-338.
- Bataller, R. C. 2011. Magnetohydrodynamic flow and heat transfer of an upper-convected Maxwell fluid due to a stretching sheet. *Fluid Dynamics and Materials Processing*. **7**(2): 153-173.
- Bejan, A. 1984. *Convection heat transfer*. New York: John Wiley.
- Bejan, A. and Kraus, A. D. 2003. *Heat transfer handbooks*. New York.: John Wiley
- Blundell, S. and Blundell, K. 2006. *Concepts in modern physics*. Oxford University Press.
- Buongiorno, J., Hu, L. W., Kim, S. J., Hannink, R., Truong, B. A. O. and Forrest, E. 2008. Nanofluids for enhanced economics and safety of nuclear reactors: An evaluation of the potential features, issues and research gaps. *Nuclear Technology*. **162**(1): 80-91.
- Buongiorno, J. 2006. Convective transport in nanofluids. *Journal of Heat Transfer*. **128**(3): 240-250.
- Burmeister, L. C. 1993. *Convective heat transfer*. New York: John Wiley and Sons Inc.
- Cebeci, T. and Bradshaw, P. 1988. *Physical and computational aspects of convective heat transfer*. New York: Springer.

- Cebeci, T. and Smith, A. M. O. 1974. Analysis of turbulent boundary layers. *NASA STI/Recon Technical Report A. 75*: 46513.
- Cebeci, T. and Cousteix, J. 2005. *Modeling and computation of boundary layer flows*. New York: Springer.
- Cengel, Y. A. 2003. *Heat and mass transfer* 3rd Edition, A Practical Approach Boston: McGraw Hill.
- Chen, T. and Armaly, B. 1987. *Mixed convection in external flow*. In *handbook of single-phase convective heat transfer*, New York:Wiley.
- Chen, T. and Mucoglu, A. 1977. Analysis of mixed forced and free convection about a sphere. *International Journal of Heat and Mass Transfer. 20*(8): 867-875.
- Cheng, C.Y. 2008. Natural convection heat and mass transfer from a sphere in micropolar fluids with constant wall temperature and Concentration. *International Communications in Heat and Mass Transfer. 35*(6): 750-755.
- Choi, S. U. S., Zhang, Z. G., Yu, W., Lockwood, F. E. and Grulke, E. A. 2001. Anomalous thermal conductivity enhancement in nanotube suspensions. *Applied Physics Letters. 79*(14): 2252-2254.
- Choi, S. 1995. Enhancing thermal conductivity of fluids with nanoparticles. *ASME-Publications-Fed. 231*: 99-106.
- Chopkar, M., Das, P. K. and Manna, I. 2006. Synthesis and characterization of nanofluid for advanced heat transfer applications. *Scripta Materialia. 55*(6): 549-552.
- Eastman, J., S. Choi, S. Li., Yu, W. and Thompson, L. 2001. Anomalously increased effective thermal conductivities of ethylene glycol-based nanofluids containing copper nanoparticles. *Applied Physics Letters. 78*(6): 718-720.

- Dasman, A., Kasim, M., Rahman, A., Mohammad, N. F., Mangi, A. and Shafie, S. 2013. Mixed convection boundary layer flow of viscoelastic fluids past a sphere. *In Defect and Diffusion Forum.* 336: 57-63.
- Das, S. K., Choi, S. U. S. and Yu, W. 2007. *Nanofluids: science and technology.* Pradet. New Jersey: Wiley.
- Daunghongsuk, W., and Wongwises, S. 2007. A critical review of convective heat transfer of nanofluids. *Renewable and Sustainable Energy Reviews.* **11**(5): 797-817.
- Duangthongsuk, W. and Wongwises, S. 2008. Effect of thermophysical properties models on the predicting of the convective heat transfer coefficient for low concentration nanofluid. *International Communications in Heat and Mass Transfer.* **35**(10): 1320-1326.
- El-Kabeir, S. M. M. and Gorla, R. S. R. 2007. MHD effects on natural convection in a micropolar fluid at a three-dimensional stagnation point in a porous medium. *International Journal of Fluid Mechanics Research.* **34**(2): 145-158.
- Eringen, A. C. 2001. *Microcontinuum field theories: ii. fluent media.* Vol. 2. Springer
- Eringen, A. C. 1966. Theory of micropolar fluids. *Journal Mathematical Mechnecl* 16, 1-18.
- Falkovich, G. 2011. *Fluid Mechanics: A Short Course for Physicists.* Cambridge University Press.
- Forbes, T. G. and Priest, E. R. 2000. *Magnetic reconnection: MHD theory and applications.* Cambridge University Press, First Edition.
- Ganesan, P. and Palani, G. 2004. Finite difference analysis of unsteady natural convection mhd flow past an inclined plate with variable surface heat and mass flux. *International Journal of Heat and Mass Transfer.* **47**: 4449-4457.

- Ghasemi, B. and Aminossadati, S. 2010. Brownian motion of nanoparticles in a triangular enclosure with natural convection. *International Journal of Thermal Sciences*. **49**(6): 931-940.
- Ghodeswar, K. 2010. *Natural convection in a porous medium saturated by nanofluid*. PhD Thesis. Cleveland State University.
- Guram, G. and Smith, A. 1980. Stagnation flows of micropolar fluids with strong and weak interactions. *Computers and Mathematics with Applications*. **6**(2): 213-233.
- Hahn, David W. and Ozisk, M. N. 2012. *Heat Conduction*, 3rd edition. New York: Wiley.
- Hayat, T., Shehzad, S. A., Qasim, M. and Alsaedi, A. 2014. Mixed convection flow by a porous sheet with variable thermal conductivity and convective boundary condition. *Brazilian Journal of Chemical Engineering*. **31**(1): 109-117.
- Hieber, C. and Gebhart, B. 1969. Mixed convection from a sphere at small reynolds and grashof numbers. *Journal of Fluid Mechanics*. **38**(1): 137-159.
- Huang, M. J. and Chen, C.K. 1987. Laminar free convections from a sphere with blowing and suction. *Journal of Heat Transfer*. **109**(2): 529-532.
- Incropera, F. P., Dewitt, D. P., Bergman, T. L. and Lavine, A. S. 2006. *Fundamentals of heat and mass transfer 6th ed*. New York: John Wiley and Sons.
- Ingham, D. B. and Pop, I. 2001. *Convective heat transfer: mathematical and computational modelling of viscous fluids and porous media*. Pergamon Oxford.
- Ishak, A., Nazar, R. and Pop, I. 2006a. Mixed convection boundary layers in the stagnation-point flow toward a stretching vertical sheet. *Meccanica*. **41**(5): 509-518.
- Ishak, A., Nazar, R. and Pop, I. 2006b. Mixed convection stagnation point flow of a micropolar fluid towards a stretching sheet. *Acta Meccanica*. **43**: 411-418.

- Ishak, A., Nazar, R. and Pop, I. 2006c. Unsteady mixed convection boundary layer flow due to a stretching vertical surface. *Arabian Journal for Science and Engineering*. **31**: 165–182.
- Ishak, A., Nazar, R., Amin, N., Filip, D. and Pop, I. 2007a. Mixed convection of the stagnation-point flow towards a stretching vertical permeable sheet. *Malaysian Journal of Mathematical Sciences*. **2**: 217-226.
- Ishak, A., Nazar, R. and Pop, I. 2007b. Mixed convection on the stagnation point flow toward a vertical continuously stretching sheet. *Journal of Heat Transfer*. **129**(8): 1087-1090.
- Ishak, A., Lok, Y. Y. and Pop, I. 2010a. Stagnation-point flow over a shrinking sheet in a micropolar fluid. *Chemical Engineering Communications*. **197**: 1417-1427.
- Ishak, A., Nazar, R., Bachok, N. and Pop, I. 2010b. MHD mixed convection flow near the stagnation-point on a vertical permeable surface. *Physica A: Statistical Mechanics and its Applications*. **389**: 40-46.
- Ishak, A., Nazar, R. and Pop, I. 2008. Post stagnation point boundary layer flow and mixed convection heat transfer over a vertical linearly stretching sheet. *Archives of Mechanics*. **60**: 303-322.
- Ishak, A. 2010. Similarity solutions for flow and heat transfer over a permeable surface with convective boundary condition. *Applied Mathematics and Computation*. **217**(2): 837-842.
- Ishak, A., Yacob N. and Bachok N. 2011. Radiation effects on the thermal boundary layer flow over a moving plate with convective boundary condition. *Meccanica*. **46**(4): 795-801.
- Jaluria, Y., Manca, O., Poulidakos, D., Vafai, K. and Wang, L. 2012. Heat transfer in nanofluids. *Advances in Mechanical Engineering*. **12**(2): 512-533.

- Jena, S. and Mathur, M. 1981. Similarity solutions for laminar free convection flow of a thermomicro-polar fluid past a non-isothermal vertical flat plate. *International Journal of Engineering Science*. **19**(11): 1431-1439.
- Jou, R. Y. and Tzeng, S.C. 2006. Numerical research of nature convective heat transfer enhancement filled with nanofluids in rectangular enclosures. *International Communications in Heat and Mass Transfer*. **33**(6): 727-736.
- Kafoussias, N. and Williams, E. 1995. The effect of temperature-dependent viscosity on free-forced convective laminar boundary layer flow past a vertical isothermal flat plate. *Acta Mechanica*. **110**(1-4): 123-137.
- Kakaç, S. and Pramuanjaroenkij, A. 2009. Review of convective heat transfer enhancement with nanofluids. *International Journal of Heat and Mass Transfer*. **52**(13): 3187-3196.
- Kang, H. U., Kim, S. H. and Oh, J. M. 2006. Estimation of thermal conductivity of nanofluid using experimental effective particle volume. *Experimental Heat Transfer*. **19**(3): 181-191.
- Kasim, A. R. M., Mohammad, N. F, Aurangzaib, S. S. and Sharidan, S. 2012. Natural convection boundary layer flow of a viscoelastic fluid on solid sphere with Newtonian heating. *World Academy of Science, Engineering and Technology*. **64**: 628-633.
- Keller, H. B. 1970. *A new difference scheme for parabolic problems. in numerical solutions of partial differential equations*. New York: Academic Press.
- Keller, H. B. and Cebeci, T. 1972. Accurate numerical methods for boundary-layer flows. two dimensional turbulent flows. *AIAA Journal*. **10**(9): 1193-1199.
- Keller, H. B. and Cebeci, T. 1972. Accurate numerical methods for boundary layer flows i. two dimensional laminar flows. *Proceedings of the Second International Conference on numerical Methods in Fluid Dynamics*. New York: Springer-Verlag.

- Khanafer, K., Vafai, K. and Lightstone, M. 2003. Buoyancy-driven heat transfer enhancement in a two-dimensional enclosure utilizing nanofluids. *International Journal of Heat and Mass Transfer*. **46**(19): 3639-3653.
- Klyachko, L. 1963. Heat transfer between a gas and a spherical surface with the combined action of free and forced convection. *Journal of Heat Transfer*. **85**: 355-362.
- Kotouc, M., Bouchet, G. and Dusek, J. 2008. Loss of axisymmetry in the mixed convection, assisting flow past a heated sphere. *International Journal of Heat and Mass Transfer*. **51**(11-12): 2686-2700.
- Kumar, S., Prasad, S. K. and Banerjee, J. 2010. Analysis of flow and thermal field in nanofluid using a single phase thermal dispersion model. *Applied Mathematical Modelling*. **34**(3): 573-592.
- Lien, F. S. and Chen, C. C. 1987. Mixed convection of micropolar fluid about a spherewith blowing and suction. *International Journal of Engineering Science*. **25**(7): 775-784.
- Lok, Y. Y., Phang, P. Amin, N. and Pop, I. 2003. Unsteady boundary layer flow of a micropolar fluid near the forward stagnation point of a plane surface. *International Journal of Engineering Science*. **4**:47-51.
- Lok, Y. Y., Amin, N, Campean, D. and Pop, I. 2005. Steady mixed convection flow of a micropolar fluid near the stagnation point on a vertical surface. *International Journal of Numerical Methods for Heat & Fluid Flow*. **15**(7):654-670.
- Lok, Y. Y., Amin, N and Pop, 2006. Unsteady mixed convection flow of a micropolar fluid near the stagnation point on a vertical surface. *International Journal of Thermal Sciences*. **45**(12):1149-1157.
- Lok, Y. Y., Amin, N and Pop, 2007. Mixed convection flow near a non-orthogonal stagnation point towards a stretching vertical plate. *International Journal of Heat and Mass Transfer*. **50**: 4855-4863.

- Luikov, A. V., Aleksashenko, V. A. and Aleksashenko, A. A. 1971. Analytical methods of solution of conjugated problems in convective heat transfer. *International Journal of Heat and Mass Transfer*. **14**(8): 1047-1056.
- Lukaszewicz, G. 1999. *Micropolar fluids: theory and applications*. Basel: Birkhuser: Springer.
- Magyari, E. 2010. Comment on 'a similarity solution for laminar thermal boundary layer over a flat plate with a convective surface boundary conditions by Aziz. *Communications in Nonlinear Science and Numerical Simulation* 2009,14:1064-1068. *Communications in Nonlinear Science and Numerical Simulation I*. **16**: 599-601.
- Maiga, S. E. B., Palm, S. J., Nguyen, C. T., Roy, G. and Galanis, N. 2005. Heat transfer enhancement by using nanofluids in forced convection flows. *International Journal of Heat and Fluid Flow*. **26**(4): 530-546.
- Makinde, O. D. and Aziz, A. 2010. MHD mixed convection from a vertical plate embedded in a porous medium with a convective boundary conditions. *International Journal of Thermal Sciences*. **49**(9): 1813-1820.
- Merkin, J. H. 1994. Natural convection boundary layer flow on a vertical surface with Newtonian heating. *International Journal of Heat and Fluid Flow*. **15**(5): 392-398.
- Merkin, J. H. and Pop, I. 2011. The forced convection flow of a uniform stream over a flat surface with a convective surface boundary conditions. *Communications in Nonlinear Science and Numerical Simulation*. **16**(9): 3602-3609.
- Mohamed, M. K. A. Salleh, M. Z, Nazar, R. and Ishak, A. 2012. Stagnation point flow over a stretching sheet with Newtonian heating. *Sains Malaysiana*. **41**(11): 1467-1473.
- Mohamed, M. K. A. Salleh, M. Z, Nazar, R. and Ishak, A. 2013. Numerical investigation of stagnation point flow over a stretching sheet with convective boundary conditions. *Boundary Value Problems*. **4**(1): 1-10

- Molla, M. M., Hossain, M. A. and Siddiqua, S. 2011. Radiation effect on free convection laminar flow from an isothermal sphere. *Chemical Engineering Communications*. **198**(12): 1483-1496.
- Molla, M. M., Saha, S. C. and Hossain, M. A. 2012. The effect of temperature dependent viscosity on MHD natural convection flow from an isothermal sphere. *Journal of Applied Fluid Mechanics*. **5**(2), 25-31.
- Molla, M. M., Taher, M. Chowdhury, M. M. and Hossain, M. A. 2005. Magneto-hydrodynamic natural convection flow on a sphere in presence of heat generation. *Nonlinear Analysis: Modelling and Control*. **10**(4): 349-363.
- Mucoglu, A. and Chen, T. 1978. Mixed convection about a sphere with uniform surface heat flux. *Journal of Heat Transfer*. **100**(3): 542-551.
- Mustafa, M., Khan, J. A., Hayat, T. and Alsaedi, A. 2015. Boundary layer flow of nanofluid over a nonlinearly stretching sheet with convective boundary condition. *IEEE Transactions On Nanotechnology*, **14**(1): 159.
- Muthtamilselvan, M., Kandaswamy, P. and Lee., J. 2010. Heat transfer enhancement of copper-water nanofluids in a lid-driven enclosure. *Communications in Nonlinear Science and Numerical Simulation*. **15**(6): 1501-1510.
- Na, T. Y. 1979. *Computational methods in engineering boundary value problems*. Academic Press. New York.
- Nadeem, S. and Haq, R. U. 2014. Effect of thermal radiation for magnetohydrodynamic boundary layer flow of a nanofluid past a stretching sheet with convective boundary conditions. *Journal of Computational and Theoretical Nanoscience*. **11**(1): 32-40.
- Nazar, R., Amin, N., Groşan, T and Pop, I. 2002a. Free convection boundary layer on an isothermal sphere in a micropolar fluid. *International Communications in Heat and Mass Transfer*. **29**(3): 377-386.

- Nazar, R., Amin, N., Groşan, T. and Pop, I. 2002b. Free convection boundary layer on a sphere with constant surface heat flux in a micropolar fluid. *International Communications in Heat and Mass Transfer*. **29**(8): 1129-1138.
- Nazar, R., Amin, N. and Pop, I. 2002c. On the Mixed convection boundary layer flow about a solid sphere with constant surface temperature. *Arabian Journal for Science and Engineering*. **27**(2): 117-135.
- Nazar, R., Amin, N. and Pop, I. 2002d. Mixed convection boundary layer flow from a sphere with constant surface heat flux in a micropolar fluid. *Journal of Energy Heat and Mass Transfer*. **29**(8): 1129-1138.
- Nazar, R., Amin, N. and Pop, I. 2002e. Mixed convection boundary layer flow from a horizontal circular cylinder with a constant surface heat flux. *International Journal of Applied Mechanics and Engineering*. **7**:409-431.
- Nazar, R., Amin, N. and Pop, I. 2003a. Mixed convection boundary layer flow about an isothermal sphere in a micropolar fluid. *International journal of thermal sciences*. **42**(3): 283-293.
- Nazar, R., Amin, N. and Pop, I. 2003b. The Brinkman model for the mixed convection boundary layer flow past a horizontal circular cylinder in a porous medium. *International Journal of Heat Mass Transfer*. **46**:3167-3178.
- Nazar, R., Amin, N. and Pop, I. 2003c. Mixed convection boundary layer flow from a horizontal circular cylinder in micropolar fluids: case of constant wall temperature. *International Journal of Numerical Methods for Heat and Fluid Flow*. **13**:86-109.
- Nazar, R., Amin, N. and Pop, I. 2004a. Mixed convection boundary layer flow from a horizontal circular cylinder with a constant surface heat flux. *Heat and Mass Transfer*. **40**:219-227.
- Nazar, R., Amin, N. and Pop, I. 2004b. Mixed convection boundary layer flow from a horizontal circular cylinder in micropolar fluids: case of constant wall heat flux. *International Journal of Fluid Mechanics Research*. **31**:143-159.

- Nazar, R., Tham, L. Pop, I. and Ingham, D. 2011. Mixed convection boundary layer flow from a horizontal circular cylinder embedded in a porous medium filled with a nanofluid. *Transport in Porous Media*. **86**(2): 517-536.
- Nazar, R. 2003. *Mathematical models for free and mixed convection boundary layer flows of micropolar fluids*. Ph.D thesis Universiti Teknologi Malaysia, Malaysia.
- Nirmalkar, N., Bose, A. and Chhabra, R. P. 2014. Mixed convection from a heated sphere in Bingham plastic fluids. *Numerical Heat Transfer, Part A: Applications*. **66**(9): 1048-1075.
- Ozisik, M. N. 1985. *Heat Transfer*. New York: McGraw-Hill Inc.
- Oztop, H. F. and Abu-Nada, E. 2008. Numerical study of natural convection in partially heated rectangular enclosures filled with nanofluids. *International Journal of Heat and Fluid Flow*. **29**(5): 1326-1336.
- Patel, H. E., Anoop, K., Sundararajan, T. and Das, S. K. 2006 A micro-convection model for thermal conductivity of nanofluids. *International Heat Transfer Conference* **13**: 243-265.
- Patel, H. E., Das, S. K., Sundararajan, T., Nair, A. S., George, B. and Pradeep, T. 2003. Thermal conductivities of naked and monolayer protected metal nanoparticle based nanofluids: Manifestation of anomalous enhancement and chemical effects. *Applied Physics Letters*. **83**(14): 2931-2933.
- Pop, I. and Na, T. Y. 1999. Natural convection over a vertical wavy frustum of a cone. *International Journal of Non-Linear Mechanics*. **34**: 925-934.
- Putra, N., W. Roetzel, and S. K. Das. 2003. Natural convection of nano-fluids. *Heat and Mass Transfer*. **39**(8-9): 775-784.
- Rashad, A. M., Chamkha, A. J. and El-Kabeir, S. M. M. 2011. Effect of chemical reaction on heat and mass transfer by mixed convection flow about a sphere in a saturated porous media. *International Journal of Numerical Methods for Heat and Fluid Flow*. **21**(4): 418-433.

- Rashad, A. M., Chamkha, A. J. and El-Kabeir, S. M. M. 2014. Effects of radiation and chemical reaction on heat and mass transfer by natural convection in a micropolar fluid-saturated porous medium with streamwise temperature and species concentration variations. *Heat Transfer Research*. **45**(8): 795–815.
- Rashad, A. M., Chamkha, A. J. and Modather, M. 2013. Mixed convection boundary-layer flow past a horizontal circular cylinder embedded in a porous medium filled with a nanofluid under convective boundary condition. *Computers and Fluids*. **86**: 380-388.
- Rashidi, M. M. and Erfani, E. 2009. A novel analytical solution of the thermal boundary-layer over a flat plate with a convective surface boundary condition using dtm-pade. *Paper presented at the 2009 International Conference on Signal Processing Systems. 15-17 May 2009*.
- Routbort, J., Wu, Y., France, D. M., Singh, D., Timofeeva, E. V. and Smith, D. S. 2009. *Gobain Corp. Argonne National Lab: Michellin North America*.
- Salleh, M. Z., Nazar, R. and Pop, I. 2009. Forced convection boundary layer flow at a forward stagnation point with Newtonian heating. *Chemical Engineering Communications*. **196**: 987-996.
- Salleh, M. Z., Nazar, R. and Pop, I. 2010a. Mixed convection boundary layer flow about a solid sphere with Newtonian heating. *Archives of Mechanics*. **62**(4): 283-303.
- Salleh, M. Z., Nazar, R. and Pop, I. 2010b. Mixed convection boundary layer flow from a solid sphere with Newtonian heating in a micropolar fluid. *SRX Physics* doi:10.3814/2010/736039.
- Salleh, M. Z., Nazar, R. and Pop, I. 2010c. Modeling of free convection boundary layer flow on a solid sphere with Newtonian heating. *Acta Applicandae Mathematicae* **112**(3): 263-274.
- Salleh, M. Z. and Nazar, R. 2010d. Free convection boundary layer flow over a horizontal circular cylinder with Newtonian heating. *Sains Malaysiana*. **39**(4): 671-676.

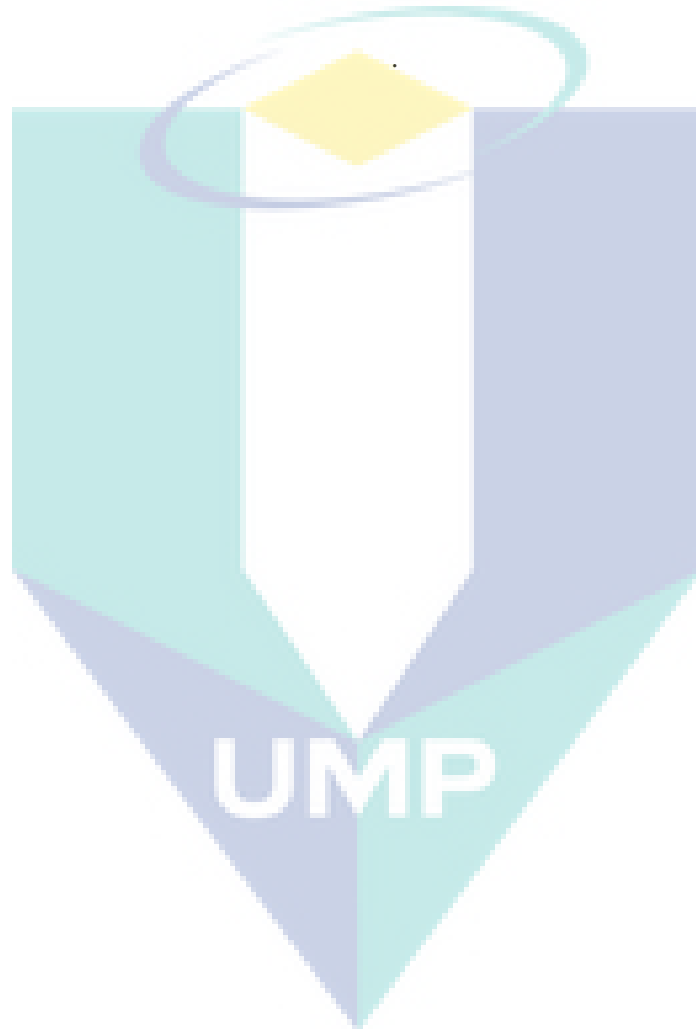
- Salleh, M. Z., Nazar, R. and Pop, I. 2010e. Mixed convection boundary layer flow over a horizontal circular cylinder with Newtonian heating. *Heat and Mass Transfer*. **46**(11-12): 1411-1418.
- Salleh, M. Z., Nazar, R. and Pop, I. 2010f. Boundary layer flow and heat transfer over a stretching sheet with Newtonian heating. *Journal of the Taiwan Institute of Chemical Engineers*. **41**(6): 651-655.
- Salleh, M. Z., Nazar, R., Arifin, N. M., Pop, I. and Merkin, J. H. 2011. Forced convection heat transfer over a circular cylinder with Newtonian heating. *Journal of Engineering Mathematics*. **69**: 101-110.
- Salleh, M. Z., Nazar, R. and Pop, I. 2012a. Numerical solutions of free convection boundary layer flow on a solid sphere with Newtonian heating in a micropolar fluid. *Meccanica*. **47**(5): 1261-1269.
- Salleh, M. Z., Najihah, S., M., Roziena, K. Khasi'ie, N. S. Nazar, R. and Pop, I. 2012b. Free convection over a permeable horizontal flat plate embedded in a porous medium with radiation effects and mixed thermal boundary conditions. *Journals of Mathematics and Statistics*. **8**(1): 122-128.
- Schlichting, H. 1979. *Boundary layer theory*. New York: McGraw-Hill Inc.
- Sivaiah, M., Nagarajan, A. and Reddy, P. S. 2010. Radiation effects on MHD free convection flow over a vertical plate with heat and mass flux. *Emirates Journal for Engg. Research*. **15**, 35-40.
- Sherman, F. S. 1990. *Viscous Flow*. New York: McGraw-Hill Inc.
- Talebi, F., Mahmoudi, A. H. and Shahi, M. 2010. Numerical study of mixed convection flows in a square lid-driven cavity utilizing nanofluid. *International Communications in Heat and Mass Transfer*. **37**(1): 79-90.
- Tanner, R. I. 1988. *Engineering rheology*. Oxford: Clarendon Press.

- Tansley, C. E. and Marshall, D. P. 2001. Flow past a cylinder on a β plane, with application to gulf stream separation and the antarctic circumpolar current. *Journal of Physical Oceanography*. **31**(11): 3274-3283.
- Tiwari, R. K. and Das, M. K. 2007. Heat transfer augmentation in a two-sided lid-driven differentially heated square cavity utilizing nanofluids. *International Journal of Heat and Mass Transfer*. **50**(9): 2002-2018.
- Trisaksri, V., and S. Wongwises. 2007. Critical review of heat transfer characteristics of nanofluids. *Renewable and Sustainable Energy Reviews*. **11**(3): 512-523.
- Tham, L. and Nazar, R. 2012. Mixed convection flow about a solid sphere embedded in a porous medium filled with a nanofluid. *Sains Malaysiana*. **41**(12): 1643-1649.
- Tham, L., Nazar, R. and Pop, I. 2011. Mixed convection boundary-layer flow about an isothermal solid sphere in a nanofluid. *Physica Scripta*. **84**(2): 025403.
- Tham, L., Nazar, R. and Pop, I. 2012. Mixed convection boundary layer flow from a horizontal circular cylinder in a nanofluid. *International Journal of Numerical Methods for Heat & Fluid Flow*. **22**(5): 576-606.
- Tran, P. X. and Lyons, D. K. 2007. Nanofluids for use as ultra-deep drilling fluids. *Fact Sheet, National Energy Technology Laboratory, Office of Fossil Energy, US Department of Energy, Jan., <http://www.netl.doe.gov/publications/factsheets/rd/R&D108>*.
- Vassallo, P., Kumar, R. and D'Amico, S. 2004. Pool boiling heat transfer experiments in silica-water nano-fluids. *International Journal of Heat and Mass Transfer*. **47**(2): 407-411.
- Wang, T. Y. and Kleinstreuer, C. 1988. Local skin friction and heat transfer in combined free-forced convection from a cylinder or sphere to a power-law fluid. *International Journal of Heat and Fluid Flow*. **9**(2): 182-187.
- Wang, X. Q. and Mujumdar, A. S. 2008. A Review on nanofluids-part ii: experiments and applications. *Brazilian Journal of Chemical Engineering*. **25**(4): 631-648.

- White, F. M. 1974. *Viscous fluid flow 3ed*. McGraw-Hill Education.
- Wong, K. V. and De Leon, O. 2010. Applications of nanofluids: current and future. *Advances in Mechanical Engineering*. doi:10.1155/2010/519659.
- Yacob, N. A. and Ishak, A. 2011. Stagnation point flow towards a stretching/shrinking sheet in a micropolar fluid with a convective surface boundary condition. *The Canadian Journal of Chemical Engineering*. **90**(3): 621-626.
- Yacob, N. A., Ishak, A. Pop, I. and Vajravelu, K. 2011. Boundary layer flow past a stretching/shrinking surface beneath an external uniform shear flow with a convective surface boundary condition in a nanofluid. *Nanoscale Research Letters*. **6**(1): 1-7.
- Yacob, N. A. M. and Nazar, R. 2006. Mixed convection boundary layer on a solid sphere with constant surface heat flux. *Journal of Quality Measurement and Analysis*. **2**(1): 63-74.
- Yao, L. S. 1980. Buoyancy effects on a boundary layer along an infinite vertical cylinder with a step change of surface temperature. *American Society of Mechanical Engineers*. **1**(11): 16-21.
- Yao, S., Fang, T. and Zhong, Y. 2011. Heat transfer of a generalized stretching/shrinking wall problem with convective boundary conditions. *Communications in Nonlinear Science and Numerical Simulation*. **16**(2): 752-760.
- Yih, K. A. 1999. Couple heat and mass transfer by natural convection adjacent to a permeable horizontal cylinder in a saturated porous medium. *International Communications in Heat and Mass Transfer*. **26**: 431-440.
- You, S. M., Kim, J. H. and Kim, K. H. 2003. Effect of nanoparticles on critical heat flux of water in pool boiling heat transfer. *Applied Physics Letters*. **83**(16): 3374-3376.

Yu, W. and Xie, H. 2012. A review on nanofluids: preparation, stability mechanisms, and applications. *Journal of Nanomaterials*. [dx.doi.org/10.1155/2012/435873](https://doi.org/10.1155/2012/435873).

Yuge, T. 1960. Experiments on heat transfer from spheres including combined natural and forced convection. *Journal of Heat Transfer (US)*. **82**(2): 587-599.



APPENDIX A

BASIC CONCEPTS

Prandtl number

The Prandtl number or Pr dimensionless number which can be defined as:

$$\text{Pr} = \frac{\nu}{\alpha} = \frac{\text{viscous diffusion rate}}{\text{thermal diffusion rate}} = \frac{c_p \mu}{k}, \quad (\text{A1})$$

where $\nu = \mu/\rho$ is the dynamic viscosity, $\alpha = k/(\rho c_p)$ is the thermal diffusivity, μ is dynamic viscosity, k is the thermal conductivity, c_p is the specific heat and ρ is the density. The Prandtl number contains no such length scale in its definition and is dependent only on the fluid and the fluid state. As such, the Prandtl number is often found in property tables alongside other properties such as viscosity and thermal conductivity.

Typical values for Pr are:

- Around 0.015 for mercury,
- Around 0.16-0.7 for mixtures of noble gases or noble gases with hydrogen,
- Around 0.7-0.8 for air and many other gases,
- Between 4 and 5 for R-12 refrigerant,
- Around 7 for water (at 20°), 13.4 and 7.2 for seawater (at 0° and 20°, respectively)
- Between 100 and 40,000 for engine oil,
- Around 1×10^{25} for Earth's mantle.

Prandtl number influenced the velocity and thermal boundary layer thickness. For $\text{Pr} \ll 1$, it is found that thermal boundary layer thickness δ_T is bigger than the velocity boundary layer thickness δ_h , while for $\text{Pr} \gg 1$, the opposite trend occurs. Furthermore, for $\text{Pr} = 1$, the value is $\delta_T = \delta_h$ (Bejan, 1984; Incropera et al., 2006). Hence, Prandtl number acts as a relative measurement between velocity boundary layer

and thermal boundary layer. In summary, an increase in Prandtl values gives an impression of high viscosity (Sherman, 1990).

Grashof number

The Grashof number or Gr is a dimensionless number in heat transfer and fluid dynamics which approximates the ratio of the buoyancy to viscous force acting on a fluid. It frequently arises in the study of situations involving natural convection. It is defined for the convective boundary conditions as:

$$Gr = g\beta(T_f - T_\infty) \frac{a^3}{\nu^2}, \quad (\text{A2})$$

where $\beta = -\frac{1}{\rho} \left(\frac{\partial \rho}{\partial T} \right)$ is the thermal expansion coefficient, ρ is the fluid density, g is the gravity acceleration, T_∞ is the ambient temperature, T_f is the temperature of the hot fluid and $\nu = \mu / \rho$ is the kinematic viscosity.

For free convection from vertical flat plates, the value of Gr is $10^8 < Gr < 10^9$ and Grashof number plays the same role as Reynolds number in forced convection. The boundary layer is turbulent at higher Grashof numbers while at lower Grashof numbers, the boundary layer is laminar (Cengel, 2003).

Reynolds number

Reynolds number or Re can be defined as a number of different situations where a fluid is in relative motion to a surface (Tansley and Marshall, 2001). This definition generally includes the fluid properties of density and viscosity, plus a velocity and a characteristic length or characteristic dimension. This dimension is a matter of convention, for example a radius or diameters are equally valid for spheres or circles, but one is chosen by convention. For aircraft or ships, the length or width can be used. For flow in a pipe or a sphere moving in a fluid, the internal diameter is generally used today. Other shapes such as rectangular pipes or non-spherical objects have an equivalent diameter defined. For fluids of variable density such as compressible gases or fluids of variable viscosity such as non-Newtonian fluids, special rules apply. The

velocity may also be a matter of convention in some circumstances, notably stirred vessels with these conventions, the Reynolds number is defined as (Falkovich, 2011)

$$\text{Re} = \frac{U_{\infty} L}{\nu} = \frac{\text{inertial forces}}{\text{viscous forces}}, \quad (\text{A3})$$

where U_{∞} is free stream velocity, L is a characteristic linear dimension, and ν is the kinematic viscosity.

Nusselt number

Nusselt number or N_u is a dimensionless number which represents the ratio of amount of heat displaced by convection to conduction. It is defined as

$$N_u = \frac{hL}{k} = \frac{\text{convective heat transfer}}{\text{conductive heat transfer}}, \quad (\text{A4})$$

where L is the characteristic length, k is thermal conductivity of the fluid and h is the convective heat transfer coefficient.

In this context, convection includes both advection and conduction it is a dimensionless number. The conductive component is measured under the same conditions as the heat convection but with a (hypothetically) stagnant (or motionless) fluid. A Nusselt number close to one, namely convection and conduction of similar magnitude, is the characteristic of "slug flow" or laminar flow. A larger Nusselt number corresponds to more active convection, with turbulent flow typically in the 100-1000 range. The convection and conduction heat flows are parallel to each other and to the surface normal of the boundary surface, and are all perpendicular to the mean fluid flow in the simple case (Incropera et al., 2006).

Radiation

Radiation is the emission of electromagnetic waves from all matter that has a temperature greater than absolute zero. It represents a conversion of thermal energy into electromagnetic energy. Thermal energy consists of the kinetic energy of random movements of atoms and molecules in matter. All matter with a temperature by

definition is composed of particles which have kinetic energy, and which interact with each other. These atoms and molecules are composed of charged particles, i.e., protons and electrons, and kinetic interactions among matter particles result in charge-acceleration and dipole-oscillation. This results in the electrodynamic generation of coupled electric and magnetic fields, resulting in the emission of photons, radiating energy away from the body through its surface boundary. Electromagnetic radiation, including light, does not require the presence of matter to propagate and travels in the vacuum of space infinitely far if unobstructed.

The characteristics of thermal radiation depend on various properties of the surface it is emanating from, including its temperature, its spectral absorptivity and spectral emissive power, as expressed by Kirchoff's law. The radiation is not monochromatic, i.e., it does not consist of just a single frequency, but comprises a continuous dispersion of photon energies, its characteristic spectrum. If the radiating body and its surface are in thermodynamic equilibrium and the surface has perfect absorptivity at all wavelengths, it is characterized as a black body. A black body is also a perfect emitter. The radiation of such perfect emitters is called black-body radiation. The ratio of any body's emission relative to that of a black body is the body's emissivity, so that a black body has an emissivity of unity, (Blundell and Blundell, 2006).

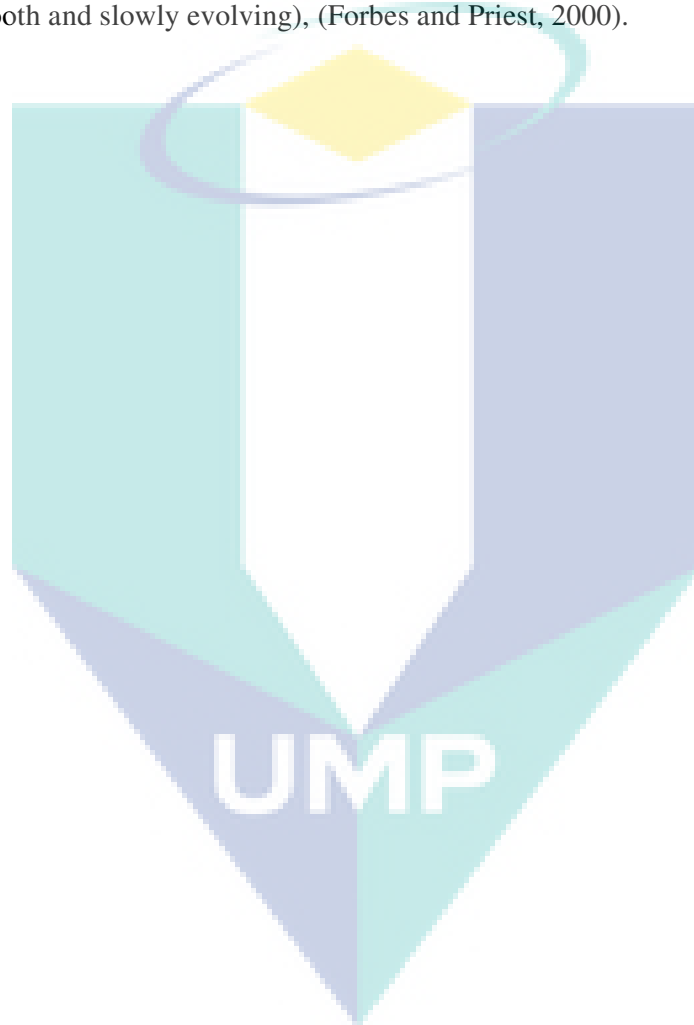
Magnetohydrodynamics (MHD)

Magnetohydrodynamics (MHD) is the study of the dynamics of electrically conducting fluids. Examples of such fluids include plasmas, liquid metals, and salt water or electrolytes. The word magnetohydrodynamics (MHD) is derived from magneto-meaning magnetic field, hydro-meaning liquid and -dynamics meaning movement. The field of MHD was initiated by Hannes Alfvén in 1942.

MHD is only strictly applicable when:

1. The plasma is strongly collisional, so that the time scale of collisions is shorter than the other characteristic times in the system, and the particle distributions are therefore close to Maxwellian.

2. The resistivity due to these collisions is small. In particular, the typical magnetic diffusion times over any scale length present in the system must be longer than any time scale of interest.
3. Interest in length scales much longer than the ion skin depth and Larmor radius perpendicular to the field, long enough along the field to ignore Landau damping, and time scales much longer than the ion gyration time (system is smooth and slowly evolving), (Forbes and Priest, 2000).



APPENDIX B

CARTESIAN COORDINATE SYSTEMS

Conservation of continuity, momentum and energy given in equations (2.1) to (2.3) are valid for any coordinate system.

$$\bar{\nabla} \cdot \bar{\nabla} = 0, \quad (\text{B1})$$

$$(\bar{\nabla} \cdot \bar{\nabla}) \bar{\nabla} = -\frac{1}{\rho_{nf}} \bar{\nabla} \bar{p} + \frac{\mu_{nf}}{\rho_{nf}} \bar{\nabla}^2 \bar{\nabla} + \frac{(\rho_{nf} - \rho_{\infty})}{\rho_{\infty}} g, \quad (\text{B2})$$

$$(\bar{\nabla} \cdot \bar{\nabla}) T = \alpha_{nf} \bar{\nabla}^2 T. \quad (\text{B3})$$

In order to write them for a Cartesian coordinate system first we need to define the velocity vector components in two dimensional , such as the following

$$\bar{\nabla} = \bar{r} (\bar{u} \mathbf{i} + \bar{v} \mathbf{j}) \quad (\text{B4})$$

Furthermore we need to use the following mathematical identities

$$\bar{\nabla} \cdot \bar{\nabla} = \frac{\partial}{\partial \bar{x}} (\bar{r} \bar{u}) + \frac{\partial}{\partial \bar{y}} (\bar{r} \bar{v}), \quad (\text{B5})$$

$$\bar{\nabla} \cdot \bar{\nabla} = \bar{r} \left(\bar{u} \frac{\partial}{\partial \bar{x}} + \bar{v} \frac{\partial}{\partial \bar{y}} \right), \quad (\text{B6})$$

$$\bar{\nabla} \bar{p} = \frac{\partial \bar{p}}{\partial \bar{x}} \mathbf{i} + \frac{\partial \bar{p}}{\partial \bar{y}} \mathbf{j}, \quad (\text{B7})$$

$$\bar{\nabla}^2 \bar{\nabla} = \bar{r} \left(\frac{\partial^2 \bar{u}}{\partial \bar{x}^2} + \frac{\partial^2 \bar{v}}{\partial \bar{x}^2} + \frac{\partial^2 \bar{u}}{\partial \bar{y}^2} + \frac{\partial^2 \bar{v}}{\partial \bar{y}^2} \right), \quad (\text{B8})$$

$$\bar{\nabla}^2 T = \frac{\partial^2 T}{\partial \bar{x}^2} + \frac{\partial^2 T}{\partial \bar{y}^2}, \quad (\text{B9})$$

Substituting (B5) into equation (B1) we get the continuity equation

$$\frac{\partial}{\partial \bar{x}}(\bar{r}\bar{u}) + \frac{\partial}{\partial \bar{y}}(\bar{r}\bar{v}) = 0 \quad (\text{B10})$$

Substituting (B4) to (B8) into equation (B2) then become

\bar{x} -momentum equation:

$$\begin{aligned} \bar{u} \frac{\partial \bar{u}}{\partial \bar{x}} + \bar{v} \frac{\partial \bar{u}}{\partial \bar{y}} = & -\frac{1}{\rho_{nf}} \frac{\partial \bar{p}}{\partial \bar{x}} + \frac{\mu_{nf}}{\rho_{nf}} \left(\frac{\partial^2 \bar{u}}{\partial \bar{x}^2} + \frac{\partial^2 \bar{u}}{\partial \bar{y}^2} \right) \\ & + \frac{\chi \rho_s \beta_s + (1-\chi) \rho_f \beta_f}{\rho_{nf}} g (T - T_\infty) \sin\left(\frac{\bar{x}}{a}\right), \end{aligned} \quad (\text{B11})$$

\bar{y} -momentum equation:

$$\begin{aligned} \bar{u} \frac{\partial \bar{v}}{\partial \bar{x}} + \bar{v} \frac{\partial \bar{v}}{\partial \bar{y}} = & -\frac{1}{\rho_{nf}} \frac{\partial \bar{p}}{\partial \bar{y}} + \frac{\mu_{nf}}{\rho_{nf}} \left(\frac{\partial^2 \bar{v}}{\partial \bar{x}^2} + \frac{\partial^2 \bar{v}}{\partial \bar{y}^2} \right) \\ & - \frac{\chi \rho_s \beta_s + (1-\chi) \rho_f \beta_f}{\rho_{nf}} g (T - T_\infty) \cos\left(\frac{\bar{x}}{a}\right) \end{aligned} \quad (\text{B12})$$

Finally, substituting (B3) into equation (B9) we get the energy equation

$$\bar{u} \frac{\partial T}{\partial \bar{x}} + \bar{v} \frac{\partial T}{\partial \bar{y}} = \alpha_{nf} \left(\frac{\partial^2 T}{\partial \bar{x}^2} + \frac{\partial^2 T}{\partial \bar{y}^2} \right) \quad (\text{B13})$$

APPENDIX C

LIST OF SYMBOLS USED IN THE MATLAB® PROGRAM

Matlab® name	Symbol
np	J
i, nx	x -station, total x -station
k, kmax	iteration count
x, delx	x, k_n or Δx
xx	α
eta, eta(np,1), deleta	$y, y_\infty, \Delta y$
deta	h_j or Δy
stop	$ \delta v_0 $
f, u, v, s, t	$f, f', f'', \theta, \theta'$
cfb, cub, cvb, csb, ctb	$f_{j-1/2}^{n-1}, u_{j-1/2}^{n-1}, v_{j-1/2}^{n-1}, s_{j-1/2}^{n-1}, t_{j-1/2}^{n-1}$
cuub, cfvb, cftb, cusb	$(u_{j-1/2}^{n-1})^2, f_{j-1/2}^{n-1} v_{j-1/2}^{n-1}, f_{j-1/2}^{n-1} t_{j-1/2}^{n-1}, u_{j-1/2}^{n-1} s_{j-1/2}^{n-1}$
cdervb, cdertb	$(v_j^{n-1} - v_{j-1}^{n-1})/h_j, (t_j^{n-1} - t_{j-1}^{n-1})/h_j$
fb, ub, vb, sb, tb	$f_{j-1/2}, u_{j-1/2}, v_{j-1/2}, s_{j-1/2}, t_{j-1/2}$
uub, fvb, ftb, usb	$(u_{j-1/2})^2, f_{j-1/2} v_{j-1/2}, f_{j-1/2} t_{j-1/2}, u_{j-1/2} s_{j-1/2}$
dervb, derpb	$(v_j - v_{j-1})/h_j, (t_j - t_{j-1})/h_j$
a1 to a8	$(a_1)_j$ to $(a_8)_j$
b1 to b8	$(b_1)_j$ to $(b_8)_j$
r1 to r5	$(r_1)_j$ to $(r_5)_j$
R1, R2	$(R_1)_{j-1/2}^{n-1}, (R_2)_{j-1/2}^{n-1}$
a, b, c	$[A_j], [B_j], [C_j]$
alfa, gamma	$[\alpha_j], [\Gamma_j]$
ww, rr, dell	$[W_j], [r_j], [\delta_j]$
delf, delu, delv, dels, delt	$\delta f, \delta u, \delta v, \delta s, \delta t$

APPENDIX D

MATLAB PROGRAM

```
%%%%%%%%%%%%%%%%%%%%%%%%%%%%%%%%%%%%%%%%%%%%%%%%%%%%%%%%%%%%%%%%%%%%%%%%
%%%%%%%%%%%%%%%%%%%%%%%%%%%%%%%%%%%%%%%%%%%%%%%%%%%%%%%%%%%%%%%%%%%%%%%%
```

```
%Problem: mixed convection boundary layer flow over a solid sphere  
with convective boundary conditions in a nanofluid with  
convective boundary conditions%
```

```
%%%%%%%%%%%%%%%%%%%%%%%%%%%%%%%%%%%%%%%%%%%%%%%%%%%%%%%%%%%%%%%%%%%%%%%%  
The answer displayed in the result sheet will be started from number  
linstead of 0
```

```
%%%%%%%%%%%%%%%%%%%%%%%%%%%%%%%%%%%%%%%%%%%%%%%%%%%%%%%%%%%%%%%%%%%%%%%%
```

```
% Data input
```

```
xend =    %('Input the endpoint of x = ');  
delx =    %('Input the step size for x = ');  
blt =     %('Input the boundary layer thickness = ');  
deleta = %('Input the step size of boundary layer thickness = ');  
nx = ( xend / delx ) + 1; np = ( blt / deleta ) + 1;  
Ga=       % ('Input the Gamma value  
pr =      %('Input the prandtl number = ');  
ge =      %('Input the value of lambda, gr/re2 = ');  
N =       %('Input nanoparticle volume fraction = ');  
ps =      %('Input density of the solid fraction = ');  
pf =      %('Input density of the fluid fraction = ');  
Bs =      %('Input thermal expansion coefficient of the solid  
          fraction = ');  
Bf =      %('Input thermal expansion coefficient of the fluid  
          fraction = ');  
ks =      %('Input thermal conductivity of the solid = ');  
kf =      %('Input thermal conductivity of the fluid = ');  
cs =      %('Input heat capacity of the solid = ');  
cn =      %('Input heat capacity of the fluid = ');  
x(1) = 0.0 ; B(1) = 1; A(1) = 1.0; E(1) = 2.0;  
for i = 2:nx  
    x(i) = x(i-1) + delx;  
    xx(i) = x(i) / (x(i) - x(i-1));  
    B(i) = sin(x(i)) / x(i);  
    A(i) = (9/4)*cos(x(i)) * B(i);  
    E(i) = 1 + (x(i) * cot(x(i)));
```

```

end
for i = 1:nx
stop = 1.0; k = 1;
while stop > 0.00001
    eta(1,1) = 0.0;
    for j = 2:np
        eta(j,1) = eta(j-1,1) + deleta;
    end
% To generate the initial value for velocity and temperature profile
% see Eq (2.110) - (2.114)
    etanpq = eta(j,1) / 4;
    etau15 = 1 / eta(np,1);
    for j = 1:np
        deta(j,k) = deleta;
        etab = eta(j,1) / eta(np,1);
        etab1 = etab^2;
        etab3 = ((3/2) - (1/2)* etab1);
    if i == 1
        f(j,1,i) = (3/2) * etanpq * B(i) * etab * (3 - ((1/2) * etab1));
        u(j,1,i) = (3/2) * etab * B(i) * etab3;
        v(j,1,i) = (9/4) * etau15 * B(i) * (1 - etab1);
        s(j,1,i) = -etab1 + 1;
        t(j,1,i) = -2* etau15*etab;
    else
% from shift profile
        f(j,1,i) = ff(j);
        u(j,1,i) = uu(j);
        v(j,1,i) = vv(j);
        s(j,1,i) = ss(j);
        t(j,1,i) = tt(j);
    end
end
end
% To define the coefficients of the linearized equations
for j = 2:np
% Previous station
    if i == 1
        cfb(j,i) = 0.0; cub(j,i) = 0.0; cvb(j,i) = 0.0;
        csb(j,i) = 0.0; ctb(j,i) = 0.0; cunb(j,i) = cub(j,i)^2;
        cfvb(j,i) = cfb(j,i) * cvb(j,i);
        cftb(j,i) = cfb(j,i) * ctb(j,i);
    end
end

```

```

cusb(j,i) = cub(j,i) * csb(j,i);
cdervb(j,i) = 0.0; cdertb(j,i) = 0.0;
else
    cfb(j,i) = ffb(j); cub(j,i) = uub(j); cvb(j,i) = vvb(j);
    csb(j,i) = ssb(j); ctb(j,i) = ttb(j);
    cunb(j,i) = cub(j,i)^2; cfvb(j,i) = cfb(j,i) * cvb(j,i);
    cftb(j,i) = cfb(j,i) * ctb(j,i);
    cusb(j,i) = cub(j,i) * csb(j,i);
    cdervb(j,i) = ddervb(j);
    cdertb(j,i) = ddertb(j);
end
% Present station (centered-difference derivatives) (see Eq (2.48)-
(2.50))
fb(j,k,i) = 0.5 * ( f(j,k,i) + f(j-1,k,i) );
ub(j,k,i) = 0.5 * ( u(j,k,i) + u(j-1,k,i) );
vb(j,k,i) = 0.5 * ( v(j,k,i) + v(j-1,k,i) );
sb(j,k,i) = 0.5 * ( s(j,k,i) + s(j-1,k,i) );
tb(j,k,i) = 0.5 * ( t(j,k,i) + t(j-1,k,i) );
unb(j,k,i) = ub(j,k,i)^2; fvb(j,k,i) = fb(j,k,i) * vb(j,k,i);
ftb(j,k,i) = fb(j,k,i) * tb(j,k,i);
usb(j,k,i) = ub(j,k,i) * sb(j,k,i);
dervb(j,k,i) = ( v(j,k,i) - v(j-1,k,i) ) / deta(j,k);
dertb(j,k,i) = ( t(j,k,i) - t(j-1,k,i) ) / deta(j,k);

% Coefficients of the difference momentum equation (see Eq (2.86))
a1(j,k) = (1/((1-N)^2.5*(1-N+ N*(ps/pf)))) + 0.5 * (E(i) + xx(i)) *
    deta(j,k) * fb(j,k,i) - 0.5 * xx(i) * deta(j,k) *
cfb(j,i);
a2(j,k) = a1(j,k) - 2.0*(1/((1-N)^2.5*(1-N+ N*(ps/pf))));
a3(j,k) = 0.5 * (E(i) + xx(i)) * deta(j,k) * vb(j,k,i) + 0.5 * xx(i) *
    deta(j,k) * cvb(j,i);
a4(j,k) = a3(j,k);
a5(j,k) = -1.0 * (1 + xx(i)) * deta(j,k) * ub(j,k,i);
a6(j,k) = a5(j,k);
a7(j,k) = ((N*ps*(Bs/Bf)+(1-N)* pf)/(1-N*pf+N*ps))*ge * B(i) * 0.5 *
    deta(j,k);
a8(j,k) = a7(j,k);
% Coefficients of the difference energy equation (see Eq (2.87))
b1(j,k) = (((ks+2*kf)-2*N*(kf-ks))/(((ks+2*kf)+N*(kf-ks))*((1-
    N)+N*((ps*cs)/(pf*cn))))*(1.0 / pr) + 0.5 * (E(i) + xx(i))

```

```

* deta(j,k) * fb(j,k,i) - 0.5 * xx(i) * deta(j,k) * cfb(j,i); b2(j,k)
= b1(j,k) - (((ks+2*kf)-2*N*(kf-ks))/(((ks+2*kf)+N*(kf-ks))* ((1-N + N
    * ((ps*cs)/(pf*cn))))))*(2.0 / pr);
b3(j,k) = 0.5 * (E(i) + xx(i)) * deta(j,k) * tb(j,k,i) + .05 * xx(i)*
    deta(j,k) * ctb(j,i);
b4(j,k) = b3(j,k);
b5(j,k) = -0.5 * xx(i) * deta(j,k) * sb(j,k,i) + 0.5 * xx(i) *
    deta(j,k) * csb(j,i);
b6(j,k) = b5(j,k);
b7(j,k) = -0.5 * xx(i) * deta(j,k) * ub(j,k,i) - 0.5 * xx(i) *
    deta(j,k) * cub(j,i);
b8(j,k) = b7(j,k);

% Expressions of Rj (see Eq (2.73)-(2.74))
R1 = deta(j,k) *(1/((1-N)^2.5*(1-N+ N*(ps/pf))))* cdervb(j,i) + (E(i)-
    xx(i)) * deta(j,k) * cfvb(j,i) +(xx(i) - 1.0) * deta(j,k) *
    . cunb(j,i) + ((N*ps*(Bs/Bf)+(1-N)* pf)/(1-N*pf+N*ps))* ge * B(i) *
    deta(j,k) * csb(j,i)+* deta(j,k) * A(i);
R2 = deta(j,k) * (((ks+2*kf)-2*N*(kf-ks))/(((ks+2*kf)+N*(kf-ks))* ((1-
    N)+N*((ps*cs)/(pf*cn))))*(1.0 / pr) * cdertb(j,i) + (E(i) -
    xx(i)) * deta(j,k) * cftb(j,i) + xx(i) * deta(j,k) * cusb(j,i);

% Expressions of rj-1/2 (see Eq (2.88))
r1(j,k) = f(j-1,k,i) - f(j,k,i) + deta(j,k) * ub(j,k,i);
r2(j,k) = u(j-1,k,i) - u(j,k,i) + deta(j,k) * vb(j,k,i);
r3(j,k) = s(j-1,k,i) - s(j,k,i) + deta(j,k) * tb(j,k,i);
if i == 1
r4(j,k) = (1/((1-N)^2.5*(1-N+ N*(ps/pf)))) * (v(j-1,k,i) - v(j,k,i)) -
    deta(j,k) * .(E(i) + xx(i)) * fvb(j,k,i) + (1.0 + xx(i)) *
    deta(j,k) * .unb(j,k,i) - xx(i) * deta(j,k) * cvb(j,i) *
    fb(j,k,i) + xx(i) * deta(j,k) * cfb(j,i) * vb(j,k,i) -
    ((N*ps*(Bs\Bf)+(1-N)* pf)\(1-N*pf+N*ps))* ge * B(i) *
    deta(j,k) * sb(j,k,i) -deta(j,k) * A(i) - R1;
end
r5(j,k) = (((ks+2*kf)-2*N*(kf-ks))/(((ks+2*kf)+N*(kf-ks))* ((1-
    N)+N*((ps*cs)/(pf*cn))))*(1.0 / pr) * (t(j-1,k,i) -
    t(j,k,i)) - (E(i) + xx(i)) * deta(j,k) * ftb(j,k,i) +
    xx(i) * deta(j,k) * usb(j,k,i) - .xx(i) * deta(j,k) *
    csb(j,i) * ub(j,k,i) + xx(i) * deta(j,k) * cub(j,i) *
    sb(j,k,i) + xx(i) * deta(j,k) *

```

```

        cfb(j,i) * tb(j,k,i) - xx(i) * deta(j,k) * ctb(j,i) *
        fb(j,k,i) - R2;
    end
% Obtain the matrices (see Eq (2.91)-(2.94))
a{2,k} = [ 0 0 1 0 0; -0.5*deta(2,k) 0 0 -0.5*deta(2,k) 0; 0 -1 0 .0 -
        0.5*deta(2,k); a2(2,k) a10 a8(2,k) a3(2,k) a1(2,k) 0; 0
        b8(2,k) b3(2,k) 0 b1(2,k)];
    for j = 3:np
a{j,k} = [ -0.5*deta(j,k) 0 1 0 0; -1 0 0 -0.5*deta(j,k) 0; 0 -1 0 0 0
        -0.5*deta(j,k); a6(j,k) a8(j,k) a3(j,k) a1(j,k) 0; b6(j,k)
        b8(j,k) b3(j,k) 0 b1(j,k)];
b{j,k} = [ 0 0 -1 0 0; 0 0 0 -0.5*deta(j,k) 0; 0 0 0 0 -0.5*deta(j,k);
        0 0 0 a4(j,k) a2(j,k) a10(j,k) 0; 0 0 0 b4(j,k) 0 0
        b2(j,k)];
    end
    for j = 2:np
c{j,k} = [ -0.5*deta(j,k) 0 0 0 0; 1 0 0 0 0; 0 1 0 0 0; a5(j,k)
        a7(j,k) 0 0 0; b5(j,k) b7(j,k) 0 0 0];
    end
% The recursion formulas
% forward sweep
% (see Eq (2.98)-(2.104))
    alfa{2,k} = a{2,k};
    gamma{2,k} = inv(alfa{2,k}) * c{2,k};
    for j = 3:np
        alfa{j,k} = a{j,k} - ( b{j,k} * gamma{j-1,k});
        gamma{j,k} = inv(alfa{j,k}) * c{j,k};
    end
% (see Eq (2.96))
    for j = 2:np
        rr{j,k} = [ r1(j,k); r2(j,k); r3(j,k); r4(j,k); r5(j,k)];
    end
% (see Eq (2.105)-(2.111))
    ww{2,k} = inv(alfa{2,k}) * rr{2,k};
    for j = 3:np
        ww{j,k} = inv(alfa{j,k}) * (rr{j,k} - (b{j,k} * ww{j-1,k}));
    end
% backward sweep (see Eq (2.89))
    delf(1,k) = 0.0; delt(1,k) = 0.0; delu(1,k) = 0.0;

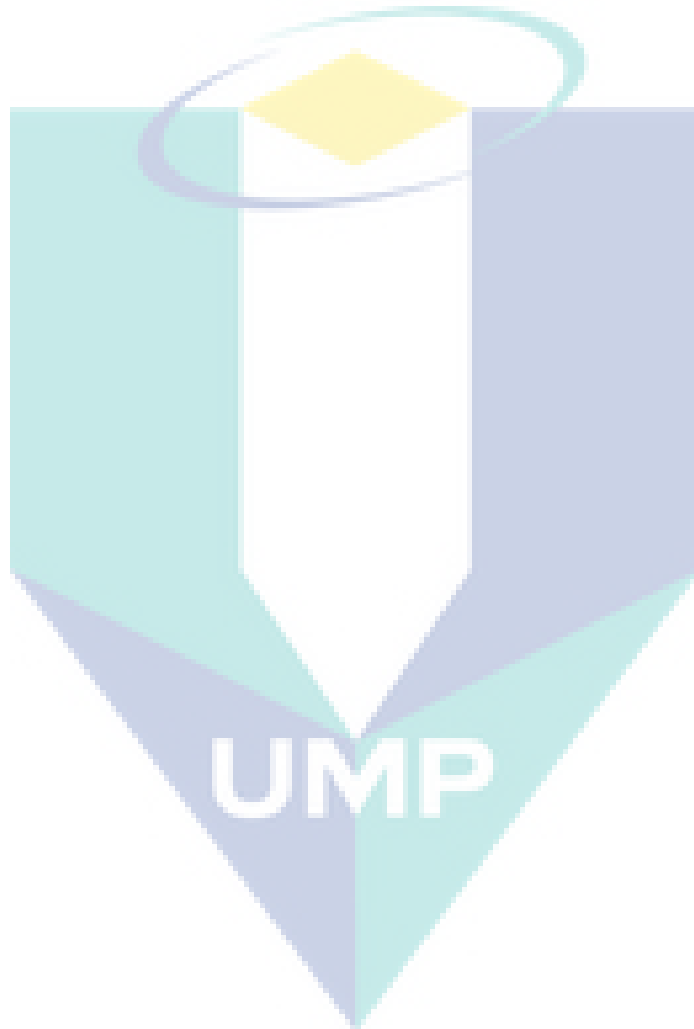
```

```

    delg(1,k) = 0.0; delu(np,k) = 0.0; dels(np,k) = 0.0;
    dell{np,k} = ww{np,k};
% (see Eq (2.107)-(2.108))
    for j = np-1:-1:2
        dell{j,k} = ww{j,k} - (gamma{j,k} * dell{j+1,k});
    end
% (see Eq (2.95))
    delv(1,k) = dell{2,k}(1,1);
    dels(1,k) = dell{2,k}(3,1);
    delf(2,k) = dell{2,k}(4,1);
    delv(2,k) = dell{2,k}(5,1);
    delt(2,k) = dell{2,k}(7,1);
    for j = np:-1:3
        delu(j-1,k) = dell{j,k}(1,1);
        dels(j-1,k) = dell{j,k}(3,1);
        delf(j,k) = dell{j,k}(4,1);
        delv(j,k) = dell{j,k}(5,1);
        delt(j,k) = dell{j,k}(7,1);
    end
    % Newton's method (see Eq (2.75))
    for j = 1:np
        f(j,k+1,i) = f(j,k,i) + delf(j,k);
        u(j,k+1,i) = u(j,k,i) + delu(j,k);
        v(j,k+1,i) = v(j,k,i) + delv(j,k);
        t(j,k+1,i) = t(j,k,i) + delt(j,k);
    end
% check for convergence of the iterations (see Eq (2.109))
    stop = abs(delv(1,k));
    kmax(i) = k;
    k = k+1;
    end
% Shift profile
    for j = 1:np
        ff(j) = f(j,k,i); uu(j) = u(j,k,i); vv(j) = v(j,k,i);
        ss(j) = s(j,k,i); tt(j) = t(j,k,i);
    end
    for j = 1:np
        ffb(j) = fb(j,kmax(i),i);
        uub(j) = ub(j,kmax(i),i);
        vvb(j) = vb(j,kmax(i),i);
    end

```

```
ssb(j) = sb(j,kmax(i),i);  
ttb(j) = tb(j,kmax(i),i);  
ddervb(j) = dervb(j,kmax(i),i);  
ddertb(j) = dertb(j,kmax(i),i);  
dderpb(j) = derpb(j,kmax(i),i);  
end
```



APPENDIX E**LIST OF PUBLICATIONS****A Journal**Published

1. **Alkawasbeh, H. T.,** Salleh. M. Z., Tahar R. M. and Nazar, R. 2014. Numerical solutions of free convection boundary layer flow on a solid sphere with convective boundary condition, *Journal of Physics: Conference Series IOP Publishing*. **495**(1): 012025. (ISI, Scopus Indexed)
2. **Alkawasbeh, H. T.,** Salleh. M. Z., Tahar R. M., Nazar, R. and Pop, I. 2014. Mixed convection boundary layer flow about a solid sphere with convective boundary conditions. *Wulfenia Journal*. **21**(3): 386-404
3. **Alkawasbeh, H. T.,** Salleh. M. Z., Tahar R. M., Nazar, R. and Pop, I. 2014. Free convection boundary layer flow on a solid sphere with convective boundary conditions in a micropolar fluid. *World Applied Sciences Journal*. **32**(9): 1942-1951. (Scopus Indexed).
4. **Alkawasbeh, H. T.,** Salleh. M. Z., Nazar, R. and Pop, I. 2014. Numerical solutions of effect of radiation and magnetohydrodynamic free convection boundary layer flow a solid sphere with Newtonian heating. *Applied Mathematical Sciences Journal*. **8**(140): 6989-7000. (Scopus Indexed).
5. **Alkawasbeh, H. T.,** Salleh. M. Z., Tahar R. M. and Nazar, R. 2014. Effect of radiation on magnetohydrodynamic free convection boundary layer flow near the lower stagnation point of a solid sphere with Newtonian heating. *Journal of Engineering and Technology. (JET)*. **5**(1): 77-88. (Scopus Indexed).
6. **Alkawasbeh, H. T.,** Salleh. M. Z., Tahar R. M., Nazar, R. and Pop, I. 2015. Effect of radiation and magnetohydrodynamic free convection boundary layer flow on a solid sphere with convective boundary conditions. *Walailak Journal of Science and Technology*. **12**(9): 849-861. (Scopus Indexed).

7. **Alkawasbeh, H. T.**, Salleh, M. Z., Tahar R. M., Nazar, R. and Pop, I. 2015. Effect of radiation and magnetohydrodynamic free convection boundary layer flow on a solid sphere with convective boundary conditions in a micropolar fluid. *Malaysian Journal of Mathematical Sciences*. 9(3): 463-480 (Scopus Indexed).
 8. **Alkawasbeh, H. T.**, Salleh, M. Z., Tahar, R. M., Nazar, R. and Pop, I. 2015. Numerical solutions of mixed convection boundary layer flow about a solid sphere in a micropolar fluid with convective boundary conditions. *World Applied Sciences Journal*. (Scopus Indexed) (Accepted).
- Submitted
9. **Alkawasbeh, H. T.**, Salleh, M. Z., Tahar, R. M., Nazar, R. and Pop, I. 2015. Mixed convection boundary layer flow about a solid sphere with convective boundary conditions in a nanofluid. *Submitted to Applied Mathematics and Computation Journal*. (ISI, Scopus Indexed) *Under Review*.
 10. **Alkawasbeh, H. T.**, Salleh, M. Z., Tahar, R. M., Nazar, R. and Pop, I. 2015. Mixed convection flow about a solid sphere embedded in a porous medium filled with convective boundary conditions in a nanofluid. *Submitted to The European Physical Journal Plus*. (ISI, Scopus Indexed). *Under Review*.
 11. Ishak, N., **Alkawasbeh, H. T.**, Wainib I, Rosli N. and Salleh, M. Z., 2015. MHD flow and heat transfer for the upper-convected Maxwell fluid over a stretching/shrinking sheet with prescribed wall temperature *Submitted to Journal of Teknologi*. (Scopus Indexed). *Under Review*.
 12. Hussanan, A., Salleh, M. Z., Khan, I, **Alkawasbeh, H. T.** 2015. MHD flow and heat transfer in a Casson fluid over a nonlinearly stretching sheet with Newtonian heating. *Submitted to Applied Mathematical Modelling Journal* (ISI, Scopus Indexed) *Under Review*.

B Proceeding

1. **Alkawasbeh, H. T.**, Salleh, M. Z., Tahar, R. M. and Nazar, R. 2013. Effect of radiation and magnetohydrodynamic free convection boundary layer flow near the stagnation point of a solid sphere with Newtonian Heating. *Proceeding of the Malaysian Technical Universities Conference on Engineering and Technology or (MUCET) to be hold between 3 -4 Dececember 2013 in Kuantan, Pahang.*
2. **Alkawasbeh, H. T.**, Salleh, M. Z., Tahar, R. M., Nazar, R. and Pop, I. 2013. Free convection boundary layer flow near the stagnation point of a solid sphere with convective boundary conditions in a micropolar fluid. *AIP Proceedings of The 3rd International Conference on Mathematical Sciences (1602): 76-82.* (ISI, Scopus Indexed).
3. **Alkawasbeh, H. T.**, Salleh, M. Z., Tahar, R. M. and Nazar, R. 2014. Numerical solution of free convection boundary layer flow on a solid sphere with convective boundary conditions. *Proceeding of the 2014 International Conference on Science and Engineering in Mathematics, Chemistry and Physics, Jakarta-Indonesia, 13-14 January 2014, 229-238.*
4. **Alkawasbeh, H. T.**, Sarif, N. M., Salleh, M. Z., Tahar, R. M., Nazar, R. and Pop, I. 2015. Effect of radiation and magnetohydrodynamic free convection boundary layer flow on a solid sphere with Newtonian Heating in a micropolar fluid. *AIP Proceedings In The 2nd Ism International Statistical Conference 2014 (ISM-II): Empowering the Applications of Statistical and Mathematical Sciences. (1643): 662-669.* (ISI, Scopus Indexed).
5. **Alkawasbeh, H. T.**, Sarif, N. M., Salleh, M. Z., Tahar, R. M. 2015. Mixed convection boundary layer flow of nanofluid near the lower stagnation point about a solid sphere with convective boundary conditions. *Proceeding In the International Conference on Global Optimization and Its Applications (ICoGOIA2015) 10 -11 August 2015 in Kuantan, Pahang.*